P O L A R F R E Q U E N C Y

D I S C R I M I N A T O R S

DAVID MALCOLM RACHMAN

A dissertation submitted to the Faculty of Engineering, University of Cape Town, Cape Town, in fulfilment of the requirements for the degree of Master of Science in Engineering.

Cape Town, 1986

ABSTRACT

This dissertation makes a study of frequency discriminators and their role in instantaneous frequency measuring (IFM) signal acquisition receivers. Frequency discriminators are the major building blocks of IFM. They are required to measure frequency accurately over very broad bandwidths and to have near unity probabilities of pulse intercept.

The major difficulties of the most commonly reported version are identified as a lack of component symmetry and a need to cross over two transmission lines while maintaining isolation. The effect on accuracy due to lack of symmetry shows up analytically. TOUCHSTONE, a micro-computer analysis package, is demonstrated as an excellent analysis tool while alternatives are also suggested.

Variations of the standard discriminator are discussed. These are intended to improve performance due to lack of symmetry. None completely solve the cross over problem. A new type of discriminator requiring fewer components is introduced. It requires no cross over and exhibits greater symmetry. Analysis indicates that it performs better than the standard version. Two prototypes show the methods to be reliable and confirm the promise of the new version.

DECLARATION

I declare that this dissertation is my own, original work. It is being submitted for the degree of Master of Science in Engineering. It has not previously been submitted in this or any other form for a degree at any university.

Signed by candidate

(Name of Candidate)

21st day of April, 1986

For Thea, my mother.
She was here for the
beginning .....

ACKNOWLEDGEMENTS

The author is indebted to the following people in particular :

Professor Barry Downing, for supervision and tireless encouragement.

Mr Johan Pretorius, for numerous discussions and much valued advice.

Mr Richard Nortier and members of NIAST, for useful discussions and assistance with materials.

The staff, and particularly the workshop staff, of the University of Cape Town's Department of Electrical and Electronic Engineering, for assistance during the project.

The CSIR Foundation for Research Development, for financial assistance.

Mrs Sally Creed, for typing the manuscript.

LIST OF ABBREVIATIONS

AC	Alternating current
A/D	Analog to digital converter
AM	Amplitude modulation
AMP	Amplifier
A/O	Acousto-optic
AOA	Angle of arrival
AOR	Acousto-optic receiver
BPF	Band-pass filter
BW	Bandwidth
CCD	Charge coupled device
CVR	Crystal video receiver
CW	Continuous wave
DC	Direct current
DIFM	Digital instantaneous frequency measurement
DLD	Delay line discriminator
FAR	False alarm rate
FD	Frequency discriminator
FOM	Figure of merit
HP	Hewlett Packard
IBM-PC	International Business Machines Personal Computer
IF	Intermediate frequency
IFM	Instantaneous frequency measurement
IFMR	Instantaneous frequency measuring receiver
LA	Limiting amplifier
LO	Local oscillator
LPF	Low pass filter
PD	Phase discriminator
PFD	Polar frequency discriminator
PIN	p-type - intrinsic - n-type
PM	Phase modulation
POI	Probability of intercept
PROM	Programmable read only memory
PTFE	Poly-tetra-fluoro-ethylene
QC	Quadrature coupler
RF	Radio frequency

ROM	Read only memory
RMS	Root mean square
SAW	Surface acoustic wave
SSD	Simultaneous signal detection
TE	Transverse electric
TEM	Transverse electromagnetic
TOA	Time of arrival
TS	TOUCHSTONE
UCT	University of Cape Town
VCO	Voltage controlled oscillator
VSWR	Voltage standing wave ratio
WC	Wilkinson coupler (in-phase power splitter)
YIG	Yttrium iron garnet

TABLE OF CONTENTS

Page

Page

LIST OF TABLES

LIST OF FIGURES

Figure **Page**

Figure **Page**

Figure **Page**

CHAPTER ONE

INTRODUCTION

Frequency discriminators (FDs), as their name suggests, are devices with frequency dependent outputs that can be used to measure signal frequency. Polar frequency discriminators provide a sine and a cosine output which can be applied to a polar display to read frequency directly once calibrated. Essentially they operate by measuring the phase difference between input and output of a transmission line of known length when a signal is passed down it.

FDs are not new. Goddard[13] reports that work on the first discriminators began at the Mullard Research Laboratories in England in 1954, while the first polar discriminator was built there in 1957. As for the principle of measuring frequency in terms of signal phase delay down a transmission line, Goddard suggests that must be nearly as old as electromagnetic science.

The main attraction of FDs is that they can operate over very large bandwidths and be sensitive to signals arriving anywhere within that band all the time. Rarely are FDs built to cover bandwidths of less than an octave and one has been reported[10] covering 2 to 18 GHz. Bandwidth is limited primarily by the bandwidths of the individual components.

The prime use of FDs is in intantaneous frequency measuring (IFM) receivers and these are just one type of signal acquisition receiver. The practical demands of such receivers can be very challenging which is why FDs are best studied in the context of IFM. Certainly IFM can be counted on to highlight any failings of FDs.

1.1 OBJECTIVES

The first objective is to gain an understanding of acquisition receivers in general and IFM in particular. This will throw light on the requirements and limitations of FDs. At the same time

all current FD realisations reported in the literature should be studied as each has advantages and disadvantages.

The next objective is to find suitable methods of analysing the broadband performance of FDs. This should allow different FDs to be properly compared and improve the design procedure. At the same time practical difficulties in constructing the different FDs should be determined.

With knowledge of the theoretical and practical difficulties of the various FDs, attempts should be made to overcome any problems. This may require the development of a new form of FD.

The final objective is to demonstrate the validity of the design and analysis methods by building and testing an FD covering the reasonably challenging bandwidth of 2 to 6 GHz.

1.2 DISSERTATION ORGANISATION

This dissertation is divided into six main chapters. The first, chapter two, looks briefly at the various different types of signal acquisition receivers, be they in use today or still in the experimental stages.

Chapter three takes an in depth look at IFM receivers with particular emphasis on digital IFM. Digital IFM is a newer field and has its roots in the early seventies.

Chapter four studies the forms and characteristics of the various FD types that have been reported in the literature. The main practical difficulties are also detailed. A new FD form is introduced which overcomes many of the difficulties of earlier versions.

Chapter five looks at the various components which make up FDs. Particular emphasis is placed on their characteristics which affect overall performance and limit bandwidth. Ways of broadbanding

the components are discussed and the methods described are used to design and build components required for the prototypes. Measured component characteristics are presented. With knowledge of both ideal and non-ideal component properties, broadband FD analysis can be tackled with greater confidence.

Chapter six looks briefly at various methods which can be used to analyse the discriminators, and chooses a 'yardstick' which allows the performance of different FDs to be compared. The best available analysis method is then used to perform several sample analyses and make comparisons between the standard or most commonly described FD and the two forms of the new version introduced in chapter four.

Chapter seven describes the building and comprehensive testing of two prototypes of the new FD version. Use is made of the components described in chapter five.

The final chapter is a conclusion and suggests some areas for future work.

CHAPTER TWO

SIGNAL ACQUISITION RECEIVERS

The subject of this dissertation is frequency discriminators. They perform a very specific task, namely the measurement of frequency (or phase, as will be seen later). To fully appreciate the special characteristics of these units it is useful to consider the systems within which they are generally used. Similarly, to better understand these systems one needs to consider the types of signals that they are designed to intercept. This chapter serves this purpose and briefly describes alternative systems, for completeness and because the wide range of techniques used makes their study particularly rewarding.

2.1 TYPICAL SIGNAL CHARACTERISTICS

Firstly it should be noted that it is the microwave frequency band that is of interest here, more particularly the range 500 MHz to 18 GHz. This is an extremely large bandwidth and any one receiver generally covers only a portion of this frequency range. Various techniques can then be used to extend coverage to the whole band. Nevertheless it must be realised that very large bandwidths are involved, typically an octave or more.

Next it must be realised that the receivers are meant to reveal the presence of signals at a given location. It is not generally known in advance even that signals are present, let alone their frequency or other characteristics. Interception of the most complex and fleeting signals should be aimed at, then detection of simpler signals will follow. It should also be borne in mind that several signals may be present in any given time interval, perhaps even active simultaneously.

A large proportion of signals in this frequency band are emitted by radar units. The simplest radar signal is CW but most are pulsed and have very short pulse durations. Typically receivers

are designed to intercept pulses as short as 100ns in duration[1-5]. Receivers should therefore aim at a very high probability of pulse intercept. More 'exotic' radars may vary their frequency within each pulse and/or from pulse to pulse. They may also vary their pulse repetition frequency or may emit several beams at different frequencies such as in 'stacked-beam' radar for measurement of both height and range[6].

Signals may also vary very widely in amplitude so that a wide dynamic range is desirable. Other obvious considerations are size, weight and cost.

Receivers may be designed to report on each pulse's carrier frequency, direction of arrival, pulse amplitude, pulse duration and time of arrival[7]. In addition after several pulses have been collected, more complex receivers endeavour to identify the signal type, (eg. 'chirped' radar or multi-beam radar) and other parameters such as pulse repetition frequency. It is the accurate, within pulse, measurement of carrier frequency that this chapter is primarily concerned with.

2.2 CRYSTAL VIDEO RECEIVER

The crystal video receiver (CVR) is the most widely used wideband receiver because of its simplicity, small size and low cost[1,8]. In its simplest form it consists of a low noise RF pre-amplifier, a square law video detector and a log video amplifier. This provides a 100 percent probability of intercept (POI), a broad bandwidth and signal amplitude information. Its major drawback is that it provides no frequency information beyond that the signal falls within the passband of the receiver. The passband is often defined by a front-end bandpass filter, typically an octave or more in bandwidth. Other disadvantages are rapid performance degradation in dense signal environments, and susceptibility to jamming.

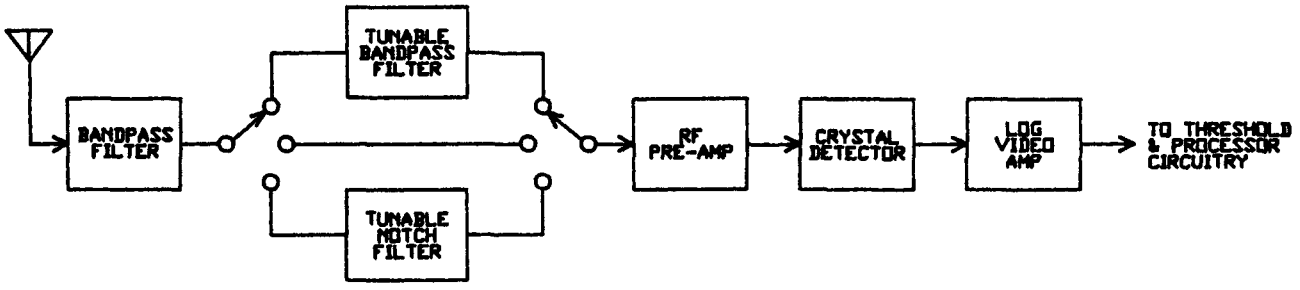

Fig 2.1 : **Typical crystal video receiver**
after Hofmann and Brown

The system can be upgraded to a tunable RF (TRF) crystal video receiver by adding a tunable bandpass filter as shown in fig 2.1. This can be a varactor-tuned or tunable yttrium iron garnet (YIG) filter, and allows frequency measurement with a resolution of between 5 and 70 MHz[8]. However, switching the filter in and out significantly reduces the POI and also degrades the false alarm rate (FAR). Another variation also shown in fig 2.1 uses a tunable notch filter to eliminate CW or any other interfering narrowband signal.

2.3 SCANNING SUPERHETERODYNE RECEIVERS

A typical scanning superheterodyne receiver[8,9] is shown in fig 2.2. The figures given in the diagram are intended purely as an example. This receiver covers an octave band in 5 MHz steps but could equally well be swept. The YIG preselector is used here to obtain a wide dynamic range and image rejection with one frequency conversion. The 5 MHz IF limits the minimum detectable pulse width to 200ns. Increasing the IF bandwidth reduces the signal acquisition time and the minimum detectable pulse width but also reduces the sensitivity[9].

The receiver's dynamic range is its main advantage, typically 50dB or greater. The accuracy of frequency information depends on oscillator stability and linearity, and the resolution of the IF bandwidth. A YIG oscillator typically gives 0.2 per cent

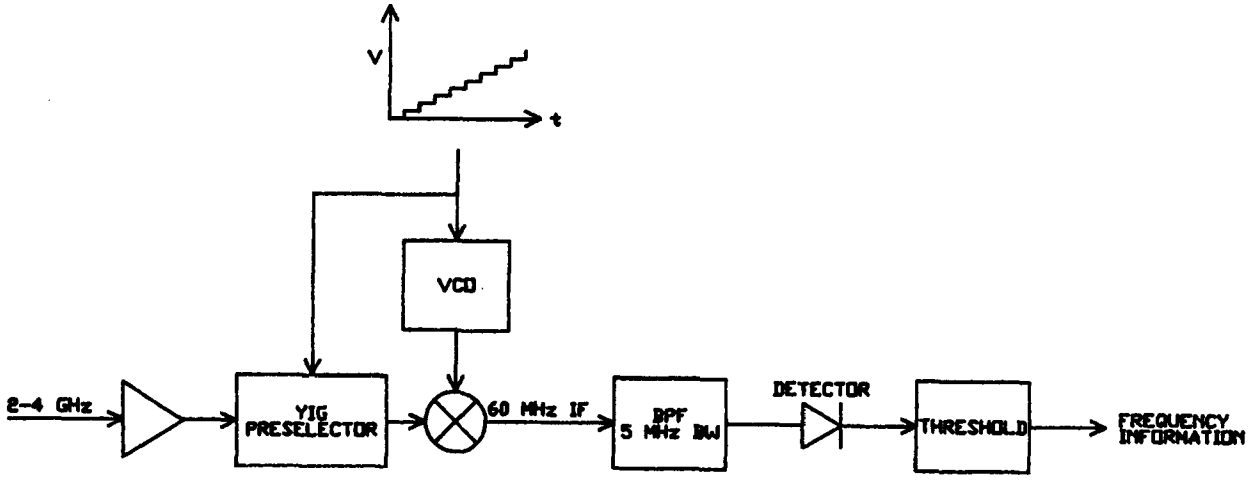

Fig 2.2 : **Typical superheterodyne implementation**
after Rappott and Stone

accuracy, or 5 to 8 MHz in the 2 to 4 GHz band[9].

The receiver exhibits excellent signal separation capability because of the frequency selectivity, and a low FAR. Its greatest disadvantage is its very low pulse POI. A given pulse will only be detected if the VCO frequency is within an IF bandwidth (5 MHz in this case) of the carrier frequency plus IF frequency while the pulse is present. If the VCO sweep period is much greater than the pulse length then the probability of intercepting a given pulse is approximately given by:

$$POI(\%) \simeq \frac{\text{IF bandwidth}}{\text{total swept bandwidth}} \times 100 \qquad \ldots\ldots (2.3.1)$$

In this example the IF bandwidth is 5 MHz and the total swept bandwidth is 2 GHz giving a 0.25 percent POI of a single pulse. The effect of this is to limit the bandwidth over which the receiver can effectively be used. However, they make excellent narrow band receivers and are widely used as such. They may also be steered by broader band receivers (often IFMR's) as in combination receivers.

2.4 COMPRESSIVE OR MICROSCAN RECEIVERS

The compressive receiver[1,7-9] is a logical step up from swept superheterodyne receivers. It attempts to improve the superhet's POI by using a very fast sweep time, ideally faster than the shortest pulse duration. An RF input pulse mixed with such an oscillator produces a 'chirped' or frequency modulated pulse. If this pulse is applied to a pulse compression filter with a slope opposite to that of the swept LO (ie. a matched filter), then the output is a compressed pulse whose position in time relative to the start of the LO sweep is a function of the frequency of the original input pulse.

The block diagram of a compressive receiver is shown in fig 2.3. The receiver provides a near unity POI while retaining the ability to separate simultaneous signals closely spaced in frequency. The IF output of the mixer scans in frequency at the same rate as the LO. The compressive filter delays the beginning of the IF pulse by the pulse width and the rest of the pulse proportionately less. In theory all the signal energy should exit the filter at the same instant but the band limiting nature of the filter gives the output a finite duration. In fact the shape of the output pulse is the Fourier transform of the IF bandpass characteristic, and its duration is approximately 1/IF bandwidth[1]. Increasing the IF bandwidth reduces the output pulse duration and increases the receiver's frequency resolution.

Image rejection in compressive receivers is good since the matched filter delay characteristics are in the same direction as the image pulse frequency modulation. As a result the image pulse will be spread to twice its initial duration and will be reduced in amplitude.

In theory there is no limit to the bandwidth of these receivers. Practical limitations on bandwidth are imposed by local oscillator scan speed and linearity, and compressive filter delay linearity. Wide bandwidth, fast tuning and very narrow output pulses mean

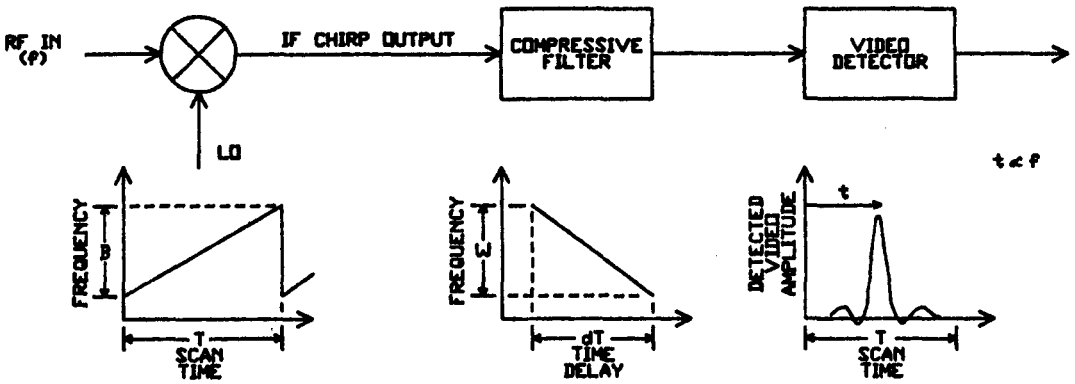

Fig 2.3 : **Block diagram of compressive receiver**
after Hofmann and Baron

that very high data rates have to be processed and that processor costs are high. Another limitation is that time-of-arrival measurements are quantised into intervals equal to the scan time.

2.5 IFM RECEIVERS

Fig 2.4 shows an analog instantaneous frequency measuring receiver (IFMR) in its simplest form. This section serves only as a very brief introduction to IFMR's to facilitate comparison with the other receivers described in this chapter. IFMR's will be covered in more detail in chapter 3.

The IFMR achieves a near unity pulse POI by having a 'wide-open' front-end requiring no tuning. Octave bandwidths are typical and recently a 2 to 18 GHz version was reported[10]. Sensitivity and dynamic range are good provided a limiting amplifier is used at the input to the frequency discriminator (FD) as shown in fig 2.4.

The FD block is the focus of this dissertation and will be discussed in depth in subsequent chapters. Its function is to accept an RF input and produce two video signals with amplitudes $\rho \sin \theta$ and $\rho \cos \theta$. ρ is a measure of the signal amplitude and θ is directly proportional to frequency. If these two signals are

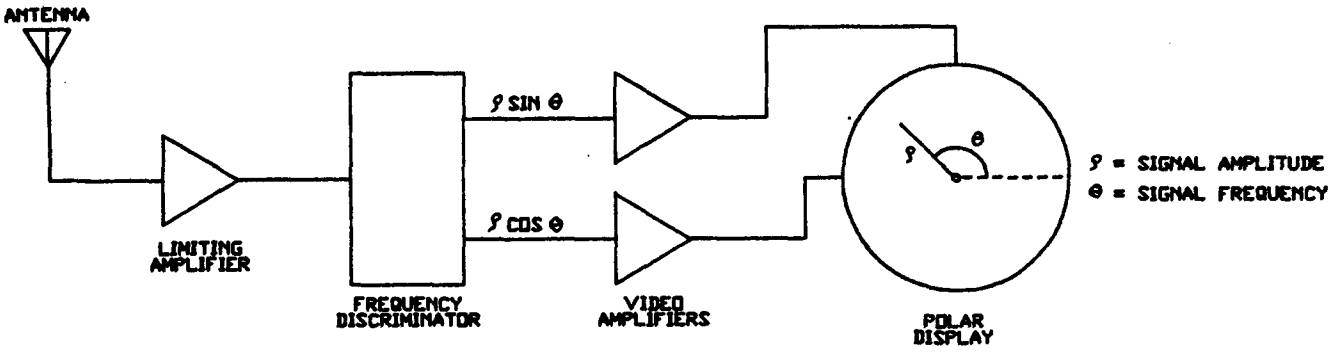

Fig 2.4 : **Simple analog IFM receiver**

applied to the vertical and horizontal plates of a polar display then ρ is the radial component and the angular component θ can be scaled to read frequency directly. The FD is often referred to as a polar frequency discriminator (PFD) because of the sine and cosine terms. Any amplitude or frequency modulation present will show up on the display as radial and angular fluctuations respectively.

Since IFMR's have no frequency dispersive components they cannot separate two or more simultaneous signals. If two signals are present the display will shown the vector sum of the two signals and thus will read neither signal correctly. The presence of multiple signals can be detected fairly easily[11] but IFMR techniques alone are not sufficient for the separate frequencies to be measured. A good solution is to use IFMR's to steer other narrow band receivers, such as the swept superheterodyne receiver, which can separate simultaneous signals.

2.6 CHANNELISED RECEIVERS

Channelised receivers consist of banks of contiguous filters covering the frequency band of interest[2,7,8,9,19]. Detectors following each filter show the presence of a signal within its associated filter. Fig 2.5 shows a very simple channelised receiver. It offers the high POI of CVRs and IFMRs and the signal

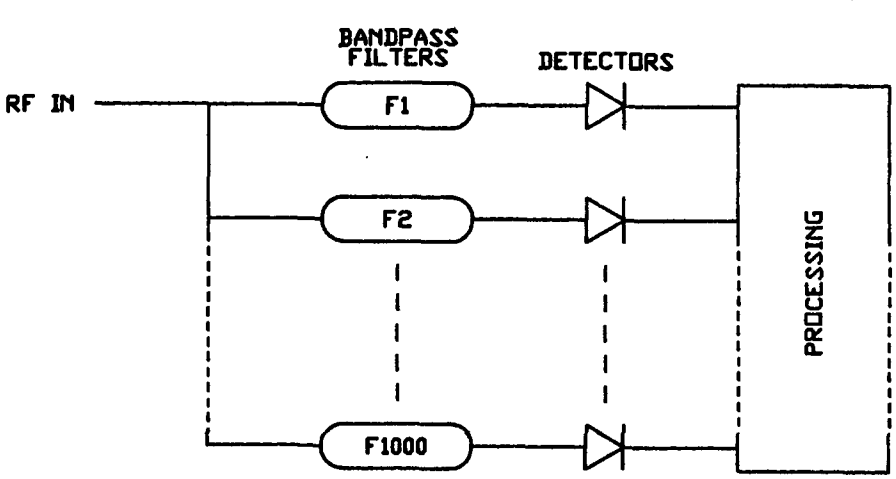

Fig 2.5 : **Simple channelised receiver**

separation ability of the superheterodyne receiver. Channelised receivers are often referred to as instantaneous Fourier transform receivers because of the way incoming signals are 'instantly' broken up into frequency cells with a resolution of half the filter bandwidths.

If a 10 GHz bandwidth is to be covered by a receiver of the type shown in fig 2.5 and each filter is 10 MHz wide (giving a resolution of ± 5 MHz) then one thousand filters are required. However if a 'folding' technique is used then the number of filters required can be greatly reduced. Fig 2.6 shows such a receiver. The frequency data given are meant purely as an example.

Every time folding takes place noise is summed into the IF channel greatly reducing the receiver sensitivity. The switches shown allow the receiver to be 'unfolded' and the sensitivity of the receiver in fig 2.5 to be regained. This also helps resolve certain ambiguities that can occur in the folded mode when multiple signals are present[7]. The price paid for folding and unfolding is an increase in signal acquisition time.

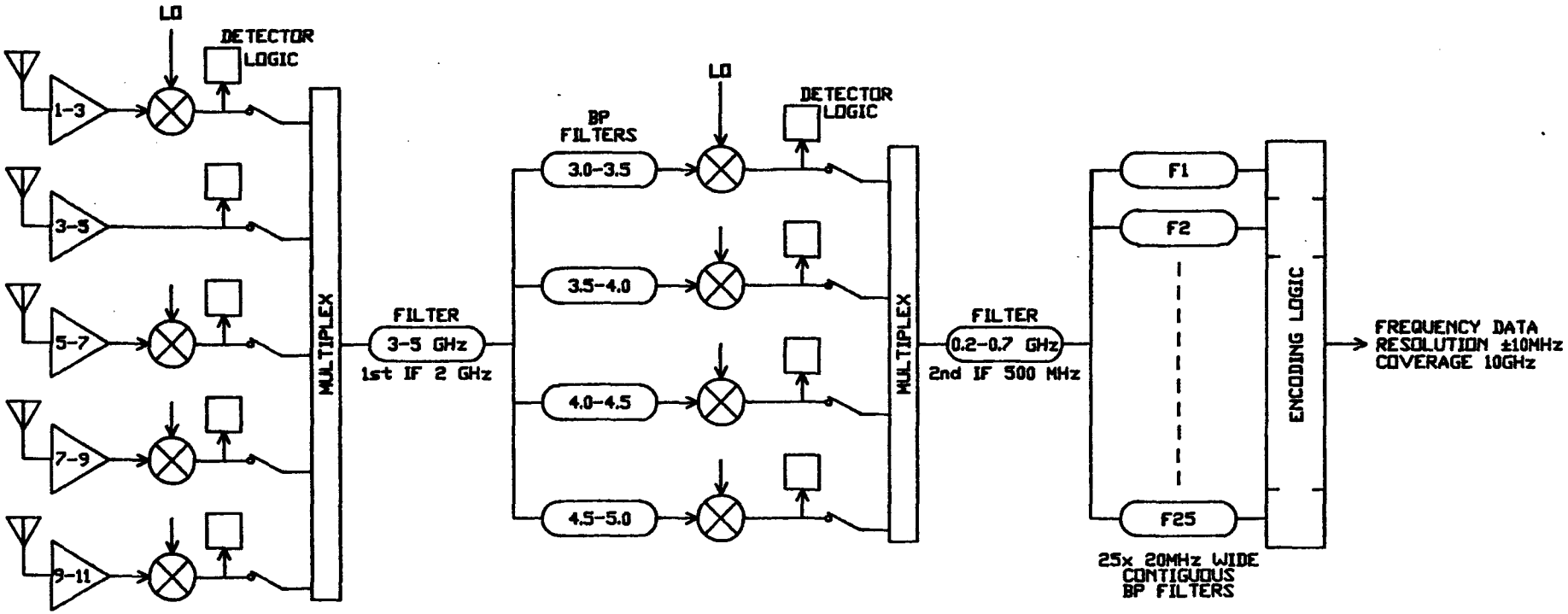

Fig 2.6 : Folded channelised receiver

Another difficulty with channelised receivers is that the frequency accuracy and resolution required is often at odds with the filter bandwidth necessary to allow measurements of the narrowest pulses expected. One solution is to carefully tailor the frequency response of the filter skirts[2]. The tendency of signals to 'overflow' from one cell to another can be used to determine the position of a signal within one cell if, for example, the signal amplitude in that cell is compared with those of adjacent cells. This can improve resolution but again increases throughput time.

The large amounts of hardware required by channelised receivers has limited their use in the past but interest in them has been revived with the introduction of surface acoustic wave (SAW) devices. Several contiguous SAW bandpass filters can now be integrated on a single piezo-electric crystal, reducing size and cost.

2.7 ACOUSTO-OPTIC RECEIVERS

An alternative form of 'instantaneous Fourier transform' or channelised receiver makes use of the interaction between monochromatic light and sound waves to synthesize the equivalent of a large bank of filters[1,7,8]. The acousto-optic interaction takes place in a Bragg cell shown conceptually in fig 2.7. The Bragg angle shown is the angle for which first order diffraction lines become intense and other orders significantly decreased.

A block diagram of an acousto-optic receiver (AOR) is shown in fig 2.8. The RF signal is fed to a transducer bonded to a crystal of piezo-electric material, causing a sound wave to be propagated along the crystal surface. A laser generates a monochromatic light beam which is spread by a lens to cover the crystal aperture. On passing through the crystal the light beam is deflected due to the variation in crystal refractive index caused by the sound wave. The angular deflection and intensity of the light beam is proportional to the frequency and power of the RF signal respectively. If more than one RF signal is present simultaneously

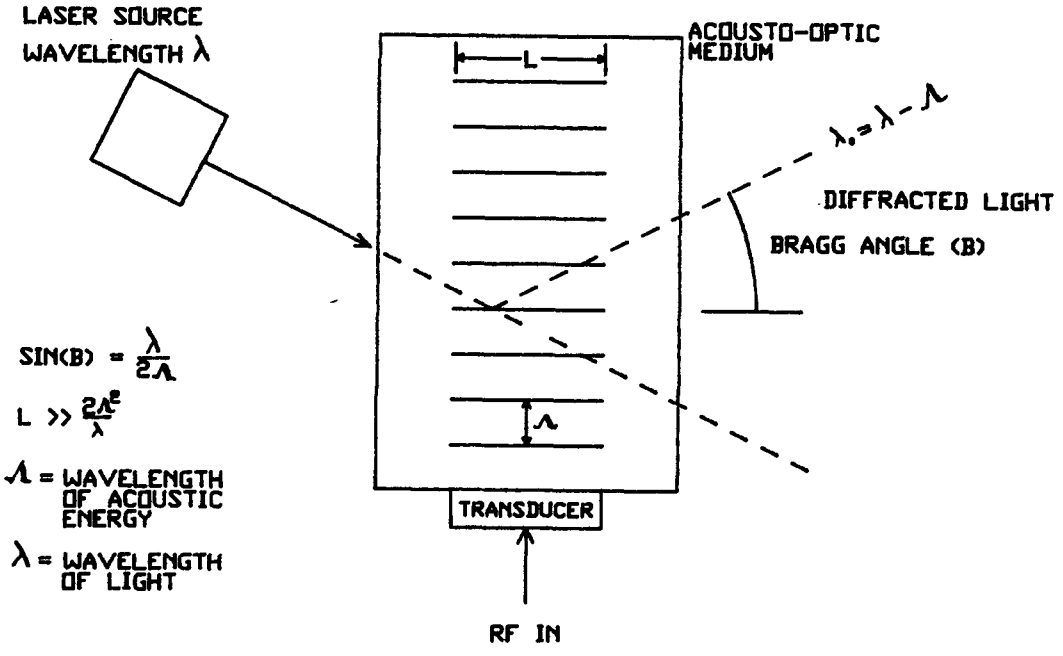

Fig 2.7 : **Bragg cell concept**
after Hofmann and Baron

the laser light will be deflected into separate beams, each representing one of the RF input frequencies. A second lens then focuses the diffracted beam onto a photosensor which may be an array of closely spaced PIN photodiodes, or a monolithic charge coupled device (CCD) array.

Although the technology is still fairly young, AORs promise the bandwidth and accuracy of IFMRs together with the ability to separate simultaneous signals. Its disadvantages include a relatively small dynamic range, complex processor interface hardware requirements for accurate pulse time-of-arrival measurements, and the bulky packaging required for the optical components. This last problem could be solved using hybrid and monolithic integrated optic techniques in which a solid state laser, Bragg cell, lenses and photosensor array are packaged on a single substrate.

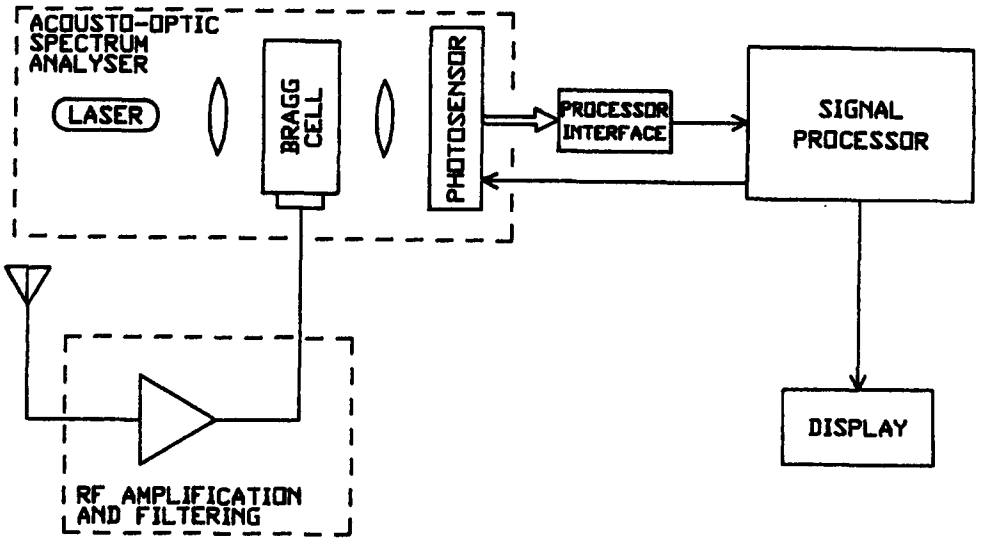

Fig 2.8 : **AOR block diagram**
after Hofmann and Brown

2.8 SUMMARY

Several different types of receiver have been discussed in this chapter. No single receiver completely outshines the rest for every situation. If, for example, size and weight are of utmost importance and frequency data is unimportant, then the CVR is best. Another set of requirements would indicate a different receiver. In fact the requirements may only be met by a combination of receivers. Commonly then, a broadband receiver is used for initial signal detection and the steering of a narrow band receiver to the correct frequency band for more complete signal analysis.

Table 2.1 summarises the advantages and disadvantages of the various receivers discussed. Margosian[3] attempts to rate each receiver qualitatively in table 2.2. The figures-of-merit he derives constitute only a very rough guide but they do indicate the prominence of IFM receivers. They also strengthen the argument for further research into these receivers and for their use as the broad-band steering component of combination receivers.

Table 2.1 : **Comparison of signal acquisition receivers**

	CVR	Superhet.	Microscan	IFM	Channelised	A/D
Sensitivity	Low	High	High	Med	High	High
Dynamic Range	Low	High	Med	High	Med	Low
Frequency Accuracy	Poor	Good	Good	Excellent	Good	Good
Simultaneous Signal Capability	Poor	Excellent	Good	Poor	Good	Excellent
TOA Availability	Excellent	Fair	Poor	Excellent	Ecellent	Poor
Bandwidth	Excellent	Good	Good	Excellent	Fair	Fair
Pulse POI	~100%	Low	~100%	~100%	~100%	~100%
Processing Complexity	Low	Med	High	Med	High	Med
Hardware Complexity	Low	Med	High	Med	High	Med
Cost	Low	Med	High	Med	High	Med
Stage of Development	Mature	Mature	Emerging	Mature	Emerging	Early

Table 2.2 : **Qualitative comparison of receivers**

after Margosian

Qualitative Key E = 1.00 G = 0.67 P = 0.33	Acousto-optical	IFM	Microscan	Channelised	Crystal-video	Superhet.
Figure of merit	0.89	0.89	0.73	0.61	0.78	0.61
Instantaneous Bandwidth	G	E	G	G	E	P
Frequency Resolution	E	E	G	G	P	E
Throughput Time	G	E	E	G	E	P
Simultaneous Signals	E	P	G	E	P	P
Size/Weight	E	E	G	P	E	E
Cost	E	E	G	P	E	G

CHAPTER THREE

DIFM AND COMBINATION RECEIVERS

Section 2.5 briefly introduced IFM receivers in their simplest form. Besides being of general interest, a closer look will illustrate how the rest of the receiver is built around the main RF component, namely the frequency discriminator. One's understanding of the fundamental characteristics of frequency discriminators can only be enhanced by such a 'black box' approach ahead of a detailed look at their internal workings.

Topics discussed in this chapter include techniques used in digital instantaneous frequency measuring (DIFM) receivers to resolve the resolution versus ambiguity problem, methods of extending the instantaneous bandwidth of IFMRs, simultaneous signal detection and the need for limiting amplifiers.

Several more complex receivers which utilise more than one of the general techniques discussed in chapter 2 have been reported in the literature. Most of them include IFM techniques and some of the more interesting versions are included at the end of this chapter to lend weight to the argument for studying further IFMRs and, in particular, frequency discriminators.

3.1 THE DELAY LINE DISCRIMINATOR

The frequency discriminator block shown in fig 2.4 can be broken up into a power splitter, delay line and phase discriminator as shown in fig 3.1. In this form it is often called a delay line discriminator (DLD)[1,3]. It makes use of the well established principle of measuring frequency in terms of phase delay when a signal is propagated down a transmission line of known length. Almost all IFM receivers reported in the literature make use of DLDs and they were pioneered at the Mullard Research Laboratories in England thirty years ago[13].

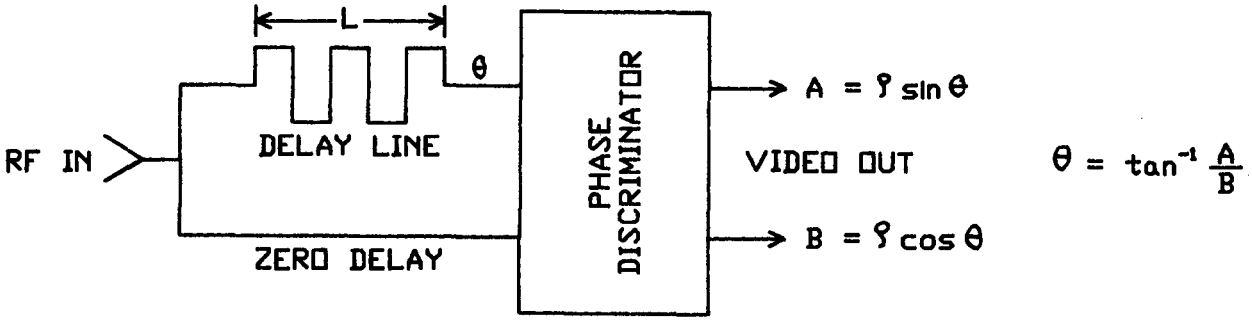

Fig 3.1 : Delay line discriminator

If a delay line of length L and phase constant β is used then the phase delay θ is given by

$$\theta = \beta L \qquad \ldots\ldots (3.1.1)$$

If the signal wavelength is λ then

$$\beta = \frac{2\pi}{\lambda} \qquad \ldots\ldots (3.1.2)$$

If v is the velocity of propagation and f is the signal frequency then

$$\lambda = v/f \qquad \ldots\ldots (3.1.3)$$

substituting in (3.1.2)

$$\beta = \frac{2\pi}{v} .f \qquad \ldots\ldots (3.1.4)$$

Substituting this in turn into (3.1.1) we get

$$\theta = \frac{2\pi}{v} .f. L \qquad \ldots\ldots (3.1.5)$$

Alternatively

$$\theta = kf \qquad \ldots\ldots (3.1.6)$$

where k is a constant and

$$k = \frac{2\pi}{v} . L \qquad \ldots\ldots (3.1.7)$$

Hence phase delay is directly proportional to signal frequency and can be used as a direct measure of frequency.

If f_1 and f_2 are the edge frequencies of the DLD's passband, and $f_2 > f_1$ then from (3.1.6)

$$\theta_1 = kf_1$$
$$\theta_2 = kf_2$$

so that

$$\theta_2 - \theta_1 = k(f_2 - f_1) \qquad \text{..... (3.1.8)}$$

The requirement for no ambiguity in the reading is

$$\theta_2 - \theta_1 < 2\pi$$

If f_{BW} is the bandwidth of the DLD, ie. $f_{BW} = f_2 - f_1$, then from (3.1.8)

$$f_{BW} = \frac{\theta_2 - \theta_1}{k} \qquad \text{..... (3.1.9)}$$

The maximum unambiguous bandwidth is

$$f_{BW_{max}} = \frac{2\pi}{k} \qquad \text{..... (3.1.10)}$$

Substituting for k from (3.1.7) we get

$$f_{BW_{max}} = \frac{v}{L} \qquad \text{..... (3.1.11)}$$

Equation (3.1.11) shows that the shorter the delay line length the larger the unambiguous bandwidth. The frequency accuracy of the DLD then depends on the accuracy of the phase discriminator. If phase inaccuracies could be reduced without limit there would be no conflict between frequency accuracy and unambiguous bandwidth. In practise, however, an accuracy of even two degrees would be very difficult and expensive to realise[1].

From (3.1.5), an indication of the frequency accuracy is given by

$$\frac{d\theta}{df} = \frac{2\pi . L}{v} \qquad \ldots\ldots (3.1.12)$$

Equation (3.1.12) shows that the longer the delay line the more accurate the frequency measurement. This is in direct conflict with unambiguous bandwidth requirements and for a receiver of the type described in section 2.5 a trade-off would have to be chosen.

For a given phase accuracy $d\alpha$ and bandwidth f_{BW} the frequency accuracy df is given by

$$df = \frac{f_{BW} . d\alpha}{2\pi} \qquad \ldots\ldots (3.1.13)$$

If, for example, a 4 GHz bandwidth is to be covered unambiguously and phase can be measured to ± 2° then frequency can at best be measured to ± 22 MHz with a single DLD.

3.2 AMBIGUITY RESOLUTION

Phase measurements made at the output of a delay line will be repeated every cycle of 2π radians, giving an unambiguous range of only 2π radians. However, as demonstrated in appendix A, if two delay lines L_n and L_p are used such that their lengths are in the ratio n:p, n>p and n and p are integers with no common factors, then the unambiguous range is extended to $2\pi n$ radians for line L_n, and $2\pi p$ radians for line L_p, and these correspond to the same frequency range.

It is simpler to consider the case n>1 and p=1, and in practise ratios are usually chosen to be of this type. For two lines with lengths in the ratio n:1, 2π radians of the shorter line defines the unambiguous bandwidth f_{BW}. Phase discriminator accuracy $d\alpha$ and the length of the long line now define the frequency accuracy

df as

$$df = \frac{f_{BW}\, d\alpha}{2\pi n} \qquad \ldots\ldots (3.2.1)$$

At first sight it would seem that after the shortest line length has been chosen to suit the desired bandwidth, the long line can be increased in length without bound for any given frequency accuracy. However for very short pulses the length of time taken to traverse the delay line becomes a significant problem. East[4] gives the minimum acceptable pulse width as

$$t_{min} = \tau + \frac{1}{2.5B_v} \qquad \ldots\ldots (3.2.2)$$

Where τ is the time delay of the delay line, and B_v the bandwidth of the video processing circuitry which follows the phase discriminator. Hence τ (or length $L = v\tau$) must be kept short for interception of short pulses.

These rules define the longest and shortest delay line lengths and two lines would appear to be sufficient for any given band coverage. This would be true if it were not, once again, for the limited phase discriminator accuracy. Consider phase errors $d\theta_p$ and $d\theta_n$ for the discriminators attached to lines L_p and L_n respectively. If large enough, these errors may cause a breakdown in ambiguity resolution leading to large frequency errors corresponding to 2π radians of the longest line L_n. This is in addition to the error caused by $d\theta_n$.

The condition for there to be no ambiguity breakdown is derived in appendix A as

$$|nd\theta_p + pd\theta_n| < \pi \qquad \ldots\ldots (3.2.3)$$

Typically the discriminator phase errors will be of the same order, ie. $d\theta_p \simeq d\theta_n$. Phase tolerances calculated from (3.2.3) for commonly used delay line ratios are given in table 3.1. The delay line ratio is hence also limited by phase measurement errors.

Table 3.1 : **Phase tolerance for typical delay-line ratios after East**

Delay line ratio n:p	2:1	3:1	4:1	5:1	8:1	10:1
Tolerance (degrees)	60	45	36	30	20	16.4

The solution to this problem is to use more than two delay lines at the cost of increased hardware requirements. Efficient processing then requires digital techniques. Good choice of delay line lengths, ratios and number of bits of quantisation simplifies the combination into a single frequency code. One such choice is given as an example in fig 3.2. Frequency accuracy is now also limited by quantisation error given by:

$$df_q = \frac{1}{\tau 2^{m+1}} \qquad \ldots\ldots (3.2.4)$$

where τ is the time delay of the longest line and m is the number of bits of quantisation associated with the discriminator attached to that line. Expression (3.2.4) leads to the description of a delay line by its characteristic frequency f_{DL} such that

$$f_{DL} = \frac{1}{\tau} \qquad \ldots\ldots (3.2.5)$$

or

$$f_{DL} = \frac{v}{L} \qquad \ldots\ldots (3.2.6)$$

where L is the length of the line. Furthermore, the characteristic wavelength λ_{DL} of a delay line is such that $\lambda_{DL} = L$. This can be seen from expression (3.2.6). Equations (3.2.1) and (3.2.4) can be re-written as

$$df = \frac{f_{DLL}}{2\pi} d\alpha \qquad \ldots\ldots (3.2.7)$$

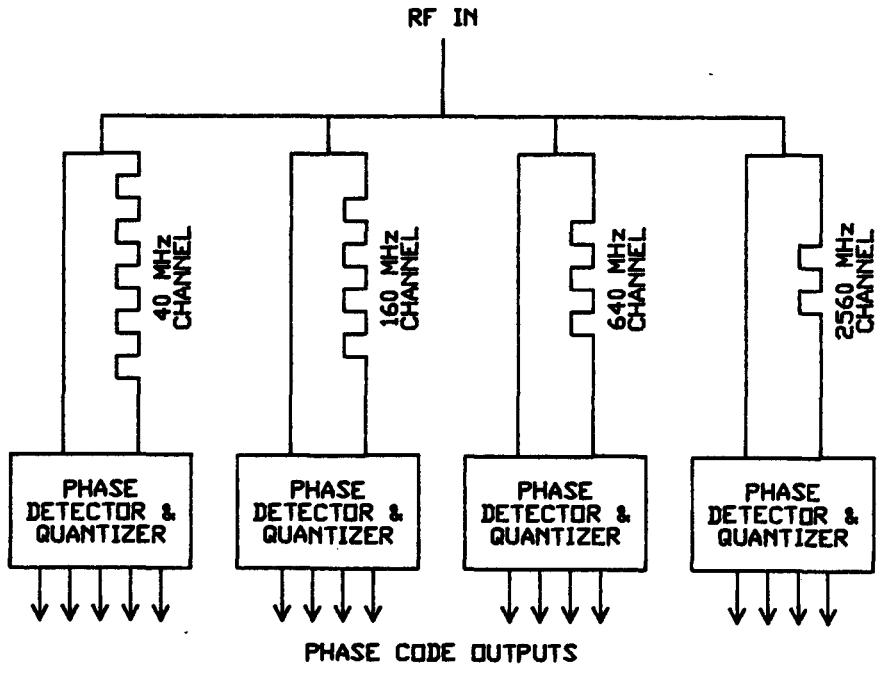

Fig 3.2 : 2-4 GHz four delay line arrangement using a 4:1 ratio after Hofmann and Baron

and

$$df_q = \frac{f_{DLL}}{2^{m+1}} \qquad \ldots\ldots (3.2.8)$$

where f_{DLL} is the characteristic frequency of the longest line.

3.3 DIGITAL IFM RECEIVERS

Fig 3.3 is a block diagram of a typical digital IFM (DIFM) receiver showing the main functional elements. IFM modules subsequently referred to in this chapter will be of this form.

The filter coarsely defines the operating band at the RF input. The RF amplifier generally has relatively poor gain roll-off characteristics and the main function of the filter is to prevent the generation of spurious signals within the RF amplifier by high-power signals outside the operating band.

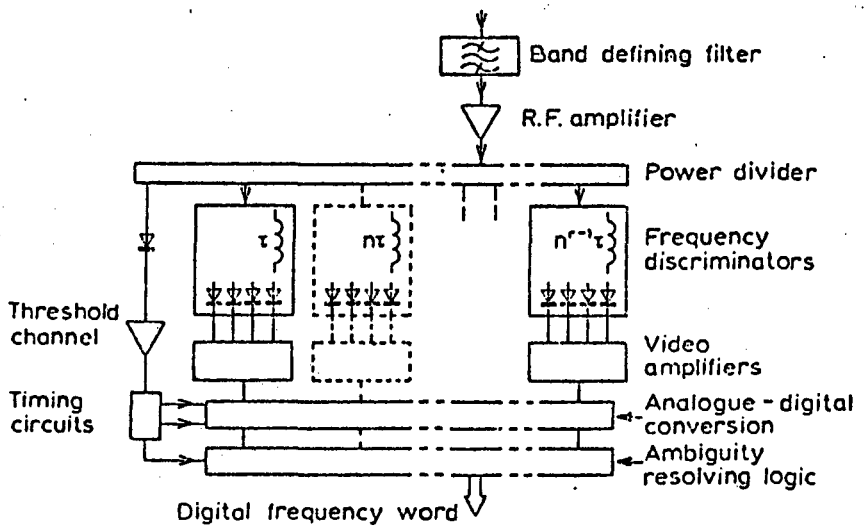

Fig 3.3 : Digital IFM receiver block diagram after East

Typically 60dB of RF gain may be required for maximum sensitivity. The amplifier should exhibit good pulse fidelity, low harmonic levels and good limiting at high signal levels. The need for limiting will be discussed in a subsequent section.

The broad-band power divider ensures that the signal is evenly split to the discriminators and the threshold channel. The video amplifiers may be AC-coupled, DC-restored or DC amplifier types. AC-coupled amplifiers are the simplest but are insensitive to CW and high duty-cycle signals. DC types respond to CW but are affected by RF amplifier noise levels and may be blocked when CW signals are present.

The threshold channel detects the presence or arrival of signals and co-ordinates the analog-to-digital conversion and logic circuitry sampling. The logic network combines the digital codes from the discriminator quantizers to provide an accurate unambiguous code representing signal frequency. Some form of error correction or temperature compensation may be included here but processing must be fast to allow a high pulse handling rate. Typical processing time for 10 to 12 bit frequency data is 150ns[4].

3.4 EXTENDED BAND COVERAGE TECHNIQUES

Most frequency discriminators reported in the literature cover bandwidths of one or two octaves but full coverage of the 2 to 18 GHz band is a common IFM requirement. Several techniques can be used to extend coverage to the full band and those most frequently used are included here.

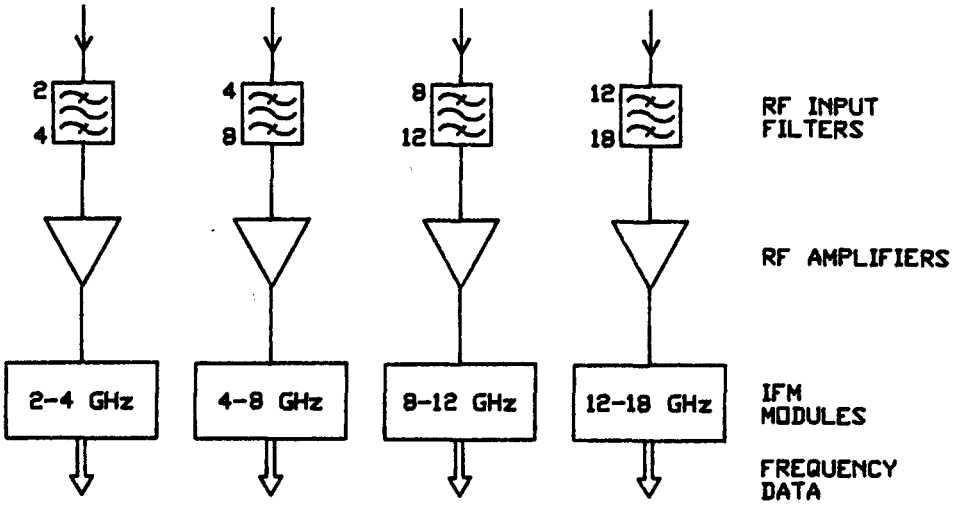

Fig 3.4 : Contiguous baseband cover after East

Fig 3.4 shows a system which gives contiguous baseband coverage. The band break-up shown is given as an example and is commonly used. Another choice becoming popular is 2-6 GHz and 6-18 GHz. The system still has a 100 per cent pulse POI but requires two or more RF receiver designs.

Fig 3.5 uses a superheterodyne mixing approach to translate the sub-bands to a common baseband, here 2-6 GHz. The IFM modules are identical and 100 per cent pulse POI is still a feature. Mixer conversion loss reduces sensitivity unless additional gain is used before mixing takes place.

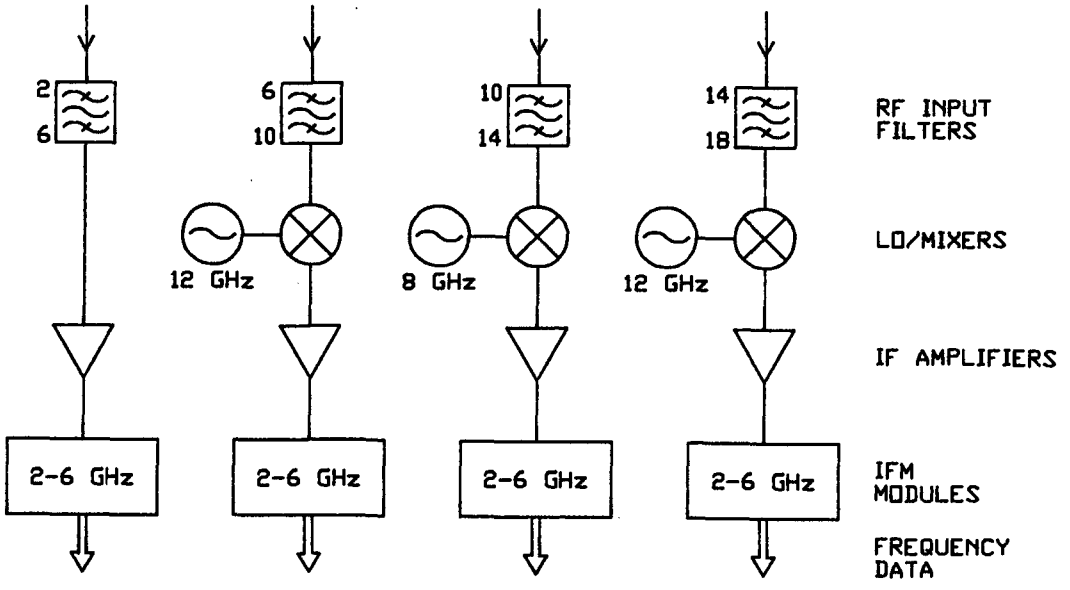

Fig 3.5 : Contiguous superheterodyne cover after East

Fig 3.6 shows a technique in which the sub-bands are 'folded' into a common IFM receiver. The IFM fine frequency output is then combined with coarse frequency information from the directional couplers to give unambiguous coverage. 100 per cent pulse POI is retained at the expense of about 6dB poorer sensitivity and increased receiver operating data rate[4].

Recently a single frequency discriminator covering the full 2-18 GHz band was reported[10]. This would appear to be the ideal solution but the development of amplifiers with the same bandwidth is still in its early stages. Secondly, the larger the instantaneous bandwidth the higher the signal density is likely to be and processing at the required rates becomes very expensive. The 2-18 GHz discriminator design does, however, form a module with the flexibility for use in almost any new IFM design, saving time and development costs.

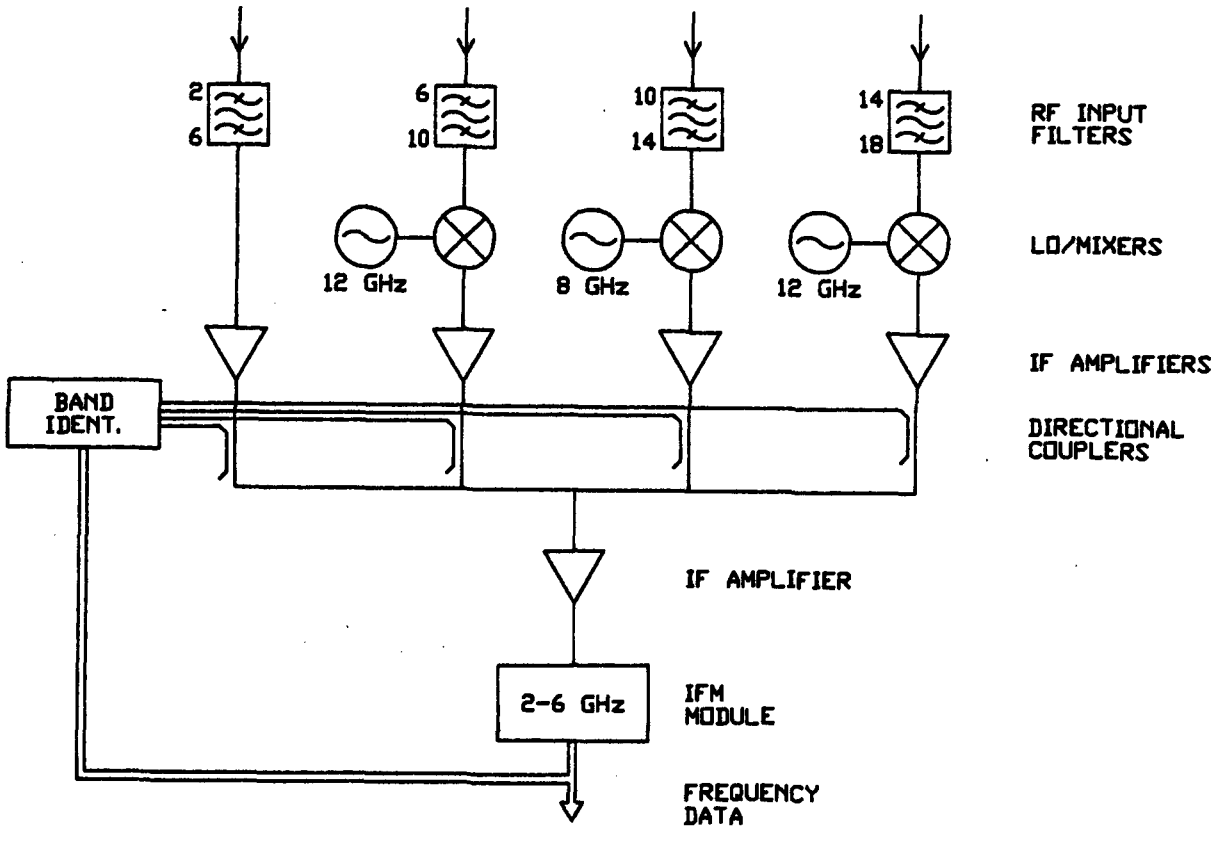

Fig 3.6 : **Band folding**
after East

3.5 SIMULTANEOUS SIGNAL DETECTION

IFM receivers offer no way of separating signals of different frequency present in the frequency discriminators at the same time. The discussion of simultaneous signals is simplified by considering the case of just two signals present. Consider a receiver of the type described in section 2.5. A single signal produces sine and cosine terms at the inputs of the polar display. A second signal produces its own sine and cosine terms so that the display plots the sum of the two sine terms against the sum of the two cosine terms giving, in general, a result reflective of neither input. In fact the result will be weighted towards the larger of the two signals and it is this signal which is usually of most interest.

The consensus of opinion expressed in the literature[1-4,11,14] is that if two simultaneous signals differ in power level by more than 6db then the error in the measurement of the largest signal is negligible (and even the figure 3dB is often mentioned). Thus to cause a significant error signals have not only to be present simultaneously but their relative power levels have to fall within a fairly narrow window.

The probability of this occurring when a CW signal is present may be quite high. However the CW signal can easily be measured when it is alone, and a tunable notch filter directed to exclude it from later measurements on incoming pulses. If both signals are pulsed then the probability of them being sufficiently close in amplitude and simultaneous is small. Nevertheless it may be important to know the integrity of every measurement as it is made so that doubtful results will be discarded and not acted upon. Many IFMR manufacturers include simultaneous signal detection (SSD) circuitry which sets a flag whenever readings are determined to be in doubt.

Before considering some of the SSD methods employed it is useful to look more closely at the case of two signals present at one time. The first situation involves two signals which have exactly coincident leading edges (or in practise within 10ns of each other). The second is that in which pulses overlap each other for a portion of their duration. This in turn may be broken up into two sub-cases. If the leading pulse is the stronger of the two then errors are infrequent[11]. If a stronger pulse follows a weaker pulse then errors are significantly more frequent. The reason for this is that the first pulse triggers a measurement which then takes place during a transition period as the stronger pulse makes its presence felt. Fig 3.7 shows this transition period with its characteristic dip.

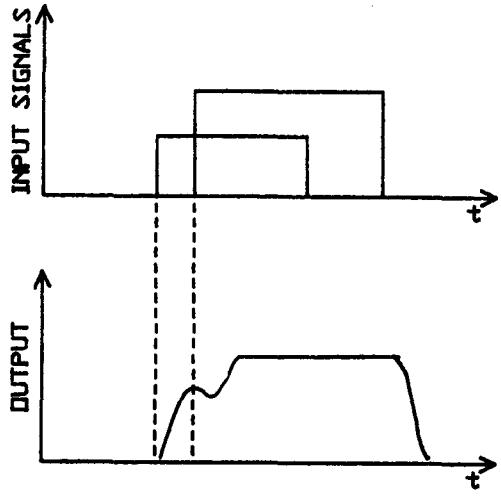

Fig 3.7 : Characteristic output dip of a strong signal following a weak signal
after Tsui, Shaw, Cisar and Ratliff

The cause of this dip can be ascribed to the mixing effect of the limiting amplifier which normally precedes the video detectors. The non-linear characteristic of the limiting amplifier generates harmonics which reduce the power level in the original frequencies. Most harmonics are generated when the signals are roughly equal in power, ie. at some time during the rising edge of the stronger pulse. The correct frequencies are then at their weakest giving the dip in detector output.

3.5.1 ANALOG SSD TECHNIQUES

The most commonly proposed SSD involves using a mixer, bandpass filter, detector and comparator as shown in fig 3.8. For a single signal entering the mixer all harmonics are generated and these are excluded by the bandpass filter. Hence in this form it is suitable only for octave bandwidths. When two or more signals arrive at the mixer, harmonics of the difference frequency will be generated and passed by the filter to the detector. If the original signals are close in amplitude so that the detected difference frequency amplitude exceeds the threshold set by the

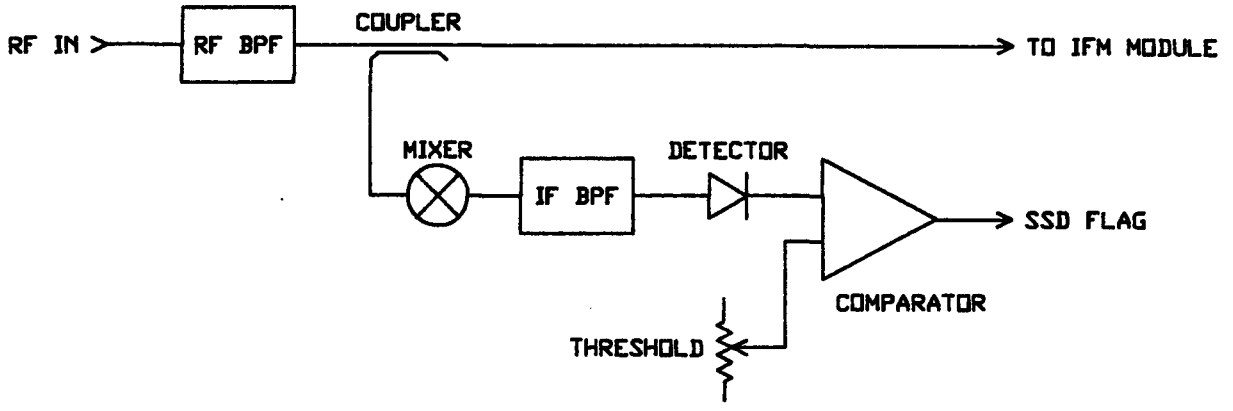

Fig 3.8 : **Mixer based SSD circuit**
after Margosian

comparator, then the SSD flag is set and the IFM reading disregarded. This circuit is useful in the first type of signal described but not so effective against overlapping pulses.

For overlapping pulses the following methods have been tried. Edge detection in the threshold channel of the IFM module (fig 3.3) allows the arrival of overlapping pulses to be sensed. The dip shown in fig 3.7 can be utilised if the IFM detector outputs are sampled and held for comparison with a later sampling. If the samples are not the same then the SSD flag is set. Alternatively the detector output can be split into two paths, one delayed on the other. The dip in output should then cause the delayed output to exceed the undelayed output momentarily, and if this happens the SSD flag is set.

The problem with these pulse overlap detection methods is that if the circuits are adjusted for good sensitivity then the false alarm rate is high, false alarm here being an indication of simultaneous signals when only a single signal is present.

3.5.2 DIGITAL SSD TECHNIQUES

A novel technique has been proposed[11] which makes use of the identity $\sin^2\theta + \cos^2\theta = 1$. If the sine and cosine outputs of a frequency discriminator are operated on in this way and the result is not unity, then two or more signals must be present. This should work for both truly simultaneous and overlapping signals.

In practise the discriminator outputs include an amplitude term which is dependent both on the original signal amplitude and its frequency, since discriminator losses vary with frequency. The actual identity used is $(A^2(f,s)\sin^2\theta+A^2(f,s)\cos^2\theta)^{\frac{1}{2}} > A_{th}(f,s)$ where f is the signal frequency and s its power level. Threshold values $A_{th}(f,s)$ are evaluated ahead of time and stored in a ROM. The ROM is accessed via the frequency data output of the IFM module. Its value varies relatively slowly with frequency so that not all the IFM data bits need be used. A ROM is also used to evaluate the function $(a^2 + b^2)^{\frac{1}{2}}$ where a and b are the sine and cosine outputs respectively.

Fig 3.9 shows a block diagram of this scheme. Provided the measured value A(f,s) exceeds the threshold value, the IFM reading is assumed to be correct. A value of A(f,s) below threshold sets the SSD flag. The system is not foolproof but dramatically reduces the undetected error rate.

A different system involves continued resampling of the discriminator outputs down the length of the pulse. Overlapping pulses will then be measured before, during and after overlap so that often the individual pulse frequencies will be correctly determined. In the case of simultaneous leading pulse edges, the trailing edges are unlikely to be simultaneous so that the frequency of the longer pulse will be measured after the end of the

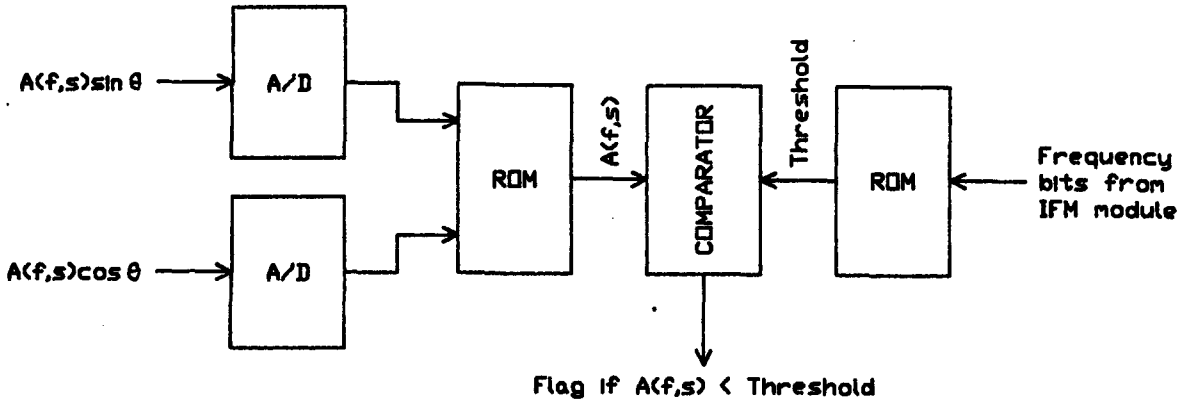

Fig 3.9 : **Digital SSD scheme**
after Tsui et al

short pulse. Measurements made during overlap may be discarded, or possibly back calculation can be used to determine the frequency of the shorter pulse.

Another advantage of this system is that modulation present within a pulse can be analysed. However this method requires fast, expensive processing if the system is still to be sensitive to pulses of say 100ns.

3.6 DYNAMIC RANGE EXTENSION

Standard frequency discriminators (FDs) employ banks of detector diodes to provide the sine and cosine outputs, usually four detectors to each FD. The detectors and their properties will be discussed in detail in subsequent chapters, but brief mention of some of their limitations is required here.

FD sensitivity is limited by the tangential sensitivity of the detector diodes and by FD losses. A very good commercial FD may have a tangential sensitivity of -40 dBm to -50 dBm[14] but when a bank of FDs is used sensitivity of the IFM module is significantly lower. Furthermore line losses contribute to overall noise figure. IFM receivers therefore require pre-amplifiers to improve sensitivity and noise figure. Typical sensitivity requirements are -60 dBm or better.

The mode of operation of the FDs requires that the detectors be well matched to each other and that their output voltage to input RF power relationship be linear. The detectors must therefore operate in their unsaturated square-law region. Input signals of high enough power to drive the detectors beyond their square-law region will suffer additional phase (and hence frequency) measurement errors. Furthermore, should the diodes be driven into saturation their recovery time will restrict the minimum pulse width that can be processed. These factors limit IFM dynamic ranges to 20 dB or 30 dB[4], whereas dynamic ranges of 60 dB or greater are generally required.

The answer to both dynamic range and sensitivity problems is the use of limiting pre-amplifiers[4,12,14]. Low power input signals can then be considerably amplified whereas high power signals drive the pre-amplifier to limiting so that the FDs are not overdriven. The requirements placed on these limiting amplifiers (LAs) are harsh, making them the single most expensive module in an IFM receiver.

The LA must have an instantaneous bandwidth that matches that of the FDs. In fact it is frequently the attainable LA bandwidth that currently limits overall IFMR bandwidth. The exception is the case in which high gain antennas of narrow bandwidth are used. Overall system dynamic range, gain and noise figure are also controlled by the LA.

Should the LA overshoot its limiting level on the leading edge of a pulse, the detectors may be driven into saturation. Accurate measurements cannot then be made before detector linearity is recovered. This limits minimum acceptable pulse width as mentioned before. Pulse envelope distortion caused by amplitude variation, phase delay, AM to PM conversion or excessive VSWR reflections may delay frequency measurements or degrade their accuracy.

The non-linear limiting characteristic causes harmonics to be generated. Usually no more than the second harmonic falls within

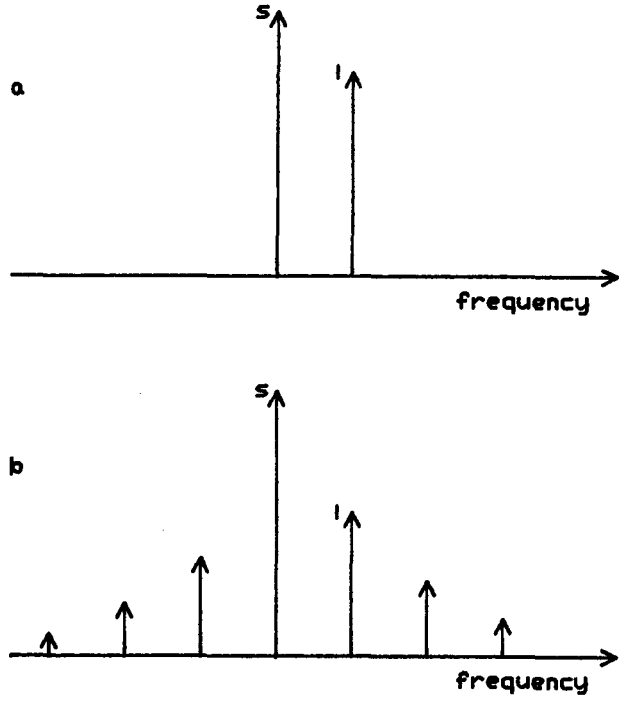

Fig 3.10 : **Limiting amplifier interfering signal suppression**
after East
a) Input spectrum
b) Output spectrum

the IFM passband so that the second harmonic level must be sufficiently low not to introduce significant phase errors or cause the SSD flag to be set.

One consequence of using limiting amplifiers is that IFM amplitude measurements may not be very meaningful. Usually a broadband detector is used on a portion of the unlimited signal to provide amplitude information.

An added bonus of using LAs is their inherent ability to suppress interfering signals by up to 6 dB or more[4], so increasing receiver interference tolerance levels. This refers to the case of simultaneous signals in which the larger signal is sufficient to cause limiting and is the wanted signal. The smaller signal is then an interfering signal. The suppression is due to the spreading of power into LA generated intermodulation components

spaced at the difference frequency as shown in fig 3.10. The symmetric spacing of these components either side of the main signal helps to reduce further the resulting phase error by counter-acting one another. This interference suppression does not, however, apply when the signals are low enough to fall in the LA's linear gain region.

3.7 COMBINATION RECEIVERS

Several different receiver types were discussed in chapter two. Each had its own particular characteristics and none were suitable for every application. Improved coverage can be obtained by combining complimentary receiver types into a single system. Cost, size and weight are major inhibiting factors but combination receivers are worthy of consideration.

Although not usually considered as such, an element of receiver mixing crept into the discussion in section 3.6. The use of limiting amplifiers reduced the usefulness of amplitude information provided by IFM modules and, to restore this capability, a broadband video detector channel was added. In reality this added channel is a crystal video receiver (CVR), and the overall receiver a combination IFM and CVR.

Commonly combined characteristics are the excellent intercept and instantaneous bandwidth properties of broadband systems, and the signal analysis and separation capabilities of narrowband systems. The task of the broadband section is then to detect signal activity, make initial measurements and steer the narrowband section to the correct frequency band for more detailed analysis. Very frequently a DIFM is chosen as the broadband component.

Fig 3.11 shows a combination IFM and scanning superheterodyne receiver[8]. Received signals are fed simultaneously to an IFM module and a bank of scanning superheterodyne receivers. The IFM output controls the IF switch and VCO for detailed signal analysis. The tunable notch filter shown is used to remove interfering CW signals automatically.

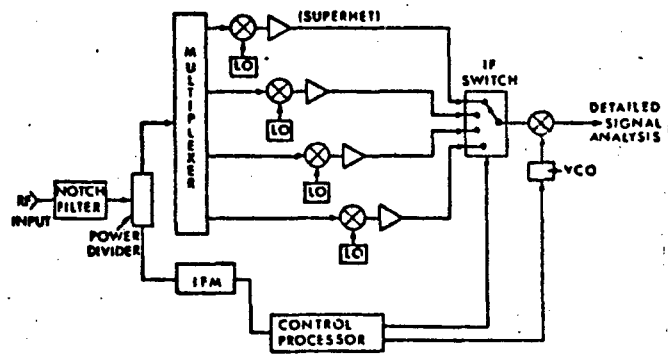

Fig 3.11 : **Combination IFM and superheterodyne receiver**
after Collins and Grant

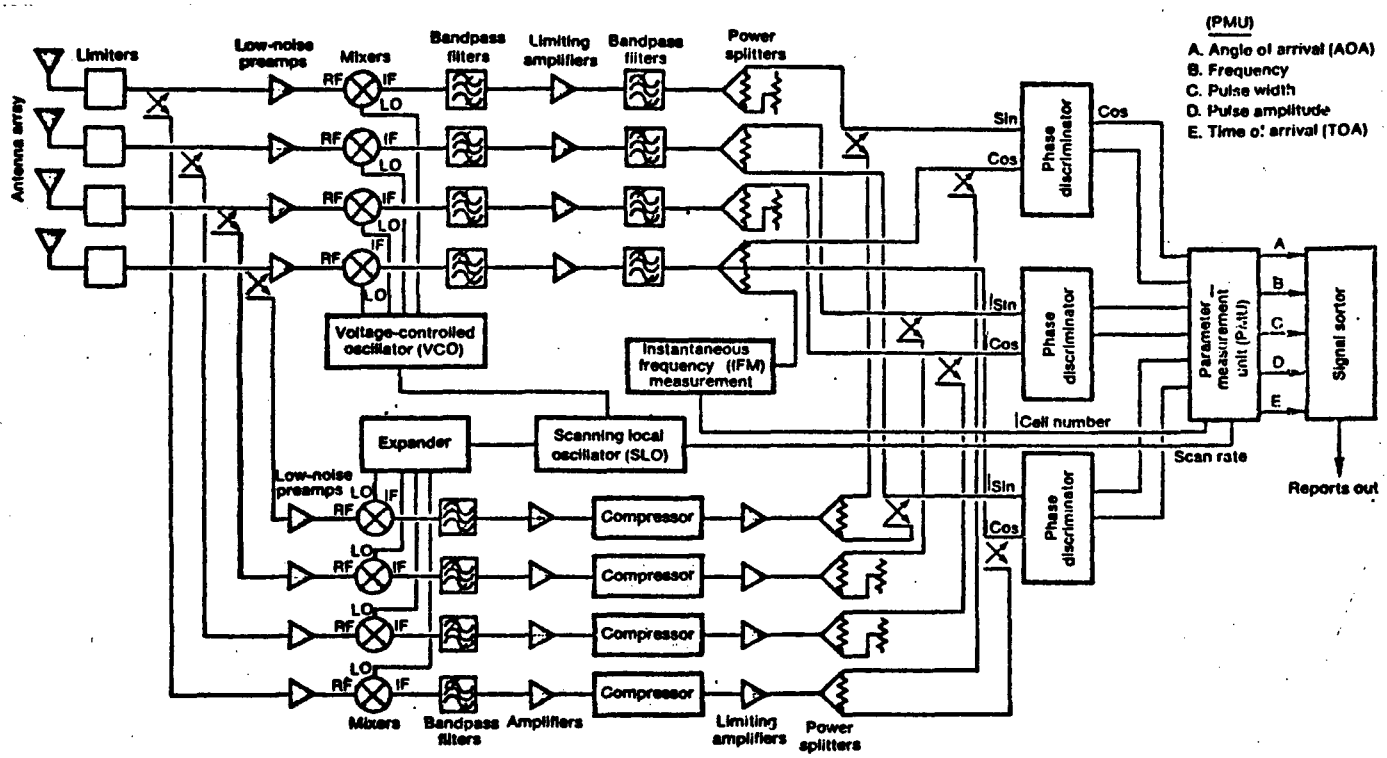

Fig 3.12 : **Combination IFM and compressive receiver**
after Konig

Fig 3.12 shows a more complex system that has been suggested[15]. This receiver combines IFM techniques with those of compressive receivers. In this case the IFM section processes relatively strong signals with large dynamic ranges, while the compressive section handles weaker signals with limited dynamic ranges. The receiver shown in fig 3.12 is particularly of interest here since it includes some detail of other measurements such as angle and time of arrival.

3.8 THREE PHASE IFM

The IFM receivers discussed in the foregoing sections of this chapter utilised delay line frequency discriminators as described in section 3.1. An alternative frequency discriminator known as a three phase discriminator has recently been described by Rhodes[5]. It consists of three phase-compensated all-pass networks which maintain a fixed phase difference between the three channels over the band. The amplitude characteristics shown in fig 3.13 can then be generated.

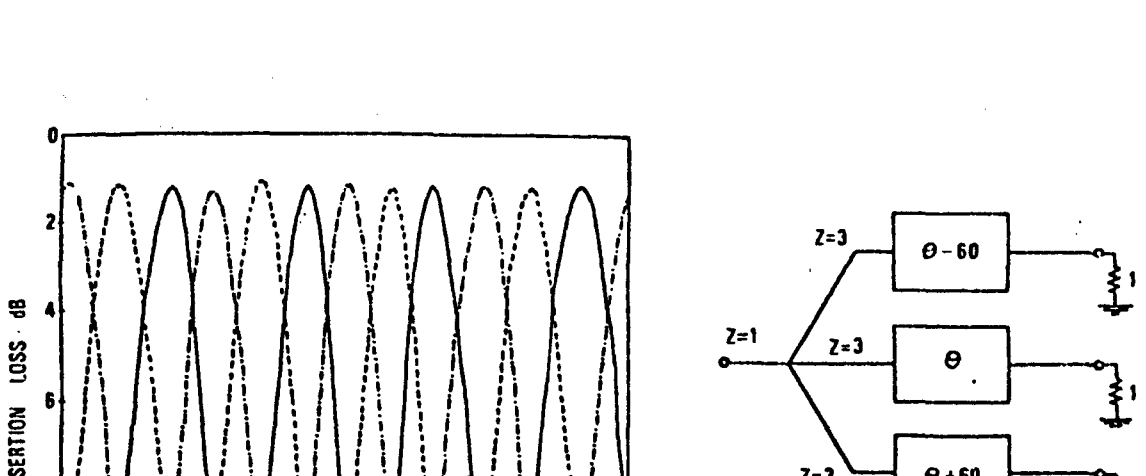

Fig 3.13 : **Three phase discriminator amplitude characteristics** after Rhodes

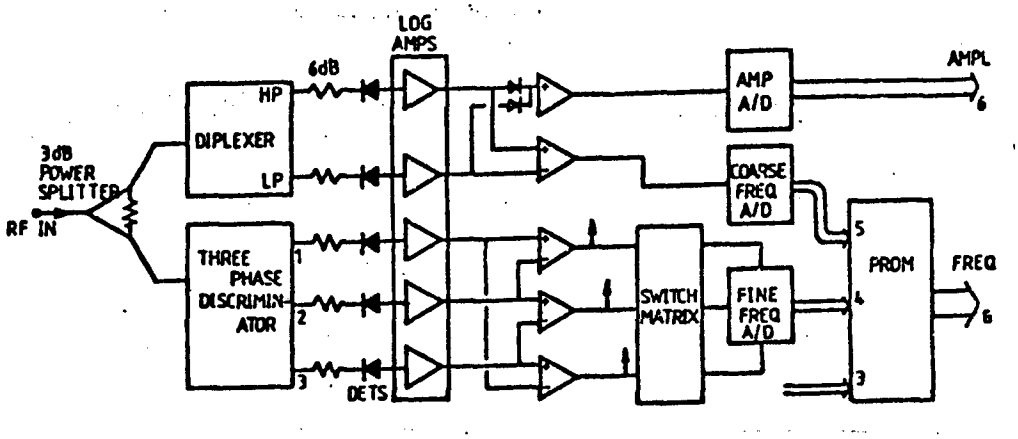

Fig 3.14 : **Three phase IFM receiver**
after Rhodes

Fig 3.14 shows a block diagram of an IFM receiver employing a three phase discriminator. Amplitude data and coarse frequency information are formed from the amplitude characteristics of a contiguous diplexer with low selectivity. The three phase discriminator and associated switch matrix provide fine frequency data. The coarse and fine frequency data are used to access a PROM which supplies the final frequency word. Rhodes also suggests using a bank of these discriminators when high integrity is required.

Like the delay line IFM three phase IFM cannot separate simultaneous signals. A higher sensitivity without RF pre-amplification is claimed as compared to delay line IFM. Dynamic range is more limited and Rhodes reports a frequency accuracy of only 50 MHz RMS whereas 1 MHz or better can be achieved with delay line discriminators.

Delay line discriminators traditionally each employ four detector diodes whereas the three phase version uses three. Rhodes cites this as one of the biggest advantages of three phase versions, particularly when banks of discriminators are used for greater integrity. However delay line discriminators using only three detector diodes have been developed as a result of this thesis[16] thus nullifying any advantage.

Three phase discriminators will certainly have their uses but they are unlikely to seriously challenge the role of delay line discriminators, hence the argument for further work on delay line discriminators is still strong.

3.9 SUMMARY

IFM receivers and their traits have been well covered in this chapter, both to illustrate their prominence and to set the scene for the following in-depth discussion of delay line discriminators. Certainly the argument for further research into frequency discriminators is strong, but sight should never be lost of the alternatives.

Other IFM topics beyond the scope of this dissertation which warrant further study are limiting amplifiers - the most expensive RF modules in IFMs - and simultaneous signal detection, particularly if this leads to the ability to resolve different frequency components in every situation.

Signal environments are becoming steadily more crowded and the signals themselves more exotic. Limits on signal processing speeds may in future halt the trend towards ever broader band receivers and bring narrow band receivers into greater prominence. Future technological advances in high speed processing, optical and filter techniques are bound to have a marked effect on the direction of evolution of signal acquisition receivers. The possibility of completely new methods being developed serves to keep the whole topic alive.

CHAPTER FOUR

DELAY LINE FREQUENCY DISCRIMINATORS

Work on building a broadband 'wide-open' or non-tuning frequency discriminator (FD) began at the Mullard Research Laboratories in 1954[13]. First results were not very successful with the relationship between frequency and any other derived parameter being too non-linear and unrepeatable for accurate measurement.

The break-through and birth of modern delay line FDs came in 1957 when the identity $\cos^2(\theta/2)-\sin^2(\theta/2) = \cos\theta$ was used to measure the phase delay θ down a delay line of known length, this being directly related to frequency. A second such operation employing an additional delay of $\pi/2$ radians at all frequencies provides the orthogonal $\sin\theta$ component.

Delay line discriminators (DLDs) have many possible circuit realisations as will be seen in this chapter. Those described in the literature are all direct descendants of the 1957 version but improved stripline and microstrip techniques have allowed greater instantaneous bandwidths to be reached. A new substantially different version is introduced at the end of this chapter.

4.1 PRINCIPLE OF DELAY LINE DISCRIMINATOR

Fig 4.1 shows the basic components of a DLD. The delay line causes a delay τ and the delayed signal is multiplied with a direct signal and, separately, with a signal shifted a fixed $\pi/2$ radians to give the sine and cosine outputs after low-pass filtering as shown.

Consider a fixed frequency, constant amplitude, sinusoidal input signal $V\cos(2\pi ft)$ where f is the signal frequency and V its amplitude. The output of the delay line is then $V\cos(2\pi ft-\theta)$ where $\theta=2\pi f\tau$. The mixing product M_1 is given by

$$M_1 = V\cos(2\pi ft).\ V\cos(2\pi ft - \theta) \qquad \ldots\ldots (4.1.1)$$

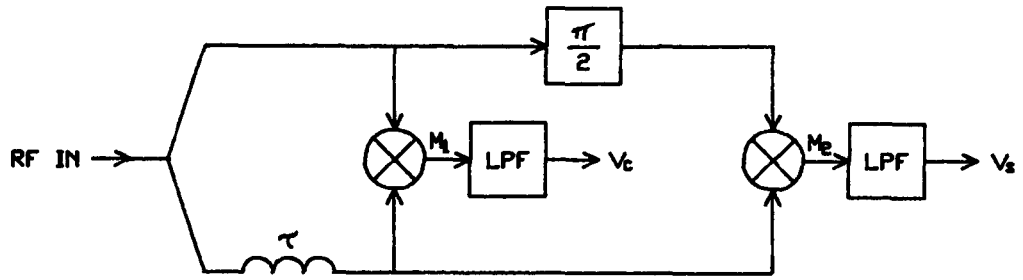

Fig 4.1 : **Basic frequency discriminator**

or

$$M_1 = \frac{V^2}{2} \cos\theta + \frac{V^2}{2} \cos(4\pi ft - \theta) \quad \ldots\ldots (4.1.2)$$

Low pass filtering rejects the sum frequency so that the output V_c is given by

$$V_c = \frac{V^2}{2} \cos\theta \quad \ldots\ldots (4.1.3)$$

The inputs to the second mixer are $V \cos(2\pi ft - \pi/2)$ and $V\cos(2\pi ft - \theta)$. The mixing product M_2 is then

$$M_2 = V\cos(2\pi ft - \pi/2).\ V\cos(2\pi ft - \theta) \quad \ldots\ldots (4.1.4)$$

or

$$M_2 = \frac{V^2}{2} \cos(-\pi/2 + \theta) + \frac{V^2}{2} \cos(4\pi ft - \pi/2 - \theta) \quad \ldots\ldots (4.1.5)$$

Low pass filtering and the use of identity $\cos(-\pi/2+\theta) = \sin\theta$ gives V_s as

$$V_s = \frac{V^2}{2} \sin\theta \quad \ldots\ldots (4.1.6)$$

If (4.1.3) and (4.1.6) are applied to the x and y plates of an oscilloscope, a dot will appear on the screen with the polar co-ordinates

$$\rho = 2K\sqrt{V_s^2 + V_c^2} \qquad \ldots\ldots (4.1.7a)$$

$$\theta = \tan^{-1}\left(\frac{V_s}{V_c}\right) \qquad \ldots\ldots (4.1.7b)$$

Where 2K is the deflection sensitivity of the display. These simplify to

$$\rho = KV^2 \qquad \ldots\ldots (4.1.8a)$$

$$\theta = 2\pi f\tau \qquad \ldots\ldots (4.1.8b)$$

Accuracy depends on the system sensitivities

$$\frac{d\theta}{df} = 2\pi\tau \qquad \ldots\ldots (4.1.9a)$$

$$\frac{d\rho}{dV^2} = K \qquad \ldots\ldots (4.1.9b)$$

A pure sinusoidal input is of course a very special case. Aside from the possibility of simultaneous signals, an intercepted signal may have amplitude modulation or angle modulation or both. A general input signal can be described by

$$v(t) = a(t)\cos(\phi(t)) \qquad \ldots\ldots (4.1.10)$$

Myers and Cumming[17] give a complete analysis of the theoretical response of FDs of the basic type shown in fig 4.1, and their results are applicable to all the FD types covered in this chapter. For completeness some of their general results are included here.

For a general signal described by (4.1.10) the polar co-ordinates become

$$\rho(t) = Ka(t)a(t-\tau) \qquad \ldots\ldots (4.1.11a)$$

$$\theta(t) = \phi(t)-\phi(t-\tau) \qquad \ldots\ldots (4.1.11b)$$

Note that $\rho(t)$ is independent of any phase modulation $\phi(t)$, and $\theta(t)$ is independent of amplitude variations $a(t)$.

Provided the rates of change of the modulations $a(t)$ and $\phi(t)$ are sufficiently slow relative to the delay τ then

$$\rho(t) \simeq Ka^2(t) \qquad \ldots\ldots (4.1.12a)$$

$$\theta(t) \simeq \tau \frac{d\phi}{dt} = 2\pi f_i(t) \qquad \ldots\ldots (4.1.12b)$$

Where f_i is the instantaneous frequency of the signal and is defined by

$$f_i(t) = \frac{1}{2\pi} \frac{d\phi}{dt} \qquad \ldots\ldots (4.1.13)$$

This is referred to as the quasi-static response.

In the case of sinusoidal angle modulation described by

$$\phi(t) = \omega_c t + M\sin(\omega_m t) \qquad \ldots\ldots (4.1.14)$$

where ω_c is the carrier angular frequency, $f_m = \omega_m/2\pi$ the modulation frequency, M the modulation index and $2Mf_m$ the peak-to-peak frequency deviation, application of equation (4.1.11) gives

$$\theta(t) = \omega_c \tau + 2M\left[\sin\frac{\omega_m \tau}{2}\cos\omega_m\left(t-\frac{\tau}{2}\right)\right] \qquad \ldots\ldots (4.1.15)$$

The total angular spread is then given by $4M\sin(\omega_m\tau/2)$ radians. If τ is sufficiently small that $\sin(\omega_m\tau/2) \simeq \omega_m\tau/2$ then the spread is $2\pi\tau$ times the peak-to-peak frequency deviation $2Mf_m$ and the quasi-static approximations hold. Of particular interest are the cases

$$\omega_m\tau/2 = k\pi, \quad k = 0, 1, 2.... \qquad ..... (4.1.16)$$

For which, from (4.1.5), there will be no angular spread. In the case of sinusoidal amplitude modulation given by

$$a(t) = A(1+m\cos\omega_m t) \qquad ..... (4.1.17)$$

where A is the carrier amplitude, m the modulation index and $\omega_m/2\pi$ the modulation frequency, application of (4.1.11) gives

$$\rho(t) = KA^2\left[1 + \frac{m^2}{2}\cos\omega_m\tau + m\cos\omega_m t + m\cos\omega_m(t-\tau) + \frac{m^2}{2}\cos(2\omega_m t - \omega_m\tau)\right] \qquad ..... (4.1.18)$$

If $\omega_m\tau \ll 1$ this reduces to

$$\rho(t) \simeq KA^2(1 + m\cos\omega_m t)^2 \qquad ..... (4.1.19)$$

which is the quasi-static response, and $\omega_m\tau \ll 1$ is a sufficient condition for quasi-static results to hold.

If pulses of duration $2t_o$ described by

$$a(t) = A, \quad -t_o < t < t_o$$
$$= 0, \quad \text{otherwise} \qquad ..... (4.1.20)$$

are applied to the input of the discriminator, mixing can only take place while the delay line output to the mixers is present simultaneously with the undelayed mixer inputs. This will not occur before a time τ has elapsed after arrival of the leading edge of the pulse. Full deflection KA^2 will occur for a time $2t_o - \tau$, so that pulses must exceed τ in duration in order to be detectable.

In practical microwave realisations of fig 4.1 phase shifting is achieved with fixed phase shifters or hybrid quadrature couplers. Mixing is performed by square-law detectors by the 'quarter-square method' in which the product gh of two functions g and h is arrived at via the relationship

$$(g + h)^2 - (g - h)^2 = 4gh \qquad \ldots\ldots (4.1.21)$$

These components will be introduced briefly in the next section and treated more fully in subsequent chapters.

4.2 STANDARD FD COMPONENTS

A brief look at the symbols and ideal behaviour of standard FD components is required at this stage. Besides the delay line itself, frequency discriminators are made up of combinations of hybrid quadrature couplers, in-phase power splitters/combiners and square-law detectors. Fig 4.2 shows the symbols used to represent these components.

For the purposes of this chapter, a quadrature coupler is a four port device as shown in fig 4.2a). A signal incident at port 1 is evenly divided between ports 2 and 3 with a 90 degree phase difference between the two out-going signals. No signal appears at port 4 as it is isolated from port 1. Similarly a signal incident at port 4 is evenly split between ports 2 and 3 while port 1 is isolated. A signal incident at port 2 or 3 is divided equally between ports 1 and 4, ports 2 and 3 being isolated from

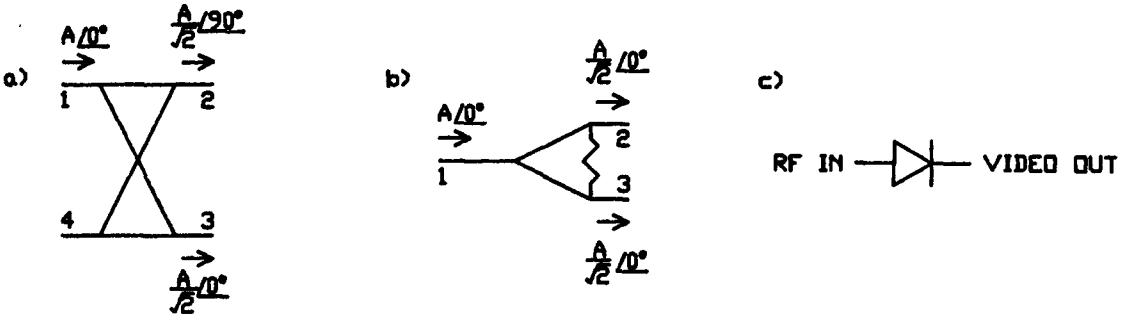

Fig 4.2 : **Standard FD component symbols**

a) Quadrature coupler

b) In-phase power splitter/combiner

c) Square-law detector

each other. The two divided or out-going signals always have a 90 degree phase difference. The physical length of the component is considered to be zero in this chapter for simplicity since this assumption does not affect the final FD outputs.

Fig 4.2(b) shows an in-phase power splitter/combiner in which a signal incident at port 1 is split equally between ports 2 and 3. In contrast with the quadrature coupler the outgoing signals are in phase with each other. The form shown here is that of a single stage Wilkinson coupler which will be fully described in chapter 5. The resistor shown causes port 2 to be isolated from port 3. Since the device is passive it is reversible. Signals incident simultaneously at ports 2 and 3 are multiplied by the same $1/\sqrt{2}$ voltage factor and then summed vectorially at port 1. Isolation between ports 2 and 3 is maintained. Again the device length is taken to be zero in this chapter since the end results are not affected.

Fig 4.2(c) shows the symbol used for a square-law detector. If an RF signal $A\cos(2\pi ft)$ is incident at the RF port then the squared result is $2KA^2\cos^2(2\pi ft)$ which can be written as $K(A^2 + A^2\cos 4\pi ft)$. $2K$ is the detector sensitivity. The detector output incorporates a low pass filter so that the output signal is KA^2 which is a DC voltage if the input is CW and has no amplitude

modulation. Often the input is a series of pulses and the output is then also a series of pulses with the same repetition frequency. This repetition frequency typically falls in the video frequency band for radar signals. To emphasise this the detector output is labelled 'video out' as shown and it should be remembered that the frequency band DC to video (eg. 10 MHz) is implied.

The properties of the quadrature coupler and in-phase divider described above strictly apply only at the designed or centre frequency f_o. Deviation from ideal behaviour away from f_o limits the bandwidth of these components and ultimately that of the discriminator. Component bandwidths and methods of extending these bandwidths will be discussed fully in chapter 5.

While no more detail than the above is required to understand the operation of the FDs discussed in this chapter, some reference to behaviour away from f_o is needed to help explain the use of certain circuit modifications, and to facilitate comparison of the various alternatives. The precise behaviour away from f_o is of course dependent on the component design but general trends can be illustrated by considering a quadrature coupler made up of a pair of coupled lines a quarter wavelength long at f_o, and a single section Wilkinson coupler or in-phase divider also a quarter wavelength long at f_o. A full explanation of what is meant by the above will be given in chapter 5.

The microwave circuit analysis package TOUCHSTONE on an IBM PC desk-top computer was used to generate the amplitude and phase data depicted in figs 4.3 and 4.4. TOUCHSTONE will be described in chapter 6. The circuit file used to plot these diagrams is included as B-1 in appendix B. The quadrature coupler is referred to as 'CPLR' in the keys, while the in-phase combiner is labelled 'WC'. The port numbering used in fig 4.2 applies here as in, for example, MAG(S31) (= magnitude of S_{31}) of CPLR or ANG(S21) (= angle of S_{21}) of WC.

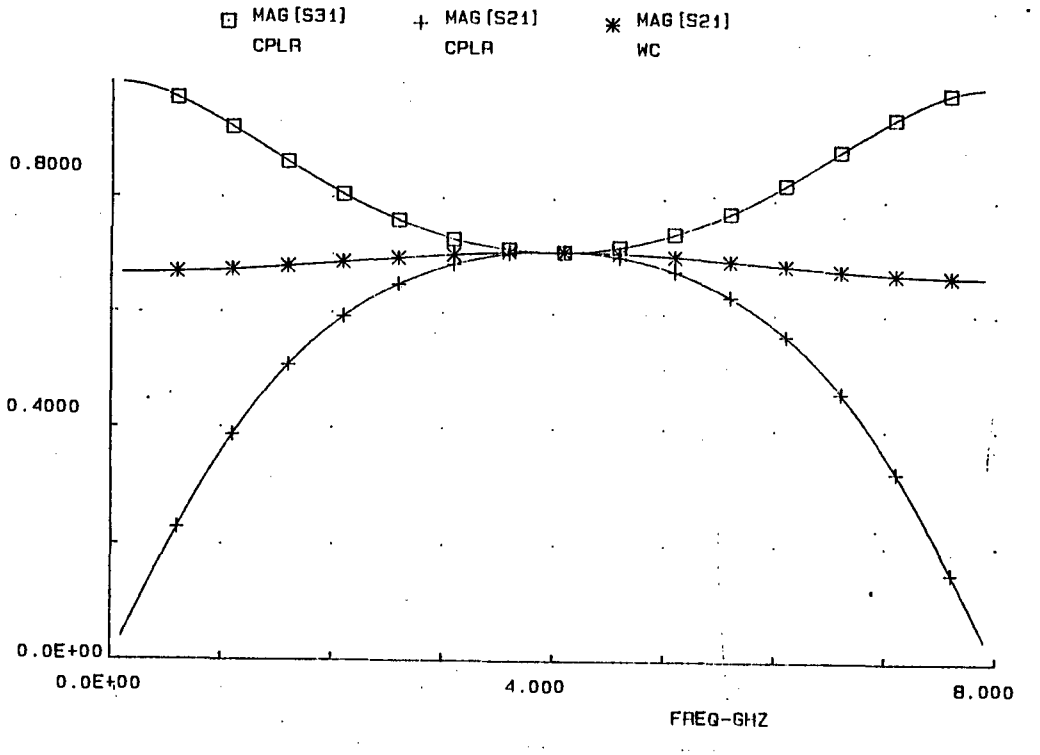

Fig 4.3 : Voltage transfer characteristic of single section quadrature coupler (CPLR) and single section Wilkinson coupler (WC)

Note that in each case the voltage transfer factor is $1/\sqrt{2} = 0.707$ at f_o, as shown in fig 4.3. This falls off slowly in the case of the in-phase divider and the two output ports are always equal and represented by the single curve. The quadrature coupler changes more rapidly and ports 2 and 3 are not equal in amplitude away from f_o. Fig 4.4 shows that the phase across the in-phase power divider is very nearly linear as expected. The deviations from linearity are due to the phase of the reflection co-efficient at port 1. In the case of the quadrature coupler there is a marked deviation from linearity although ports 2 and 3 are always 90 degrees apart. In this case the non-linearity is a property of the coupling itself. If k is the mid-band coupling factor ($0 \leq k \leq 1$, $k = \sqrt{2}$ in figs 4.3 and 4.4) and θ is the electrical length of the coupling section such that

$$\theta = \frac{\pi f}{2f_o} \qquad \ldots\ldots (4.2.1)$$

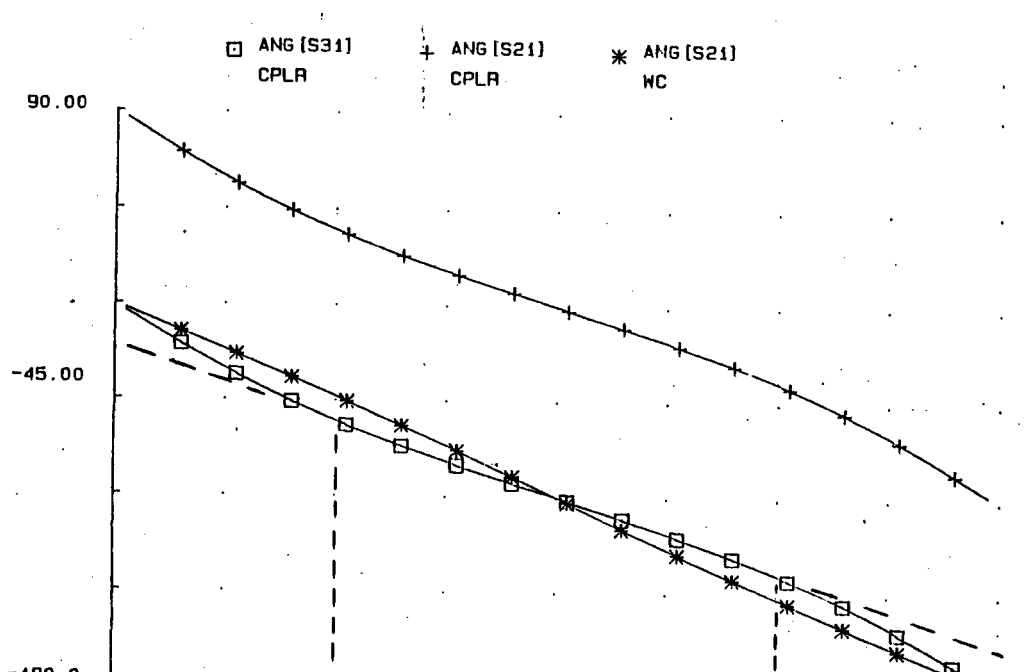

Fig 4.4 : Phase transfer characteristic of single section quadrature coupler (CPLR) and single section Wilkinson coupler (WC)

then Young[18] gives the transfer characteristics S_{21} and S_{31} as

$$S_{21} = \frac{jk\sin\theta}{\sqrt{1-k^2}\cos\theta + j\sin\theta} \qquad \ldots\ldots (4.2.2)$$

$$S_{31} = \frac{\sqrt{1-k^2}}{\sqrt{1-k^2}\cos\theta + j\sin\theta} \qquad \ldots\ldots (4.2.3)$$

The corresponding phase transfer functions are thus

$$\mathrm{Ang}(S_{21}) = \frac{\pi}{2} - \tan^{-1}\left[\frac{\tan\theta}{\sqrt{1-k^2}}\right] \qquad \ldots\ldots (4.2.4)$$

$$\text{Ang}(S_{31}) = -\tan^{-1}\left[\frac{\tan\theta}{\sqrt{1-k^2}}\right] \qquad \ldots\ldots (4.2.5)$$

As will be seen it is the difference between the in-phase divider and quadrature coupler phase characteristics that is important, since the 90 degree phase difference is always maintained within the quadrature coupler.

4.3 COMMON FD CIRCUIT

Fig 4.5 shows the FD circuit configuration most frequently described in the literature[4,10,16,20,21,22]. It consists of a phase discriminator (PD) fed by delayed and undelayed outputs of an in-phase power splitter (WC). The PD section is composed of three hybrid quadrature couplers (QCs) and a WC. These feed four detectors arranged as shown.

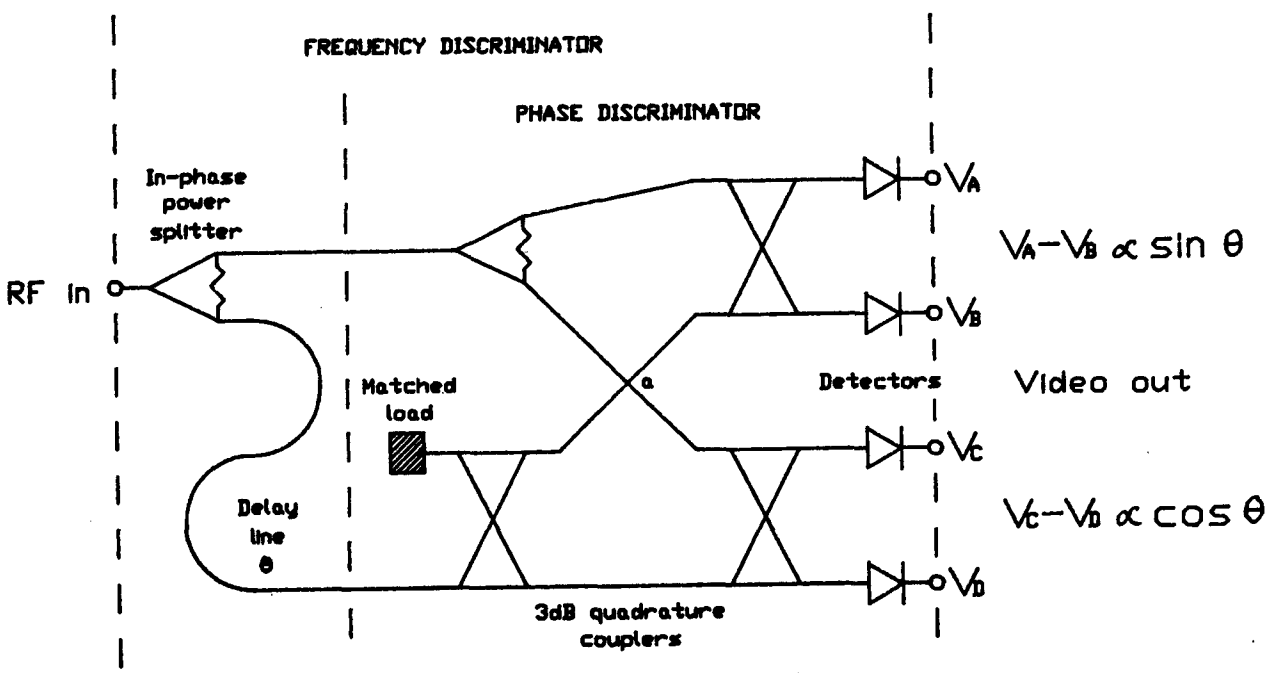

Fig 4.5 : Common FD configuration

A mathematical proof of the operation of this circuit using the ideal components described in the last section and a lossless delay line is given in appendix C. If A is the amplitude of an input signal, θ the electrical length of the delay line at the input signal frequency and 2K the sensitivity of the detectors then the final outputs are

$$(V_A - V_B) = KA^2 \sin\theta \qquad \ldots\ldots (4.3.1)$$

$$(V_C - V_D) = KA^2 \cos\theta \qquad \ldots\ldots (4.3.2)$$

θ can then be determined from the relationship

$$\theta = \tan^{-1}\left[\frac{V_A - V_B}{V_C - V_D}\right] \qquad \ldots\ldots (4.3.3)$$

to give the input signal frequency. In theory the input signal amplitude can also be determined from

$$A^2 = \frac{1}{K}\left[(V_A - V_B)^2 + (V_C - V_D)^2\right]^{\frac{1}{2}} \qquad \ldots\ldots (4.3.4)$$

But in practise this data is rarely very meaningful since FDs are normally fed by limiting amplifiers.

The instantaneous bandwidth of the circuit is limited by the individual component deviations from ideal behaviour away from the designed or centre frequency f_o. These deviations cause errors in the measurement of the phase angle θ so that FD bandwidth is determined primarily by the largest phase error that can be tolerated. For a given set of components the errors caused are determined by circuit layout and, in general, the more symmetrical the phase discriminator the smaller the errors or, alternatively, the larger the usable bandwidth.

The PD of fig 4.5 is symmetric except for the two front end components where a WC is set against a QC. At the centre frequency f_o the theoretical error is zero if the components described in the latter part of section 4.2 and depicted in figs 4.3 and 4.4 are used. Away from f_o both the amplitude and phase characteristics introduce errors.

The amplitude variation between the two outputs of the QCs will affect accuracy even when there is perfect symmetry unless the delay line is lossless, as will be shown in chapter 6. The amplitude trend of the WC is very different from both QC outputs so that the error is compounded by lack of symmetry.

The phase differences shown in fig 4.4 are perhaps even more significant. Ideally the phase relationship should be precisely linear. The WC shows very nearly linear phase slope and although the QC curves are definitely non-linear they remain a fixed 90 degrees apart. Errors are caused by the varying phase difference between the QC and WC outputs which should always be 0 degrees or 90 degrees.

A slightly more subtle effect can be shown by considering a bandwidth such as that marked at its limits by the vertical dashed lines in fig 4.4. The line marking the best linear approximation to the actual phase curve of the QC within this bandwidth is marked at its extremes by dashed lines. This line would be the phase characteristic of a component slightly shorter in length and encompassing a fixed phase shift, since the slope is reduced in magnitude and the line does not pass through 0 degrees at zero frequency. In this case the component appears to have an electrical length at f_o of approximately 70 degrees as opposed to an actual length of 90 degrees, and the fixed phase shift is about 20 degrees. In contrast the WC shows its true length of 90 degrees at f_o and no fixed phase shift.

The difference in effective component length can be absorbed into the delay line by calculating an effective delay line length for

the equations of section 4.1, rather than using the actual length. In general the components themselves may differ in physical length, usually by a multiple of quarter wavelengths at f_o, and this can be accounted for in the same way. The fixed phase shift is not so easily accounted for. An additional RF component giving a fixed phase shift can be used, or digital processing can make corrections by direct calculation or by accessing a PROM for the final frequency word. The PROM is then programmed immediately after manufacture and testing of each individual FD and is supplied with it. This is the usual technique adopted since processing time must be kept to a minimum.

Various circuit modifications such as the additional phase shifter have been used in the past to improve theoretical error performance, and these are summarised in section 4.4. Best performance and smallest size are achieved by integrating the entire FD onto a single substrate. The main practical obstacle to this is the cross-over required at the point marked a) in fig 4.5. This is dealt with fully in section 4.5.

4.4 VARIATIONS OF STANDARD FD CIRCUIT

Since the FD shown in fig 4.5 is the most commonly described FD, and since other circuits reported in the literature are easily recognisable as being derivatives of it, it may be referred to as the standard version. The variations described in the literature are discussed below. Their mode of operation is the same as that of the standard version and they are offered here without mathematical proof.

4.4.1 SCHIFFMAN COMPENSATION

Fig 4.6 shows an adaptation described by Margosian[3]. It makes use of a class of broad-band microwave phase shifters first described by Schiffman[23] in 1958. The Schiffman compensator consists of coupled line sections as does the QC and can be used to compensate for the QC phase dispersion shown in fig 4.4.

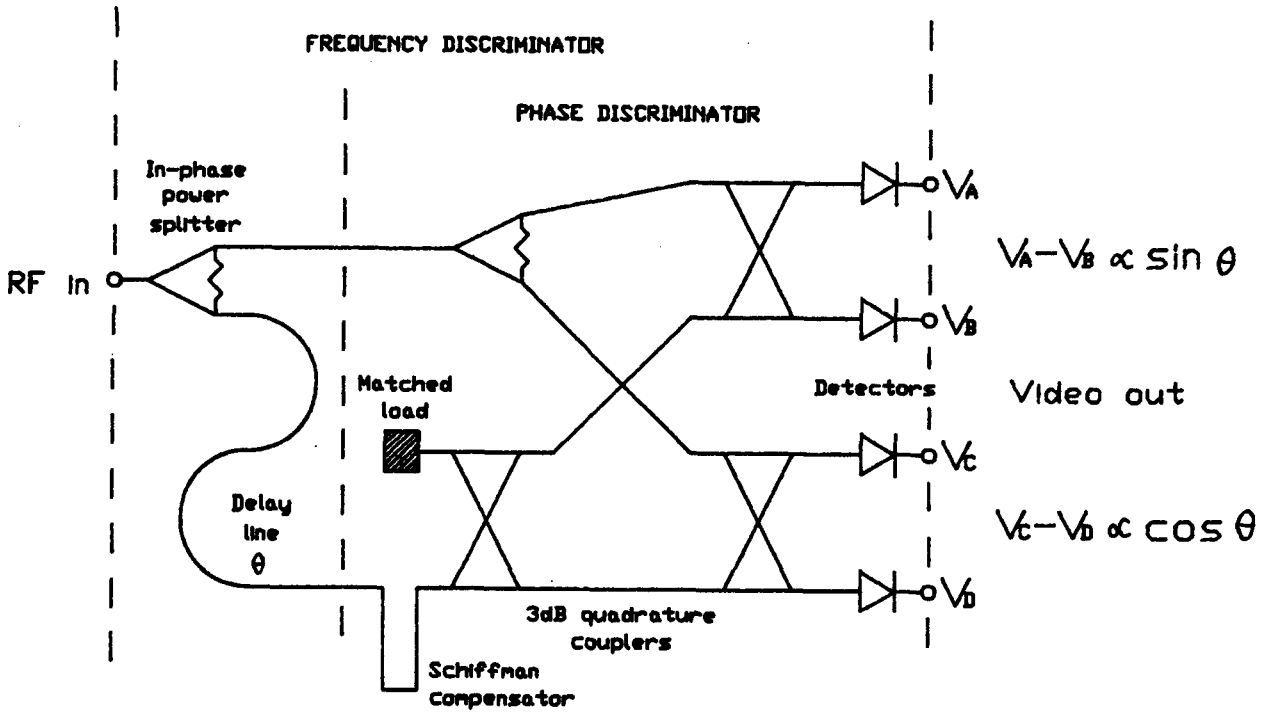

Fig 4.6 : **Schiffman compensated FD**

Fig 4.7, which was generated by the TOUCHSTONE circuit file given in appendix B-2, clearly shows how this compensation works. The curve labelled CPLR is the QC phase curve given in fig 4.4 but shifted up 180 degrees for convenience. The curve labelled SL is the ideal linear relationship and the curve labelled S is that of a Schiffman compensator. The Schiffman is constructed of a single coupled line section which is a quarter wavelength long at the centre frequency f_o = 4 GHz, as is the QC coupled section. To give the QC the same physical length as the Schiffman, extra uncoupled transmission line sections a quarter wavelength long at f_o have been added.

The odd and even mode impedances, Z_{oe} and Z_{oo}, of the Schiffman coupled line section must be carefully chosen to reflect as closely as possible the QC curve. If the base characteristic impedance is Z_o then the relationship

$$Z_o = \sqrt{Z_{oe}\, Z_{oo}} \qquad \ldots\ldots (4.4.1)$$

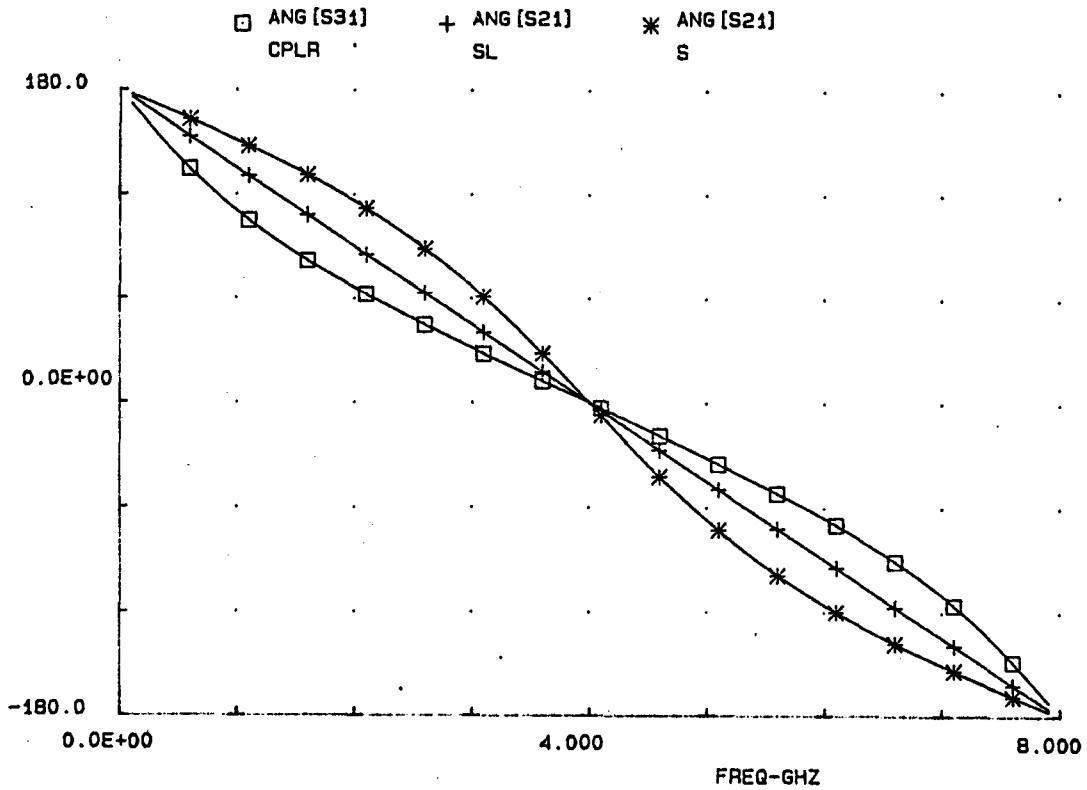

Fig 4.7 : **QC and Schiffman compensator phase characteristics**

should hold to ensure the Schiffman is properly matched to the rest of the circuit. Odd and even mode impedances of coupled lines will be discussed in more detail in chapter 5.

Schiffman gives the phase ϕ, across the compensator as

$$\phi_1 = \cos^{-1}\left[\frac{\rho - \tan^2\theta}{\rho + \tan^2\theta}\right] \qquad \ldots\ldots (4.4.2)$$

where $\theta = \pi f/2f_o$ as in equation (4.2.1), and

$$\rho = \frac{Z_{oe}}{Z_{oo}}, \qquad \rho \geq 1 \qquad \ldots\ldots (4.4.3)$$

Compare ϕ_1 with the phase ϕ_2 across the QC plus added transmission line section. From equation (4.2.5)

$$\phi_2 = \theta + \tan^{-1}\left[\frac{\tan\theta}{\sqrt{1-k^2}}\right] \qquad \ldots\ldots (4.4.4)$$

For full compensation the following relation must hold at all values of θ that fall within the bandwidth of interest

$$\frac{\phi_1 + \phi_2}{2} = 2\theta \qquad \ldots\ldots (4.4.5)$$

The phase deviation function ϕ_d can then be defined as

$$\phi_d = 4\theta - \phi_1 - \phi_2 \qquad \ldots\ldots (4.4.6)$$

or, from equations (4.4.2) and (4.4.4)

$$\phi_d(\theta,\rho,k) = 3\theta - \cos^{-1}\left[\frac{\rho - \tan^2\theta}{\rho + \tan^2\theta}\right] - \tan^{-1}\left[\frac{\tan\theta}{\sqrt{1-k^2}}\right] \qquad \ldots\ldots (4.4.7)$$

Note that $\phi_d = 0$ for all θ if $k = 0$ and $\rho = 1$ but that this is the trivial un-coupled solution. In general k is determined by bandwidth requirements and ρ is chosen so that ϕ_d is a minimum over the range of θ of interest. Note also that for $\theta = 0$, 90 degrees and 180° (corresponding to f = 0, 4 GHz and 8 GHz in fig 4.7) $\phi_d = 0$ for all k and ρ.

If k is not zero ρ cannot be chosen so that ϕ_d is zero for all θ. Determination of the value of ρ that gives minimum phase deviation is not trivial and is beyond the scope of this dissertation. Microwave components are never

lossless and nor do they have perfect input and output matches, so there will be some contribution to phase error from the reduction in signal amplitude. Finally RF circuitry size is increased which in turn increases weight and cost.

4.4.2 FOUR QC VERSION

An obvious and commonly used solution to the non-symmetry problem is to replace the WC of the phase discriminator section of fig 4.5 with an identical QC, and to correct the phase relationships with a fixed ninety degree phase shifter[5,24,25]. Fig 4.8 shows this FD configuration.

The phase shifter must operate properly over the whole instantaneous bandwidth. Shifters of the type introduced by Schiffman[23] are usually used. They have similar phase properties to the compensator described in section 4.4.1. Lower coupling than that required by the QC ensures that

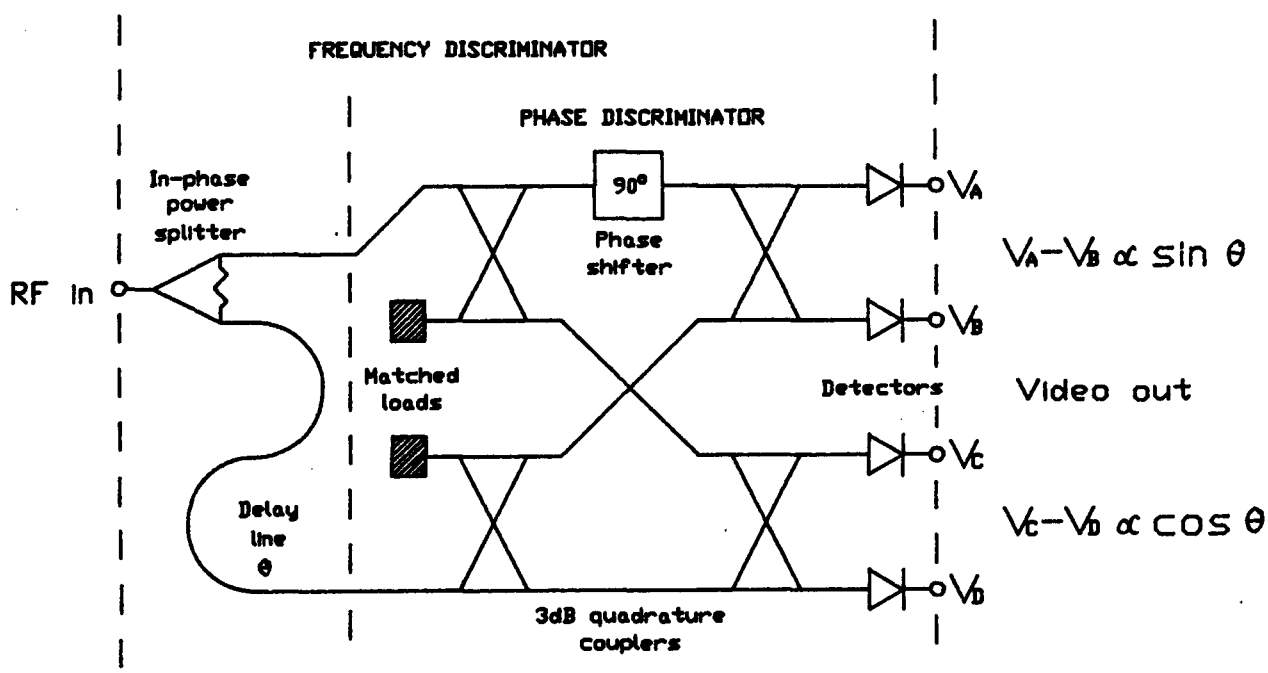

Fig 4.8 : Four QC frequency discriminator

phase deviations are much less pronounced than in the original symmetry problem.

Once again component losses and mis-matches reduce signal amplitude at the output and hence affect overall accuracy. RF circuit size, weight and cost are increased as in the Schiffman compensation case. Often the front-end WC is also replaced by a QC to reduce the number of different broad-band RF components that must be designed. The extra 90 degree shift adds to the frequency dependent delay line phase and must be accounted for by the processor.

4.4.3 180 DEGREE HYBRID VERSION

Fig 4.9 shows an FD version described by Hofmann and Baron[1] and by Myers and Cumming[17]. Essentially it is the same as that shown in fig 4.8 except that the ninety degree phase shifter and preceding quadrature coupler have been

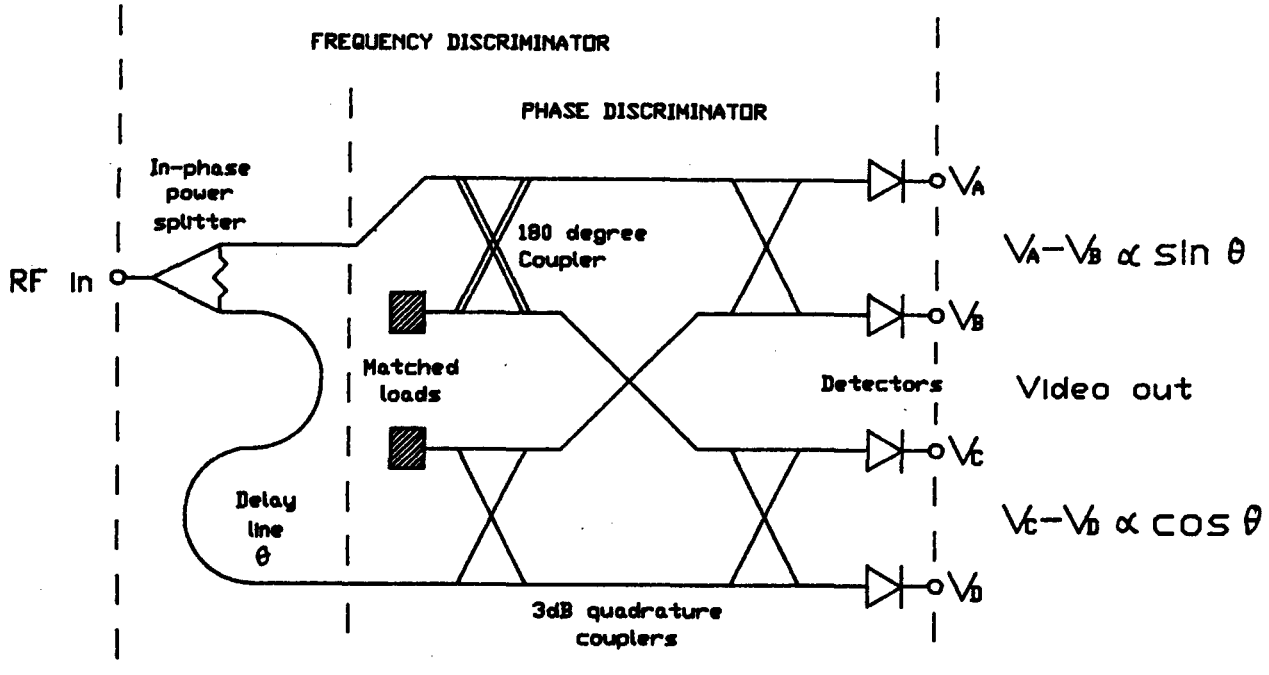

Fig 4 .9 : 180 degree hybrid version

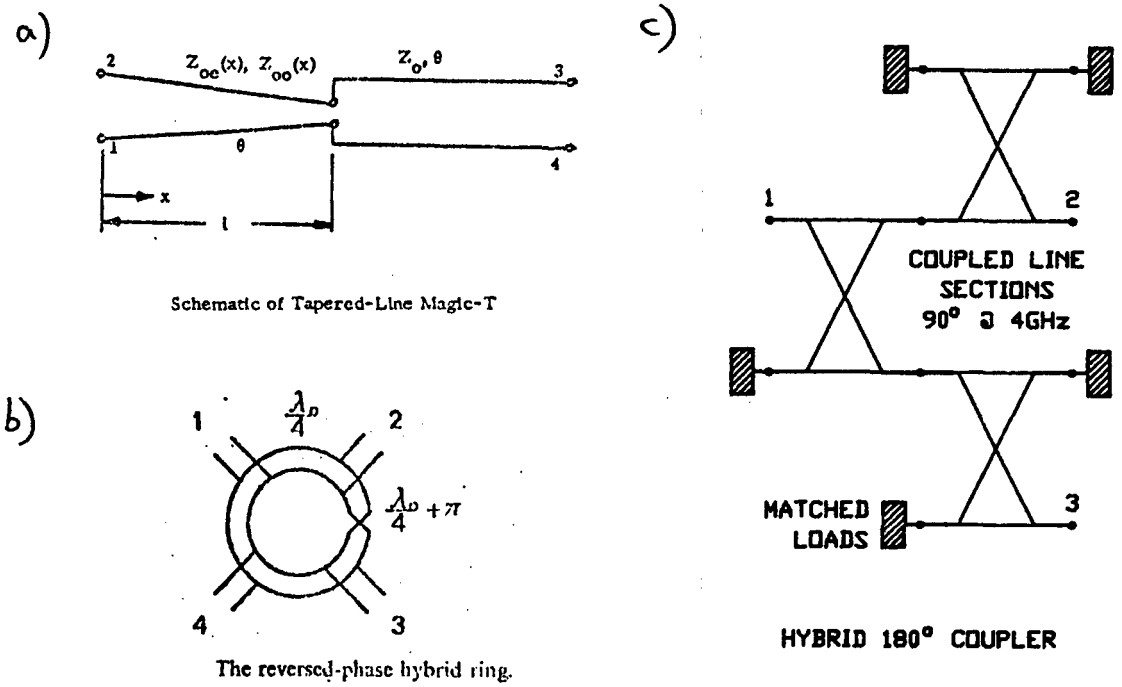

Fig 4.10 : 180 degree hybrids

a) Tapered-line magic-T
after Duhamel and Armstrong

b) Reversed-phase hybrid ring
after Rehnmark

c) 3-QC-Section hybrid coupler

replaced by a single device. The new component splits the input signal equally to the two output ports and ensures that there is a 180 degree phase difference between the outputs.

There are several ways in which this new component can be made. Some versions of stepped asymmetric couplers exhibit a 180 degree output phase at the centre frequency f_o, but phase is not independent of frequency. Stepped multi-section couplers, both symmetric and assymmetric, are covered in chapter 5.

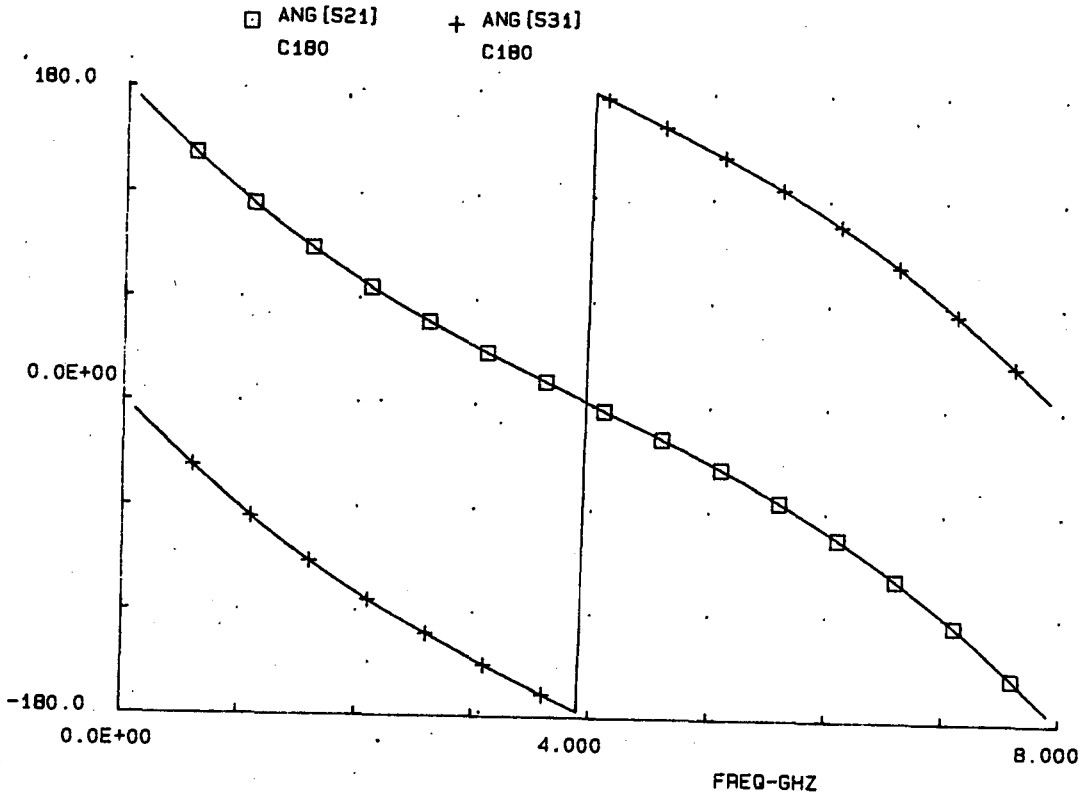

Fig 4.11 : Output phase characteristics of hybrid 180 degree coupler

Duhamel and Armstrong[26] describe a 'magic-T' made up of a tapered coupled transmission line section and two uncoupled lines as shown in fig 4.10(a). It may be designed to exhibit a 3dB power split with a 180 degree or zero phase difference between the outputs. The phase difference is independent of frequency but the phase across the device is likely to be different to that of the QC in the other channel, as was the case when the WC was used.

Rehnmark[27] describes a reversed-phase hybrid ring derived from the well-known 'rat race' hybrid ring. This is shown in fig 4.10(b). It does require a frequency independent 180 degree phase shifter but Rehmark suggests that in twin line this can be accomplished by twisting the lines over as shown. In other media this is not so simple and it is unlikely that this technique can be applied to microwave integrated circuits.

Fig 4.10(c) shows an alternative version made up of three single section quadrature couplers. Good choice of centre frequency coupling factors for the three QCs can probably help broaden the bandwidth of the device, as is done with the multi-section quadrature couplers described in the following chapter. Fig 4.11, generated by the TOUCHSTONE circuit file in appendix B-3, shows the output phase difference to be 180 degrees independent of frequency.

A drawback of this last technique is that the device has an inherent 3dB loss. This loss is probably tolerable since FDs are driven by amplifiers, but the other channel must include a 3dB attenuator to keep amplitudes equal. A better alternative to the attenuator is to change the 1:1 power split at the front end to a 2:1 split so that the 180 degree hybrid channel starts 3dB above the level of the other channel.

Fig 4.11 shows a very similar phase dispersion trend to the QC trend shown in fig 4.7. Although full compensation is unlikely, errors due to dispersion can probably be greatly reduced if this device is used. This last method has been used by Myers and Cumming[17].

4.5 THE CROSSOVER PROBLEM

All of the FD versions discussed so far share the need to cross over two transmission lines at the point marked (a) in fig 4.5. Ideally the crossover must be accomplished with no coupling between the lines or power reflection due to changing impedances occurring. The crossover problem is a significant stumbling block to integrating the entire FD on a single substrate.

At low frequencies in microstrip a 'true' crossover can be achieved with an air-bridge, ie. a conducting ribbon suspended above one of the tracks. The height of the bridge is limited by structural problems and the resulting VSWR. However the lower the bridge

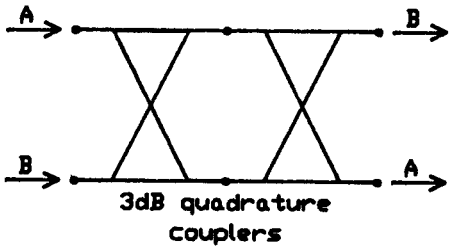

Fig 4.12 : **Signal crossover with cascaded QC hybrids**

the greater the coupling between the lines. In practise air-bridges can be used without large errors if the isolation between the lines is greater than about 25dB. These factors limit the frequency up to which this method can be used to about 6 GHz[21]. The air-bridge also affects phase through parasitic reactances and as far as possible these have to be taken into account in the design of the rest of the circuit.

Chelli et al[21] suggest using two cascaded 3dB quadrature couplers to perform the crossover as shown in fig 4.12. However, to keep phases in step, identical cascaded couplers must also be used in the other arms as shown in fig 4.13. Note that this doubles the total number of components required. Also imperfections in the QCs cause errors, especially at higher frequencies. Chelli et al achieved reasonable results with this method only up to C band.

The solution usually adopted[10,21] is to integrate the phase discriminator section separately and attach the delay line externally, although sometimes the front-end power splitter is integrated as well. The layout used is shown in fig 4.14. This method can cause problems when the front-end power splitter is integrated and the shorter delay lines cannot reach across the board.

One last solution sometimes used[4,20] is to bring the video outputs of the detectors out from internal positions on the board with co-axial cables, rather than take the outputs directly to the

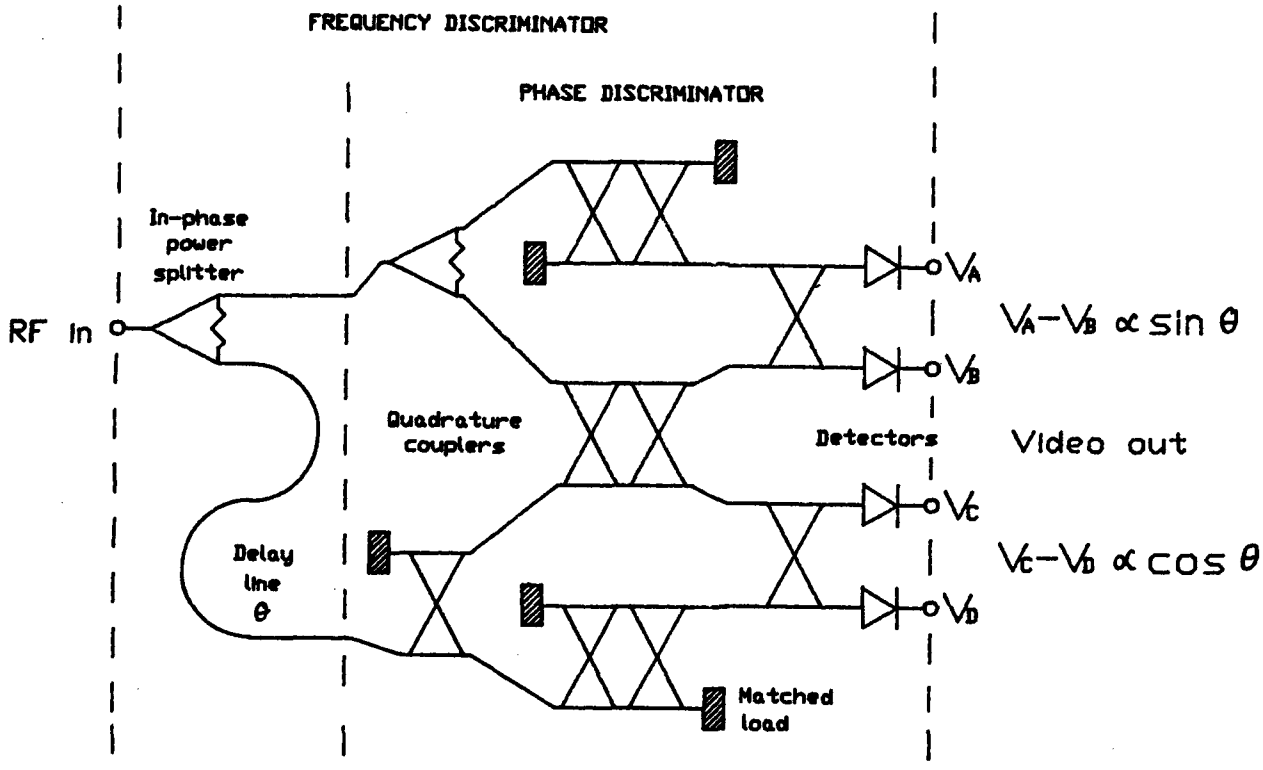

Fig 4.13 : FD with cascaded QCs to perform crossover

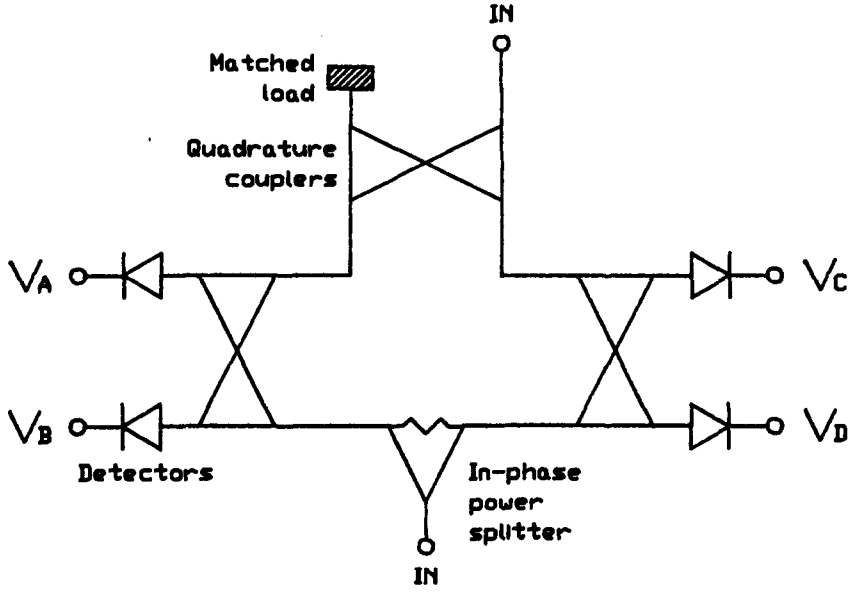

Fig 4.14 : Phase discriminator layout for separate integration

edge of the board. Care must be taken to ensure the co-axial cables do not affect the operation of the RF circuitry. This method does not easily allow co-axial packaged screw-on detectors to be used during testing stages.

Although these last two methods in particular are workable, they are certainly not the ideal solution which is to eliminate the need for a crossover altogether.

4.6 SINGLE QUADRATURE COUPLER DISCRIMINATOR

Two main difficulties with previous FD circuits have already been discussed. The first was a non-symmetry problem at the front end of the phase discriminator section which caused phase measurement errors. The second problem was a practical difficulty in crossing over two transmission lines. Fig 4.15 shows an alternative FD that was developed during the course of this work to solve these problems[16].

There are several advantages to this version which are immediately apparent. Firstly the circuit can be integrated with a layout exactly as shown. No lines need to be crossed over. Secondly no components different to those used in the standard version need to be developed. In fact the total number of components required is reduced since no matched load and only three detectors are needed. This reduces size and cost.

As will be shown in chapter 5, once constructed WC's generally exhibit more nearly ideal behaviour than quadrature couplers. They are also easier to broad-band than QCs, particularly in microstrip. This version requires only a single QC compared to three in the standard version, and even more in some of the variations discussed.

The problem of non-symmetry at the front end of the phase discriminator has also been eliminated by using only one completely symmetrical component in this position. The last WC at the V_2

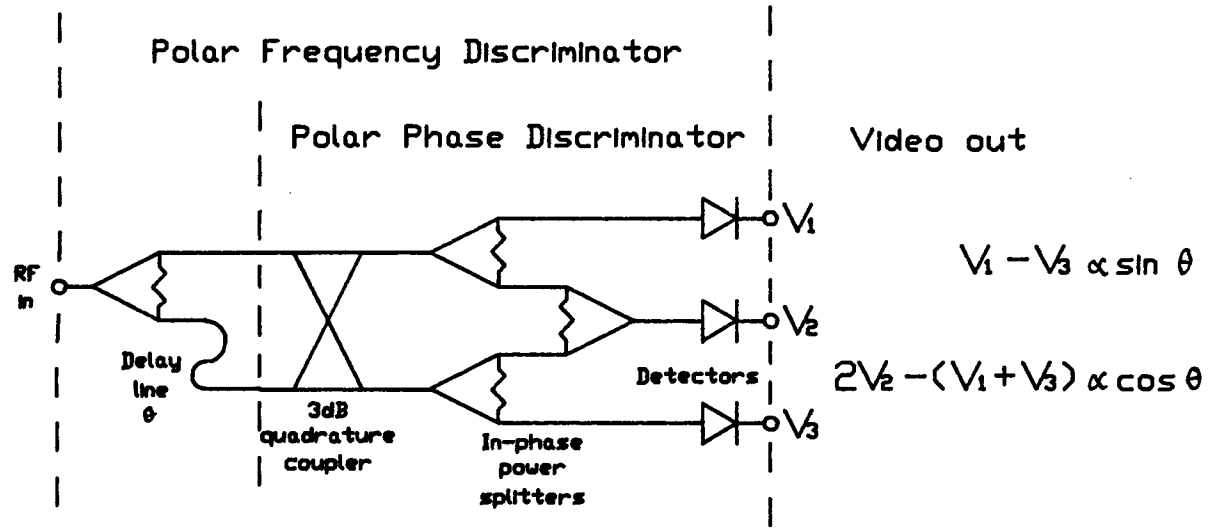

Fig 4.15 : **Single quadrature coupler FD**

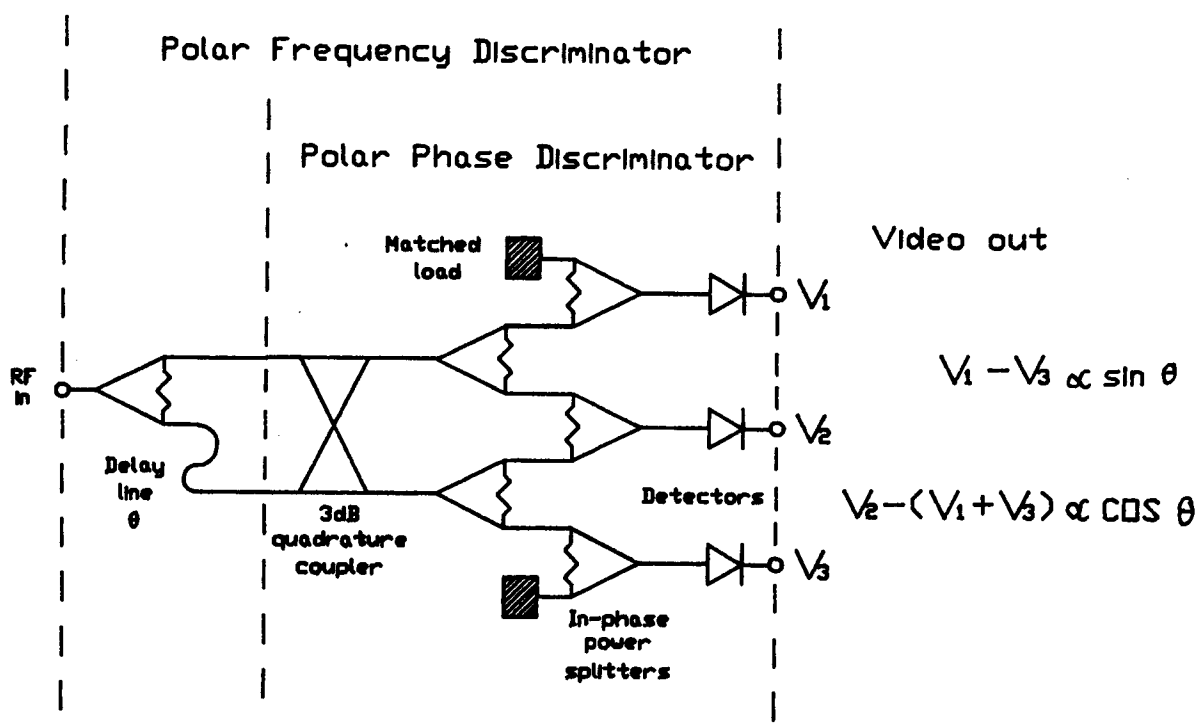

Fig 4.16 : **Alternative single QC FD**

output is not matched by similar WCs in the V_1 and V_3 outputs. This lack of symmetry does produce phase errors but, as will be shown in chapter 6, these are far less significant than in the standard version. An indication of this is given when one considers that amplitude variations alone cause these errors, and not both phase and amplitude as was the case before. Fig 4.16 shows an alternative version which eliminates even this last non-symmetry difficulty at the expense of added components. However, as will be demonstrated in chapter 6, the added complexity is rarely justified.

A mathematical proof of the operation of these circuits using ideal components is given in appendix D. In the case of the version in fig 4.15 the following apply

$$(V_1 - V_3) = KA^2 \sin\theta \qquad \ldots\ldots (4.6.1)$$

$$2V_2 - (V_1 + V_3) = KA^2 \cos\theta \qquad \ldots\ldots (4.6.2)$$

where 2K is the detector sensitivities, A the input signal amplitude, θ the electrical length of the delay line at the input signal frequency, and V_1, V_2 and V_3 are the output voltages as shown. Note that the right hand sides of these equation are identical to those of equations (4.3.1) and (4.3.2). Thus, with the associated video processing circuitry, this new FD can be inserted into existing IFM receiver designs with no other alterations.

The factor 2 required on the left of equation (4.6.2) can be realised with a video amplifier of gain 2, but is probably better incorporated as a higher gain channel in the processing circuitry that follows. If this is done the video processing circuitry need be little larger than that of the standard version despite the slightly more complex operations.

For the version of fig 4.16 the following apply

$$(V_1 - V_3) = \tfrac{1}{2}Ka^2 \sin\theta \qquad \ldots\ldots (4.6.3)$$

$$V_2 - (V_1 + V_3) = \tfrac{1}{2}KA^2 \cos\theta \qquad \ldots\ldots (4.6.4)$$

Note that the factor 2 is no longer present so that no additional video gain in the V_2 channel is required.

The two disadvantages of these circuits are the slightly more complex video processing and some inherent RF loss in the FD circuitry. This arises from using WCs as power combiners with inputs that in general are not in phase. The second version has greater RF loss than the first and it is this that causes the factor 2 to be dropped. Since frequency discriminators are always fed by limiting amplifiers, this loss, which is a maximum of 3dB, can usually be tolerated.

4.7 SINGLE HYBRID TEE FREQUENCY DISCRIMINATOR

Several waveguide frequency discriminators have also been described in the literature[28,29]. They are usually equivalent to a single channel in the FDs previously discussed so that their accuracy is more limited. They are usually meant to be quickly assembled laboratory tools and the simplest of them is described here for interest.

In the usual form of these waveguide discriminators the input signal is first divided into two paths by either a 3dB power splitter or hybrid tee. The two signals then pass down transmission lines of length L_1 and L_2 with frequency dependent phase constant β. The outputs of these lines are then recombined in a power combiner and square-law detected. The amplitude of the detected signal is dependent on both the input signal frequency f and amplitude A. If the detector sensitivity is 2K then the output provided by these discriminators is usually[29] given by

$$V_{out} = KA^2 \cos\beta(L_1 - L_2) \qquad \ldots\ldots (4.7.1)$$

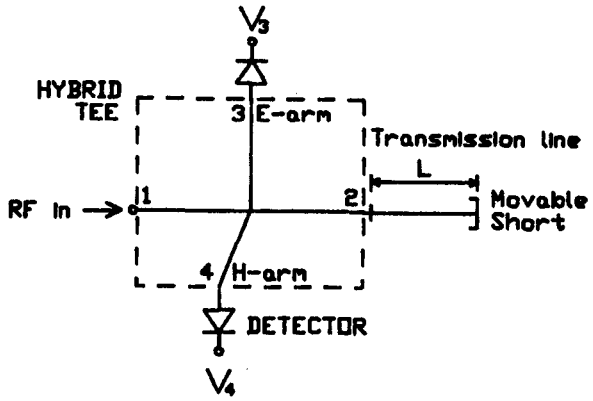

Fig 4.17 : **Single hybrid tee frequency discriminator**

Replacing $\beta(L_1 - L_2)$ by θ and comparing with equations (4.3.2) and (4.6.2) shows that the output is identical to that of a single channel of the previously described FDs.

Nigrin et. al.[29] describe what is probably the simplest such discriminator. It consists of a transmission line with a movable short circuit, two detectors and a single hybrid tee shown schematically in fig 4.17. It is only useful over narrow bands in which the s-parameters of the hybrid tee vary little. If the s-parameters of the hybrid tee have their usual definitions and symbols, K_3 and K_4 are the sensitivities of the detectors at ports 3 and 4 respectively, L is the transmission line length, ϕ_{12} is the phase angle of the S_{12} parameter,

$$D = \left[1 + S_{22}e^{-j\beta.2L}\right]^{-1} = |D|e^{j\phi} \quad \ldots\ldots (4.7.2)$$

then

$$\begin{aligned} V_{out} &= V_3 - V_4 \\ &= (K_3|S_{13}|^2+K_4|S_{14}|^2)|D||S_{12}|2\cos(\beta 2L-\phi_{12}-\phi) \\ &\quad + (K_3|S_{13}|^2-K_4|S_{14}|^2)(1+|D|^2|S_{12}|^2) \end{aligned} \quad \ldots\ldots (4.7.3)$$

Provided the hybrid tee s-parameters are such that the cosine term in (4.7.3) predominates, the output is similar to that of a single channel of an FD.

4.8 SUMMARY

This chapter started with a look at the basic theory of frequency discriminators and the ideal components used to realise them. The standard FD version was discussed and its two main problems were found to be a lack of symmetry and the need for a crossing over of transmission lines.

Several variations of the standard version were also looked at. These were intended to lessen the symmetry problem and none completely overcame it. Methods of getting around the cross-over problem were also discussed but none were entirely satisfactory.

A new frequency discriminator was introduced which had no need for a cross-over and largely eliminated the symmetry problem.

An FD's bandwidth is limited by the bandwidths of its constituent components. A closer look at ways of implementing and broad-banding these components needs to be taken, along with a look at FD analysis techniques. This will facilitate the good design of FDs for given bandwidths.

CHAPTER 5

FREQUENCY DISCRIMINATOR COMPONENTS

In order to confirm the feasibility of frequency discriminators, and in particular the new single QC versions, prototypes must be constructed and tested. Before doing so, the individual components must be designed, built and tested. The advantage of doing this before completing the theoretical analysis of FDs is that non-ideal properties which are not indicated by theory are highlighted. These difficulties can then be borne in mind while the more complete analysis is undertaken.

Firstly a frequency band should be chosen. This band should be wide enough to be challenging and to demonstrate suitability for wideband applications. The upper frequency limit should not be so high that discontinuity effects, due to the use of fairly rudimentary laboratory construction techniques, are likely to mask the correct operation of the circuit. To fulfil these requirements a 3:1 bandwidth was chosen, with lower and upper limits of 2 GHz and 6 GHz respectively.

Quadrature couplers and in-phase power splitters can be realised in many different ways and using many different transmission structures. The best choice of component design and transmission medium depends on factors like bandwidth, size and ease of use. Choice of a single medium eliminates the need for (never perfect) broadband transitions between different media, but different components may be better suited to different media.

This chapter looks closely at the construction and bandwidths of FD components and presents measured results of devices actually constructed.

5.1 CHOICE OF CIRCUIT CONSTRUCTION MEDIUM

5.1.1 MICROWAVE TRANSMISSION STRUCTURES

Fig 5.1 summarizes the media choices available to microwave circuit designers. Each media has its own particular

properties and are thus suited to different applications. Waveguide, for example, exhibits very low loss making it ideal for the top end of the microwave spectrum. At lower frequencies waveguide becomes large, heavy and unwieldy. It is not suited to integration, is generally not flexible and, apart from ridged waveguide, has a limited bandwidth. It is certainly not suited to broadband frequency discriminators in the 2 GHz to 6 GHz range.

Co-axial cable may be small and flexible but becomes lossy at high frequencies. It is very useful for interconnecting equipment but mounting components into co-axial cable in the laboratory is difficult. Co-axial cable is not suited to integration but commercial co-axial packaged devices such as attenuators and detectors are very useful in the laboratory as screw on devices.

The other three commonly used media are microstrip, stripline and slotline. All are suited to integration. Microstrip is particularly attractive as components are very easily mounted and circuits are compact and light, the more so the higher the dielectric constant of the base material. Microstrip circuits are also best suited to tuning with metal discs which is particularly useful in amplifier and oscillator work. Microstrip suffers from radiation losses - a property which can be used to great advantage in the design of flat profile antennas - and dielectric losses become excessive above about 20 GHz.

Stripline has similar properties to microstrip but doesn't suffer radiation losses and has higher dielectric losses. It is less easy to use, particularly when mounted components are required.

Slotline is less commonly used. High impedance lines, series stubs and short circuits are more easily used in slotline than in microstrip and stripline. Sometimes

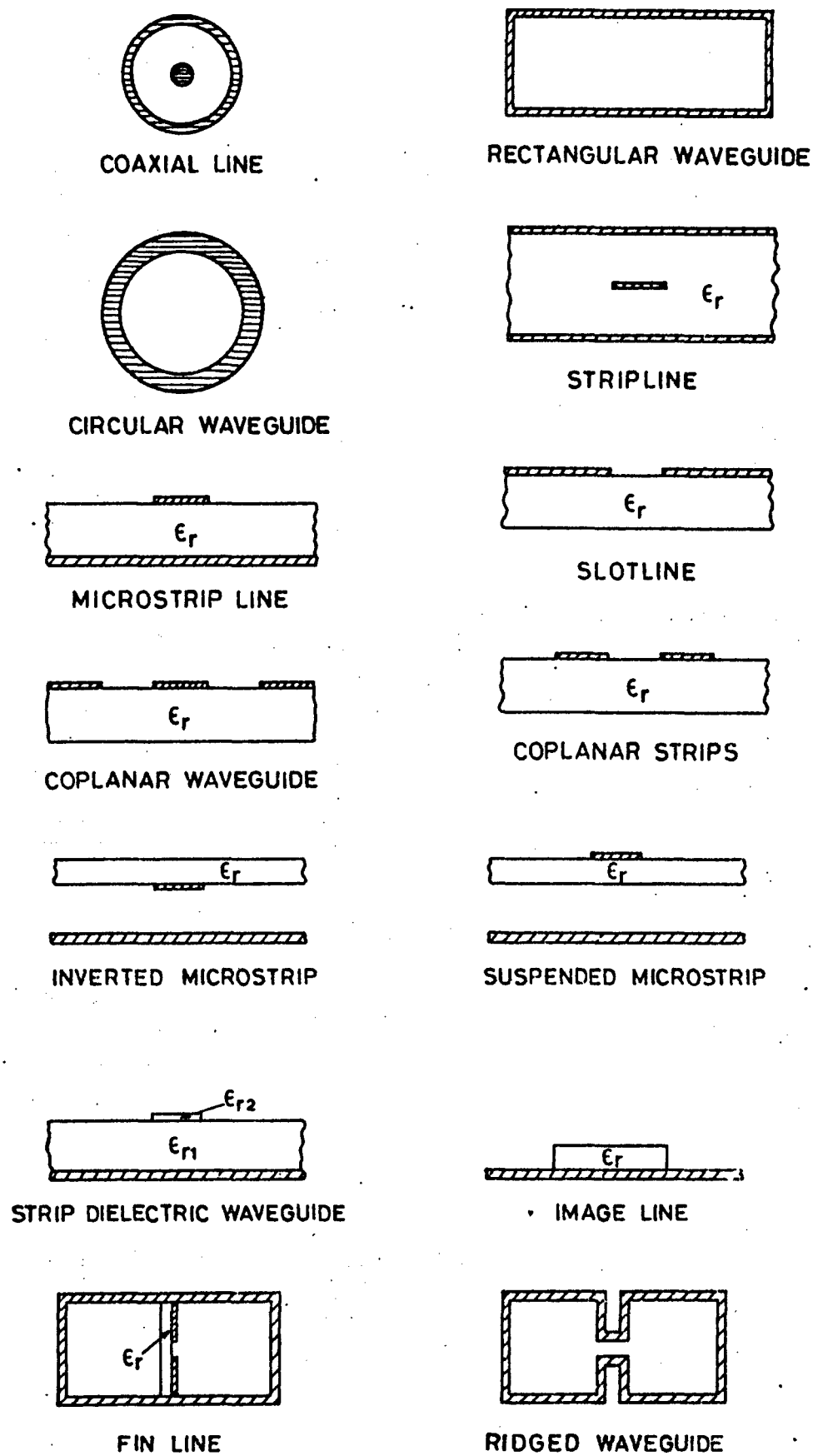

Fig 5.1 : Transmission structures for microwave circuits
after Gupta et al

slotline and microstrip are used together as in slotline couplers, but this requires accurate alignment of the etching masks on either side of the board.

Ideally microstrip would be best suited to the construction of frequency discriminators. However coupled lines with coupling as tight as 3dB cannot be made in microstrip simply by running lines very close together. Interdigitated couplers can produce tight coupling but these require very fine etching and bonding facilities which were not available.

Tight coupling can be achieved in stripline and in-phase power splitters can be constructed in stripline without very fine etching and bonding facilities, although construction is more difficult than in microstrip. Thus stripline was the medium chosen for construction of the prototypes. A full explanation of the influence of coupling factor on this decision will be given in section 5.3.

5.1.2 CHOICE OF SUBSTRATE

The main factors governing the choice of substrate for the prototypes were availability and the ease with which the material could be worked or machined. More important considerations for production would be cost and overall performance related to operating environment.

Ceramic dielectrics such as alumina are very hard and difficult to machine. Soft boards such as those made by the Rogers Corporation and 3M are much easier to work.

The next choice is between high and low dielectric constant material. Generally the relative dielectric constant ε_r of high dielectric constant commercial materials is about ten, and that of low dielectric constant material a little above two. In general the lower the dielectric constant the lower the loss and the larger the circuit.

The next choice is the thickness of dielectric to use. For a given characteristic impedance, the thicker the dielectric the broader the transmission strip so that this choice is governed primarily by specific circuit requirements. In the case of the FD prototypes the determining factor was the line widths of the coupled sections of the quadrature couplers.

A choice of copper thickness and method of fixing to the dielectric should also be made. The thicker the copper the more uncertainty in the design equations in general, and the greater the likelihood of marked under-cutting of copper edges during etching. Also the thicker the copper the larger the airgap between dielectric layers in stripline applications so that usually the thinnest available copper layers are preferable. The copper layers may be electro-deposited or rolled copper foil. The latter has lower loss and is more suitable in critical applications but has poor adhesion properties making it more likely to lift from the dielectric during solering.

The dielectric may be copper clad on both sides or one side may be clad with aluminium foil or with aluminium, brass or copper plate. Brass and copper are much heavier and harder than aluminium. For initial prototype work, aluminium plate backings make it very simple to fix on co-axial to microstrip or stripline transitions, and lends strength to the structure.

It was decided to use soft board for ease of machining, and a low dielectric constant was preferred so that losses and step discontinuities were less likely to mask circuit operation. The available material was RT/duroid 5880 which is made of glass microfiber reinforced poly-tetra-fluoro-ethylene (PTFE). This material has a relative dielectric constant of 2.20 ± 0.02. Its full specifications are tabled in appendix E.

Two different thicknesses were used for the three layer structures needed to make stripline overlay couplers. The first, for the outer two layers, had a dielectric thickness of 0.062 ± 0.002 inches with a quarter inch thick aluminium backing plate, and a one ounce per square foot cladding of electro-deposited copper. The second board for the centre layer had a dielectric thickness of 0.005 ± 0.0005 inches and was clad on both sides by a half ounce per square foot layer of electro-deposited copper.

5.1.3 STRIPLINE

Stripline consists of a conducting strip suspended in a dielectric between two (ideally infinite in extent) ground planes. Usually the strip is suspended mid-way between the two ground planes. However if a three layer structure is used, as is necessary for the construction of overlay coupled lines, the conducting strip will be offset from the centre as shown in fig 5.2.

Howe[22] presents formulae developed by Rosenzweig which allow the calculation of characteristic impedance Z_o from the dimensions indicated in fig 5.2. These formulae have

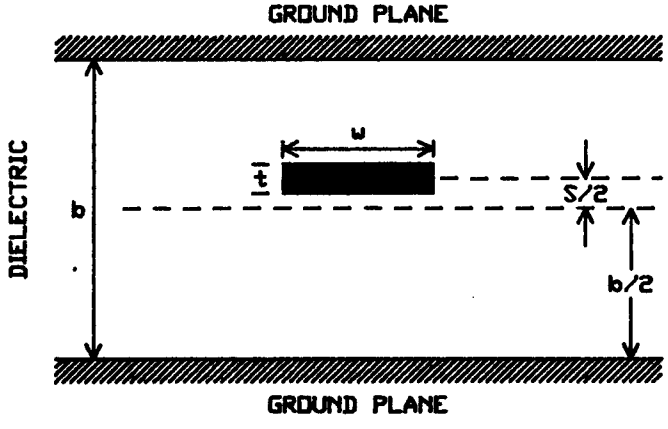

Fig 5.2 : **Stripline with offset centre conductor**

been rewritten in appendix F in a form which allows the calculation of strip width W for a given value of Z_o. A BASIC program which implements these formulae is also given as a useful design tool.

Rosenweig's method gives good results providing the following condition is met

$$\frac{W_{min}}{b - t} \geq 0.35 \qquad \ldots\ldots (5.1.1)$$

The minimum width lines calculated by this method are presented in table 5.1 for both boards used.

The BASIC program was applied to the substrates described in section 5.1.2 to provide widths of 50 ohm transmission lines etched on either board. The data and results are summarised in table 5.1.

The dominant mode of propagation in stripline is transverse electromagnetic (TEM). The maximum frequency of operation of stripline is the frequency at which transverse electric (TE) modes are excited. For wide lines the cut-off for the lowest order TE mode is given directly in GHz by[30]

$$f_T = \frac{15}{b\sqrt{\varepsilon_r}} \quad \frac{1}{(w/b + \pi/4)} \qquad \ldots\ldots (5.1.2)$$

Table 5.1 : **50 ohm strip transmission data**

	t (mm)	w_{min} (mm)	w(mm) (50Ω)	f_T (GHz)
0.062" board	0.036	1.134	2.610	19.5
0.005" board	0.018	1.141	2.657	19.3
b=3.277mm	s=0.127mm		ε_r=2.2	

where b and w are in cm. The cutoff frequencies for 50 ohm line are also included in table 5.1.

5.1.4 COUPLED STRIP TRANSMISSION LINES

Any section of transmission line whose electric and magnetic fields touch or encompass another transmission line can couple power to and from that line. Normally it is preferred that coupling be kept to a minimum but this property can be used to great advantage in hybrid circuits.

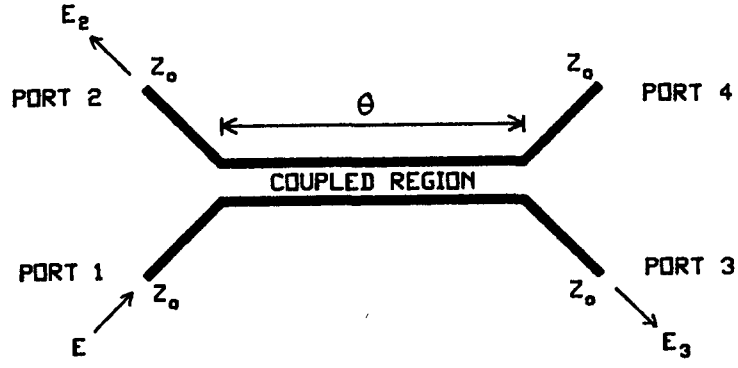

Fig 5.3 : **Pair of coupled transmission lines**

Fig 5.3 shows a pair of coupled transmission lines of electrical length θ. The centre frequency f_o is defined as the frequency at which $\theta = \pi/2$ radians, and is the frequency at which coupling is maximum. Let C_o be the centre frequency coupling factor, then in decibels the coupling is given by

$$C(dB) = -20 \log_{10}(C_o) \qquad \ldots\ldots (5.1.3)$$

If an incident wave E enters port 1 then waves E_2 and E_3 exit ports 2 and 3 respectively. No wave exits from port 4. Conservation of energy gives

$$|E|^2 = |E_2|^2 + |E_3|^2 \qquad \ldots\ldots (5.1.4)$$

The coupled outputs E_2 and E_3 are given by Young[18] as

$$\frac{E_2}{E} = \frac{jC_o \sin\theta}{\sqrt{(1-C_o^2)}\cos\theta + j\sin\theta} \qquad \ldots\ldots (5.1.5)$$

$$\frac{E_3}{E} = \frac{\sqrt{(1-C_o^2)}}{\sqrt{(1-C_o^2)}\cos\theta + j\sin\theta} \qquad \ldots\ldots (5.1.6)$$

Note that the factor j in the numerator of (5.1.5) is not present in the numerator of (5.1.6). This implies, since the denominators are identical and C_o is real, $0 \leq C_o \leq 1$, that there is a fixed ninety degree phase difference between outputs E_2 and E_3, independent of frequency.

Two orthogonal TEM modes can propagate on a pair of parallel coupled lines and these are termed the even and odd modes. In the even mode the respective voltages and currents on the two conductors are equal in magnitude and sign. In the odd mode the respective voltages and currents are equal in magnitude but are opposite in sign. Any set of voltage, current and field conditions can be expressed as a linear combination of these modes. Fig 5.4 shows the electric field patterns of each of these two modes.

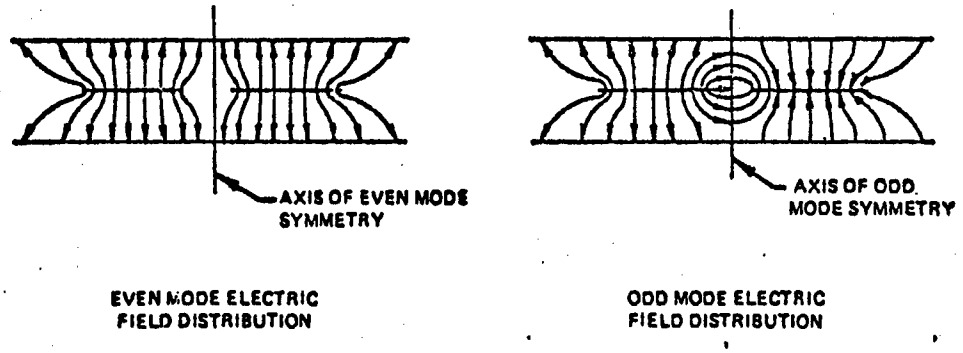

Fig 5.4 : **Even and odd mode electric field distributions**

If Z_{oe} and Z_{oo} are the odd and even mode impedances of a coupled line section then the overall characteristic impedance Z_o of the coupled line section is given by

$$Z_o^2 = Z_{oe}\, Z_{oo} \qquad \ldots\ldots (5.1.7)$$

Z_o should of course be matched to the rest of the circuit.

The coupling factor is then given by

$$C_o = \frac{(Z_{oe}/Z_{oo})-1}{(Z_{oe}/Z_{oo})+1} \qquad \ldots\ldots (5.1.8)$$

Alternatively normalised even and odd mode impedances Z_{oen} and Z_{oon} can be defined:

$$Z_{oen} = \frac{Z_{oe}}{Z_o} \qquad \ldots\ldots (5.1.9)$$

$$Z_{oon} = \frac{Z_{oo}}{Z_o} = \frac{1}{Z_{oen}} \qquad \ldots\ldots (5.1.10)$$

$$Z_{oen} = \sqrt{\frac{1 + C_o}{1 - C_o}} \qquad \ldots\ldots (5.1.11)$$

In stripline three different parallel coupled configurations can be used. These are shown in fig 5.5 and for convenience are termed edge-coupled, broadside-coupled and overlay-coupled, although of course overlay coupled lines may also be referred to as being broadside-coupled.

Edge coupled lines cannot achieve the very tight coupling necessary for 3dB couplers. Overlay couplers are preferable to broadside coupled lines since they are easier to construct with commercially available substrates.

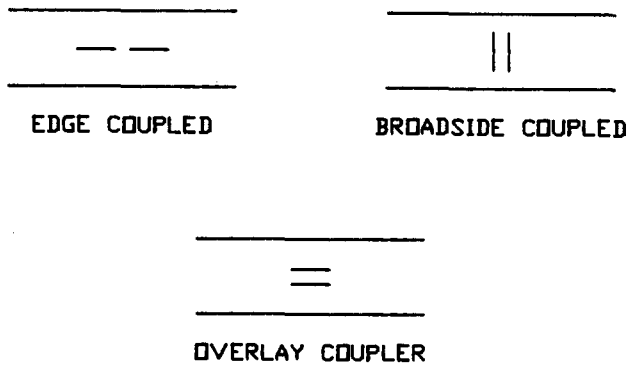

Fig 5.5 : Stripline coupled line structures

Cohn[31] has analysed the case of directly overlaid lines as shown in fig 5.6. The limitation of this method is that if b, s and relative dielectric constant ε_r are manufacturer specified as is usual, then Z_o cannot also be independently chosen but depends on coupling factor as does w. However, as will be shown in section 5.3 there are uses for Cohn's method. Appendix G gives a BASIC program useful for calculating w and Z_o from a modified version of Cohn's method, since Cohn intended that Z_o be specified and both s and w be chosen to suit the wanted coupling factor. The method is limited to cases in which

$$\frac{w}{s} > 0.35 \qquad \ldots\ldots (5.1.12)$$

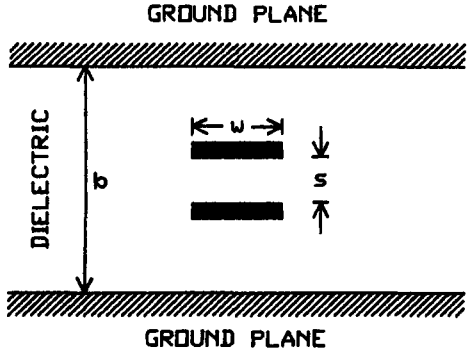

Fig 5.6 : Directly overlaid coupled striplines

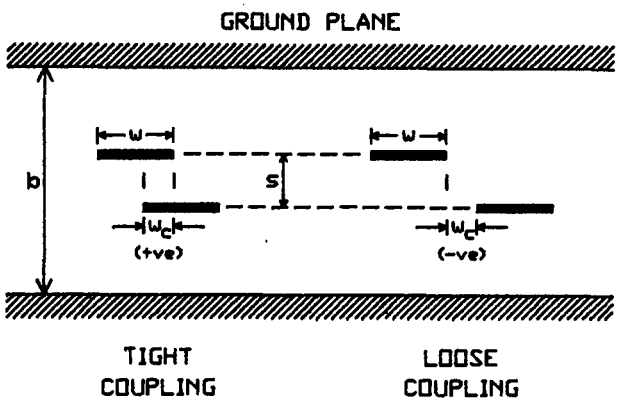

Fig 5.7 : Offset parallel coupled strip transmission lines

In general $w > s$ so this is rarely a problem. For $s = 0.127$ mm, $w > 0.04$ mm which is much narrower than the available etching facilities could produce.

Shelton[33] gives an alternative method in which the coupled lines are not directly overlaid but are offset from one another as shown in fig 5.7. This introduces a new overlap variable w_c which is positive in tight coupling cases and negative in loose coupling cases. This new variable allows Z_o to be specified independently and w and w_c to be calculated for a given coupling factor.

Appendix H contains a BASIC program useful for implementing Shelton's method. There are certain approximation conditions which must be met to ensure that the calculated values are reliable. The program reports when the method does not give usable results.

5.2 IN-PHASE POWER SPLITTERS

In-phase power splitters have frequently been referred to in the preceding text. A closer look at various types is needed to explain the choice of divider that was made.

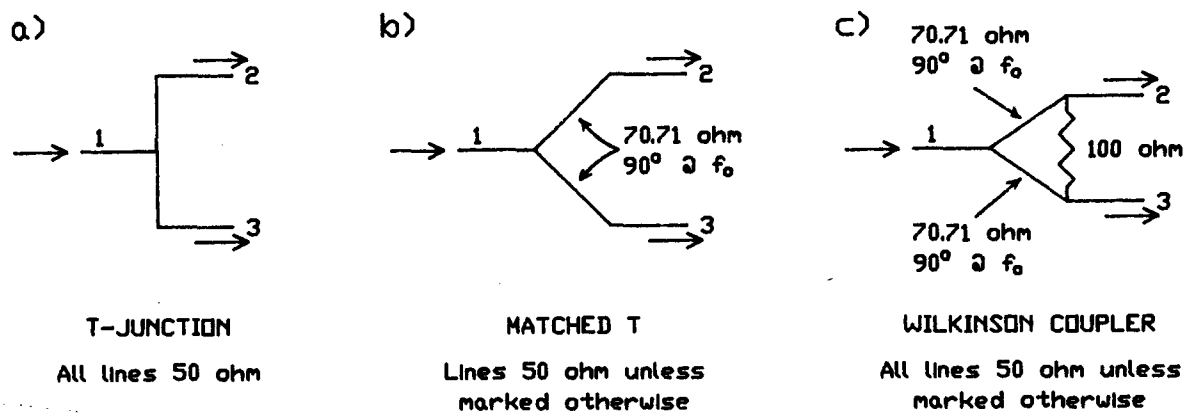

Fig 5.8 : In-phase power splitter types

5.2.1 SPLITTER TYPES

Reference was made in section 4.4.2 to using a quadrature coupler with an added ninety degree phase shifter as an in-phase power divider. This method has already been rejected as being unnecessarily large and complicated, and the discussion here will be limited to much simpler devices which, in any event, have better broadband characteristics.

Fig 5.8 shows the three different types of two way in-phase power splitters that should be considered. A comparison of the important ideal properties of the splitters at their designed frequency f_o is given in table 5.2.

The 'T junction' is simplest and has frequency independent properties. It's disadvantages are poor input and output matches and poor isolation between the output ports 2 and 3.

The 'matched T' uses quarter wave transformers to match the input port. For a quarter wave section of transmission line of characteristic impedance Z_o and load impedance Z_L, the input impedance Z_{in} is given by

Table 5.2 : Ideal properties of in-phase power splitters at their designed frequencies

	T JUNCTION	MATCHED T	WILKINSON
Power split	3.5 dB	3.01 dB	3.01 dB
Phase	In phase	In phase	In phase
S_{11}	-9.5 dB	zero	zero
S_{22} and S_{33}	-9.5 dB	-6 dB	zero
Isolation (S_{32})	3.5 dB	6 dB	Infinite

$$Z_{in} = \frac{Z_o^2}{Z_L} \qquad \ldots\ldots (5.2.1)$$

Thus if Z_o = 70.71 ohms and Z_L = 50 ohms then Z_{in} = 100 ohms. If placed in parallel with another 100 ohms the overall input impedance is 50 ohms. Thus the T of fig 5.8b) is matched to a source impedance of 50 ohms. However the matches at ports 2 and three and the isolation between ports 2 and 3 remain poor.

The 'Wilkinson Coupler' (WC) employs an isolating chip resistor as shown in fig. 5.8c). Note that aside from this it is identical to the matched T and thus has a properly matched input port. The isolating resistor causes a proper match at ports 2 and 3 and complete isolation between ports 2 and 3 at the designed frequency. The input match is not affected by the resistor. The WC is obviously the best choice. Power dividers of this type were first proposed by Wilkinson in 1960.

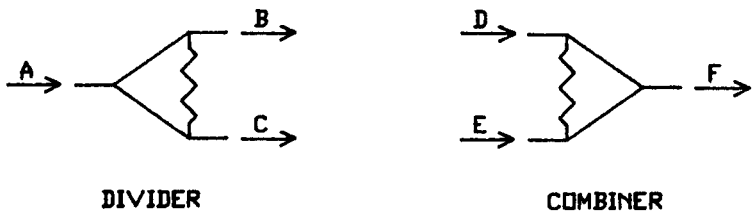

Fig 5.9 : **Wilkinson coupler as a divider and combiner**

5.2.2 WILKINSON COUPLER AS A POWER COMBINER

The Wilkinson Coupler (WC) described in section 5.2.1 is a passive device and hence must operate in the reverse direction in the same way it does in the forward direction. Fig 5.9 shows a WC used in forward and reverse directions as a power combiner and divider respectively.

In the case of the power divider, symmetry ensures that outputs B and C are equal in phase and magnitude. As a result the voltage across the isolating resistor is zero and there is no power loss in the device.

With the power combiner, inputs D and E may differ in both phase and amplitude. Consider first D and E equal in both phase and magnitude. The device is then operating precisely in reverse of the divider and no power is dissipated in the resistor.

Consider D and E equal in magnitude but differing in phase. The output power will not then equal the summed input powers and in the special case of the phase difference being 180 degrees no power will exit the device. All power entering the device will then be dissipated in the resistor. This is true at the designed frequency f_o, but away from f_o some power will be reflected back to the sources.

Although in the above case power is dissipated, it cannot be considered unwanted loss since signals in anti-phase should sum to zero and no power should be reflected. Consider now D and E equal in phase but not magnitude. Power loss in decibels is defined as

$$\text{loss (dB)} = -10\log_{10}\left[\frac{P_{out}}{P_{in}}\right] \quad \ldots\ldots (5.2.2)$$

where P_{out} is the power exiting the device and P_{in} the total power entering. Applying equation (5.2.2) to the WC combiner gives

$$\text{loss (dB)} = -10\log_{10}\left[\frac{\frac{1}{2}(D + E)^2}{D^2 + E^2}\right] \quad \ldots\ldots (5.2.3)$$

Power loss is plotted against the input amplitude ratio D/E in fig 5.10. Note that the loss varies between zero and 3dB, the lost power being dissipated in the resistor.

Once again this cannot really be considered unwanted loss since it is essential to the FD of fig 4.15 performing correctly. However this loss is the source of the factor 2 on the left hand side of equation (4.6.2). This loss

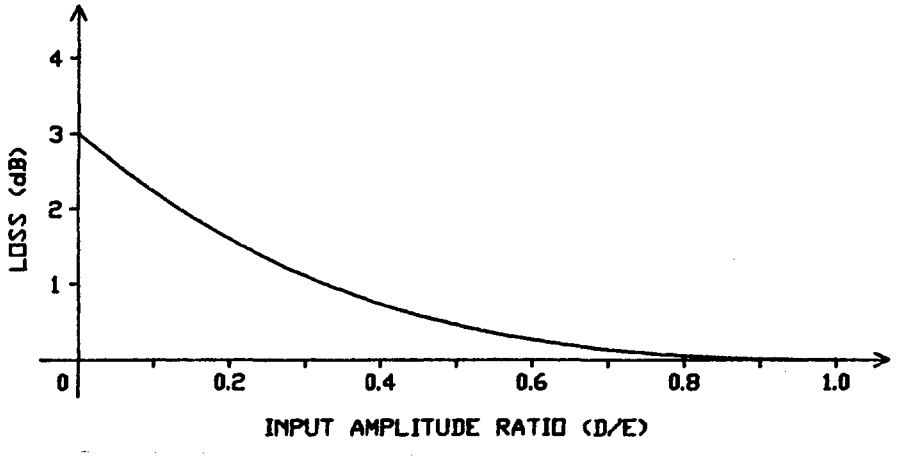

Fig 5.10 : Power loss in a WC combiner

must be borne in mind when factors like minimum sensitivity and required front-end amplifier gain are considered.

In the case of the FD in fig 4.16 there is always a total power loss of 3dB dissipated in the three WC combiners. This is usually acceptable in FDs since they are always driven by limiting amplifiers, and in any case additional loss is often added in the form of resistive detector input matching whatever the FD design.

5.2.3 BROAD-BANDING THE WILKINSON COUPLER

Sections of transmission lines a quarter wavelength long are frequently used as impedance matching networks. A single section (or pair of lines) was used in the matched T and WC described in section 5.2.1. These sections are generally designed to give a proper match at a centre frequency f_o, and the match becomes progressively less good away from f_o.

Usable bandwidth depends very much on what properties are of particular importance in a given application. For example bandwidth may be defined as the set of frequencies for which input VSWR is less than 1.2:1. In another application a 2:1 limit may be acceptable. Often in broad-band applications a single quarter wave matching section will not have sufficient bandwidth.

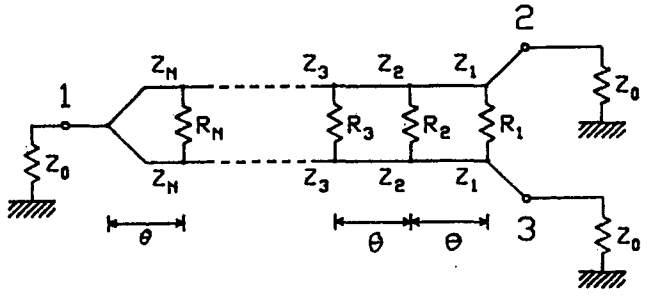

Fig 5.11 : **N-section Wilkinson coupler**
after Cohn

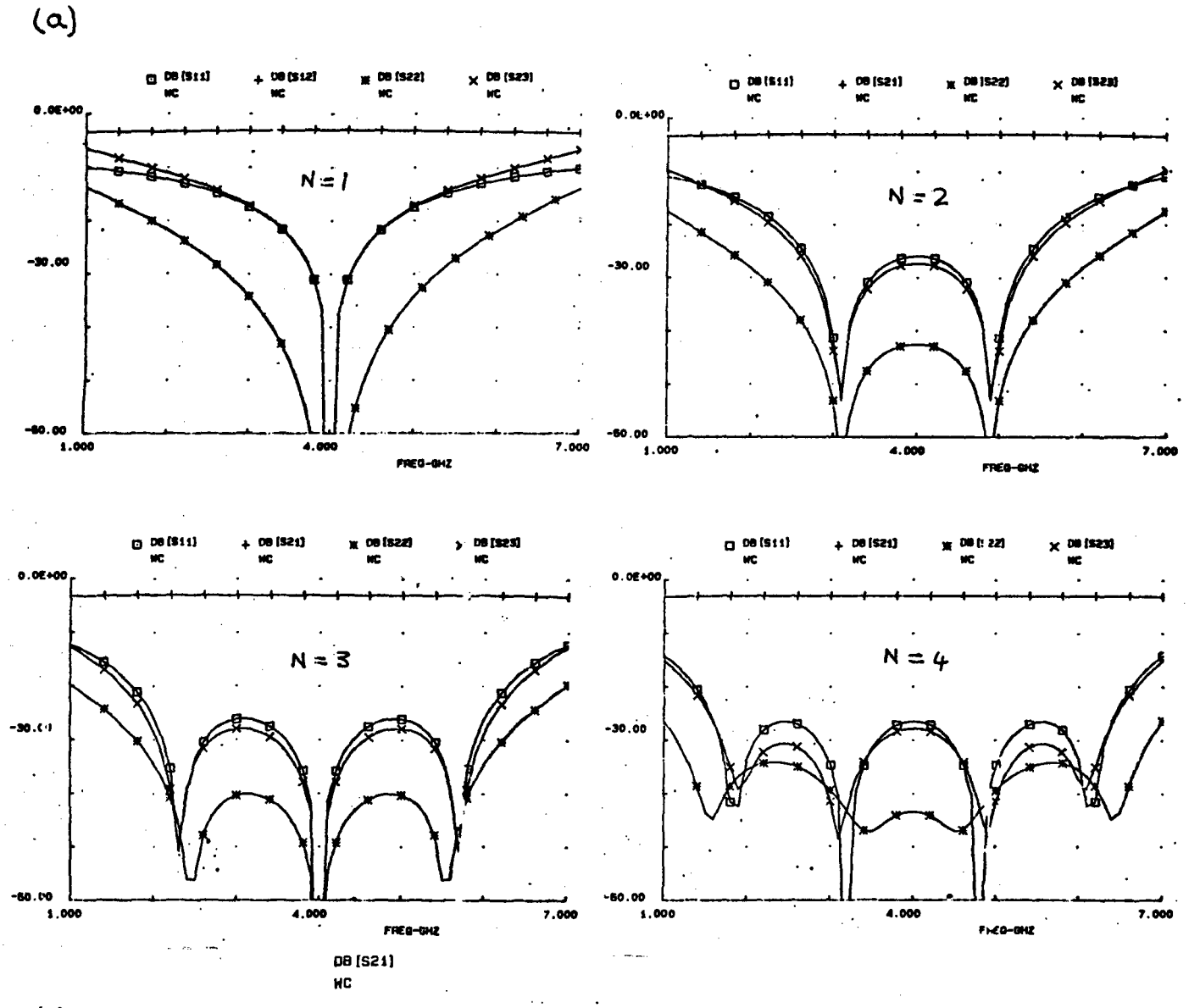

Fig 5.12 : Characteristics of WCs of 1 to 4 sections

a) Return loss and isolation

b) Transmission

The technique of increasing bandwidth by using cascaded quarter wave matching sections is well known. The same technique has been applied by Cohn[34] to broadband the Wilkinson coupler. Fig 5.11 shows a generalised N-section WC, θ = 90 degrees at f_o.

Z_1 to Z_n need to be carefully chosen to realise, for example, an equal-ripple or maximally flat pass-band characteristic. R_1 to R_n must then be selected for best input matches at ports 2 and 3, and best isolation between ports 2 and 3. Cohn[34] presents a useful table of values of Z_i and R_i for equal ripple WCs. These values were used in conjunction with TOUCHSTONE to produce the input match, isolation and transfer curves in fig 5.12 for WCs of one to four sections. A sample TOUCHSTONE circuit file for a three section WC is given in appendix B-4.

Cohn's tabulated values were used to design WCs prior to prototyping various FDs.

5.2.4 EXPERIMENTAL WILKINSON COUPLERS

A number of WCs of different lengths and on different substrate thicknesses were constructed during the course of this project. The measured results of two of them are presented here since the first was used in the FD prototypes and the second for detector matching. Their results are in any case indicative of the observations made in the other cases. A single section WC constructed on microstrip performed most nearly ideally but did not have sufficient bandwidth. All the WCs constructed were designed for a centre frequency of 4 GHz to suit the 2 to 6 GHz band requirement.

All results presented were measured on a Hewlett Packard HP 8410C network analyser controlled by an accuracy enhancement program on an HP 85 desk-top computer.

Fig 5.13 : **Disassembled stripline 3-section Wilkinson coupler**

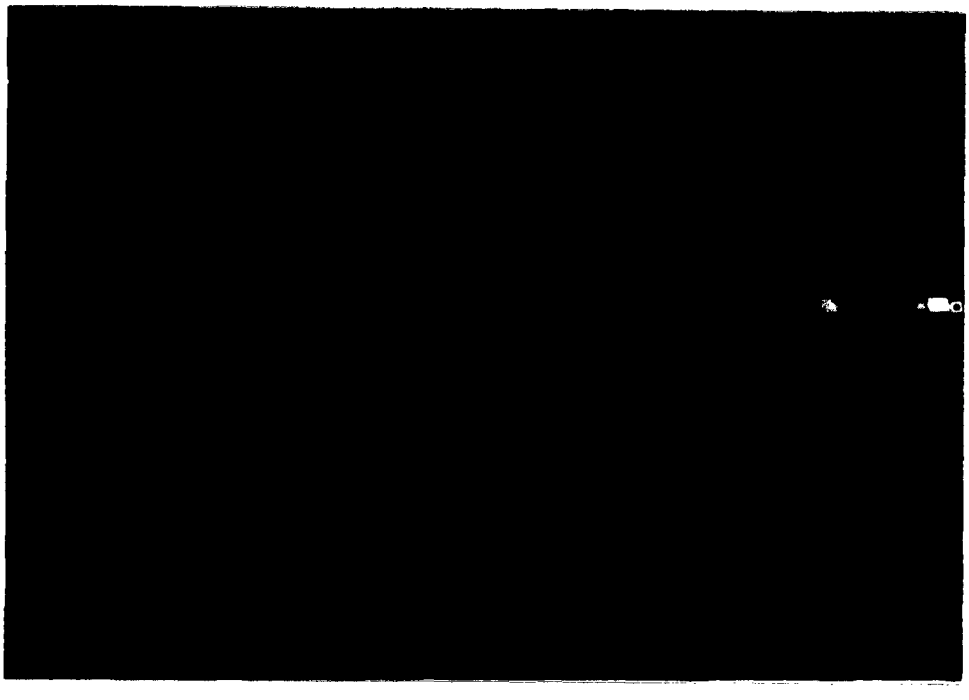

Fig 5.14 : **4-Section microstrip WC as used for detector matching**

Table 5.3 : 3-Section stripline WC design data

SECTION N	IMPEDANCE Z_N	WIDTH (mm)	$\lambda/4$ LENGTH (mm)	$R_{nominal}$ (ohms)	R_{used} (ohms)
1	57.49	2.08	12.64	400.0	400
2	70.71	1.41	12.64	211.5	200
3	86.98	0.91	12.64	107.2	100
	50.00	2.61	12.64		

Fig 5.13 shows a disassembled stripline 3-section WC which was designed for use in the FD prototypes. Cohn's[34] tabulated parameters for a three section WC of nominal 3:1 bandwidth were used. Bandwidth here is the ratio of the high frequency band limit to the low frequency limit. A three layer structure was used since overlay quadrature couplers were also required for the FD prototypes. The materials used were those described at the end of section 5.1.2. The program of appendix F was used to design the strip widths. Available resistor values closest to Cohn's nominal values were chosen. These were thick film chip resistors since microwave chip resistors were not available. Table 5.3 summarises the design data.

Fig 5.15 shows the measured data of the stripline WC. Deviation from ideal behaviour is fairly marked for several reasons. The use of available rather than nominal resistance values has only a small effect on matches S_{22} and S_{33}, and isolation S_{23} as demonstrated on TOUCHSTONE. The use of thick film chip resistors has the effect of raising the frequency at which S_{22}, S_{33} and S_{23} are best. This can best be seen by considering a single section WC. Isolation occurs because the signal passing through the

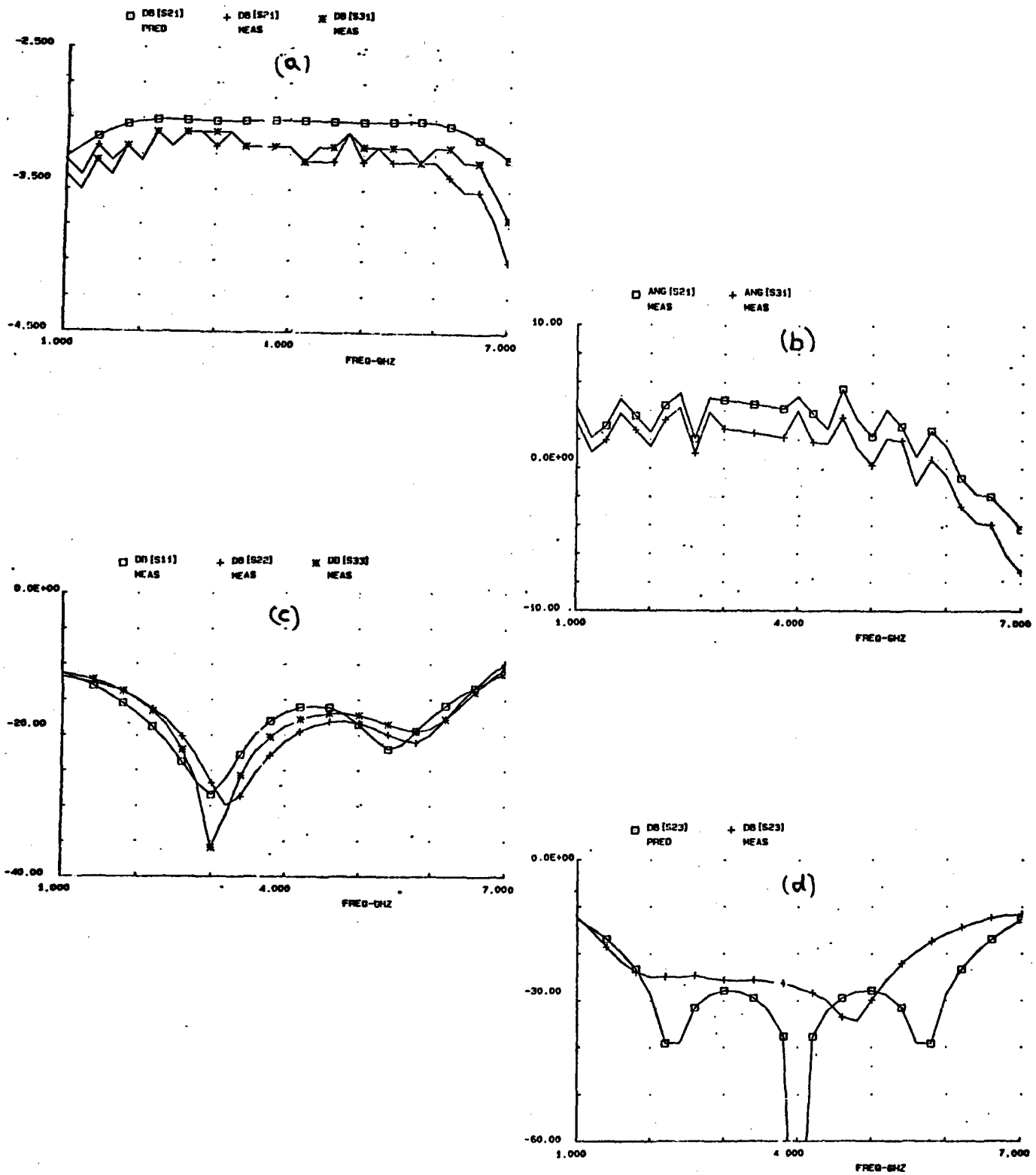

Fig 5.15 : **Measured results of 3-section stripline WC**

a) S_{21} and S_{31} compared with ideal S_{21}
b) Deviation from linearity of S_{21} and S_{31} phases
c) Input matches S_{11}, S_{22} and S_{33}
d) Measured and theoretical isolations S_{23}

zero length resistor is equal in magnitude to but 180 degrees out of phase with the signal passing along the two arms of the matching section. If, say, the resistor has an electrical length of ten degrees then isolation occurs at the frequency for which the combined length of the matching arms is 190 degrees. The higher the frequency the greater the electrical length of a transmission line so isolation must now be best at a higher frequency. This is a gross simplification but it does indicate the trend. This effect is seen most easily in fig 5.15(c) where the dips of S_{22} and S_{33} occur slightly higher in frequency than those of S_{11}. This effect can be minimised by using physically small microwave chip resistors which have short electrical lengths.

Errors are also caused by impedances not being quite correct due to approximations in the design formulae and errors arising from photographic reduction and etching. The co-axial to stripline transitions visible in fig 5.13 cause the actual measured values to be slightly different from the true values. Allowances must be made for the fact that slight instability in the sweep signal generator of the network analyser meant that amplitudes could only be measured to about ± 0.2dB, and phases to about ± 1 degree. Phase deviations between outputs 2 and 3 are also due to slight differences in the attached lengths of transmission line.

The centre frequency was a little low due to the difficulty of determining exactly what length constituted ninety degrees at 4 GHz. The use of curved sections complicated this, and parasitic reactances due to fairly tight curves was yet another cause of deviation from ideal behaviour. Straight lines would have been easier but curved lines were chosen to reduce the overall component length.

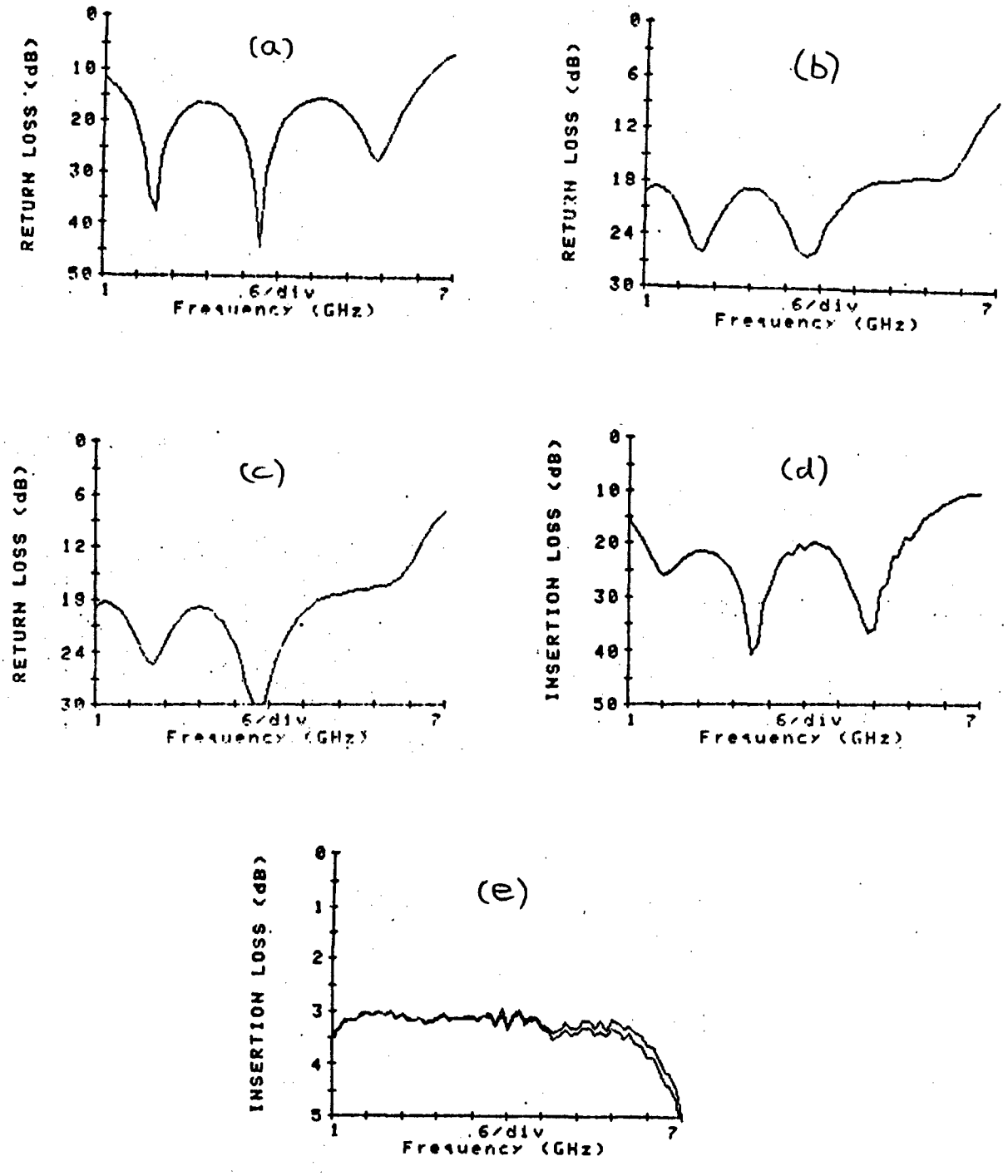

Fig 5.16 : Measured results of 4-section microstrip WC

a) input match S_{11}

b) output match S_{22}

c) output match S_{33}

d) isolation S_{32}

e) transfer S_{21} and S_{31}

Table 5.4 : **4-Section microstrip WC design data**

SECTION N	IMPEDANCE Z_N	WIDTH (mm)	$\lambda/4$ LENGTH (mm)	$R_{nominal}$ (ohms)	R_{used} (ohms)
1	55.79	2.05	13.70	482.2	470
2	64.79	1.61	13.80	291.6	270
3	77.18	1.19	13.91	172.6	180
4	89.63	0.89	14.01	103.2	100
	50.00	2.43	13.63		

Nevertheless the worst case input return loss was 14.9dB and the worst case isolation 15.7dB over 2 to 6 GHz. The power split was 3.2dB indicating a 0.2dB loss and the maximum difference in amplitude between the outputs was 0.2dB. Fig 5.15(b) shows that the phases were fairly linear up to about 6 GHz and the maximum phase difference was two degrees. It was decided that these values were suitable for demonstrating the operation of prototype FDs.

Fig 5.14 shows a four section microstrip WC that was used for matching detectors as described in section 5.4. This WC was built on RT/Duroid 5880 with a dielectric thickness of 0.031". Once again Cohn's tabulated parameters were used for a nominal 4:1 bandwidth. The program of appendix I was used to design the strip widths. Again available thick film chip resistors were used. Table 5.4 summarises the design data.

Fig 5.16 shows the measured data of the microstrip WC. Again there are marked deviations from the ideal behaviour shown in fig 5.12. The reasons are essentially the same

as for the stripline WC. The measured centre frequency is still below the designed frequency of 4 GHz. This is particularly well shown by (b), (c) and (e) of fig 5.16.

Over 2 to 6 GHz the worst case return loss is 15.4dB, and the worst case isolation is 15.5dB. Over 1.2 to 5.8 GHz, however, the worst case isolation is 19dB. The transfer characteristics S_{21} and S_{31} are centred about 3.2dB suggesting a 0.2dB loss. The maximum phase difference between these outputs is one degree.

5.3 QUADRATURE COUPLERS

Ideal quadrature coupler (QC) behaviour has already been described in section 4.2. Several different types of couplers have been reported in the literature and a brief look at some of these, plus methods of broadbanding, will help to explain the QC choice that was made for construction of the FD prototypes.

5.3.1 QUADRATURE COUPLER TYPES

Quadrature couplers described in the literature are generally variations or combinations of the four basic types of QC illustrated in fig 5.17. The parallel coupled line QC shown in fig 5.17a) is the most commonly used type since it can easily be applied to almost every transmission medium. This type has already been covered theoretically in section 5.1.4. It is particularly easy to construct in both microstrip and stripline, but in microstrip only edge coupling can be used. Practical difficulties in etching extremely narrow gaps between lines make 3dB edge coupling all but impossible.

Lange[35] introduced interdigitated couplers in 1969, as illustrated in fig 5.17(b). This method allows 3dB coupling to be achieved in microstrip but requires very accurate etching since finger widths and gaps are of the order of

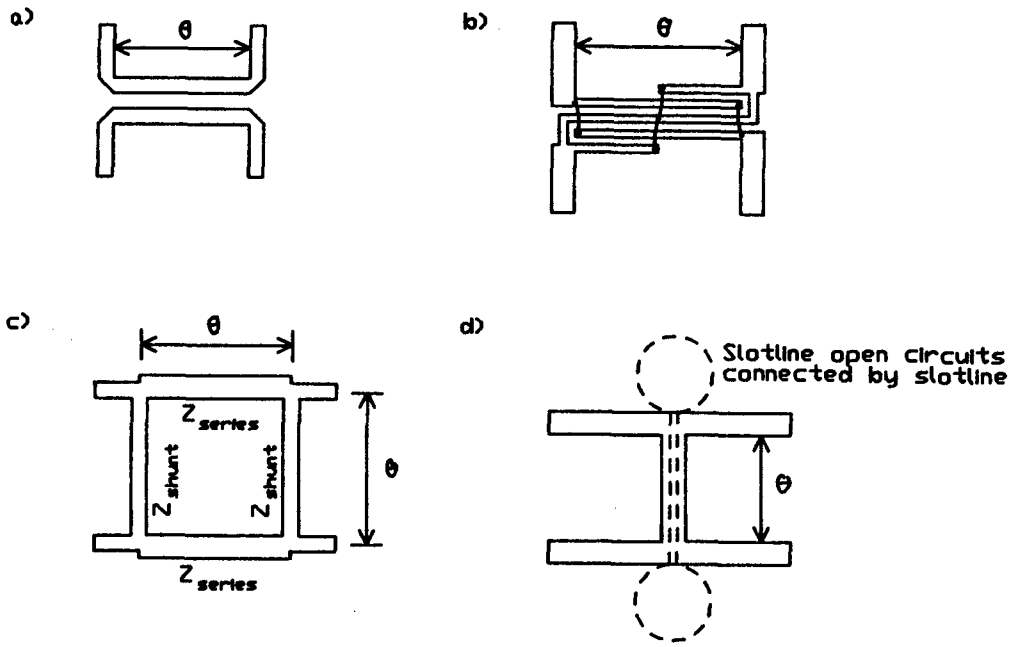

Fig 5.17 : **Basic quadrature coupler types**

a) Parallel coupled lines

b) Lange coupler

c) Branch-arm coupler

d) Slotline coupler

θ = ninety degrees at centre frequency.

0.05 mm[36]. Bond wires are required to interconnect the fingers as shown. Neither bonding nor suitable etching facilities were available which ruled out this choice.

Branch-arm couplers, as shown in fig 5.17(c), are another well known 3dB coupling structure[22]. These are well suited to both microstrip and stripline but are difficult to broadband since the phase difference between outputs is frequency dependent. The quadrature relationship holds only at the centre frequency f_o.

In broad-band applications slotline couplers shown in fig 5.17(d) are frequently used.[20,37,38] These are generally combinations of microstrip and slotline etched on opposite sides of the board. 3dB coupling can be achieved but

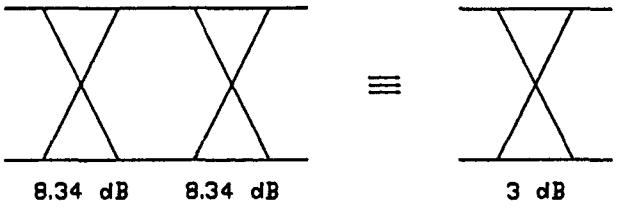

Fig 5.18 : **Achieving 3dB coupling through cascaded 8.34dB couplers**

accurate etching and alignment of both sides of the board is required.

There is a way of constructing 3dB couplers from cascaded 8.34 dB couplers as shown in fig 5.18. Edge coupled lines may then be more easily used. Disadvantages are that circuits increase in size and deviations from ideal behaviour are compounded in both couplers. Also when couplers are broadbanded some of the coupling sections require tighter coupling that the nominal coupling, so that this method may not overcome the original problem.

With the available facilities and required bandwidths the parallel coupled line QC was the only suitable choice. 3dB coupling requirements eliminated microstrip and stripline was the medium chosen.

5.3.2 BROADBANDING THE QUADRATURE COUPLER

There are two main methods of broadbanding the quadrature coupler. Fig 4.3 shows the transfer curves of a single parallel coupled line section QC designed to give exactly 3dB coupling at the centre or designed frequency f_o. The first method involves allowing the transfer curves to overlap each other and defining the bandwidth as indicated by the dashed lines in fig 5.19.

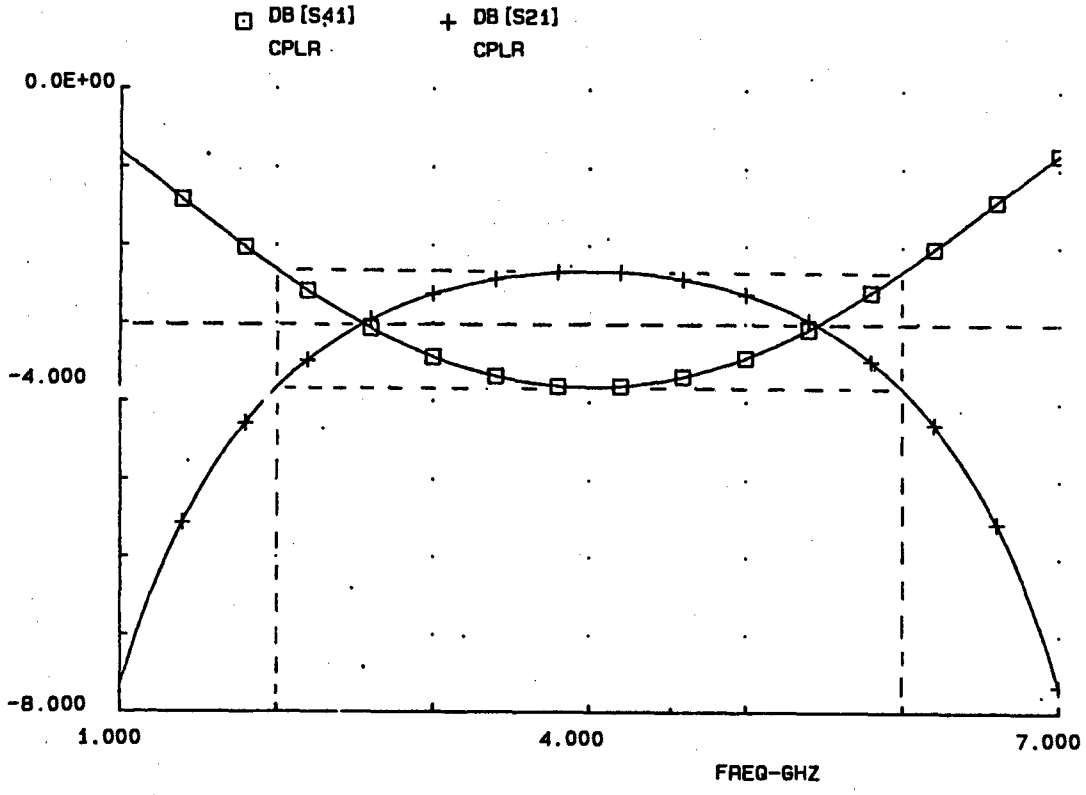

Fig 5.19 : 2-6 GHz single section coupling characteristic

The coupler whose characteristics are shown in fig 5.19 covers the bandwidths 2 to 6 GHz. The penalty is that the coupling is actually 3 ± 0.8dB. In some applications this will be acceptable and in others not. Note that the nominal centre frequency coupling is now 2.3dB.

The second method of improving bandwidth involves using multiple cascaded sections as shown in fig 5.20. Note that each section is a quarter wavelength long at the designed centre frequency, and that the pairs are drawn closer together to indicate tighter coupling.

Fig 5.20(a) shows a symmetric five section coupler in which the centre section is most tightly coupled. Symmetric couplers of this form retain the fixed ninety degree output phase difference of single section couplers. In general the more coupled sections the greater the bandwidth and the flatter the response.

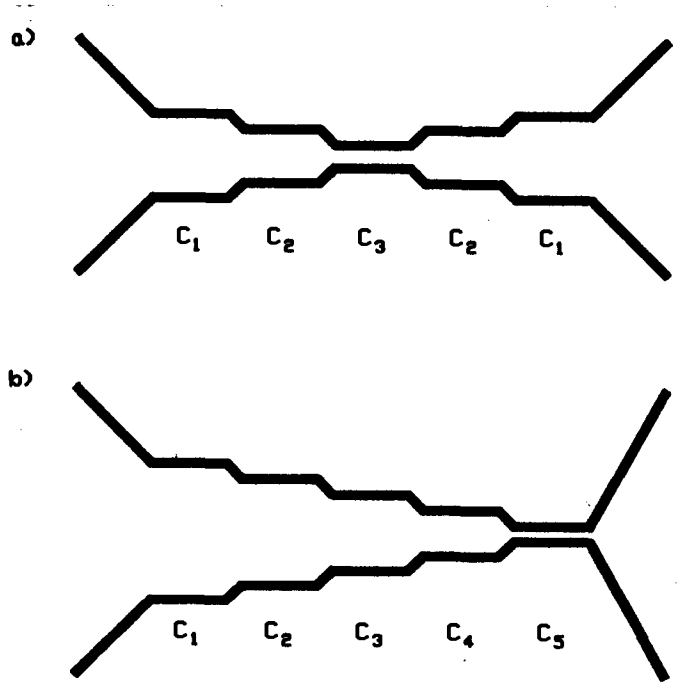

Fig 5.20 : **Stepped 5-section directional couplers**

a) symmetric

b) assymmetric

The coupling factors C_i must be carefully chosen to give, for example, an equal-ripple or maximally flat response. Cristal and Young[39] give very useful design tables for symmetric couplers. Note that the centre section is always more tightly coupled than the overall coupling factor.

Fig 5.20(b) shows an assymmetric coupler in which tightest coupling occurs at one end. Couplers of this sort do not, however, retain the fixed ninety degree phase difference between outputs. Instead the phase difference is frequency dependent and the actual form depends on the number of sections. Whereas symmetric couplers are limited to odd numbers of coupled sections assymmetric couplers are not, but the phase characteristic rules out couplers of this type for the FD prototypes.

The QCs described above have step discontinuities at the junctions between sections of different coupling co-efficient. At the lower end of the microwave range, and certainly below 6 GHz, these discontinuities cause only minor errors. The alternative to using stepped quarter wave sections is to use continuously tapered coupled lines. These work better at higher frequencies but are more difficult to design and are usually slightly larger than equivalent stepped couplers[22]. Most reported 3dB tapered line couplers are in fact cascaded 8.34dB couplers[40,41] which increases the size further.

Stepped symmetric couplers were chosen for the FD prototypes because of their ease of construction in stripline, broad bandwidths and good phase properties.

5.3.3 CENTRE SECTION SYMMETRY

Accurate phase performance of quadrature couplers depends very much on symmetrical design.[42,43] Fig 5.21 illustrates the problem for single section couplers but applies equally to the centre section of multi-section symmetric couplers. To ensure that the coupled and direct outputs exit from the same side of the coupler, the lower and upper conducting strips of an overlay coupler must cross over each other.

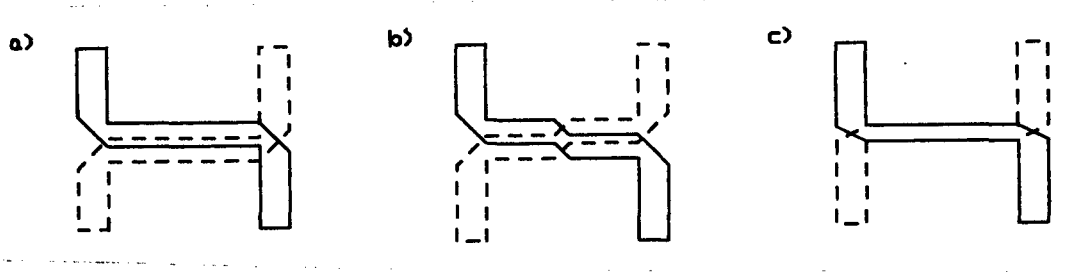

Fig 5.21 : Single section overlay coupler layouts

If offset parallel coupled lines are used, as is preferable since both coupling and characteristic impedance can be controlled for given materials, then the simplest construction is that shown in fig 5.21(a). Note however the difference in form at each end of the coupled region. This is a potential source of phase errors and a coupler of this type that was built in the early stages of this project had a very poor phase performance above the designed frequency of 4 GHz.

Symmetry can be regained by using the form shown in fig 5.21(b). The difficulty with this is that the centre crossing section has to be very carefully tailored to maintain a constant coupling factor. Even if this is done, characteristic impedance cannot be properly controlled through this region unless the separation between the conductors (s in fig 5.6) can also be varied. An initial attempt at a five section 8.34dB coupler proved to be overcoupled to the extent of nearly 2dB on testing.

The best solution is to use directly overlaid lines as shown in fig 5.21(c). Characteristic impedance is then determined by the materials used and in general will not equal the terminating impedances. In this case the coupler must be matched to the rest of the circuit as shown in the next sub-section.

5.3.4 MATCHING THE CENTRE SECTION

The impedance mis-matches at the inputs and outputs of networks can often be matched for broad-band operation by using multiple quarter wave sections. The temptation is to treat any given n-section coupler as a black box and try to match the input impedances seen at the four ports. Fig 5.22(a) shows the ideal transfer characteristic of a symmetrical five section QC (from the tables of Cristal and Young[39]). The impedance data for figs 5.22 and 5.23 are tabulated in table 5.5.

Table 5.5 : **Impedance data for figs 5.22 and 5.23**

SECTION N	Normalised Z_{oe}	Z_N (ohms) fig 5.22a)	Z_N (ohms) 5.22b) & c)	Z_N (ohms) 5.22d) & e)	Z_N (ohms) 5.23a) & b)	Z_N (ohms) 5.23c) & d)	Z_N (ohms) 5.23e) & f)
3	3.81243	50.0	33.1	33.1	33.1	33.1	33.1
2	1.32624	50.0	50.0	50.0	40.6	37.9	35.9
1	1.05972	50.0	50.0	50.0	50.0	43.7	40.7
external	—	—	—	40.6	—	—	46.1

If materials limitations give a characteristic impedance for a directly overlaid centre coupling section of 33 ohms, then the unmatched transfer and isolation characteristics are shown in figs 5.22(b) and (c). The input impedance at 4 GHz seen at the four ports is also 33 ohms. The quarter-wave matching relation

$$Z_{in} = \frac{Z_o^2}{Z_L} \qquad \ldots\ldots (5.3.1)$$

where we require the input impedance Z_{in} to be 50 ohms and the load impedance is 33 ohms, indicates the characteristic impedance Z_o of the matching section should be 40.6 ohms. The dip in fig 5.22(e) shows that this does match the coupler at 4 GHz. Note, however, that fig 5.22(d) shows the effect is extremely narrow band (note also that the scale is different from (b)), and that the transfer characteristic is worsened even only a short way from 4 GHz. This is because the original input impedance was frequency dependent. Other matching techniques, such as the use of open circuit or short circuit stubs, can be used but these greatly increase the size and complexity of the coupler.

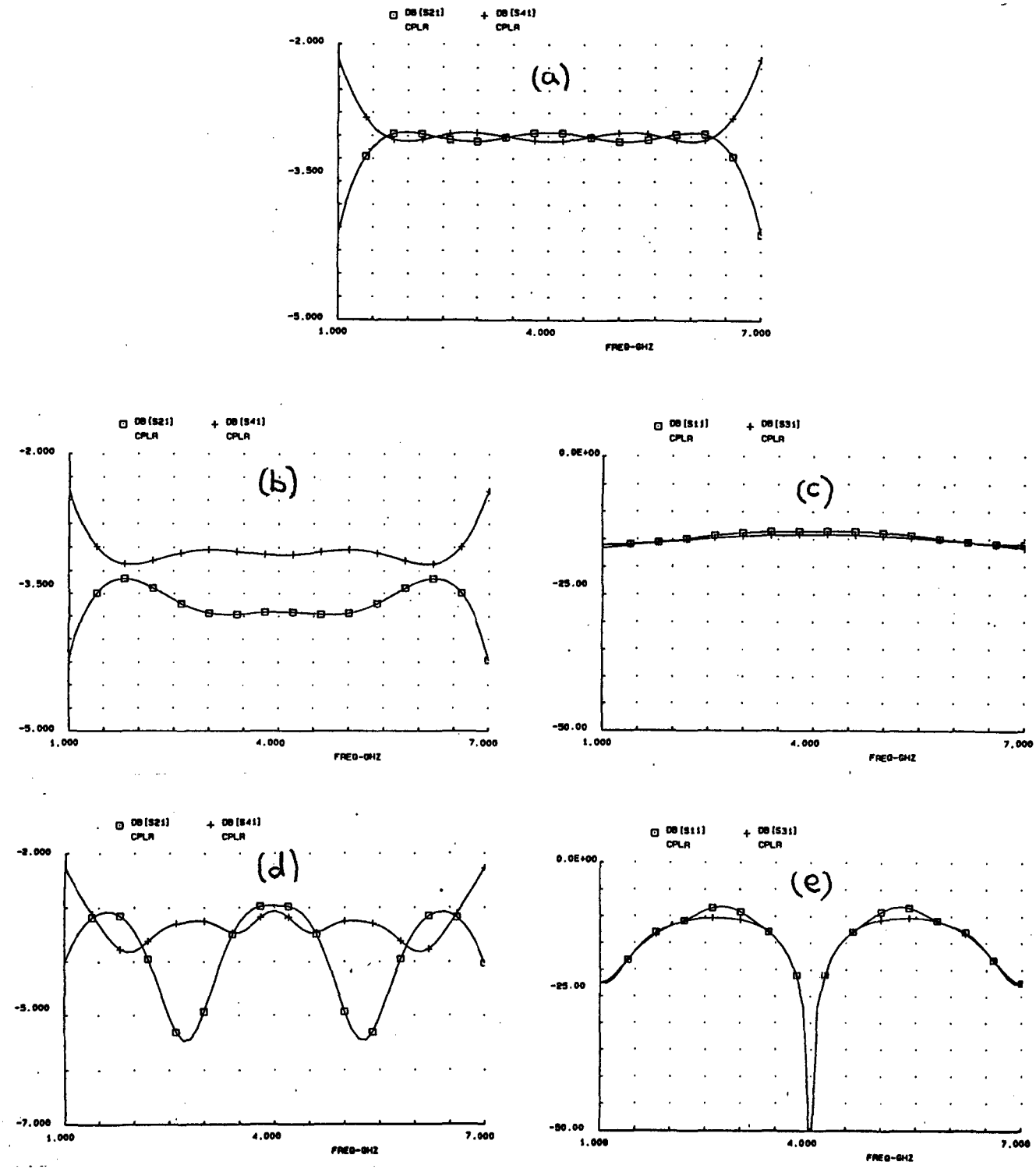

Fig 5.22 : Five section coupler characteristics

a) Ideal transfer curves, all sections 50 ohm

b) Transfer curves for centre section 33 ohm

c) Mismatch (S_{11}) and isolation (S_{31}) for case (b)

d) Transfer curves with one external matching section

e) Mismatch (S_{11}) and isolation (S_{31}) for case (d)

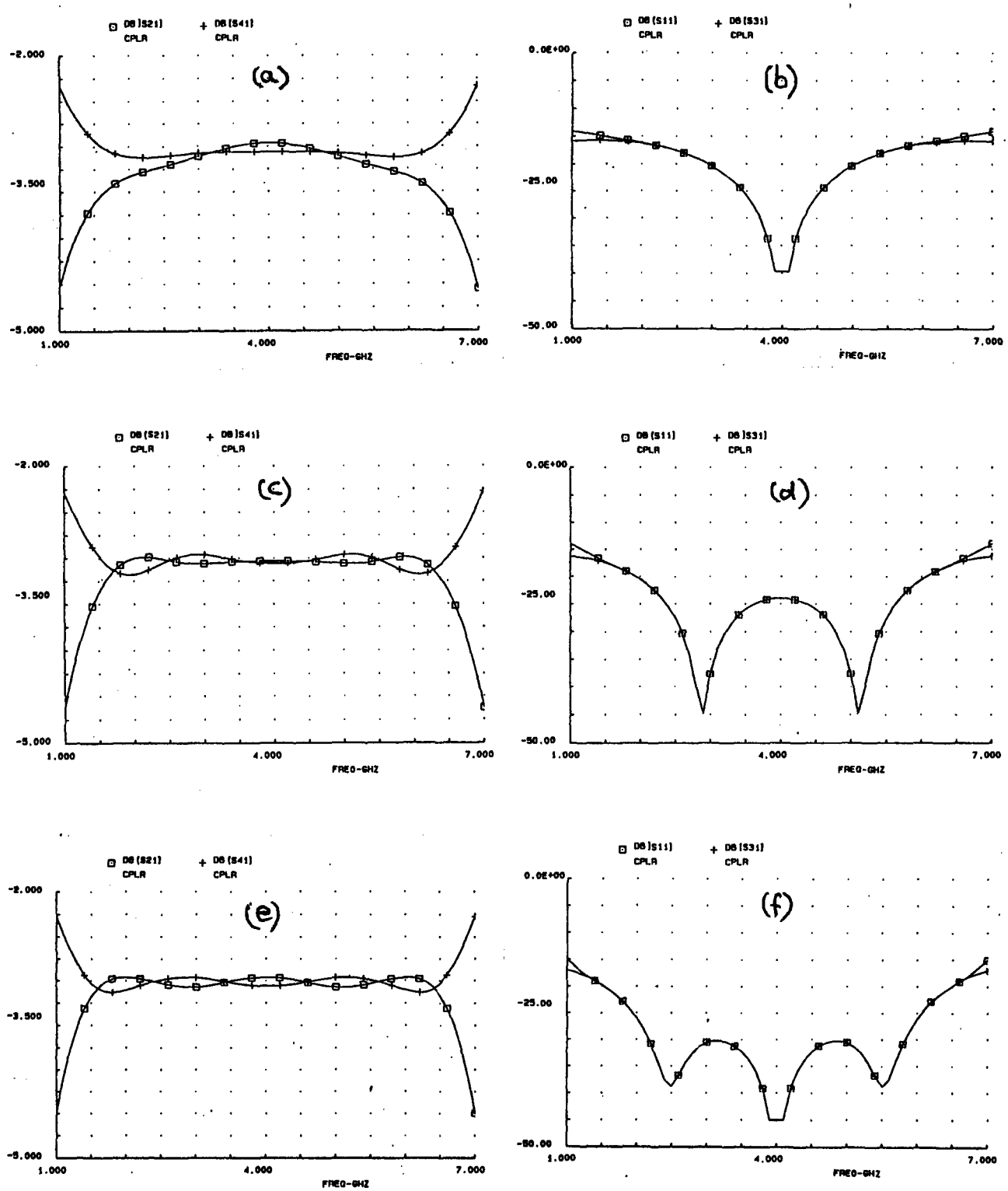

Fig 5.23 : **Five section coupler characteristics, part 2**

a) One internal matching section
b) Mismatch (S_{11}) and isolation (S_{31}) for (a)
c) Two internal matching sections
d) Mismatch (S_{11}) and isolation (S_{31}) for (c)
e) Two internal and one external matching section
f) Mismatch (S_{11}) and isolation (S_{31}) for (e)

Young[18] equated analytically TEM-mode directional couplers and stepped-impedance filters. This suggests that the quarter wave coupling sections already present in multi-section couplers, can be used to match the impedance of the centre pair. This can be done by varying their characteristic impedances in exactly the same way as is done with the more familiar quarter-wave matching.

For example, the sections on either side of the centre section can be designed to have a characteristic impedance of 40.6 ohms as was required for the external matching sections. Figs 5.23(a) and (b) show the effect of doing just that. Comparison with figs 5.22(b) and (c) shows that there is a marked improvement in performance.

When more than one matching section is used, the impedances should be chosen to give some desired trend (eg. equal-ripple or maximally flat) and bandwidth. Matthaei et al[44] present very useful tables for Tchebyscheff quarter-wave transformers. These have been used for two and three section matching to select the data tabulated in the last two columns of table 5.5.

Figs 5.23(c) and (d) show the effect of double section matching. The bandwidth has notably improved. To demonstrate that additional external matching sections can also be used, figs 5.23(e) and (f) show the result of using three matching sections. In this case the first two sections are the internal coupling sections and the last is added externally as an uncoupled section on each of the four ports. The result is a characteristic very close to the original form shown in fig 5.22(a).

5.3.5 MEASURED RESULTS OF THREE-SECTION OVERLAY COUPLER

Mathematical analysis (see chapter 6) indicated that single section overlay couplers would have been sufficient for

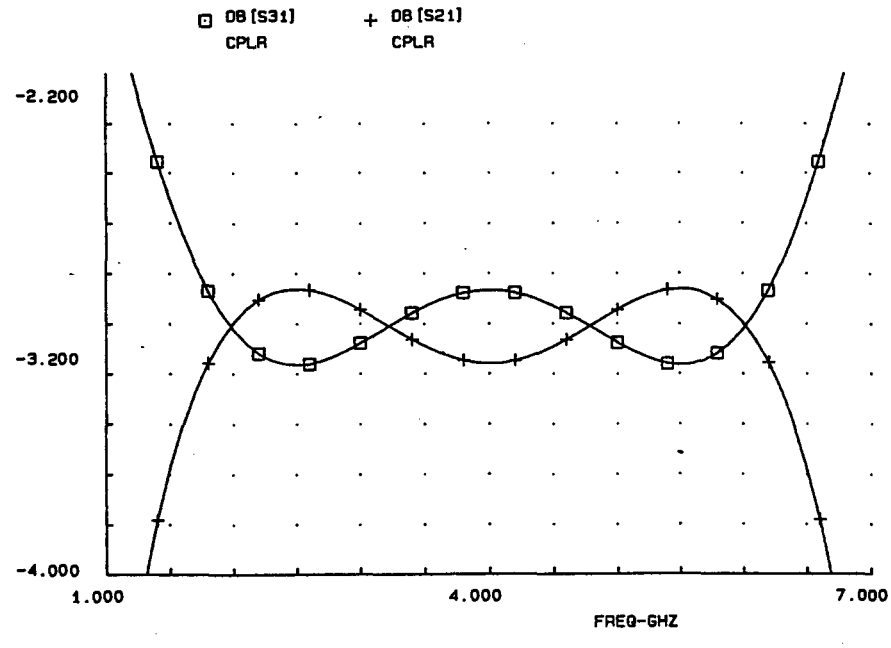

Fig 5.24 : Theoretical response of 3 section, 3dB, ± 0.15dB ripple coupler

the 2 to 6 GHz prototypes. However for directly overlaid couplers the characteristic impedance would have been very different from fifty ohms, the actual value being dependent on the precise mid-band coupling. This would require quarter wave matching, thus enlarging the coupler so that three section couplers might just as well be used. The choice of the fifty ohm base impedance was necessary to suit the available test equipment. An alternative solution would be to accept the coupler centre section impedance and use that as a base impedance for the rest of the circuit.

A look at Cristal and Young's design tables[39] for three section 3dB equal ripple couplers, showed that the centre section of the ± 0.15dB ripple version had a characteristic impedance of 50.04 ohms for directly overlaid lines in the available materials. This coincidence made this coupler an obvious choice since the theoretical mis-match was better than -60dB. Choosing the characteristic impedance of the

Table 5.6 : **Design data for 3-section coupler**

Section N	Normalised even mode impedance	Z_o (ohms)	Conductor width (mm)	Conductor offset (mm)	$\lambda/4$ (mm)
1	1.19039	50.02	2.540	-0.520	12.63
2	3.34049	50.04	0.870	-	12.63
b = 3.277 mm		s = 0.127 mm		ε_r = 2.2	

outer sections to be 50.02 ohms to match the centre section is not really necessary and almost certainly beyond the available etching resolution, but nothing is lost in including it in the design.

Fig 5.24 shows the theoretical response of this coupler. The design data is included in table 5.6. Fig 5.25 shows the coupler design actually used magnified by a factor of two. Cohn's and Shelton's design procedures were used to generate the conductor widths and gaps given in table 5.6. The data for the attached 50 ohm lines is given in table 5.1. The coupler was etched on both sides of the 0.005" board.

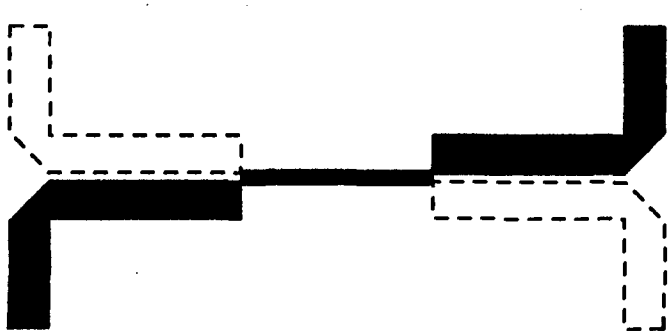

Fig 5.25 : **3-section coupler layout, twice actual size**

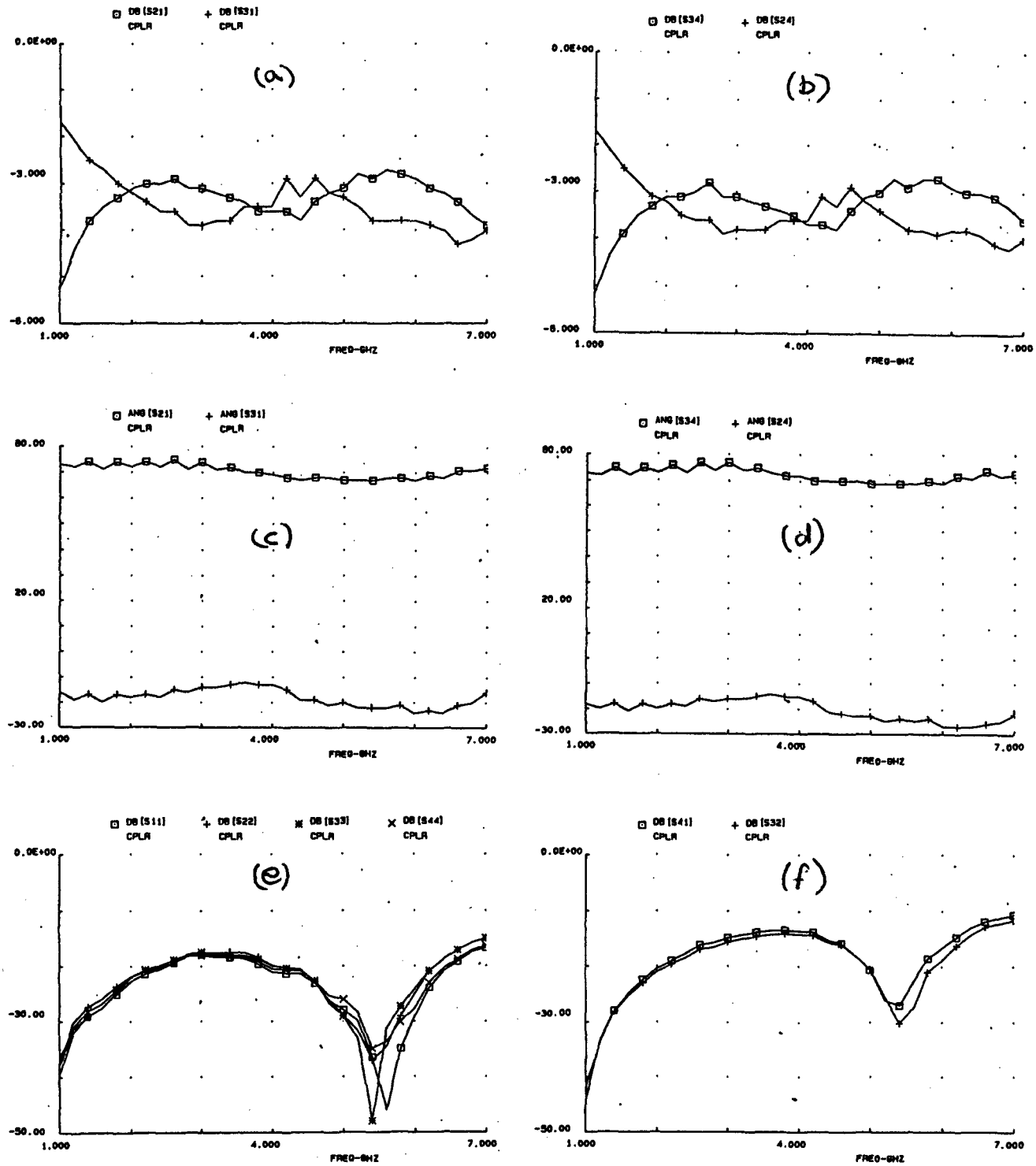

Fig 5.26 : **Measured 3-section coupler characteristics**

a) transfer functions S_{21} and S_{31}

b) transfer functions S_{24} and S_{34}

c) linearly adjusted phases of S_{21} and S_{31}

d) linearly adjusted phases of S_{24} and S_{34}

e) mis-matches S_{11}, S_{22}, S_{33} and S_{44}

f) isolation S_{41} and S_{32}

Fig 5.26 shows the measured results of the three section coupler. The transfer characteristics S_{21}, S_{31}, S_{34} and S_{24} are shown in (a) and (b). The trend is clear although performance deteriorates above 6 GHz. The coupling is approximately 3.3 ± 0.5dB indicating an overall loss of about 0.3dB. The ripple is much greater than predicted. The bandwidth also appears larger and the centre frequency is about 300 MHz above the designed 4 GHz.

Fig 5.26(c) and (d) show the corresponding phase responses corrected for the length of the coupler but not for the fixed ninety degree difference. The precise values on the y-axis do not mean much. The ninety degree difference is easily apparent although the greatest deviation from 90 degrees is 8 degrees.

Fig 5.26(e) and (f) show the input match trends and the isolations S_{41} and S_{32}. The trends are very similar as expected since the isolation and mis-match curves of fig 5.22(e) and 5.23(f) are so similar. The worst case mis-match is -17.4dB and the worst case isolation 13.4dB. This last value is not good (20dB isolation should be aimed at) but was typical of all the couplers built. Analysis showed that this coupler was at least sufficient for the prototypes.

The last point worth noting is that the larger than expected ripple and the measured mis-matches and isolation compared with theoretical values, indicates that the Wilkinson couplers performed more nearly ideally than the quadrature couplers. This may not be true in other media and even in stripline if more professional construction techniques are used.

5.4 DIODES AND DETECTORS

A wide range of diodes is currently used in microwave electronics. Each type has its own particular properties which make it suitable for a particular set of applications. Diode types commonly used as detectors are point-contact crystal diodes, Schottky barrier diodes, backward diodes and tunnel diodes[45]. Factors that should be considered when choosing diodes include frequency range, voltage sensitivity, tangential sensitivity, VSWR and temperature dependence. Once again, however, the main criterion here was availability. For this reason Schottky barrier diode's were used.

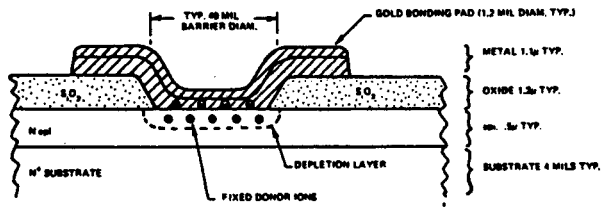

Fig 5.27 : **Schottky barrier diode cross section (reference 46)**

5.4.1 SCHOTTKY BARRIER DIODES

As in point-contact diodes, the Schottky barrier diode's rectifying junction is formed by contact between a metal and n-type or p-type semi-conductor. Fig 5.27 shows a typical Schottky diode cross-section[46].

The physics of the device is complex and covered in the literature by, for example, references 45 and 46. The discussion here will be limited to some of the more relevant simplified theory. Some insight into the device can be gained from consideration of the simple equivalent circuit given in fig 5.28.

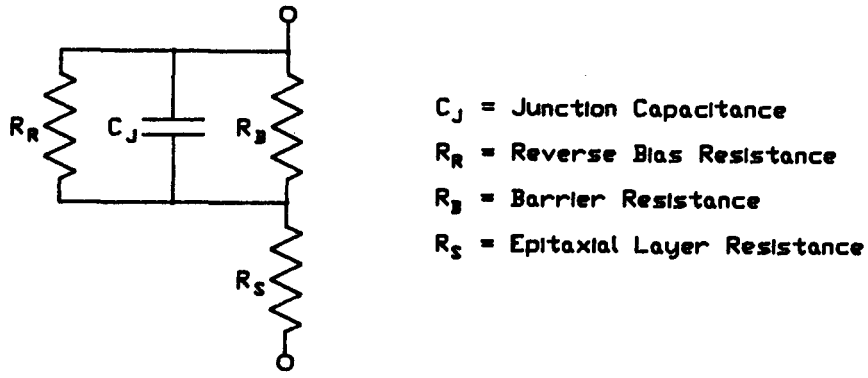

Fig 5.28 : **Diode equivalent circuit**

Ignoring junction capacitance the forward I-V curve of the diode at room temperature is

$$I = I_S \left[\exp\left(\frac{V_j}{0.028} \right) - 1 \right] \qquad \ldots\ldots (5.4.1)$$

where
- V_j = $V - IR_S$ = junction voltage
- I_S = saturation current (and is temperature dependent)
- "0.028" = nkT/q at room temperature ($n = 1.08$)
- n = forward slope factor
- k = Boltzmann's constant
- T = absolute temperature
- q = electron charge

Detection occurs because of this non-linear I-V characteristic. If the DC current is held constant by a current regulator or large resistor, and a constant low level RF signal is fed into the divide, then

$$V_{DC} = V_o - \frac{V_j^2}{0.112} \qquad \ldots\ldots (5.4.2)$$

where

V_{DC} = voltage at DC side of detector
V_o = bias voltage
V_j = junction voltage
"0.112" = 4nkT/q and is temperature dependent

Thus the DC voltage decrease from V_o depends only on the square of the RF junction voltage.

The output voltage of the detector (V_{det}) can then be specified for a given RF base impedance (eg. 50Ω), as

$$V_{det} = V_{DC} - V_o \propto P_{RF} \quad \ldots\ldots (5.4.3)$$

where P_{RF} = available RF power

It is this last relation that is of importance here. Note that it applies only to low level inputs which do not drive the detector into or near saturation. A detector operating in this mode is said to be in its "square-law region".

Schottky diodes can be obtained commercially in several different packages or in un-packaged chip form. Chip diodes are particularly useful for mounting in microstrip integrated circuits because of their small size. Ultimately it would be desirable to integrate the detectors with the rest of the RF circuit but at the prototype stage it is useful to use packaged detectors which can easily be connected to and removed from the circuit. Detectors in SMA co-axial packages were used since they could easily be screwed on and off. RF shunts and DC returns are supplied in the package as shown in fig 5.29. The RF shunt has the effect of low pass filtering the output and ensures that video frequencies are the highest frequencies that can be passed on to the IF circuitry.

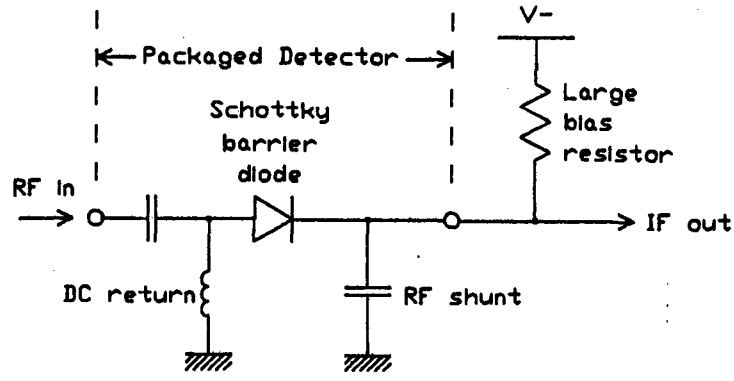

Fig 5.29 : **Packaged detector with external bias**

The diodes actually used were Aertech Industries SMA packaged biased Schottky barrier detectors, type A9X652B. They can be seen attached to the power splitter in fig 5.14.

5.4.2 DETECTOR RETURN LOSS AND RESISTIVE MATCHING

Detectors generally have very poor VSWRs. When biased for best return loss the detectors used for the prototypes had VSWRs varying between 2.3:1 and 3:1 over the 2 to 6 GHz bandwidth. Fig 5.30 shows the results of return loss measurements performed on one of the detectors. The other detectors were very similar. Fig 5.30(a) gives the results of tests performed on the detector when no matching was used. Note the dependence on bias current I_q. Best results were obtained for I_q = 81µA with this detector.

For broadband matching the easiest way to match the detectors is to pad the inputs with 6dB or 10dB attenuators. These give maximum return losses of 12dB and 20dB respectively. Fig 5.30(b) shows the results of tests performed on the same diode with pads placed between the RF source and the detector RF inputs. The price paid for this form of matching is a loss of voltage sensitivity. Resistive matching is often used with FDs[10,21], the associated loss usually being acceptable since frequency discriminators are always driven by limiting amplifiers.

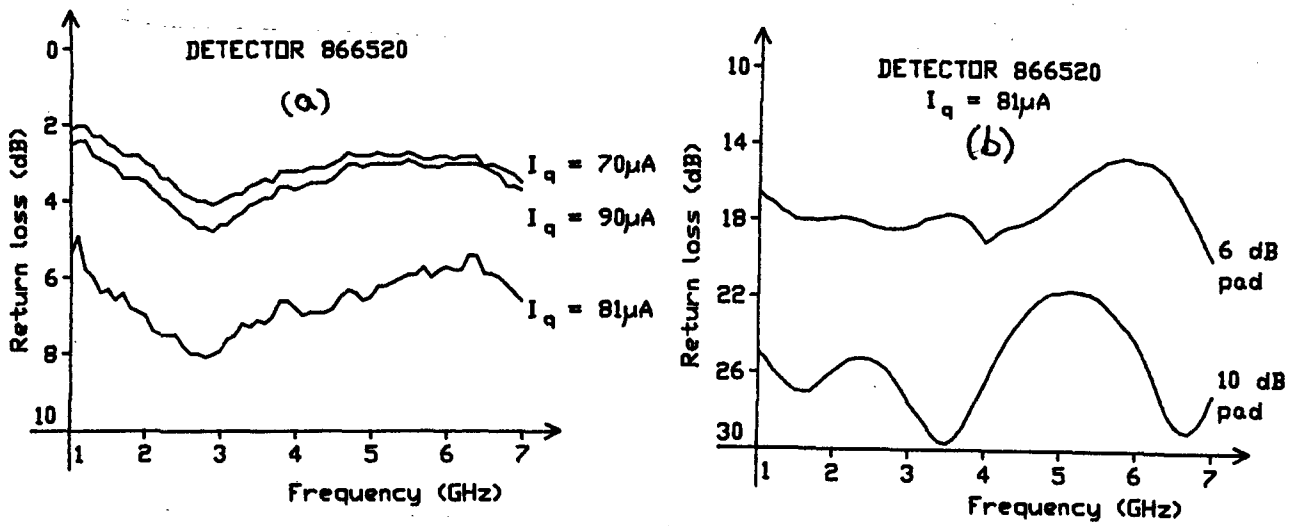

Fig 5.30 : **Measured detector return loss**

a) no resistive matching

b) with resistive matching

5.4.3 MATCHING DETECTOR VOLTAGE SENSITIVITIES

The correct operation of frequency discriminators relies on the voltage sensitivities of each detector being as similar as possible. A flat characteristic is preferable but of lesser importance. Detectors can be bought in pre-matched sets, although as such they are very expensive. An alternative is to buy detectors from the same batch, usually with consecutive serial numbers, and to match the responses as closely as possible over the required band by varying the bias currents used. The detectors used for the prototypes fell into this last category. Two sets of three detectors were available, each set having consecutive serial numbers. It was decided to pick the three of the six which were most similar.

Testing each detector separately for different bias currents is extremely laborious and a very unsatisfactory method of matching the responses. A more interactive method was required which allowed detector responses to be viewed simultaneously, and their bias currents to be varied

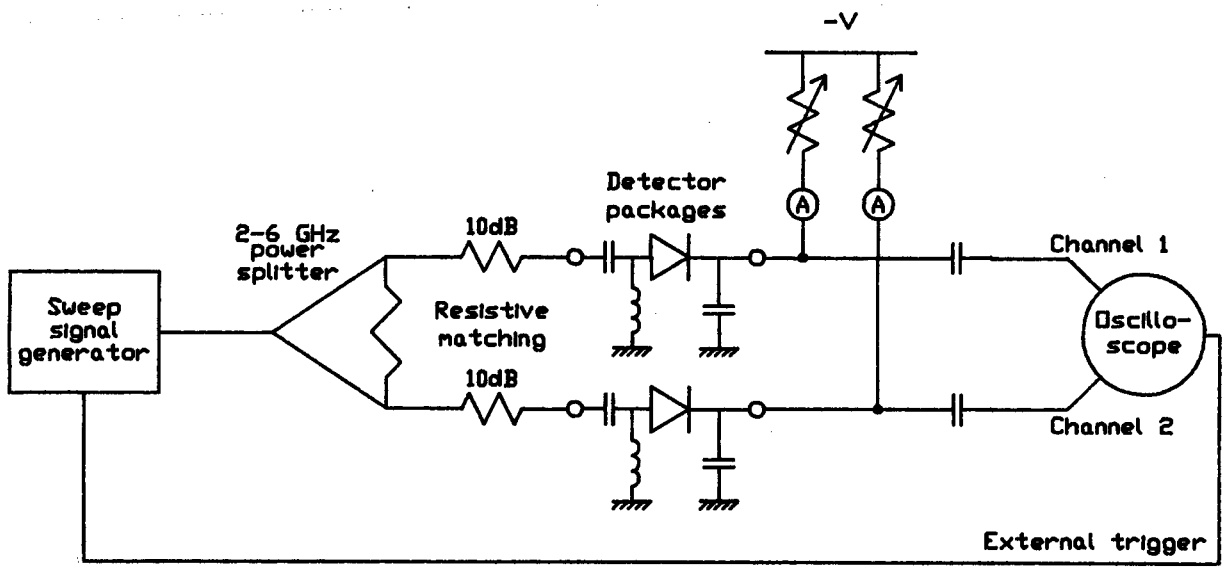

Fig 5.31 : **Detector matching circuit**

independently. The solution adopted was to use a power splitter to feed two detectors with equal RF input powers. The detector outputs were AC coupled to separate input channels of an oscilloscope. A sweep signal generator provided a signal sweeping from 2 GHz to 6 GHz in 30 ms. The sweep rate was sufficient for the detector ouputs to be passed by the DC blocking capacitor so the signal did not have to be 'chopped' (ie. switched on and off rapidly). Fig 5.31 shows the circuit used for matching the detectors. Each detector was driven by a -20dBm RF signal.

Detector 866520 was chosen as a standard since it had already been determined that it exhibited minimum VSWR for a bias current of 81μA. The other detectors were then screwed on and off and their bias currents varied to see which two were closest in performance. Fig 5.32 shows the appearance of the oscilloscope for badly matched detectors (a) and for the same detectors matched as closely as possible (b).

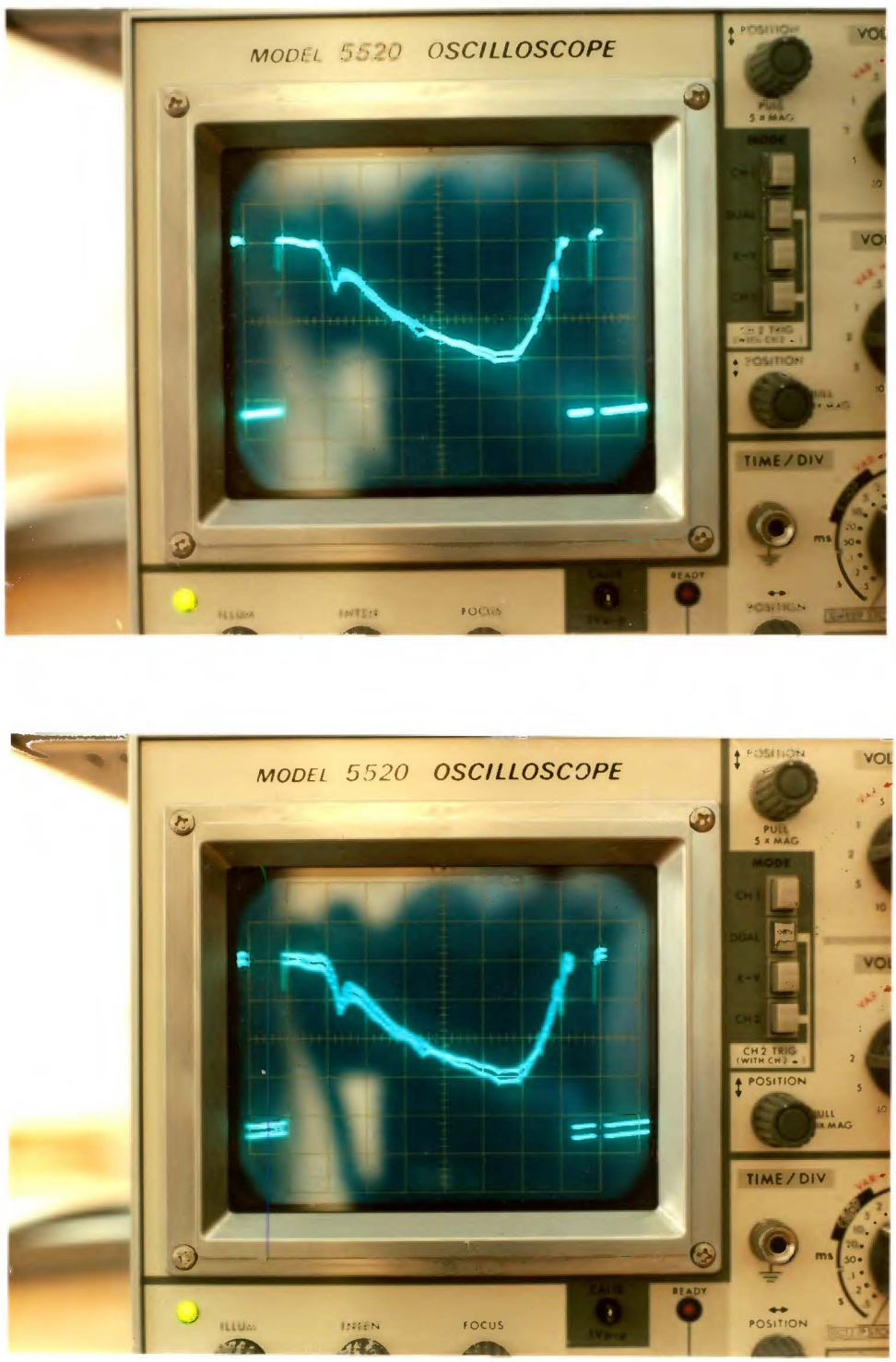

Fig 5.32 : **Oscilloscope screen appearance during sensitivity matching**

a) Detectors unmatched

b) Same detectors, bias currents varied for best match

x-axis scale : 5 ms/division

y-axis scale : 20 mV/division

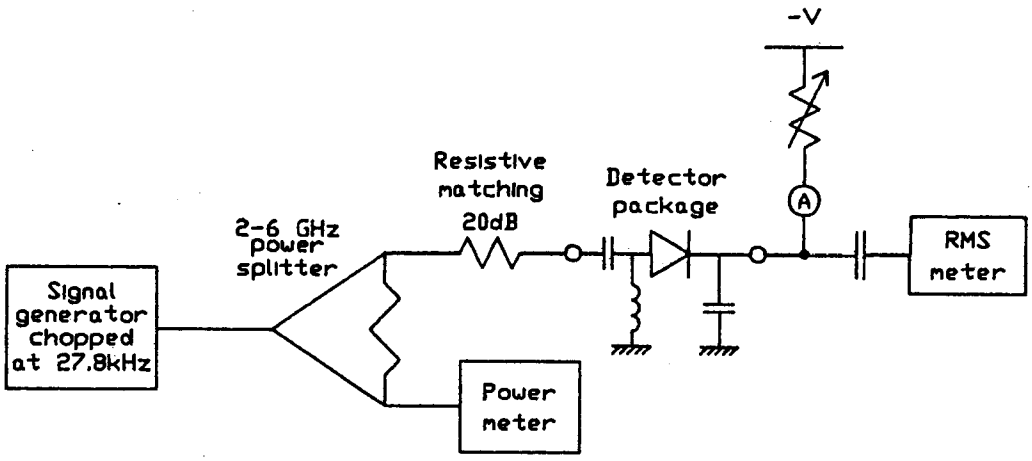

Fig 5.33 : **Voltage sensitivity measurement**

Once three detectors had been selected, their sensitivities were more accurately measured to confirm the validity of the method described above. Fig 5.33 shows the circuit used to perform these measurements. The signal generator output was 'chopped' at 27.8 kHz to allow AC coupling to the RMS volt-meter to be used. The power splitter allowed the incident RF power to the detector to be measured at the same time as the RMS voltage. Fig 5.34 shows the results of these measurements and also the numbers and bias currents of the chosen detectors. The maximum variation achieved

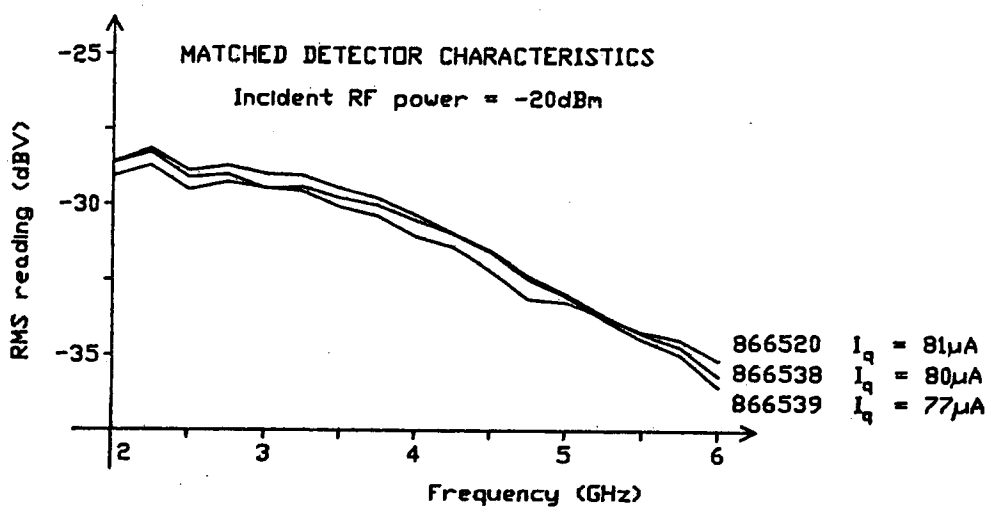

Fig 5.34 : **Matched detector voltage sensitivities**

was ± 0.4dB which falls within the specification of ± 0.5dB commonly used when broad-band pre-matched detector sets are purchased.

5.4.4 SQUARE-LAW REGION

To complete the tests on the detectors it remains to determine the range of RF input powers over which the detectors operate in the square-law region. Detectors are in their square low region if

$$V_{det} \propto P_{RF} \qquad \ldots\ldots (5.4.4)$$

where V_{det} = detected voltage

P_{RF} = available RF input power

Alternatively

$$\log (V_{det}) \propto \log (P_{RF}) \qquad \ldots\ldots (5.4.5)$$

Hence if V_{det} in dBV is plotted against P_{RF} in dBm then the square-law region is the region for which the curve is a straight line. The circuit shown in fig 5.33 was used to make the measurements.

Fig 5.35 shows the results for one of the detectors and is representative of the other two. The tests were done at 2, 4 and 6 GHz as shown. The resulting curves were very similar in shape but displaced from each other as expected. Below -20dBm the curves are very linear and even up to -10dBm they have curved down only slightly. If it is ensured that -20dBm is the maximum drive to the detectors, then they will always be operating in their square-law region.

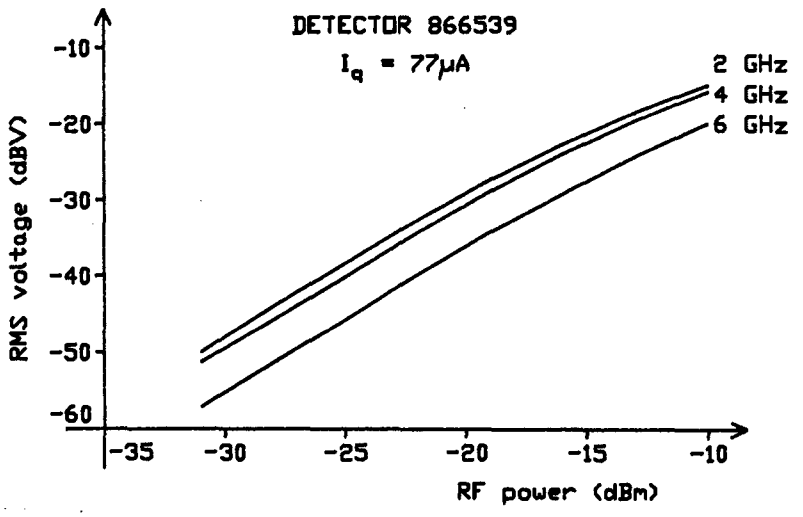

Fig 5.35 : **Determination of square-law region**

5.5 SUMMARY

Stripline has been chosen as the construction medium so that overlay quadrature couplers may be used. Wilkinson couplers have been determined to be the most suitable in-phase power splitters and a three section WC covering the 2 to 6 GHz band has been built and characterised.

Overlay couplers have been selected as easiest to implement for the prototypes. A three section QC covering 2 to 6 GHz has been built and tested.

Schottky barrier diodes have been selected for the detectors because of their ready availability. SMA co-axial packaged detectors have been obtained, properly matched and fully characterised.

CHAPTER SIX

FD ANALYSIS METHODS

Chapter 4 describes several different frequency discriminator types and demonstrates correct narrow band operation theoretically. Now that the components themselves have been characterised, the broad-band operation and error performance of FDs can be studied. Building and testing the components highlighted their non-ideal properties. Analysis methods are required which allow these factors to be included.

This chapter considers a few different methods of analysing FDs and then makes use of the best method to make some comparisons between the standard FD and the new types introduced in chapter 4. The number of factors that can be included is huge, so that only a few can be presented here as illustrative examples.

The best analysis tool, the micro-computer package TOUCHSTONE, is expensive and may not be available to a designer. In that case he or she can still make use of one of the other methods presented here, which is why they are included.

6.1 DIRECT FORMULAE APPROACH

Direct mathematical analysis is always attractive as formulae can usually be re-written to allow synthesis questions to be answered, such as what is the minimum QC isolation required for a given error performance? There are so many factors to be taken into account, however, that formulae attempting to include even a few factors at one time can become too complex to work with. Factors can be taken into account separately, but that requires new formulae to be developed each time and obscures the interaction between different factors. Certain interesting features do emerge from simple analyses and it is useful to adopt the method followed by East.[4]

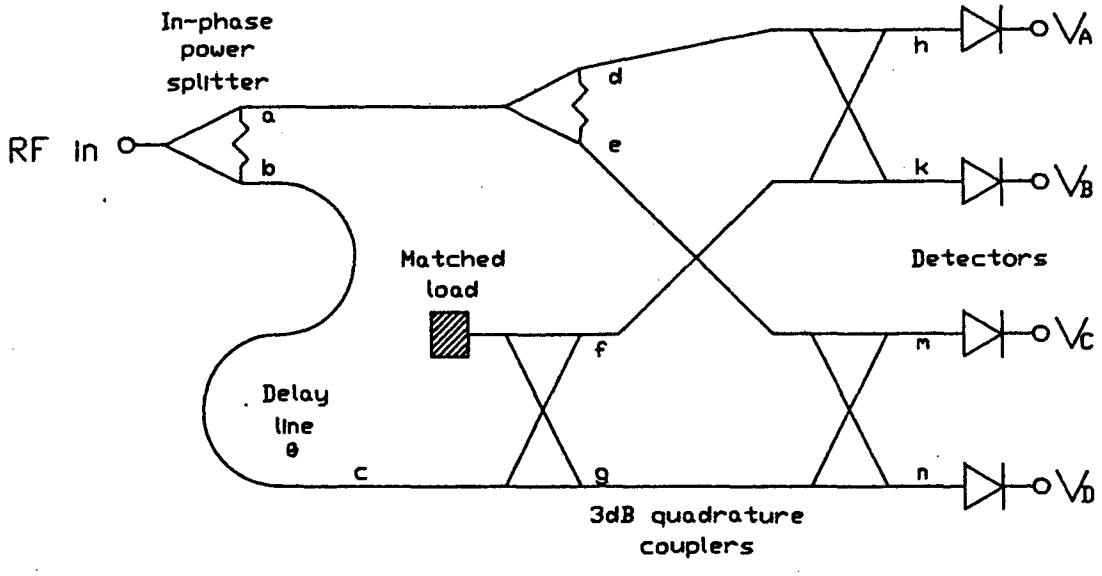

Fig 6.1 : **Standard frequency discriminator**

To represent more real components than considered in chapter 4, let

a = WC voltage transfer factor
b = QC direct output voltage transfer factor
c = QC coupled output voltage transfer factor
d = delay line attenuation factor

Consider first the standard frequency discriminator. For simplicity an input signal with unity amplitude is present at 'RF in' in fig 6.1. The signals at the points marked by lower case letters are then given by:

at a) and b) : $a\angle 0°$
at c) : $ad\angle\theta$
at d) and e) : $a^2\angle 0°$
at f) : $abd\angle\theta$
at g) : $acd\angle\theta + 90°$
at h) : $a^2c\angle 90° + ab^2d\angle\theta$
at k) : $a^2b\angle 0° + abcd\angle\theta + 90°$
at m) : $a^2c\angle 90° + abcd\angle\theta + 90°$
at n) : $a^2b\angle 0° + ac^2d\angle\theta + 180°$

Then, taking detector sensitivities to be unity

$$V_A = |a^2c \angle 90° + ab^2d \angle \theta|^2$$
$$= a^2|ac\cos 90° + jac \sin 90° + b^2d\cos\theta + jb^2d\sin\theta|^2$$
$$= a^2|b^2d\cos\theta + j(ac + b^2d\sin\theta)|^2$$
$$= a^2\,(b^4d^2\cos^2\theta + a^2c^2 + 2ab^2cd\sin\theta + b^4d^2\sin^2\theta)$$

therefore

$$V_A = a^4c^2 + a^2b^4d^2 + 2a^3b^2cd\sin\theta \qquad \ldots\ldots (6.1.1)$$

Similarly

$$V_B = a^4b^2 + a^2b^2c^2d^2 - 2a^3b^2cd\sin\theta \qquad \ldots\ldots (6.1.2)$$

$$V_C = a^4c^2 + a^2b^2c^2d^2 + 2a^3bc^2d\cos\theta \qquad \ldots\ldots (6.1.3)$$

$$V_D = a^4b^2 + a^2c^4d^2 - 2a^3bc^2d\cos\theta \qquad \ldots\ldots (6.1.4)$$

Outputs (V_A-V_B) and (V_C-V_D) can be evaluated from equations (6.1.1) to (6.1.4):

$$V_A - V_B = 4a^3b^2cd\left[(\tfrac{1}{4})\left(\frac{a}{bd} - \frac{bd}{a}\right)\left(\frac{b}{c} - \frac{c}{b}\right) + \sin\theta\right] \qquad \ldots\ldots (6.1.5)$$

$$V_C - V_D = 4a^3b^2cd\left[(\tfrac{1}{4})\left(\frac{a}{cd} - \frac{cd}{a}\right)\left(\frac{c}{b} - \frac{b}{c}\right) + \cos\theta\right] \qquad \ldots\ldots (6.1.6)$$

From equations (6.1.5) and (6.1.6)

$$\frac{(V_A - V_B)}{(V_C - V_D)} = \frac{b}{c}\left[\frac{(\tfrac{1}{4})\left(\frac{a}{bd} - \frac{bd}{a}\right)\left(\frac{b}{c} - \frac{c}{b}\right) + \sin\theta}{(\tfrac{1}{4})\left(\frac{a}{cd} - \frac{cd}{a}\right)\left(\frac{c}{b} - \frac{b}{c}\right) + \cos\theta}\right] \qquad \ldots\ldots (6.1.7)$$

Note that East appears to have left out the factor b/c in his equations labelled 13, but otherwise the above agrees with his work. Note also that if b=c then delay line loss and WC voltage split factor do not cause errors.

An error function can now be defined:

$$\theta_{error} = \theta - \tan^{-1}\left[\frac{V_A - V_B}{V_C - V_D}\right] \qquad \ldots\ldots (6.1.8)$$

Formulae can often be written for b and c as a function of frequency. For example, for single section couplers b and c are defined by the magnitudes of equations (4.2.2) and (4.2.3). Equation (6.1.8) can then be used to predict errors.

Consider now the simpler single QC FD introduced in chapter 4 and shown in fig 6.2. This will be referred to as 'type 1' from here on. Again take the detectors to have unity sensitivities and consider an input signal of unity amplitude. The signals at the points marked by lower case letters are then given by:

at a) and b) : $a\angle 0°$

at c) : $ad\angle\theta$

at d) : $ac\angle 90° + abd\angle\theta$

at e) : $ab\angle 0° + acd\angle\theta + 90°$

at f) and g) : $a^2c\angle 90° + a^2bd\angle\theta$

at h) : $a^2b\angle 0° + a^2cd\angle\theta + 90°$

at m) : $a^3c\angle 90° + a^3bd\angle\theta + a^3b\angle 0° + a^3cd\angle\theta + 90°$

Then, using the same techniques as for the standard FD

$$V_1 = a^4c^2 + a^4b^2d^2 + 2a^4bcd \sin\theta \qquad \ldots\ldots (6.1.9)$$

$$V_2 = a^6b^2 + a^6c^2 + a^6b^2d^2 + a^6c^2d^2 + 2a^6d(b^2 + c^2)\cos\theta \qquad \ldots\ldots (6.1.10)$$

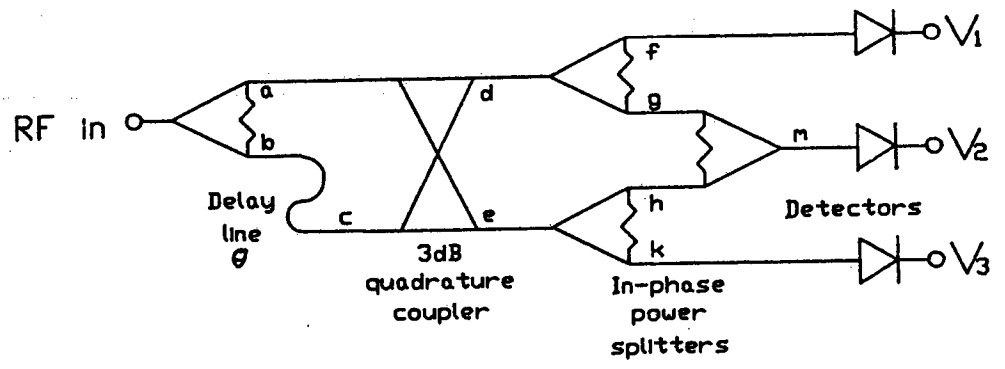

Fig 6.2 : **Single QC frequency discriminator (type 1)**

$$V_3 = a^4b^2 + a^4c^2d^2 - 2a^4bcd \sin\theta \qquad \text{..... (6.1.11)}$$

To bring V_2 into line with the others it should be multiplied by a factor a^{-2}. In chapter 4 this was approximated as $a^{-2}=2$ for the type 1 version. The more complex single QC version (shown in fig 4.16 and referred to from here on as 'type 2') performs the equivalent by multiplying V_1 and V_3 by a^2. Considering this case first, V_2 becomes:

$$V_2' = V_2a^{-2} = a^4b^2+a^4c^2+a^4b^2d^2+a^4c^2d^2+2a^4d(b^2+c^2)\cos\theta \qquad \text{..... (6.1.12)}$$

Output (V_1-V_3), from equations (6.1.9) and (6.1.11), is given by

$$(V_1-V_3) = 4a^4bcd\left[(\tfrac{1}{4})\left(\frac{1}{d} - d\right)\left(\frac{c}{b} - \frac{b}{c}\right) + \sin\theta\right] \qquad \text{..... (6.1.13)}$$

and

$$V_2' - (V_1 + V_3) = 2a^4d(b^2 + c^2)\cos\theta \qquad \text{..... (6.1.14)}$$

Then

$$\frac{V_1 - V_3}{V_2' - (V_1+V_3)} = \frac{2\left[(\tfrac{1}{4})\left(\frac{1}{d} - d\right)\left(\frac{c}{b} - \frac{b}{c}\right) + \sin\theta\right]}{\left(\frac{b}{c} + \frac{c}{b}\right)\cos\theta} \qquad \ldots\ldots (6.1.15)$$

Note that the WC voltage transfer factor a does not appear in the above, and once again b=c implies that delay line loss has no error causing effect. The error function is then

$$\theta_{error} = \theta - \tan^{-1}\left[\frac{V_1 - V_3}{V_2 a^{-2} - (V_1 + V_3)}\right] \qquad \ldots\ldots (6.1.16)$$

If we instead multiply V_2 by 2, as is the case with the type 1 FD, then

$$2V_2 - (V_1 + V_3) = 4a^6 d(b^2 + c^2)\left[(\tfrac{1}{4})\left(\frac{1}{d} + d\right)(2-a^{-2}) + \cos\theta\right] \qquad \ldots\ldots (6.1.17)$$

Then

$$\frac{V_1 - V_3}{2V_2 - (V_1+V_3)} = \frac{(a^{-2})\left[(\tfrac{1}{4})\left(\frac{1}{d} - d\right)\left(\frac{c}{b} - \frac{b}{c}\right) + \sin\theta\right]}{\left(\frac{b}{c} + \frac{c}{b}\right)\left[(\tfrac{1}{4})\left(\frac{1}{d} + d\right)(2-a^{-2}) + \cos\theta\right]} \qquad \ldots\ldots (6.1.18)$$

The error function is

$$\theta_{error} = \theta - \tan^{-1}\left[\frac{V_1 - V_3}{2V_2 - (V_1 + V_3)}\right] \qquad \ldots\ldots (6.1.19)$$

Assuming perfect components except for the imbalance in the QC outputs denoted by b and c, ie. setting d=1 and $a=1/\sqrt{2}$ in equations (6.1.7) and (6.1.18), gives the following.

For the standard FD:

$$\frac{V_A - V_B}{V_C - V_D} = \left(\frac{b}{c}\right)\left[\frac{(\frac{1}{4})\left(\frac{1}{b\sqrt{2}} - b\sqrt{2}\right)\left(\frac{b}{c} - \frac{c}{b}\right) + \sin\theta}{(\frac{1}{4})\left(\frac{1}{c\sqrt{2}} - c\sqrt{2}\right)\left(\frac{c}{b} - \frac{b}{c}\right) + \cos\theta}\right] \qquad \ldots\ldots (6.1.20)$$

For FD types 1 and 2 :

$$\frac{V_1 - V_3}{2V_2 - (V_1 + V_3)} = \frac{2\tan\theta}{\left(\frac{b}{c} + \frac{c}{b}\right)} \qquad \ldots\ldots (6.1.21)$$

The lesser dependence of the type 1 and 2 FDs on b and c is expected since they use only one QC as compared to the standard version's three.

In all the above, factors such as deviation in phase from 90 degrees in the QCs, and even theoretically predicted factors such as WC VSWR have not been considered. These are very difficult to include while keeping the equations manageable. A computer based approach is really required.

Before looking at some computer based approaches, some additional useful information can be obtained. From equations (6.1.19) and (6.1.21):

$$\theta_{error} = \theta - \tan^{-1}\ (x \tan\theta) \qquad \ldots\ldots (6.1.22)$$

$$\text{where } x = \frac{2}{\left(\frac{b}{c} + \frac{c}{b}\right)} \qquad \ldots\ldots (6.1.23)$$

The greater the absolute value of (1-x) the greater the error. Alternatively the greater the absolute value of (b-c) the greater the error, and for symmetric equal-ripple couplers this occurs at the centre-frequency, band limits and at a number of other

points depending on the number of coupled sections.

From (6.1.22)

$$\frac{\partial\theta}{\partial\theta}\,\text{error} = 1 - \frac{x\sec^2\theta}{1 + x^2\tan^2\theta} \qquad \ldots\ldots (6.1.24)$$

Maximum error for a given value of x occurs for $\partial\theta_{error}/\partial\theta = 0$, or

$$\theta = \sin^{-1}\left[\frac{x-1}{x^2-1}\right]^{\frac{1}{2}} \qquad \ldots\ldots (6.1.25)$$

For most cases studied x will be very close to unity. For example for a single stage 2 to 6 GHz coupler, which is the worst case, the centre-band coupling factor is $c = 0.7655$ and $b = \sqrt{1-c^2} = 0.6434$. Then $x = 0.985$ and from (6.1.25)

$$\theta \simeq \frac{m\pi}{4}\ ,\ m = 1,\ 3,\ 5\ \ldots\ldots \qquad \ldots\ldots (6.1.26)$$

Thus to ensure worst case errors are considered for discriminator types 1 and 2, the electrical length of the delay line θ should be $m\pi/4$ radians at the centre frequency. A good choice is probably 315 degrees, ie. the delay line length should be such that $\theta = 315$ degrees at f_o. This is close to the maximum unambiguous length of 360 degrees for a bandwidth equal to f_o, as is the case with $f_o = 4$ GHz and a band of 2 to 6 GHz.

6.2 CASCADED S-PARAMETER APPROACH

The most convenient way of describing networks at microwave frequencies is in terms of their scattering or s-parameters. For a general two port network shown in fig 6.3, if a_i represents a wave incident at port i and b_i the wave reflected from port i, then the following relationship defines the s-parameters of that network:

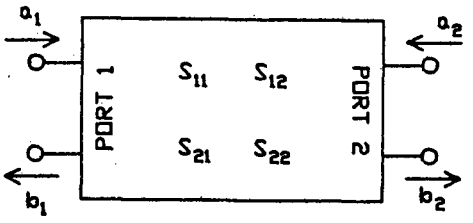

Fig 6.3 : **General two port network**

$$\begin{bmatrix} b_1 \\ b_2 \end{bmatrix} = \begin{bmatrix} S_{11} & S_{12} \\ S_{21} & S_{22} \end{bmatrix} \begin{bmatrix} a_1 \\ a_2 \end{bmatrix} \qquad \ldots\ldots (6.2.1)$$

There is no simple operation, such as addition or multiplication, that can be performed on S-matrices to write the result of cascading two separate networks, represented by their S-parameters, as a single set of S-parameters. Transfer or T-matrices, on the other hand, can merely be multiplied together if they are defined as follows:

$$\begin{bmatrix} b_1 \\ a_1 \end{bmatrix} = \begin{bmatrix} T_{11} & T_{12} \\ T_{21} & T_{22} \end{bmatrix} \begin{bmatrix} a_2 \\ b_2 \end{bmatrix} \qquad \ldots\ldots (6.2.2)$$

For two-port networks conversion between S- and T-parameters appears fairly straight forward:

$$T_{11} = (-S_{11}\, S_{22} + S_{12}\, S_{21})/S_{21} \qquad \ldots\ldots (6.2.3)$$

$$T_{12} = S_{11}/S_{21} \qquad \ldots\ldots (6.2.4)$$

$$T_{21} = -S_{22}/S_{21} \qquad \ldots\ldots (6.2.5)$$

$$T_{22} = 1/S_{21} \qquad \ldots\ldots (6.2.6)$$

and

$$S_{11} = T_{12}/T_{22} \qquad \ldots\ldots (6.2.7)$$

$$S_{12} = T_{11} - (T_{12}\ T_{21}/T_{22}) \qquad \ldots\ldots (6.2.8)$$

$$S_{21} = 1/T_{22} \qquad \ldots\ldots (6.2.9)$$

$$S_{22} = -\ T_{21}/T_{22} \qquad \ldots\ldots (6.2.10)$$

There is a pitfall in the method, however. If S_{21} is zero then the T-parameters are undefined. This may appear to be a trivial case where two port networks are concerned, but if the method is generalised and some ports are 'dummy' or un-connected ports, then divisions by zero can be a serious problem.

It is useful at this point to illustrate the method by dividing the standard FD into cascaded networks. Note that if several methods are to be cascaded then each must have as many input ports as output ports, so that 8 port networks consisting of 4 input ports and 4 output ports are required for the standard FD. This is clearly demonstrated in fig 6.4. Several un-connected 'dummy' ports must be defined, but these can easily be removed from the final S-parameter matrix to yield a five port result .

Using the port numbers shown in fig 6.4, V_A, V_B, V_C and V_D can be determined directly from the S-parameters according to:

$$V_A = |S_{52}|^2 \qquad \ldots\ldots (6.2.11)$$

$$V_B = |S_{62}|^2 \qquad \ldots\ldots (6.2.12)$$

$$V_C = |S_{72}|^2 \qquad \ldots\ldots (6.2.13)$$

$$V_D = |S_{82}|^2 \qquad \ldots\ldots (6.2.14)$$

We now require a method of cascading the 8-port networks by manipulating the s-parameters directly. The following method works well and is particularly easy to program.

Consider two n-port networks A and B, n even, cascaded together. Each network has n/2 input ports numbered 1 to n/2, and n/2 ouput

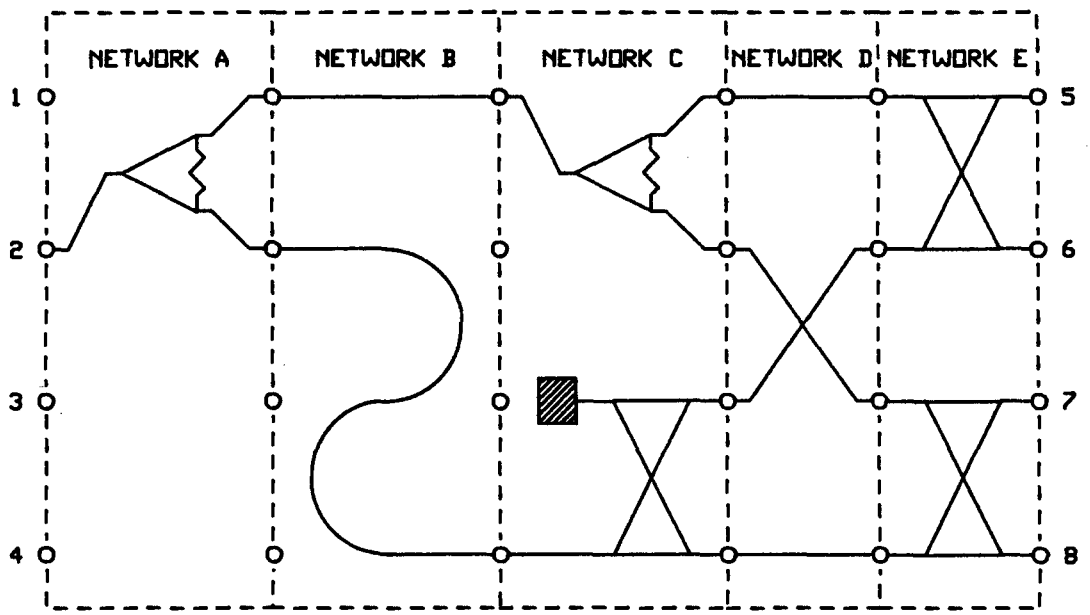

Fig 6.4 : **Standard FD as cascaded 8-ports**

ports numbered n/2+1 to n as shown in fig 6.5. Let A_{ij} be the S-parameter of network A, and B_{ij} be those of network B. Let a_i and b_i respectively be the waves entering and leaving port i of network A. Let c_i and d_i respectively be the waves entering and leaving port i of network B. Then

$$\begin{bmatrix} b_1 \\ b_2 \\ \vdots \\ b_n \end{bmatrix} = \begin{bmatrix} A_{11} & A_{12} & \cdots\cdots & A_{1n} \\ A_{21} & A_{22} & \cdots\cdots & A_{2n} \\ \vdots & \vdots & & \vdots \\ A_{n1} & A_{n2} & \cdots\cdots & A_{nn} \end{bmatrix} \begin{bmatrix} a_1 \\ a_2 \\ \vdots \\ a_n \end{bmatrix} \qquad \ldots\ldots \text{(6.2.15)}$$

and

$$\begin{bmatrix} d_1 \\ d_2 \\ \vdots \\ d_n \end{bmatrix} = \begin{bmatrix} B_{11} & B_{12} & \cdots\cdots & B_{1n} \\ B_{21} & B_{22} & \cdots\cdots & B_{2n} \\ \vdots & \vdots & & \vdots \\ B_{n1} & B_{n2} & \cdots\cdots & B_{nn} \end{bmatrix} \begin{bmatrix} c_1 \\ c_2 \\ \vdots \\ c_n \end{bmatrix} \qquad \ldots\ldots \text{(6.2.16)}$$

Waves leaving ports n/2+1 to n of network A must enter ports 1 to n/2 of network B, ie.:

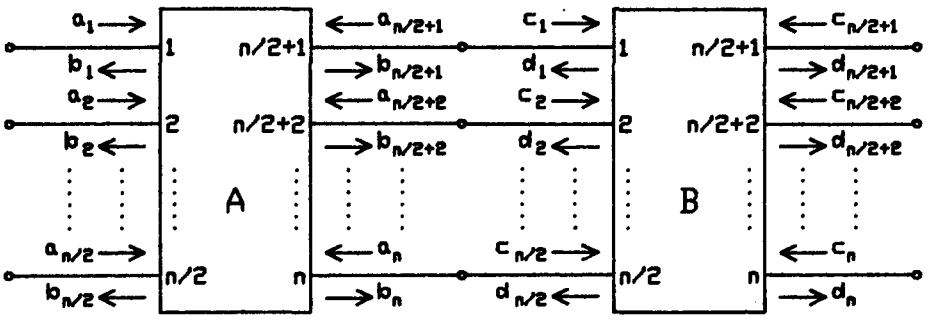

Fig 6.5 : **Cascaded n-port networks**

$$b_{i+n/2} = c_i, \quad i = 1, 2, \ldots n/2 \qquad \ldots\ldots (6.2.17)$$

Similarly

$$d_i = a_{i+n/2}, \quad i = 1, 2, \ldots n/2 \qquad \ldots\ldots (6.2.18)$$

Equation (6.2.17) can be substituted into (6.2.15) to eliminate $b_{n/2+1}$ to b_n, leaving:

$$\begin{bmatrix} b_1 \\ b_2 \\ \vdots \\ b_{n/2} \\ c_1 \\ c_2 \\ \vdots \\ c_{n/2} \end{bmatrix} = \begin{bmatrix} A_{11} & A_{12} \ldots\ldots A_{1n} \\ A_{21} & A_{22} \ldots\ldots A_{2n} \\ \vdots & \vdots \\ A_{n1} & A_{n2} \ldots\ldots A_{nn} \end{bmatrix} \begin{bmatrix} a_1 \\ a_2 \\ \vdots \\ a_n \end{bmatrix} \qquad \ldots\ldots (6.2.19)$$

Equations (6.2.18) and (6.2.16) can be used similarly to eliminate d_1 to $d_{n/2}$:

$$\begin{bmatrix} a_{n/2+1} \\ a_{n/2+2} \\ \vdots \\ a_n \\ d_{n/2+1} \\ d_{n/2+2} \\ \vdots \\ d_n \end{bmatrix} = \begin{bmatrix} B_{11} & B_{12} & \cdots & B_{1n} \\ B_{21} & B_{22} & \cdots & B_{2n} \\ \vdots & \vdots & & \vdots \\ B_{n1} & B_{n2} & \cdots & B_{nn} \end{bmatrix} \begin{bmatrix} c_1 \\ c_2 \\ \vdots \\ c_n \end{bmatrix} \quad \ldots\ldots (6.2.20)$$

c_1 to $c_{n/2}$ can now be eliminated by substituting the lower n/2 rows of equation (6.2.19) into (6.2.20), giving :

$$\begin{bmatrix} 0 \\ 0 \\ \vdots \\ 0 \\ d_{n/2+1} \\ d_{n/2+2} \\ \vdots \\ d_n \end{bmatrix} = \begin{bmatrix} C_{11} & C_{12} & \cdots & C_{1n} & B_{1,n/2+1} & B_{1,n/2+2} & \cdots & B_{1,n} \\ C_{21} & C_{22} & \cdots & C_{2n} & B_{2,n/2+1} & B_{2,n/2+2} & \cdots & B_{2,n} \\ \vdots & \vdots & & \vdots & \vdots & \vdots & & \vdots \\ C_{n1} & C_{n2} & \cdots & C_{nn} & B_{n,n/2+1} & B_{n,n/2+2} & \cdots & B_{n,n} \end{bmatrix} \begin{bmatrix} a_1 \\ a_2 \\ \vdots \\ a_n \\ c_{n/2+1} \\ c_{n/2+2} \\ \vdots \\ c_n \end{bmatrix}$$

$\ldots\ldots$ (6.2.21)

where $C_{ij} = \sum_{\ell=1}^{n/2} B_{i\ell}\, A_{\ell+n/2,j}$ $\qquad i = 1, 2, \ldots n$, $j = 1, 2, \ldots n$, $j \neq i+n/2$

$$C_{ij} = \sum_{\ell=1}^{n/2} B_{i\ell}\, A_{\ell+n/2,j-1}, \qquad i = 1, 2, \ldots n, \quad j = i+n/2 \qquad \ldots\ldots (6.2.22)$$

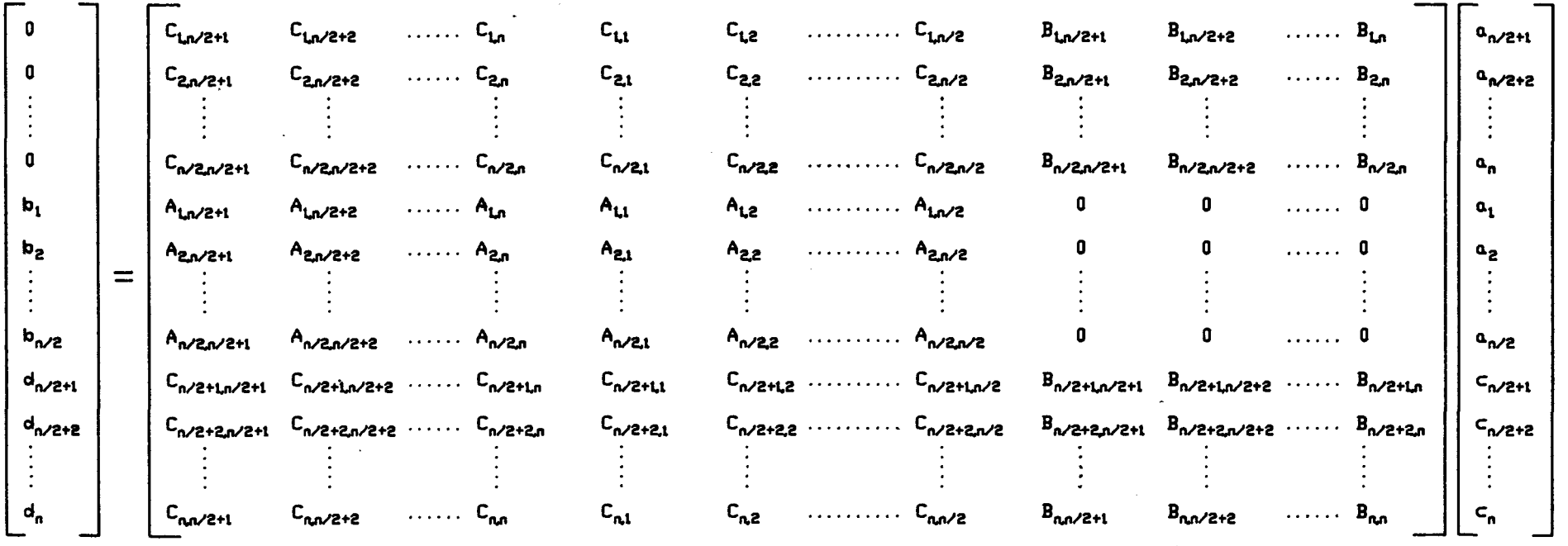

Fig 6.6 : **Equation (6.2.23)**

The top n/2 rows of equation (6.2.19) and all the rows of (6.2.20) can be written into the single set of equations (6.2.23) shown in fig 6.6. Note that the order has been chosen to simplify the remaining steps.

Let **D** be the n+n/2 by n+n/2 matrix in equation (6.2.23) (fig 6.6), such that D_{ij} is the jth element of the i'th row. Gauss reducing this matrix in the normal fashion to remove the top n/2 rows leaves an n x n matrix which is the S-parameter matrix of the cascaded network. Since the original networks are properly described by S-parameter matrices, the cascaded network must be describable by a unique set of S-parameters. Thus the equations cannot be inconsistent and nor can any parameters be undefined.

To remove the first row, find the largest element in the left most column (excluding the bottom n rows) and make this row the top one by swopping it with the row actually at the top. Swopping rows does not affect the final result, however the bottom n rows should not be swopped to retain the original node numbering format. Set up a new matrix **E** such that

$$E_{ij} = D_{i+1,j+1} - \frac{D_{i+1,1}\, D_{1,j+1}}{D_{11}} \quad , \quad \begin{matrix} i = 1, 2, \ldots n+n/2-1 \\ j = 1, 2, \ldots n+n/2-1 \end{matrix} \qquad \ldots\ldots (6.2.24)$$

Repeat this process by eliminating the top row of matrix **E** to set up a new matrix. After n/2 such reductions a single n x n matrix **E** will remain and :

$$\begin{bmatrix} b_1 \\ b_2 \\ \vdots \\ b_{n/2} \\ d_{n/2+1} \\ d_{n/2+2} \\ \vdots \\ d_n \end{bmatrix} = \begin{bmatrix} E_{11} & E_{12} & \cdots & E_{1n} \\ E_{21} & E_{22} & \cdots & E_{2n} \\ \vdots & \vdots & & \vdots \\ E_{n1} & E_{n2} & \cdots & E_{nn} \end{bmatrix} \begin{bmatrix} a_1 \\ a_2 \\ \vdots \\ a_{n/2} \\ c_{n/2+1} \\ c_{n/2+2} \\ \vdots \\ c_n \end{bmatrix} \qquad \ldots\ldots (6.2.25)$$

Equation (6.2.25) is identical to equation (6.2.2) which defines S-parameters, except that it is generalised to n-ports. Hence **E** is the required n x n set of S-parameters describing the overall cascaded network.

For the example shown in fig 6.4, five 8x8 matrices must be cascaded together and the final result should really be a 5x5 matrix. Nodes 1, 3 and 4 are dummy nodes in this case and matrix elements relating to these nodes can simply be eliminated. The remaining five nodes can be re-numbered if required. The resulting 5x5 matrix is the S-parameter matrix of the overall five port network.

Appendix J gives a FORTRAN program which implements the above method by printing the result of cascading two n x n S-parameter matrices. The advantage of the method is that the original S-parameter matrices can easily be amended to take account of any non-ideal property, or to be actual measured values. The disadvantage is that the program has to be re-run for each different frequency of interest with the applicable S-parameters. It would however be a fairly simple matter to adapt the program to calculate and organise its own S-parameters. The program may be relatively slow on a micro-computer, but it is far cheaper than acquiring a more versatile commercial analysis package.

6.3 USING COMMON CIRCUIT ANALYSIS PACKAGES

Many engineers undertaking FD design will already have access to common circuit analysis programs. SPICE is one such package and is available on UCT's main-frame computer. Programs of this type are generally not meant to calculate S-parameters and SPICE is no exception. The question is, can these programs be used to model FDs and print out S-parameters?

Whether a package can be used to model FDs or not depends firstly on the component models available in the package. The components required are transmission lines and coupled lines (and of course resistors). If either of these models is not available then some

means of including user defined components is required. The available version of SPICE had transmission line but not coupled line models. Nor did it have the facility for including user defined components (unless those components could be modelled entirely in terms of existing components). SPICE, therefore, is not really suitable for modelling FDs.

Should the required component models be available the question of 'persuading' the package to calculate S-parameters directly needs to be answered. Most packages allow voltages to be measured at any point in a circuit, and currents to be measured in any line. SPICE allows this and can therefore be used as an example.

If certain rather neat tricks are employed SPICE can be used to generate circuit S-parameters. The technique is demonstrated here for a two port network and can easily be generalised. Fig 6.3 shows a general two port network with the usual S-parameter incident (a_i) and reflected (b_i) wave conventions. From equation (6.2.1) the S-parameters are defined by:

$$b_1 = S_{11}a_1 + S_{12}a_2 \qquad \text{..... (6.3.1)}$$

$$b_2 = S_{21}a_1 + S_{22}a_2 \qquad \text{..... (6.3.2)}$$

More directly they are given by :

$$S_{11} = \left.\frac{b_1}{a_1}\right|_{a_{2=0}} \qquad \text{..... (6.3.3)}$$

$$S_{21} = \left.\frac{b_2}{a_1}\right|_{a_{2=0}} \qquad \text{..... (6.3.4)}$$

$$S_{12} = \left.\frac{b_1}{a_2}\right|_{a_{1=0}} \qquad \text{..... (6.3.5)}$$

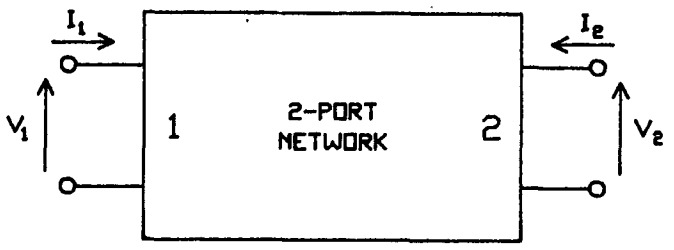

Fig 6.7 : **General 2-port network showing voltage and current conventions**

$$S_{22} = \left.\frac{b_2}{a_2}\right|_{a_1=0} \qquad \ldots\ldots (6.3.6)$$

If Z_o is the base characteristic impedance to which the ports of the network are connected, then a_i can be set to zero by connecting a load equal to Z_o to port i, and having no source attached to that node.

If the voltage (V_i) and current (I_i) conventions for a general two port network are adopted as shown in fig 6.7, then the following hold :

$$a_1 = \frac{1}{2\sqrt{Z_o}} (V_1 + Z_o I_1) \qquad \ldots\ldots (6.3.7)$$

$$a_2 = \frac{1}{2\sqrt{Z_o}} (V_2 + Z_o I_2) \qquad \ldots\ldots (6.3.8)$$

$$b_1 = \frac{1}{2\sqrt{Z_o}} (V_1 - Z_o I_1) \qquad \ldots\ldots (6.3.9)$$

$$b_2 = \frac{1}{2\sqrt{Z_o}} (V_2 - Z_o I_2) \qquad \ldots\ldots (6.3.10)$$

Using a normalised base impedance of Z_o=1 simplifies matters:

$$a_1 = \tfrac{1}{2}(V_1 + I_1) \qquad \ldots\ldots (6.3.11)$$

$$a_2 = \tfrac{1}{2}(V_2 + I_2) \qquad \ldots\ldots (6.3.12)$$

$$b_1 = \tfrac{1}{2}(V_1 - I_1) \qquad \ldots\ldots (6.3.13)$$

$$b_2 = \tfrac{1}{2}(V_2 - I_2) \qquad \ldots\ldots (6.3.14)$$

Substituting equations (6.3.11) to (6.3.14) into (6.3.7) to (6.3.10) gives :

$$S_{11} = \left.\frac{V_1 - I_1}{V_1 + I_1}\right|_{a_{2=0}} \qquad \ldots\ldots (6.3.15)$$

$$S_{21} = \left.\frac{V_2 - I_2}{V_1 + I_1}\right|_{a_{2=0}} \qquad \ldots\ldots (6.3.16)$$

$$S_{12} = \left.\frac{V_1 - I_1}{V_2 + I_2}\right|_{a_{1=0}} \qquad \ldots\ldots (6.3.17)$$

$$S_{22} = \left.\frac{V_2 - I_2}{V_2 + I_2}\right|_{a_{1=0}} \qquad \ldots\ldots (6.3.18)$$

If an AC voltage source with an RMS voltage equal to V_s and a source impedance R_s equal to one ohm (the normalised base impedance) is connected to port 1, and port 2 is matched to ensure a_2 is zero as shown in fig 6.8(a), then :

$$V_1 = V_s - I_1 R_s = V_s - I_1 \qquad \ldots\ldots (6.3.19)$$

and

$$V_1 + I_1 = V_s - I_1 + I_1 = V_s \qquad \ldots\ldots (6.3.20)$$

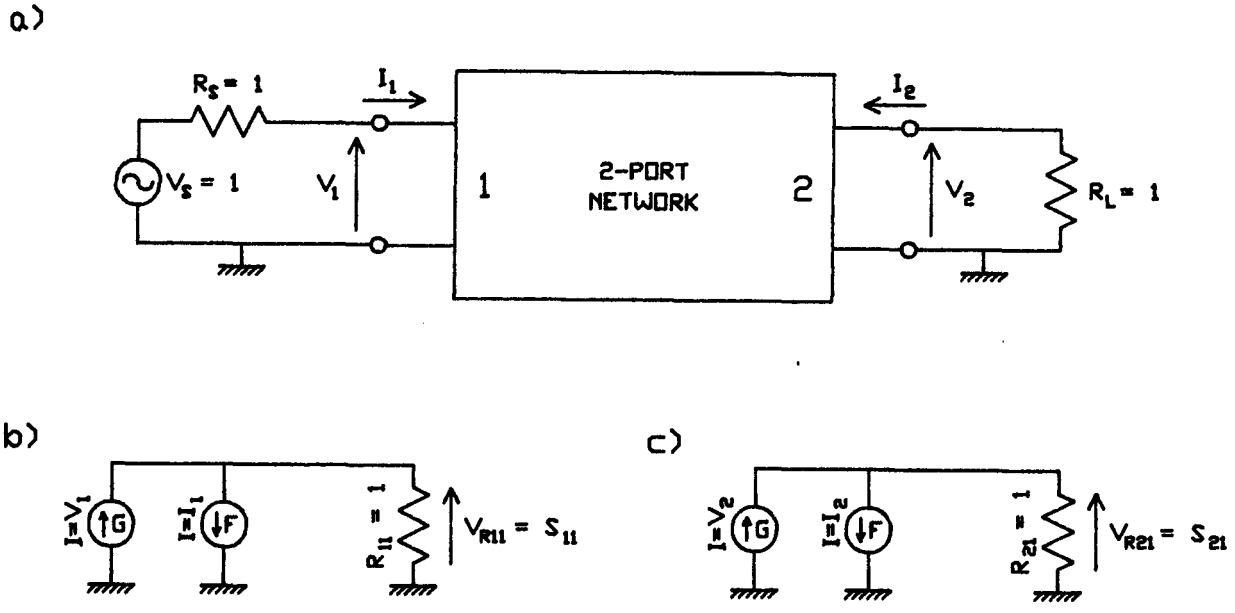

Fig 6.8 : **Circuits required for 2-port S-parameter measurements on SPICE**

a) main circuit

b) S_{11} auxiliary circuit

c) S_{21} auxiliary circuit

From equation (6.3.20) it can be seen that if V_s = 1 volt then $V_1 + I_1 = 1$ and S_{11} and S_{21} simplify to :

$$S_{11} = (V_1 - I_1)_{a_{2=0}} \qquad \text{..... (6.3.21)}$$

$$S_{21} = (V_2 - I_2)_{a_{2=0}} \qquad \text{..... (6.3.22)}$$

Auxiliary circuits can now be used to perform the subtractions. SPICE has an element called a linear voltage-controlled current-source (G) which, with a unity transconductance, gives a current equal to a voltage at a specified point. Similarly a linear current-controlled current source can be used to generate a current equal to the current in a specified branch of the circuit. Fig 6.8(b) shows such a circuit set up so that the current sources are paralleled and loaded with a one ohm resistor. The voltage

across the resistor V_{R1} is then given by :

$$V_{R1} = V_1 - I_1 = S_{11} \qquad \ldots\ldots (6.3.23)$$

A second auxiliary circuit connected as shown in fig 6.8(c) gives :

$$V_{R2} = V_2 - I_2 = S_{21} \qquad \ldots\ldots (6.3.24)$$

Thus asking SPICE to point out V_{R1} and V_{R2} in both magnitude and phase over the range of frequencies of interest, gives S_{11} and S_{21} for the network directly. Exactly the same procedure can be used to generate S_{12} and S_{22} by simply swopping the port connections.

Since S-parameters cannot be entered or modified directly, the inclusion of non-ideal properties requires adding components to cause, for example, poor VSWRs or additional phase shifts. The difficulty is that models of this sort rarely approximate the actual broad-band performance.

SPICE was used to model a single section Wilkinson power divider in this way and the S-parameters were correctly predicted. The conclusion then is that general circuit analysis programs can be used to calculate S-parameters of an FD provided the basic component models are available.

6.4 TOUCHSTONE

TOUCHSTONE is a circuit analysis package designed specifically for RF and microwave circuit analysis. It runs on an IBM PC micro-computer and compatibles. It is designed to work directly on S-parameters which is what makes it so suited to high frequency work. A few different versions are available and TOUCHSTONE/RF was used for this project.

TOUCHSTONE is extremely easy to use and can display results in several different formats. The ease of use is indicated by the

simplicity of the circuit files in appendix B. A great many circuit files were used during the course of this project and only a representative sample can be included.

S-parameters can be entered directly into TOUCHSTONE and S-parameter files created by TOUCHSTONE can be modified. This allows any non-ideal property or the measured component characteristics to be taken into account. Some versions also have physical models of microstrip and stripline transmission lines, and also discontinuity models of, for example, bends in transmission lines, step changes in line widths and T-junctions. TOUCHSTONE/RF does not.

All the above points to TOUCHSTONE being an ideal tool for FD analysis and it certainly was the best available for this project. Nevertheless there are some features of TOUCHSTONE which could be improved, and its biggest drawback is its cost and the cost of the computer equipment.

TOUCHSTONE does allow multi-port networks to be defined as sub-components of other circuits, but measurements cannot be made on networks with more than four ports. The standard FD is a five port network so that to model it it has to be divided into two three port networks with the additional ports matched with fifty ohm loads. This is clearly demonstrated in sample circuit file B-5.

Using the above method the five port FD can be analysed in a single run. However if it is required that TOUCHSTONE create S-parameter files for later analysis, then two separate runs are required since in any one run TOUCHSTONE can create only one S-parameter file. Happily the single QC FD types 1 and 2 are four port networks and can be properly handled in a single run.

Circuit file B-5 also illustrates a fault in TOUCHSTONE which is worth mentioning. Occasionally when TOUCHSTONE is asked to 'sweep' a circuit, ie. make measurements on a circuit described

in a circuit file, it appears to get stuck in an infinite loop. The only way out when this happens is to abort the run by re-setting the computer. These infinite loops occur at one or more isolated frequencies with some circuit files. Identifying these frequencies is an extremely frustrating and time consuming procedure. The 'FREQ' paragraph of circuit file B-5 is divided into two sweep commands to ensure that 4 GHz is left out. This problem did not affect the single QC FDs and the reason for it happening at all is not clear.

A feature missing from TOUCHSTONE that would be very useful, is a processing block which allows the calculated S-parameters to be manipulated to provide more meaningful information. In this case it would be very convenient to have TOUCHSTONE calculate phase or frequency errors directly. The processing block that is available in TOUCHSTONE/RF allows manipulation of corresponding parameters of two defined networks but not, for example, S_{31} to be subtracted from S_{21} of the same or a different network.

S-parameters calculated by TOUCHSTONE (TS) and stored away in disk files can be read as sequential files by BASIC programs. This provides suitable means of calculating peak and RMS errors before and after performance of linear regression. Linear regression is required for the standard version because of the phase characteristic differences between WCs and QCs, as discussed in section 4.2. Appendix K lists the program that was written for this purpose. Data required by the program, ie. the type of discriminator, centre frequency, band limits and delay line length, is passed from TS by means of a dummy S-parameter file.

S-parameter files created by TS can be very large so that disks quickly become full, particularly if several circuit files are already stored away. It is also convenient to always use the same circuit file names so that the error calculation program really has to be run after each TS circuit sweep. A batch run which automatically loads and runs the various programs is the fastest way of performing a series of analyses. User participation

is required only while TS is running to amend and 'sweep' the circuits, but it is required **each** time TS is loaded. The batch method is fully described in appendix K.

Even with batch runs the process can be very time consuming. If a great deal of FD design is to be undertaken and access to a main-frame computer is available, attention should probably be given to using the method described in section 6.2 to write a specialised but efficient analysis program. Not only would analyses take less time but user participation would only be required to enter data at the beginning of the run.

The following discussions use TS in the manner described above to focus on various aspects of the standard FD as compared to the single QC version types 1 and 2. Only a subset of the total number of factors can be considered, and those included were chosen because they highlighted certain particularly interesting features and/or demonstrated useful techniques.

6.5 BROAD-BAND DISCRIMINATOR ANALYSIS

What follows is a series of analyses made using theoretical components to compare the broadband performances of the standard FD and single QC and FDs. Some common unit of measure is required in any such comparison, and it was decided to use peak and RMS errors over a 2 to 6 GHz bandwidth as the yardstick. Phase errors are directly proportional to frequency so frequency errors could be used instead. However, frequency errors, through the proportionality constant, depend very much on the delay line length whereas phase errors depend less so. Phase errors give a more easily comparable indication of performance.

Most of the analyses were made by asking TOUCHSTONE to calculate S-parameters at frequencies spaced 100 MHz apart. This does mean that actual error peaks may be missed and peak errors may be under-estimated. RMS errors are less affected as evidenced by the comparative smoothness of the RMS error curves in the graphs in

this and subsequent sections. Some analyses were made using 200 MHz frequency intervals, and comparison with predictions made with 100 MHz intervals were favourable. This suggests that the measurements made were sufficiently accurate for comparison purposes.

It has already been mentioned that error correction through linear regression is necessary for the standard FD but not for the single QC types 1 and 2. Table 6.1 demonstrates this for FDs made of single section WCs, single section QCs and delay lines of 315 degrees at 4 GHz.

Table 6.1 : **Effect of linear regression**

Single section WCs Single section QCs Delay at 4 GHz = 315°		Standard FD errors (degrees)	Type 1 FD errors (degrees)	Type 2 FD errors (degrees)
Before linear regression	Peak	11.6	2.6	5.9
	RMS	7.56	0.78	1.54
After linear regression	Peak	3.9	2.5	3.0
	RMS	1.72	0.81	1.40

In the case of the standard FD improvement is dramatic. In the case of the type 1 FD the peak error dropped slightly while the RMS error rose. Sometimes the opposite is true and almost always one improves slightly while the other worsens. There is certainly no justification for using linear regression. In the case of the type 2 discriminator there is a small improvement in this isolated case. Usually the type 2 discriminator shows the same trends as the type 1 version.

Of particular interest is the performance of the three discriminator types with different size components. Table 6.2 answers this

Table 6.2 : **PFD error performance with different components**

Components		Single section quad. coupler		Three-section quad. coupler	
	PFD	Peak(deg)	RMS(deg)	Peak(deg)	RMS(deg)
Single section Wilkinson	Type 1	2.6	0.78	7.2	1.30
	Type 2	5.9	1.54	3.8	1.03
	Std. FD	3.9	1.72	0.8	0.16
Two-section Wilkinson	Type 1	1.9	0.30	1.0	0.18
	Type 2	1.6	0.27	0.6	0.11
	Std. FD	3.6	1.42	2.0	0.84
Three-section Wilkinson	Type 1	0.5	0.15	0.4	0.09
	Type 2	0.5	0.15	0.2	0.08
	Std. FD	3.7	1.52	1.9	0.70

question. The Wilkinson couplers were all centred on 4 GHz, as were the QCs. For the latter the coupled and direct output curves were overlapped just sufficiently to cover a band of 2 to 6 GHz. The length of the delay line was chosen to be 315 degrees in each case, since the analyses done in section 6.1 indicated that this would give worst case errors for FD types 1 and 2.

Table 6.2 shows that for the standard FD the size of the WCs makes very little difference to error performance. The corresponding is true for the size of the QCs used in FD types 1 and 2. In each case the size of the other component has a substantial effect, the larger the component the better the performance as expected. Thus for this bandwidth a single section QC should be used for discriminators 1 and 2, and a single section WC is suited to the

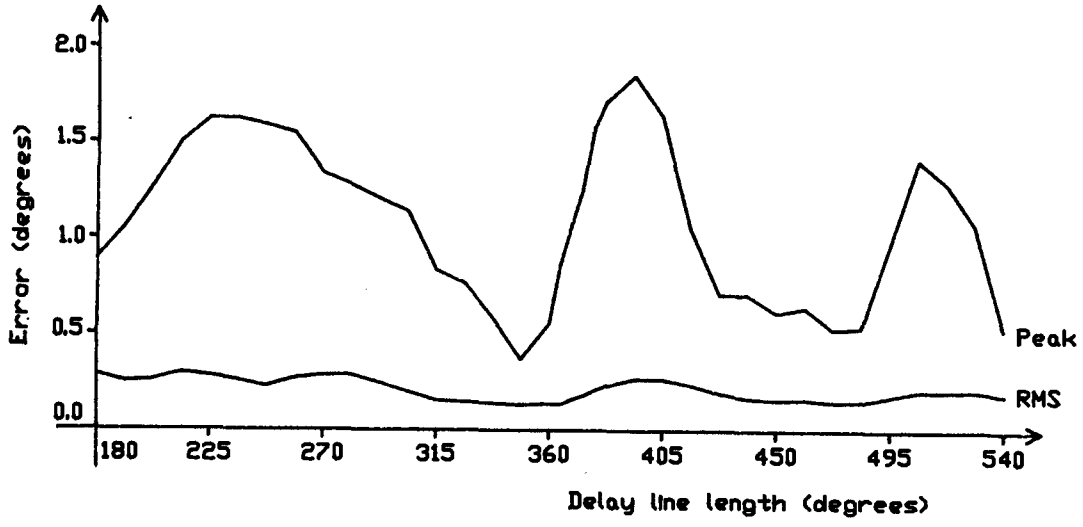

Fig 6.9 : **RMS and peak errors plotted against delay line length for a standard FD consisting of 3-section QCs and single section WCs**

standard version. Choice of the remaining component depends on required accuracy and size, and should be tempered by a knowledge of how ideal the components can be made.

The trends for FD types 1 and 2 with a single section QC and varying WC sizes are interesting. When a very narrow band WC is used type 2 does not perform as well as type 1. This is because the poor VSWRs at the band limits is more significant as a cause of error than the roll off of the power split characteristic. When a two-section WC is used the VSWR improves to the point that type 2 gives slightly better results than type 1. However when a 3-section WC is used both VSWR and flatness of the power split characteristic are improved to the point that the FDs perform equally well. The conclusion is that use of the larger type 2 FD is not warranted.

The entries in table 6.2 for the standard FD with three-section QCs and single section WCs are surprisingly good. Note however that they should really be compared with the entries for type 1 and 2 FDs with single section QCs and 3-section WCs. The analyses in section 6.1 suggest that discriminators 1 and 2 give worst

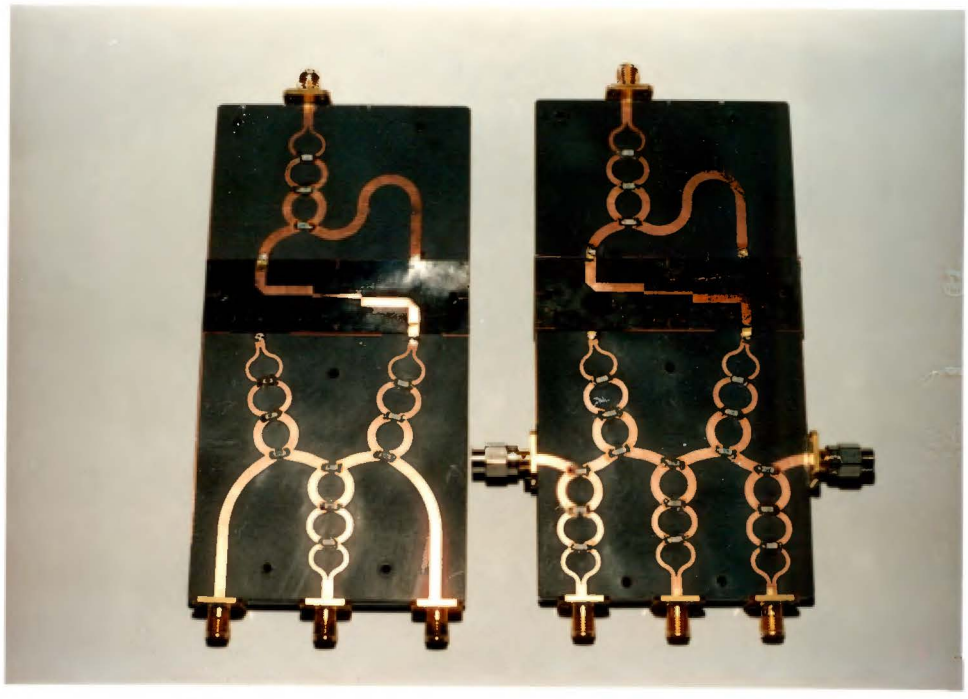

Fig 7.1 : Disassembled type 1 (left) and type 2 FD prototypes

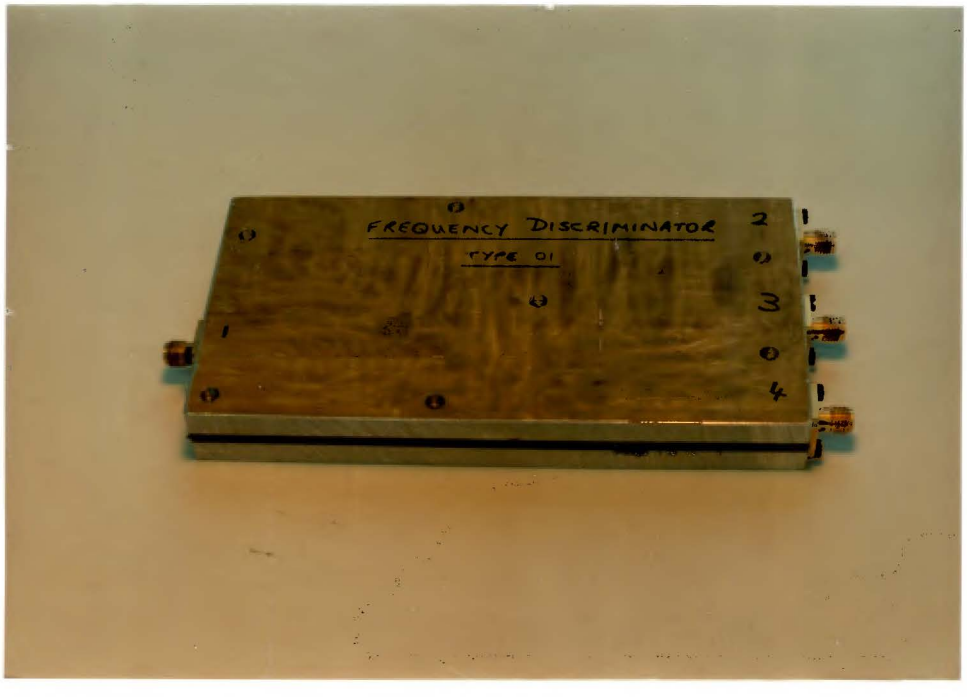

Fig 7.2 : Assembled type 1 prototype

overall size and weight can be greatly reduced by using materials with higher dielectric constants, thinner ground planes and by using microstrip rather than stripline. Ultimately the detectors would be integrated with the rest of the RF circuit, but this was not desirable for the prototypes since it would reduce flexibility during testing.

Connections between the QCs and the rest of the circuit were made by soldering small brass foil strips onto the 0.062" board conductors. Contact with the QC was maintained by pressure alone, as was contact between the tabs of the SMA co-axial to stripline launchers and the copper tracks. Thick film chip resistors were used for the WCs and these were soldered in place on the copper tracks. Small slots had to be cut into the top dielectric to accommodate the resistors. Their exact location was found by screwing the top and bottom plates together before the slots were cut. The chip resistors caused very slight indentations in the upper dielectric surface and these were used as guides to chisel away the minimum amount of dielectric.

Given more professional facilities it would have been far better to etch the entire circuit on the 0.005" board. Connections through the board, as required by the overlay couplers, would then be achieved by through-hole plating. This would eliminate the need for foil strips to make connections and ensure that the QCs are properly aligned. Mis-alignment causes differences in the lengths of transmission lines connecting to the other components. On the delay line side these differences can be absorbed into the effective length of the delay but on the phase discriminator side these differences cause errors in the summing process of the power combiner giving the centre output.

7.2 S-PARAMETER MEASUREMENTS OF TYPE 1 PROTOTYPE

After construction of the type 1 prototype shown on the left in fig 7.1 and before the addition of the detectors, its s-parameters were measured on the HP 8410C network analyser. Port numbering

for all the s-parameters given below is as follows. The input port is port one and outputs V_1, V_2 and V_3 of fig 4.15 are numbered 2, 3 and 4 respectively.

The important parameters from which phase accuracy can be calculated are S_{21}, S_{31} and S_{41}. These are shown graphically in fig 7.3(a). From these results it was possible, as will be seen, to infer an effective delay line length of 308.5 degrees at 4 GHz. Fig 7.3(b) shows predicted curves using ideal three section WCs and QCs and a 308.5 degree delay. The frequencies at which the dips in the curves occur agree to within the 0.1 GHz frequency steps that were used.

Fig 7.3(c) shows the predictions made using the measured values of the individual components as given in chapter 5. Again a delay line of 308.5 degrees at 4 GHz was used. The rather disappointing shallowness of the S_{21} dip in fig 7.3(a) is predicted by these measurements and indicates that accuracy may be poorest between 5 and 6 GHz. This time the frequencies at which the dips occur differ by 0.1 GHz at the top end of the frequency range. The reason for this is that when the components were built it was practically impossible to make the attached fifty ohm transmission lines equal in length to within about ± 0.2 degrees at 4 GHz or ± 0.3 mm. These transmission lines could not be excluded from the s-parameter measurements and affect the effective delay line length for fig 7.3(c), thus lowering slightly the frequencies at which the dips occur. Accuracy calculations are also affected and linear regression can be used to improve things somewhat, as was done for table 6.3.

Although not required to assess error performance, the measured return losses due to S_{11}, S_{22}, S_{33} and S_{44} are plotted in fig 7.4 for completeness. Similarly the isolations S_{23}, S_{24} and S_{43} are given in fig 7.5.

Error predictions from the S_{21}, S_{31} and S_{41} measurements can be made exactly as is done when TOUCHSTONE is used. The first step

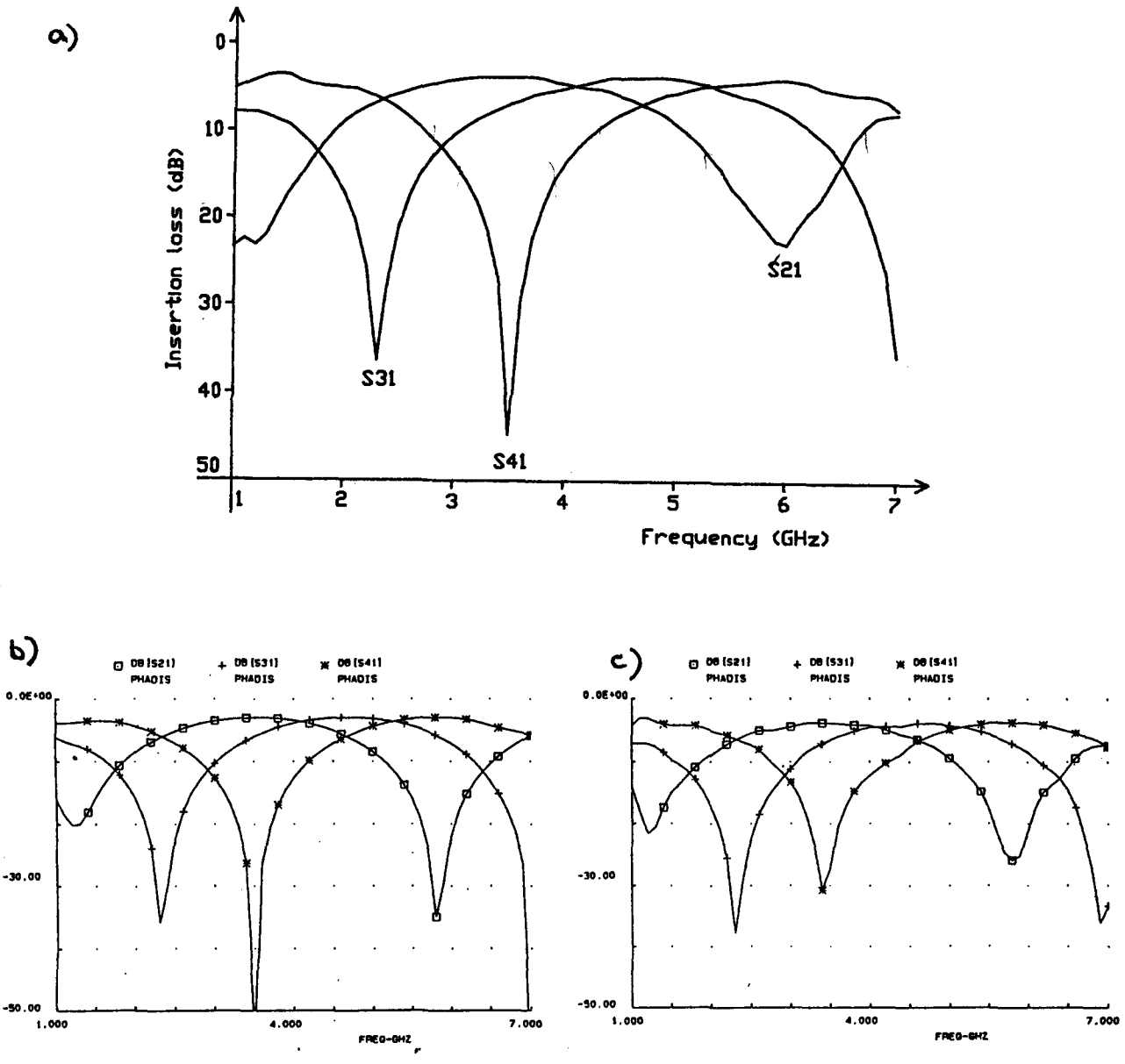

Fig 7.3 : **Type 1 S_{21}, S_{31} and S_{41} curves**

a) measured prototype results

b) predicted results using ideal components

c) predicted results using measured components

is to determine the effective length of the delay line. Direct calculations indicate that the phase is 308.5 degrees at 4 GHz. The best fit straight line through all the data in the band 2 to 6 GHz calculated by least squares linear regression is:

$$\theta = 4.07 + 76.12f \qquad \ldots\ldots (7.2.1)$$

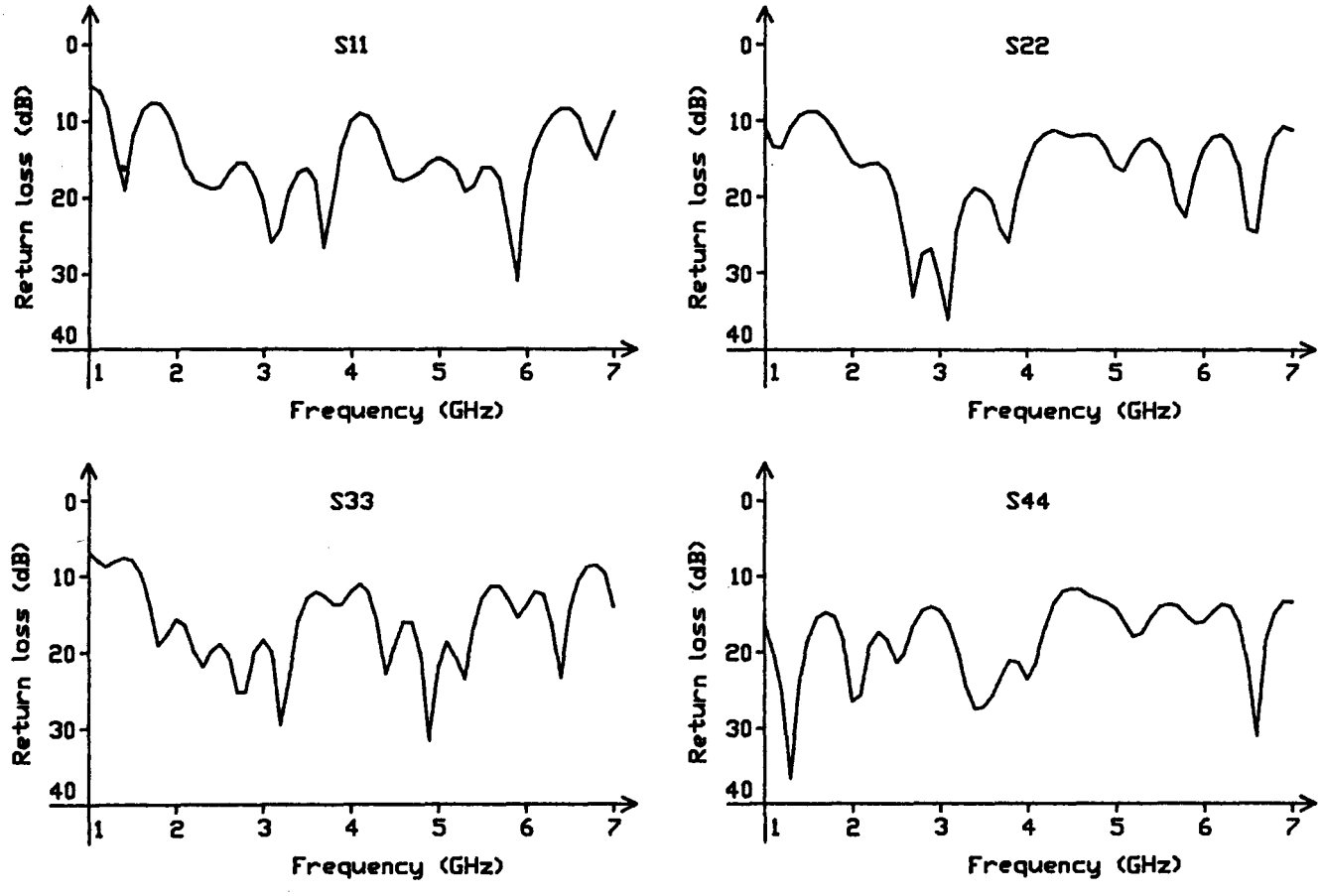

Fig 7.4 : **Measured return losses for type 1 prototype**

where θ is the phase in degrees and f the frequency in GHz. This suggests a delay line length of 304.5 degrees at 4 GHz and a constant offset of 4 degrees. The offset is due to errors caused by mis-alignment of the quadrature coupler as mentioned in the previous section

Using the measured data and taking the delay line length to be 304.5 degrees at 4 GHz gives peak and RMS errors of 6.9 and 4.0 degrees respectively. The corresponding errors assuming a delay line of 308.5 degrees are 4.2 degrees peak and 1.6 degrees RMS. After linear regression the result is precisely the same in each case as expected. Peak and RMS errors then become 3.3 degrees and 1.4 degrees respectively.

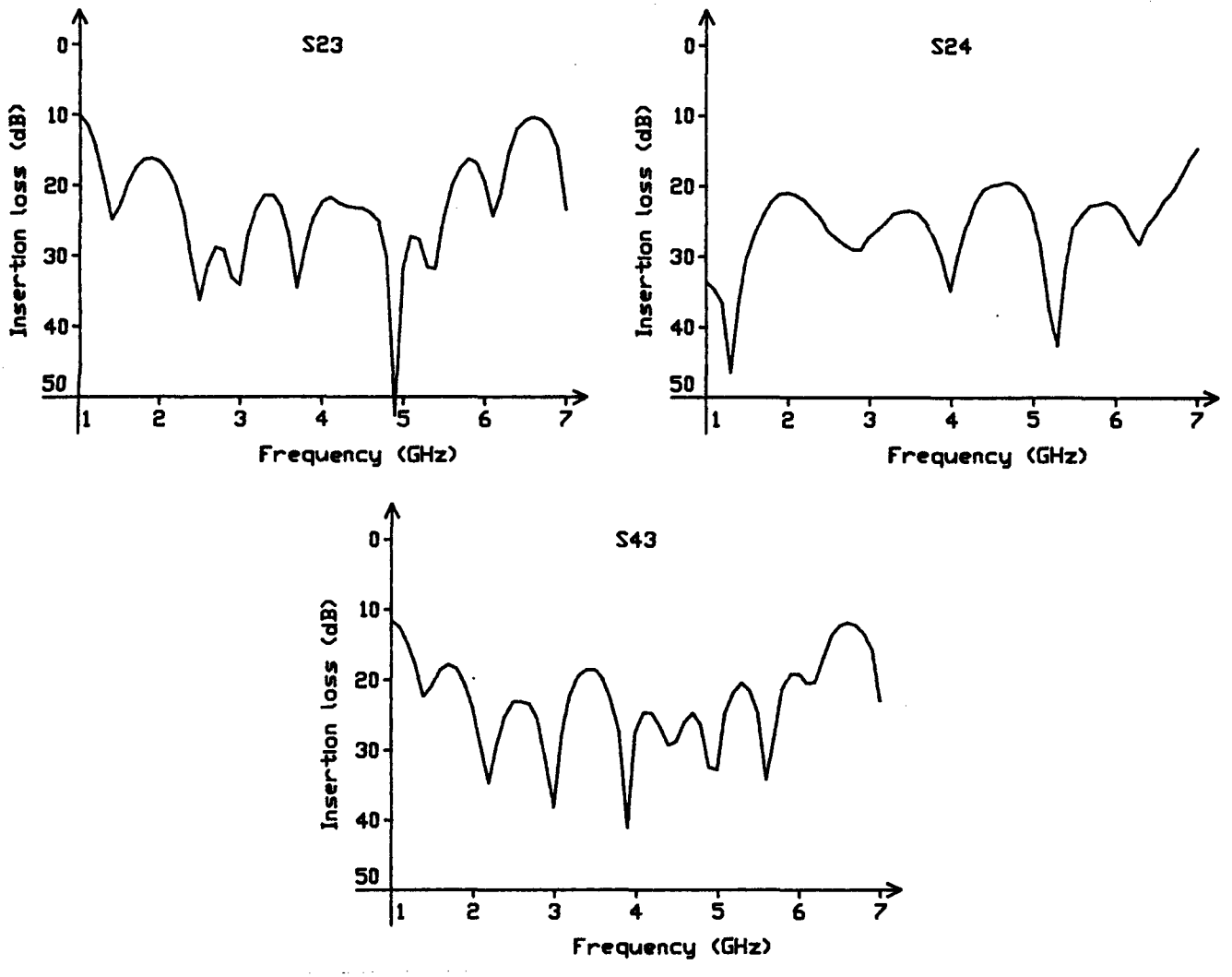

Fig 7.5 : **Measured isolations for type 1 prototype**

The above plus the frequency agreement at which the dips occur in figs 7.3(a) and 7.3(b) suggest that the effective delay line length is 308.5 degrees at 4 GHz. Furthermore the use of linear regression is justified with the prototypes to reduce errors due to QC mis-alignment.

Fig 7.6 shows the error performance of the type 1 prototype after linear regression. In contrast fig 7.7 shows the predicted curve using measured parameters of the individual components after linear regression. There is very little agreement between the two cases. There are several reasons for the disagreement. The problem of

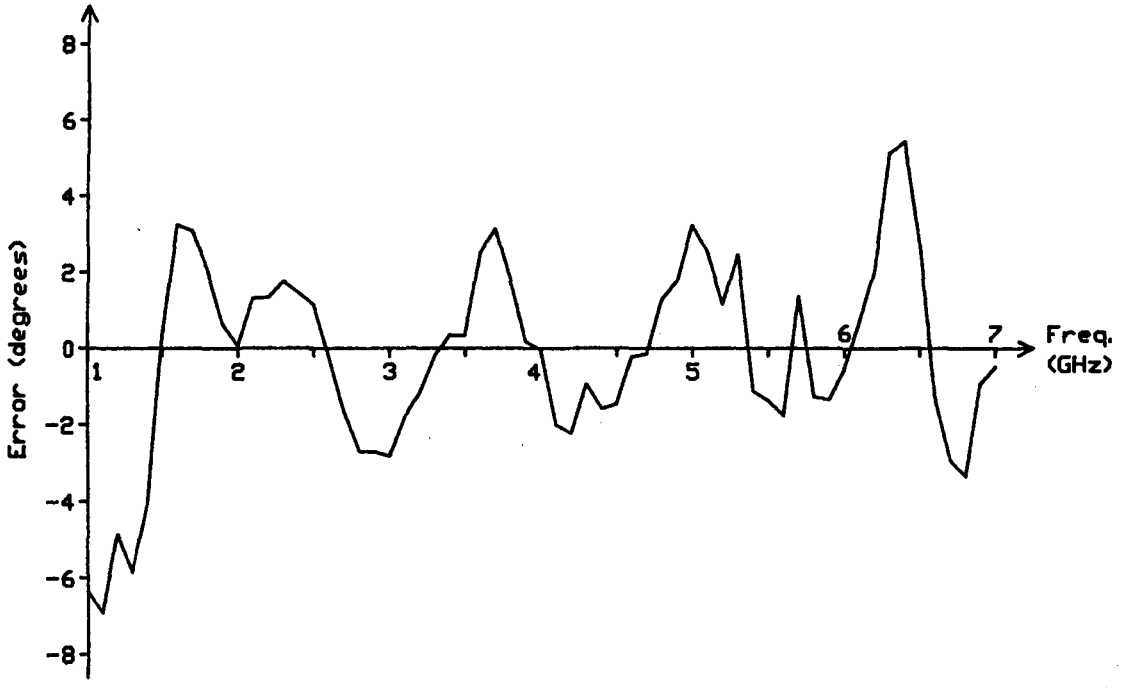

Fig 7.6 : S-parameter measurement error predictions for type 1 prototype after linear regression

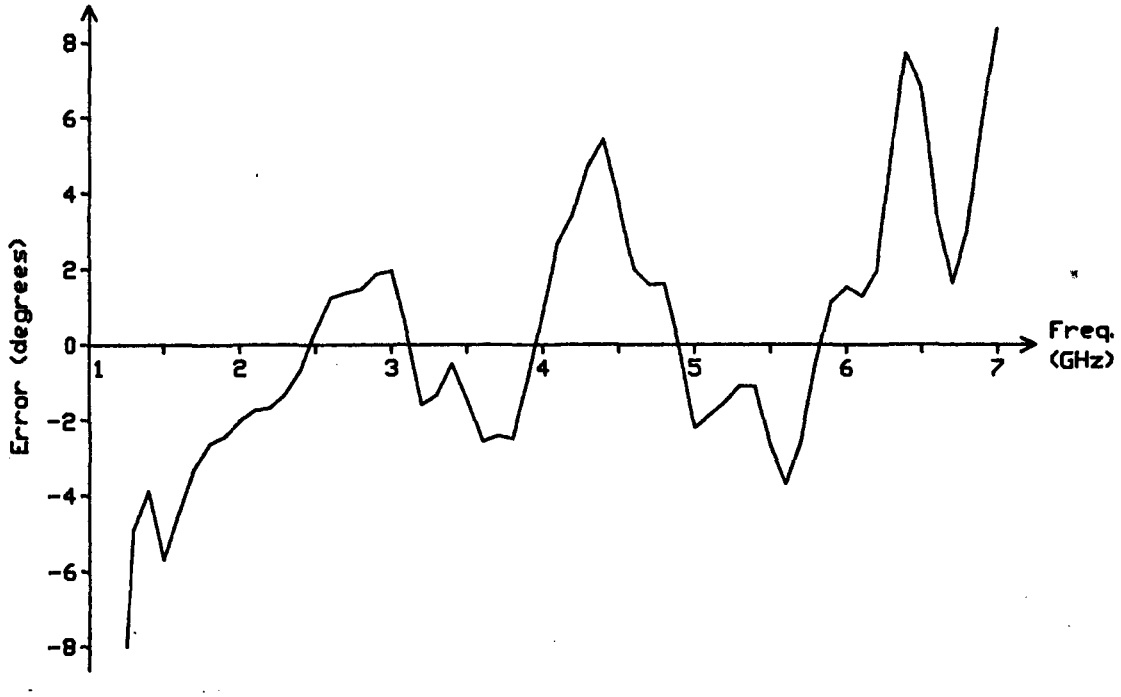

Fig 7.7 : Error predictions for type 1 FD from component s-parameter measurements after linear regression

the different transmission line lengths has already been mentioned. The co-axial to stripline launchers which were used to make the original component measurements also affected the accuracy of the original measurements. Since the QC was inserted as a separate component it could be measured separately. In the case of the WCs this was not possible and they are unlikely to have been identical to the test version or each other. All the above reasons suggest that the prototype should be better behaved than the component measurements suggest. This is indeed the case.

7.3 S-PARAMETER MEASUREMENTS OF TYPE 2 PROTOTYPE

Before adding the detectors to the type 2 prototype shown on the right in fig 7.1, its s-parameters were measured on the HP 8410C network analyser. Port numbering is exactly the same as for the type 1 discriminator for all the s-parameter references below.

Fig 7.8(a) gives the measured S_{21}, S_{31} and S_{41} curves. These are all that is required for an accuracy analysis. Once again these results suggest a delay line length of 308.5 degrees at 4 GHz. This is not surprising since the delay line is identical in design to that used in the type 1 prototype, and the rest of the circuits of both prototypes are so similar. Fig 7.8(b) gives the corresponding results predicted by TOUCHSTONE when ideal three section WCs and QCs are used with a delay of 308.5 degrees at 4 GHz. Once again the frequencies at which the dips occur are in agreement.

Fig 7.8(c) shows the predictions made using the measured values of the individual components as given in chapter 5. The rather shallow dips of S_{21} are correctly predicted. For the same reasons as described in section 7.2, the predicted dips are lower in frequency then were actually measured.

The S_{21}, S_{31} and S_{41} parameters were used to assess the error performance of the type 2 prototype as was done for type 1. Once again linear regression may be used to reduce the effect of QC

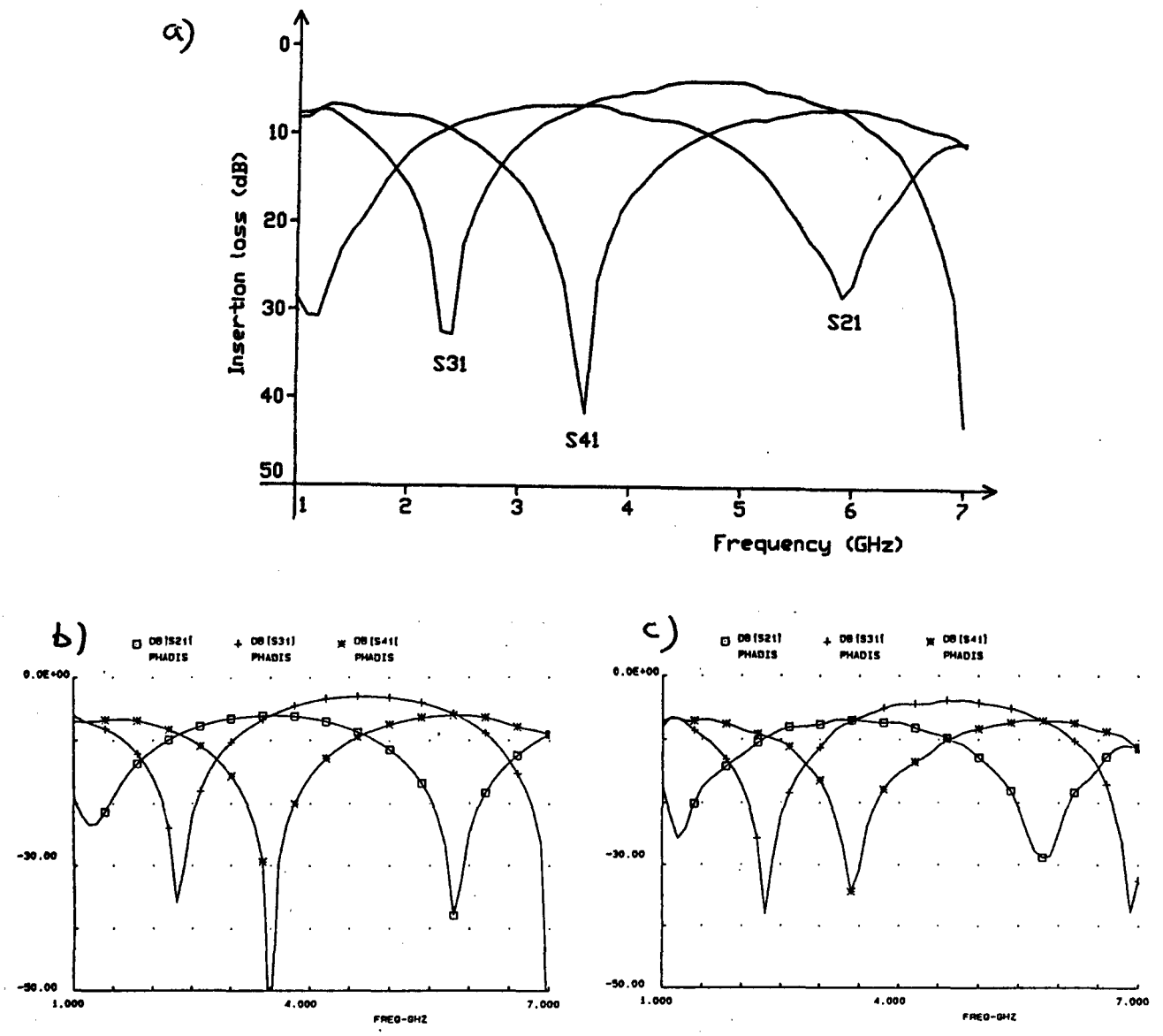

Fig 7.8 : **Type 2 S_{21}, S_{31} and S_{41} curves**

a) measured prototype results

b) predicted results using ideal components

c) predicted results using measured components

mis-alignment. Before linear regression the peak and RMS errors assuming a 308.5 degree delay line were calculated as 6.5 and 1.6 degrees respectively. After linear regression they become 6.0 and 1.4 degrees respectively. Using the individual measured components the prediction is 6.5 degrees peak and 1.9 degrees RMS after linear regression. These values were expected to be

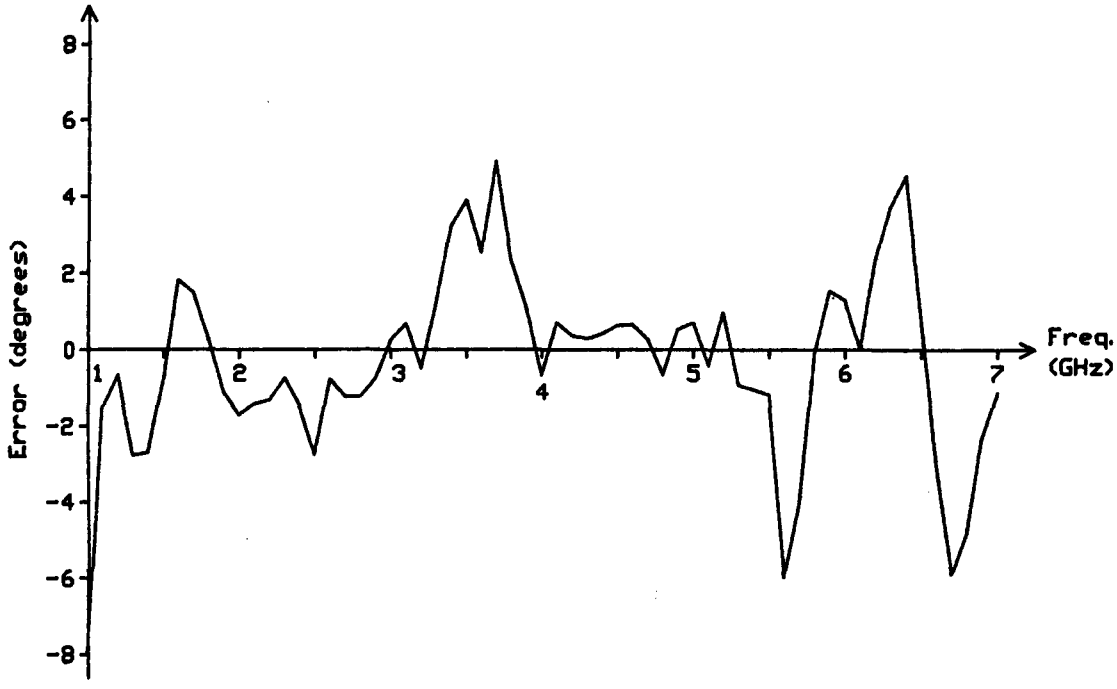

Fig 7.9 : **S-parameter measurement error predictions for type 2 prototype after linear regression**

worse than the prototype s-parameter measurements predict for the same reasons as discussed in section 7.2. Fig 7.9 shows the errors predicted by the prototype measurements plotted against frequency.

7.4 PROTOTYPE PERFORMANCE WITH DETECTORS ATTACHED

The next step in evaluating the performance of the prototypes is to add the detectors and measure their outputs over the 2 to 6 GHz frequency range. This gives quantities V_1, V_2 and V_3 which must be manipulated to calculate phase and hence accuracy. All the accuracy results quoted here were obtained assuming a delay line of 308.5 degrees at 4 GHz.

Fig 7.10 shows the circuit used for the analyses discussed in this section. The signal generator output was 'chopped' by a 27.8 kHz square wave to allow AC coupling to the voltmeter and

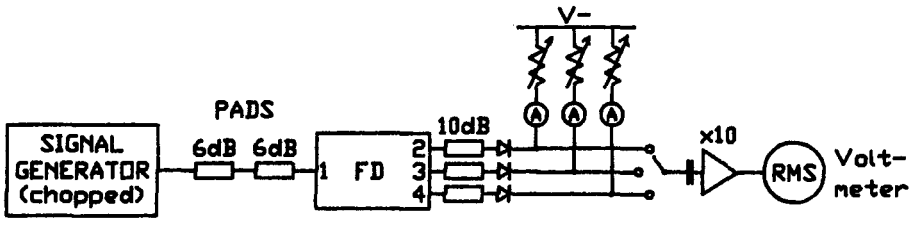

Fig 7.10 : **Circuit for performance analysis of FDs with detectors attached**

hence exclude the relatively large DC bias voltages. An RMS voltmeter was used to measure the outputs in dBV. An amplifier with voltage gain ten was used to improve sensitivity. A multi-way switch was used to allow the amplifier and RMS voltmeter to be quickly switched from one output to another.

Unless otherwise stated, detectors 866538, 866520 and 866539 were connected to FD ports 2, 3 and 4 respectively. To provide broad-band input matching to the detectors, 10dB or 6dB pads were added to give minimum return losses of 20dB and 12dB respectively. The pads at the front of the FD were required because the minimum drive level of the signal generator was -5dBm.

The first test performed on the type 1 prototype used exactly that circuit shown in fig 7.10. To provide a maximum detector drive level of -20 dBm, and hence ensure that they operate in their square-law region, a drive level of 9.5 dBm at the signal generator was required to overcome the effects of the pads, and losses in the transmission cables and in the discriminator itself. Measurements were performed at steps of 200 MHz.

Fig 7.11 shows the results measured without the use of linear regression. A peak error of 6.6 degrees at 5.4 GHz is indicated. A peak around this frequency is not surprising considering the shallowness of the dip at this frequency in fig 7.3(a). The RMS error was found to be 2.5 degrees. After linear regression the peak and RMS errors became 6.6 degrees and 2.2 degrees, but the

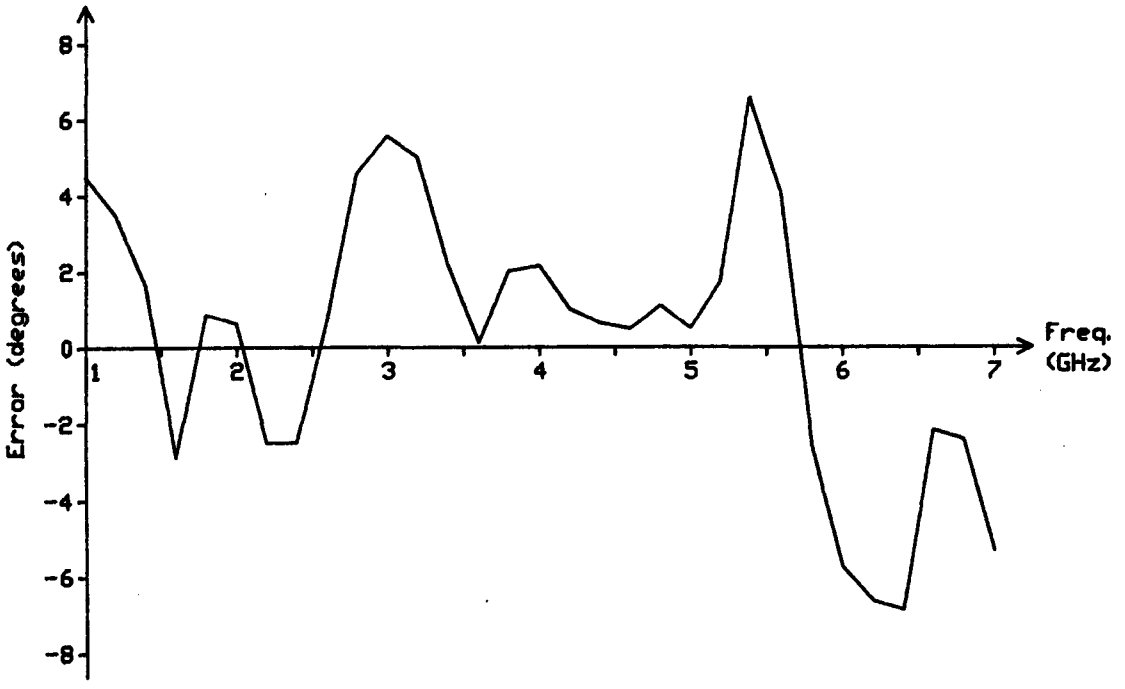

Fig 7.11 : **Error performance of type 1 discriminator with detectors attached**

peak occurs at a different frequency (6 GHz). The improvement was nominal and it was decided not to use linear regression in subsequent tests.

The detectors are of course not precisely identical and switching the detectors around must affect the results. If, for example, the detectors attached to ports 2 and 3 are swopped then the peak and RMS errors become 8.3 and 3.4 degrees respectively if the rest of the circuit remains unchanged. The detector arrangement described initially gave best results and was used in all subsequent tests.

The effects of detector drive levels exceeding slightly the square-law region can be seen by increasing the drive at the signal generator to 12dBm. The peak drive to the detectors is then -17.5 dBm. Errors worsen slightly to 7.9 degrees peak at 6 GHz and 3.1 degrees RMS.

The 10dB pads used to match the detector inputs may cause an excessive amount of loss and could worsen error performance by reducing sensitivity. Of interest then is the effect of using say 6dB pads. For this test the 10dB matching pads were replaced with 6dB pads. The two front end 6dB pads shown in fig 7.10 were replaced with a single 10dB pad. The signal generator drive level was reduced to 3.5dBm to ensure a maximum detector drive of -20 dBm. Peak and RMS errors worsened to 8.8 and 4.0 degrees respectively. The peak again occurred at 5.4 GHz.

Similar tests were performed on the type 2 prototype and the same general trends described above were seen. Overall performance was worse than for type 1. With a maximum detector drive of -20 dBm and 6dB detector matching pads, the peak error was 11.9 degrees at 5 GHz and the RMS error was 5.1 degrees. 10dB matching pads improved performance to 8.1 degrees peak at 3.8 GHz and 4.2 degrees RMS.

7.5 PROTOTYPE PERFORMANCE WITH SIMPLE PROCESSING CIRCUITRY

To complete the tests on the prototypes some processing circuitry is required. Ideally, to allow the processing of RF pulses 100ns wide, the processing circuitry should be able to operate at least up to 10 MHz. It is not quite so important that the gain responses be flat up to this frequency but that the individual channel gains be equal. The HP 8350B sweep oscillator that is part of the HP 8410C network analyser has an inbuilt facility allowing the RF output to be 'chopped' or switched on and off rapidly at 27.8 kHz. This gives a pulse length of 18μs and it was decided to test the concept with simple circuitry capable of handling at least 60 kHz.

Fig 7.12 shows simple circuits that can be used to perform the required operations. Factor 'a' in fig 7.12(b) can be varied to suit either discriminator type. Fig 7.13 shows the actual circuit that was used. Operational amplifier balancing and power supply details have been omitted. The basic circuits of fig 7.12

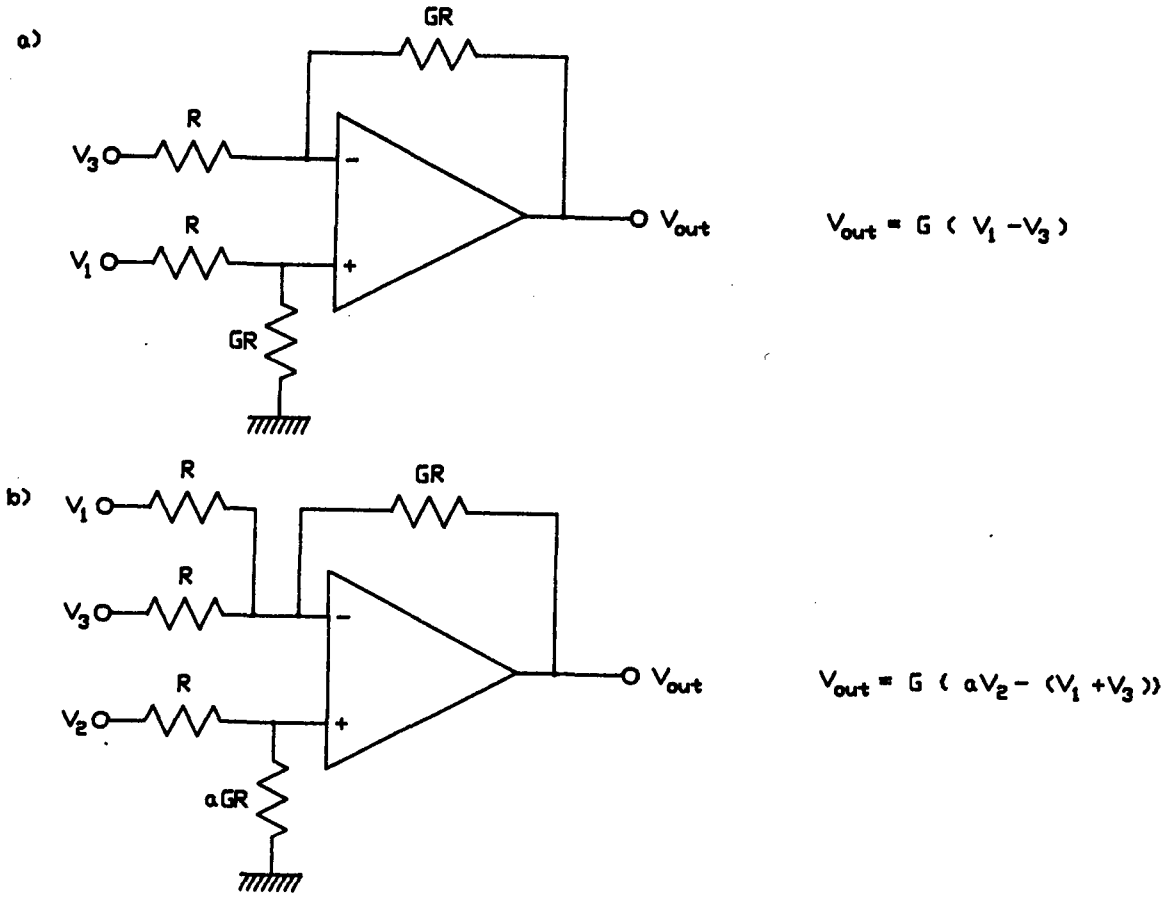

Fig 7.12 : Operation of processing circuit

are clearly evident but front-end buffer amplifiers have been used. These allow equal input impedances to be presented to each detector. The voltage gain of the front-end amplifiers is five and that of the summing circuits two, giving an overall voltage gain of ten.

To accommodate the extra factor two appearing in the type 1 discriminator relationships, the centre input amplifier of fig 7.13 has a switch allowing the gain to be stepped up to ten. Presets were used to allow the channel gains to be individually adjusted. AC coupling with a cutoff of 10 Hz was used to provide immunity from the DC biasing.

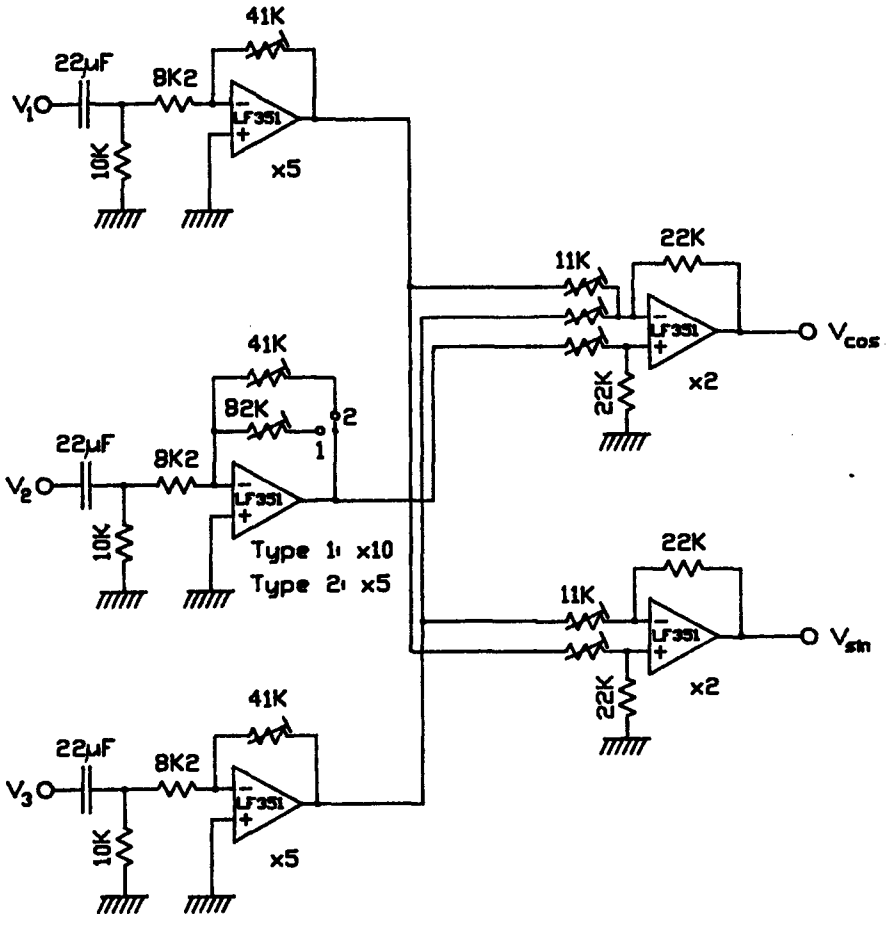

Fig 7.13 : **Simple processing circuit for both prototypes**

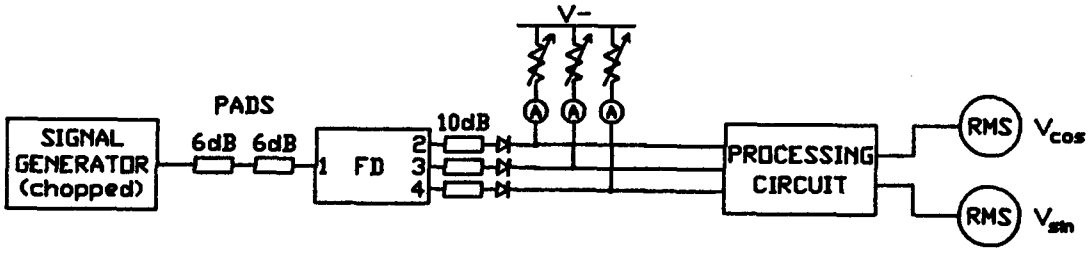

Fig 7.14 : **Error analysis with processing circuit**

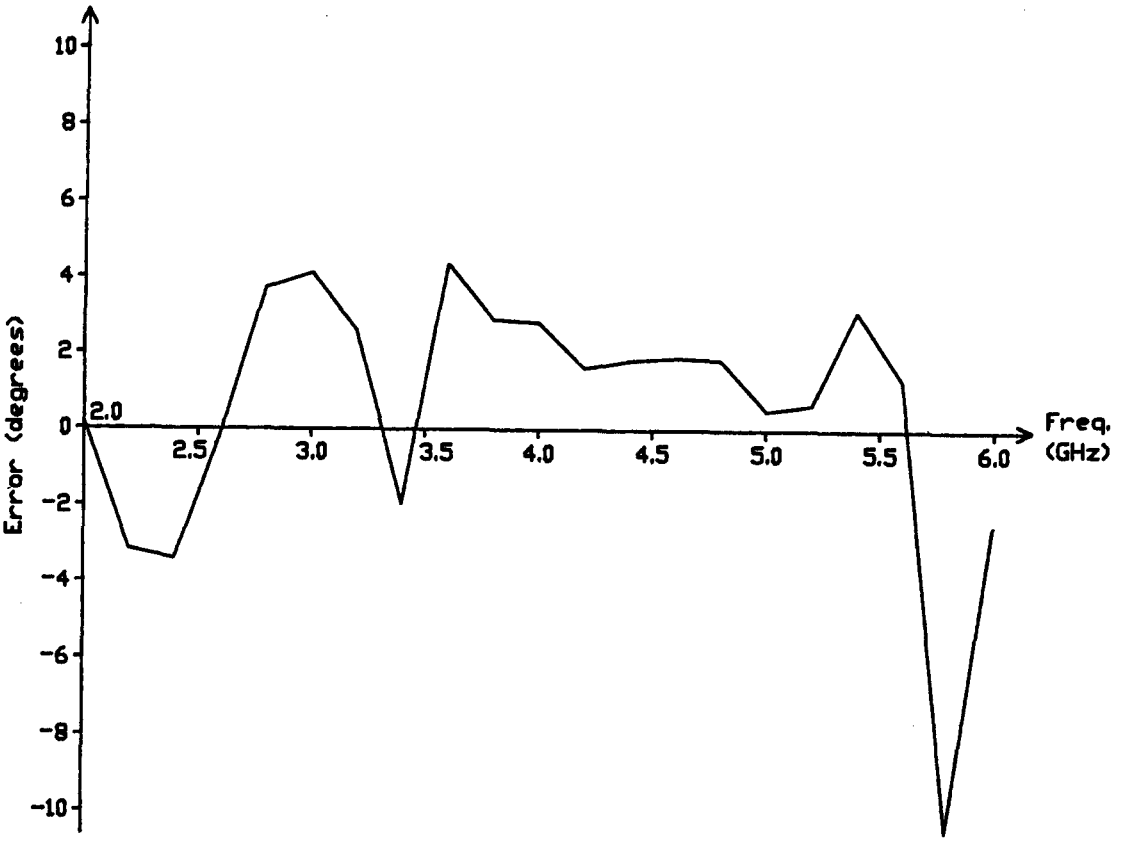

Fig 7.15 : **Error plot for type 1 prototype with processing circuitry**

Fig 7.14 shows the complete circuit used to analyse the performance of the prototypes with the processing circuit. 10dB pads were used to match the detectors as these gave best results in the previous section. The drive level at the signal generator was set as in section 7.4 to ensure that the maximum detector drive was -20dBm. Detectors 866538, 866520 and 866539 were connected to ports 2, 3 and 4 respectively.

Fig 7.15 shows the error plot for the type 1 prototype. Except for a large spike of 10.5 degrees at 5.8 GHz performance is good as indicated by the RMS error of 2.6 degrees. Before the addition of the processing circuit the RMS error was calculated to be 2.5 degrees. Fig 7.16 shows the equivalent plot for the type 2 prototype. The peak error is 7.6 degrees at 4.2 GHz and the RMS error is 4.0 degrees. These compare well with the 8.1 degrees

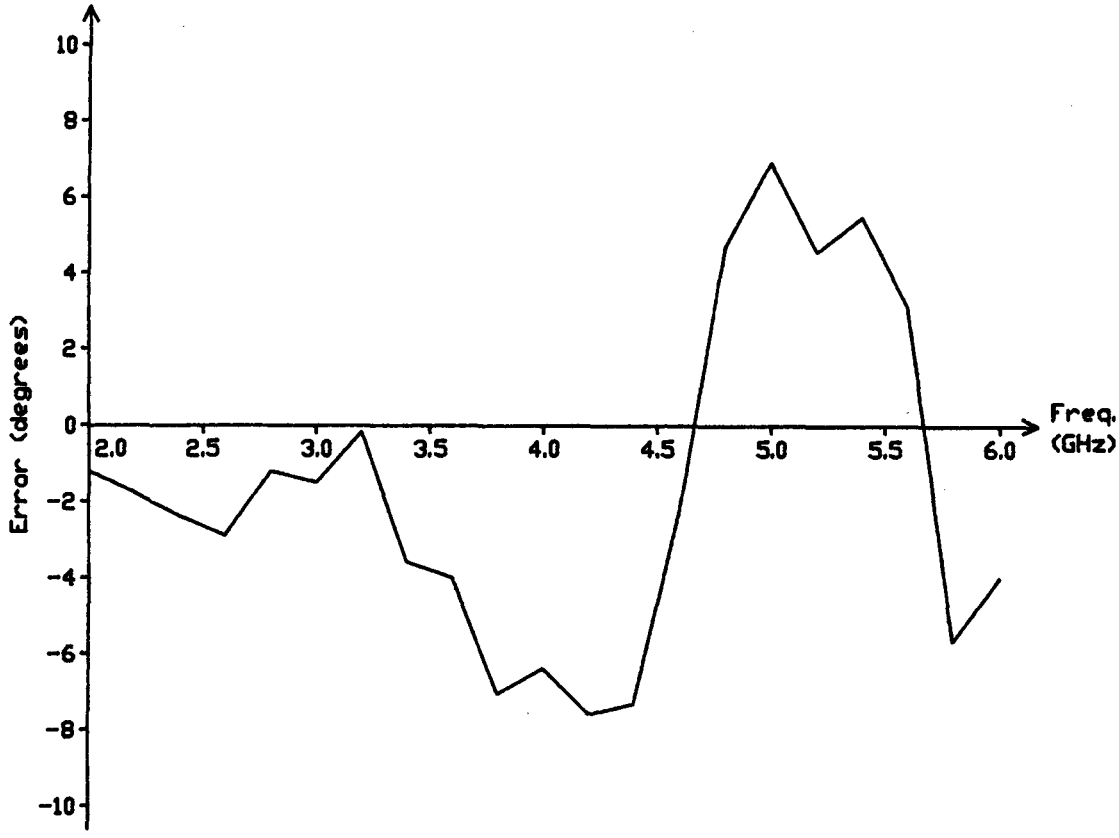

Fig 7.16 : **Error plot for type 2 prototype with processing circuitry**

peak and 3.8 degrees RMS measured prior to the addition of the processing circuit. The RMS values give a more consistent indication of performance than peak values because of the need to use frequency steps.

7.6 REPORTED STANDARD DISCRIMINATOR ACCURACIES

It is difficult to make direct performance comparisons with FDs reported in the literature because of different bandwidths used. Furthermore it is usually not made clear whether, for example, quoted errors include processing circuitry or whether performance is based on s-parameter measurements or actual detector outputs. Often errors are quoted in MHz which is very dependent on delay line length.

Table 7.1 : **Standard FD phase errors**

REFERENCE	BANDWIDTH (GHz)	ERROR (degrees)	
		PEAK	RMS
24	1 - 2	5	-
24	2 - 4	5	-
21	2 - 4	9	3.5
24	4 - 8	7	-
21	4 - 8	9	3.5
24	8 - 12	7	-
21	8 - 12	10.5	4.5
24	8.5 - 9.6	7	-
24	11 - 18	11	-
21	12 - 18	12.5	5.5
20	22.5 - 37.5	15	-

Table 7.1 summarises some of the results that have been reported for standard discriminators or variations of the standard form. Both prototypes and particularly type 1 compare very favourably, especially considering their fairly crude construction. Their 3:1 bandwidth is larger than any of those listed although they cover the lower end of the band.

7.7 SUMMARY

Prototype type 1 and type 2 FDs have been built in stripline to cover the band 2 to 6 GHz. Simple processing circuitry has been built to handle fairly long RF input pulses to demonstrate the

overall operation. The prototypes have been broadly analysed and compare favourably with reported standard FD performances.

More professional construction techniques have also been suggested. This should improve overall performance and remove any large error spikes that occur, such as that for the type 1 discriminator shown in fig 7.15.

CHAPTER EIGHT

CONCLUSIONS

This dissertation began by briefly looking at various acquisition receiver types, including the instantaneous frequency measuring (IFM) receiver. With current technology levels IFM is at least as good as any other type. The main advantages of IFM are their large instantaneous bandwidths and near unity probabilities of intercept. Its main disadvantage is its inability to deal properly with simultaneous signals. Often IFM is used in conjunction with one of the more narrow band receiver types to provide more comprehensive band coverage.

IFM receivers place certain requirements on FDs since FDs form their major RF circuitry. FDs must be small, light and cheap. Size and weight are best reduced by using microstrip integration techniques. FDs must be broad band and accurate, hence their components must have equally large bandwidths and be well behaved.

The various FD forms covered in the literature have been studied. Essentially these consist of a front end power splitter, delay line and phase discriminator (PD). One particular version is very frequently described and can be considered the standard version. Its main theoretical source of errors is a lack of component symmetry. The other FDs reported are generally variations of the standard one and are meant to reduce errors due to lack of symmetry. All result in a larger discriminator. The main practical difficulty of the standard version and its variations is the need to cross over two transmission lines while maintaining isolation between them. In the past the usual solution has been to integrate the phase discriminator section and attach the front-end delay line assembly externally.

A new version has been introduced which eliminates the need for the cross-over and exhibits greater component symmetry. It does so without increasing the number of components required and in fact reduces the number of matched detectors required from four to three. Its disadvantage is that it requires slightly more complex video processing.

A few different broadband analysis methods have been considered. The best available for this project was the IBM PC micro-computer based package "TOUCHSTONE". Several sample analyses have been carried out to compare the standard version with the new one. In all cases the new version performed as well as or better than the standard version.

Two prototype versions of the new FD form have been built to cover the band 2 to 6 GHz. Compared with reported results for the standard version and its variations, the new version performed very favourably despite rather crude construction. Better construction techniques have been suggested.

The overall conclusion is that both types of the new FD, and particularly the smaller one, are a definite improvement on the standard version and its variations. TOUCHSTONE is a good analysis tool. Peak and RMS phase discriminator errors over the operating band are a good indication of performance and allow comparisons between different FDs to be made.

8.1 SUGGESTIONS FOR FUTURE WORK

For any institution intending to do a lot of FD design time spent writing a more specialised analysis program independent of TOUCHSTONE should be well worth it. Such a program should be faster in the long run and should require less user interaction while running. Automatic computer controlled test equipment would also be a distinct advantage.

The size of the FDs should be reduced by using materials with higher dielectric constants and by building in microstrip rather than stripline. The detectors should of course be integrated with the rest of the circuit.

Further work should probably go into finding better methods of handling simultaneous signals. Currently simultaneous signals are detected by additional circuitry and the corresponding IFM data is discarded. In some simultaneous signal situations it

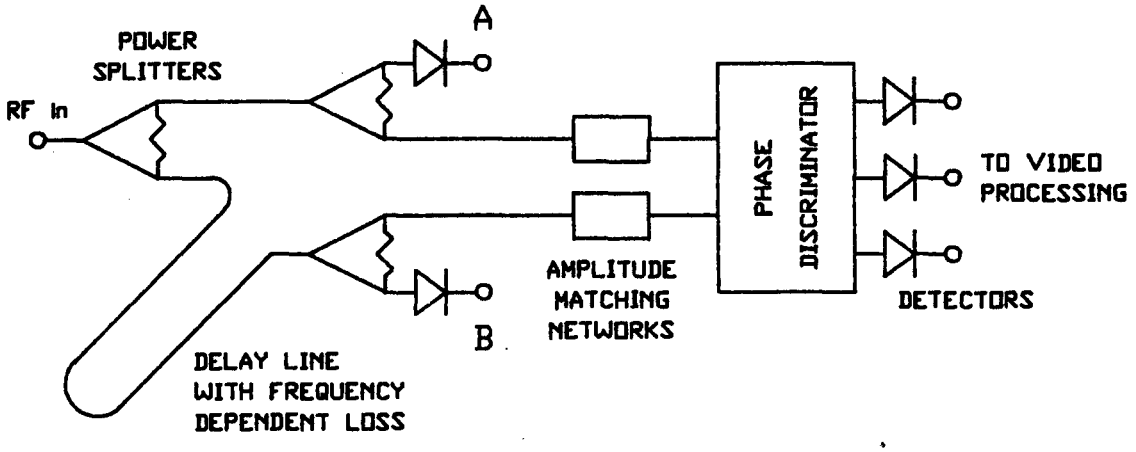

Fig 8.1 : **Possible FD giving both coarse and fine frequency data**

should be possible to determine the frequency of the largest amplitude signal or that with the longest duration. Perhaps, when two signals are present, the frequency of both signals could be inferred using prior and subsequent readings.

Another area where research work should continue is into the possibility of using a single discriminator with a long delay line that has a frequency dependent loss. The difference in amplitude between the signals entering and leaving the delay line could be used as a coarse frequency indication, rather than using an additional discriminator with a shorter delay line. The difference in amplitude between the two signals entering the phase discriminator (PD) may possibly be catered for in processing. Alternatively some amplitude matching technique may be used to ensure the amplitudes are equal at the PD inputs. Perhaps similar techniques to those used in limiting amplifiers, which are in any case always used to feed FDs, can be used. Fig 8.1 shows a possible realisation. The ratio A/B gives a coarse frequency indication whereas fine frequency information is obtained from the phase discriminator in the usual manner.

B-6 Sample S-parameter file for perfect Wilkinson coupler

The following TOUCHSTONE S-parameter file models a perfect power splitter except that the entries which are 0.100 describe an isolation of only 20dB between the two output ports. The entries would be 0.000 if isolation was also perfect.

```
! IDEAL POWER SPLITTER DESCRIPTION

1.0   0.000   0     0.707   0     0.707   0
      0.707   0     0.000   0     0.100   0
      0.707   0     0.100   0     0.000   0

7.0   0.000   0     0.707   0     0.707   0
      0.707   0     0.000   0     0.100   0
      0.707   0     0.100   0     0.000   0
```

The two left most entries are frequency data. The other entries are pairs of magnitude and phase (in degrees) data. The S-parameters are grouped as they would be in matrix form, and the node numbering is the same as that given in fig 4.2(b).

B-7 Sample S-parameter file for perfect quadrature coupler

The following TOUCHSTONE S-parameter file models a perfect quadrature coupler except that the entries which are 0.100 describe imperfect isolations of 20 dB. If perfect, the isolations would be 0.000.

To ensure that the device remains free of loss or gain the power splits are kept equal but modified to 0.704. If isolation is ideal these values should be 0.707.

```
! IDEAL QUADRATURE COUPLER DESCRIPTION

1.0   0.000   00    0.704   90    0.704   00    0.100   00
      0.704   90    0.000   00    0.100   00    0.704   00
      0.704   00    0.100   00    0.000   00    0.704   90
      0.100   00    0.704   00    0.704   90    0.000   00

7.0   0.000   00    0.704   90    0.704   00    0.100   00
      0.704   90    0.000   00    0.100   00    0.704   00
      0.704   00    0.100   00    0.000   00    0.704   90
      0.100   00    0.704   00    0.704   90    0.000   00
```

The two left most entries are frequency data. The other entries are pairs of magnitude and phase (in degrees) data. The S-parameters are grouped as is usual in matrix form, and the node numbering is the same as that given in fig 4.2(a).

B-8 Sample circuit file modelling imperfect detector VSWRs

The following TOUCHSTONE circuit file models the type 1 frequency discriminator with imperfect load VSWRs. Gyrators or impedance converters are used to give the wanted VSWR as described in section 6.8.

```
! MODEL POOR LOAD VSWRs ATTACHED TO TYPE 1 FD

VAR
    R1=100.000

CKT
    S3PA 1 2 16 W3
    TLIN 16 5 Z=50 E=315 F=4
    S4PA 2 3 4 5 3SECCPL1
    S3PA 3 6 7
    S3PA 4 9 10
    S3PA 8 7 9
    GYR 6 13 R^R1
    GYR 8 14 R^R1
    GYR 10 15 R^R1
    DEF4P 1 13 14 15 PHADIS

OUT
    PHADIS MAG[S21]
    PHADIS MAG[S31]
    PHADIS MAG[S41]

FREQ
    SWEEP 1 7 .1
```

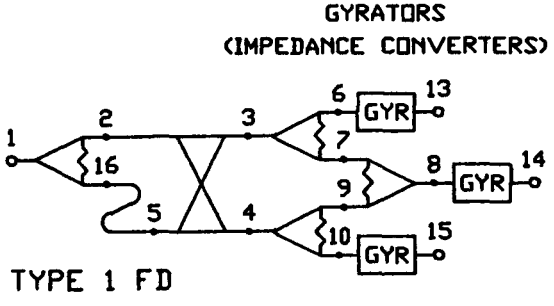

APPENDIX C

MATHEMATICAL OPERATION OF COMMON FREQUENCY DISCRIMINATOR

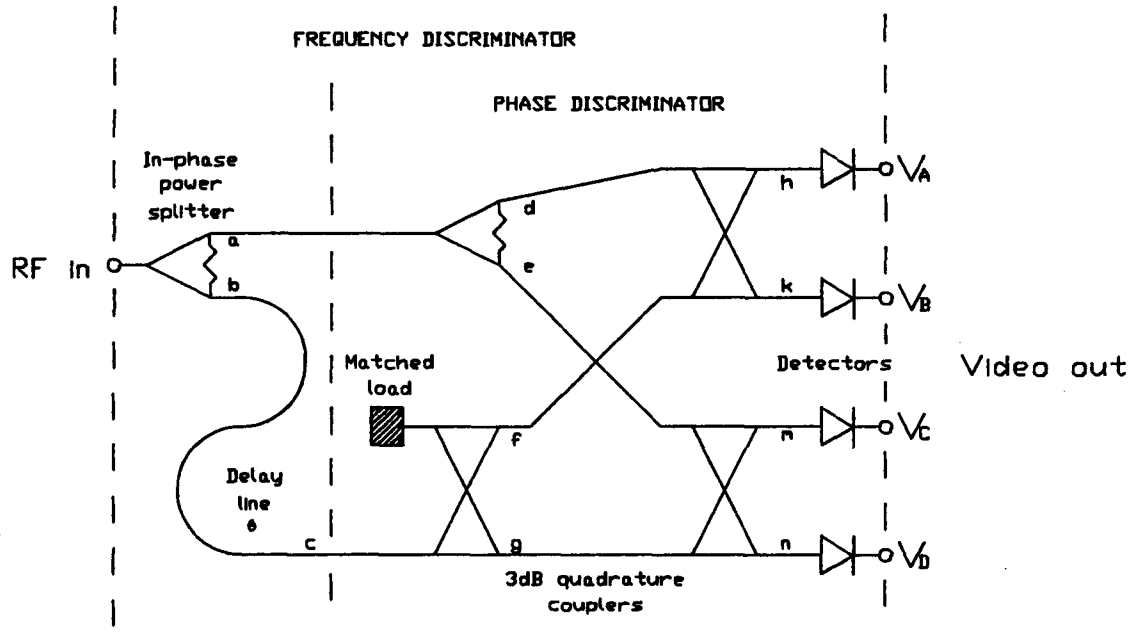

Fig C.1 : **Common frequency discriminator**

Fig C.1 shows the RF circuit configuration of a commonly used frequency discriminator[4,10,16,20,21,22]. Consider a signal incident at the RF input port and described by $A\cos(2\pi ft + 0°)$ or $A\angle 0°$. The delay line has an electrical length θ at frequency f, and for simplicity the detector sensitivities are 2K.

The operation of the circuit is best shown by considering the signals present at the points marked by lower case letters.

$$\text{Signal at RF in} : A\angle 0°$$

$$\text{at (a) and (b)} : \frac{A}{\sqrt{2}}\angle 0°$$

$$\text{at (c)} : \frac{A}{\sqrt{2}}\angle \theta$$

The signals at a) and c) are thus equal in amplitude and differ only in phase by an angle θ equal to the electrical length of the delay line at this frequency. θ is directly proportional to frequency and the task of the phase discriminator section is to measure θ, so allowing the original frequency to be determined.

$$\text{Signal at (d)} : \frac{A}{2}\angle 0^\circ \qquad \text{at (e)} : \frac{A}{2}\angle 0^\circ$$

$$\text{at (f)} : \frac{A}{2}\angle \theta \qquad \text{at (g)} : \frac{A}{2}\angle \theta + 90^\circ$$

Note that (d) and (f) constitute the two signals applied to the mixer labelled M1 in fig 4.1, and that (e) and (g) are the same two signals except that they are separated by an additional 90 degrees in phase as required by mixer M2.

$$\text{Signal at (h)} : \frac{A}{2\sqrt{2}}\angle 90^\circ + \frac{A}{2\sqrt{2}}\angle \theta$$

$$\text{at (k)} : \frac{A}{2\sqrt{2}}\angle 0^\circ + \frac{A}{2\sqrt{2}}\angle 90^\circ + \theta$$

$$\text{at (m)} : \frac{A}{2\sqrt{2}}\angle 90^\circ + \frac{A}{2\sqrt{2}}\angle 90^\circ + \theta$$

$$\text{at (n)} : \frac{A}{2\sqrt{2}}\angle 0^\circ + \frac{A}{2\sqrt{2}}\angle 180^\circ + \theta$$

The operation of the detectors (encompassing their low pass filtering section) is to square the modulus of their input signals and multiply by the sensitivity 2K.

$$V_A = 2K\left|\frac{A}{2\sqrt{2}}\angle 90^\circ + \frac{A}{2\sqrt{2}}\angle \theta\right|^2$$

$$= \frac{A^2K}{4}\,|\,1\angle 90^\circ + 1\angle \theta\,|^2$$

$$= \frac{A^2K}{4}\,|\,\cos 90^\circ + j\sin 90^\circ + \cos\theta + j\sin\theta\,|^2$$

$$V_A = \frac{A^2K}{4} \left| \cos\theta + j(1 + \sin\theta) \right|^2$$

$$= \frac{A^2K}{4} (\cos^2\theta + 1 + 2\sin\theta + \sin^2\theta)$$

$$= \frac{A^2K}{4} (2 + 2\sin\theta)$$

$$= \frac{A^2K}{2} (1 + \sin\theta) \quad \ldots\ldots (C.1)$$

Similarly

$$V_B = 2K\left| \frac{A}{2\sqrt{2}} \angle 0° + \frac{A}{2\sqrt{2}} \angle 90° + \theta \right|^2$$

$$= \frac{A^2K}{2} (1 - \sin\theta) \quad \ldots\ldots (C.2)$$

$$V_C = 2K\left| \frac{A}{2\sqrt{2}} \angle 90° + \frac{A}{2\sqrt{2}} \angle 90° + \theta \right|^2$$

$$= \frac{A^2K}{2} (1 + \cos\theta) \quad \ldots\ldots (C.3)$$

$$V_D = 2K\left| \frac{A}{2\sqrt{2}} \angle 0° + \frac{A}{2\sqrt{2}} \angle 180° + \theta \right|^2$$

$$= \frac{A^2K}{2} (1 - \cos\theta) \quad \ldots\ldots (C.4)$$

From C.1 and C.2,

$$V_A - V_B = \frac{A^2K}{2} \left[(1 + \sin\theta) - (1 - \sin\theta) \right]$$

$$= KA^2 \sin\theta \quad \ldots\ldots (C.5)$$

and

$$V_C - V_D = KA^2 \cos\theta \quad \ldots\ldots (C.6)$$

Mathematically θ can be determined from

$$\theta = \tan^{-1}\left[\frac{V_A - V_B}{V_C - V_D}\right] \qquad \ldots\ldots \text{(C.7)}$$

and

$$A^2 = \frac{1}{K}\left[(V_A - V_B)^2 + (V_C - V_D)^2\right]^{\frac{1}{2}} \qquad \ldots\ldots \text{(C.8)}$$

APPENDIX D

MATHEMATICAL OPERATION OF SINGLE QUADRATURE COUPLER FREQUENCY DISCRIMINATOR

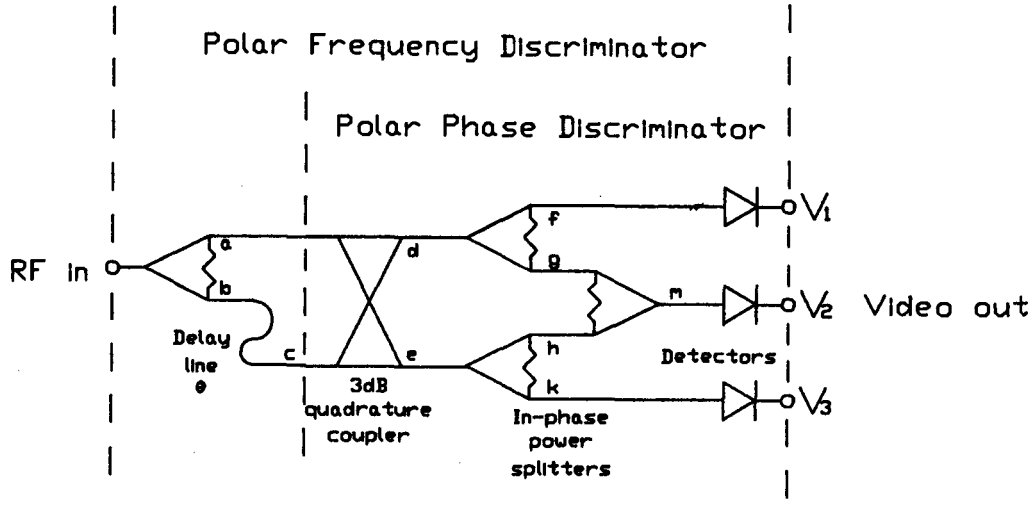

Fig D.1 : Single quadrature coupler frequency discriminator

Fig D.1 shows the RF circuit configuration of a frequency discriminator that requires only one quadrature coupler[16]. Consider a signal incident at the RF input port and described by $A\cos(2\pi ft + 0°)$ or $A \angle 0°$. The delay line has an electrical length θ at frequency f, and for simplicity the detector sensitivities are 2K.

The operation of the circuit is best shown by considering the signals present at the points marked by lower case letters.

$$\text{Signal at RF in} : A \angle 0°$$

$$\text{at (a) and (b)} : \frac{A}{\sqrt{2}} \angle 0°$$

$$\text{at (c)} : \frac{A}{\sqrt{2}} \angle \theta$$

The signals at (a) and (c) are thus equal in amplitude and differ only in phase by an angle θ equal to the electrical length of the delay line at this frequency. θ is directly proportional to frequency and the task of the phase discriminator section is to measure θ, so allowing the original frequency to be determined.

$$\text{Signal at (d)} : \frac{A}{2}\angle 90^\circ + \frac{A}{2}\angle\theta$$

$$\text{at (e)} : \frac{A}{2}\angle 0^\circ + \frac{A}{2}\angle(90^\circ + \theta)$$

$$\text{Signal at (f) and (g)} : \frac{A}{2\sqrt{2}}\angle 90^\circ + \angle\frac{A}{2\sqrt{2}}\,\theta$$

$$\text{at (h) and (k)} : \angle\frac{A}{2\sqrt{2}}\angle 0^\circ + \frac{A}{2\sqrt{2}}\angle(90^\circ + \theta)$$

$$\text{at (m)} : \frac{A}{4}\angle 90^\circ + \frac{A}{4}\angle\theta + \frac{A}{4}\angle 0^\circ + \frac{A}{4}\angle(90^\circ + \theta)$$

The operation of the detectors (encompassing their low pass filtering section) is to square the modulus of their input signals and multiply by the sensitivity 2K.

$$V_1 = 2K\left|\frac{A}{2\sqrt{2}}\angle 90^\circ + \frac{A}{2\sqrt{2}}\angle\theta\right|^2$$

$$= \frac{A^2K}{4}\,|\,1\angle 90^\circ + 1\angle\theta\,|^2$$

$$= \frac{A^2K}{4}\,|\cos 90^\circ + j\sin 90^\circ + \cos\theta + j\sin\theta|^2$$

$$= \frac{A^2K}{4}\,|\cos\theta + j(1 + \sin\theta)|^2$$

$$= \frac{A^2K}{4}(\cos^2\theta + 1 + 2\sin\theta + \sin^2\theta)$$

$$V_1 = \frac{A^2K}{4}(2 + 2\sin\theta)$$

$$= \frac{A^2K}{2}(1 + \sin\theta) \qquad \ldots\ldots (D.1)$$

similarly,

$$V_3 = 2K\left|\frac{A}{2\sqrt{2}}\angle 0^\circ + \frac{A}{2\sqrt{2}}\angle 90^\circ + \theta\right|^2$$

$$= \frac{A^2K}{2}(1 - \sin\theta) \qquad \ldots\ldots (D.2)$$

$$V_2 = 2K\left|\frac{A}{4}\angle 90^\circ + \frac{A}{4}\angle\theta + \frac{A}{4}\angle 0^\circ + \frac{A}{4}\angle 90^\circ + \theta\right|^2$$

$$= \frac{A^2K}{8}\left|1\angle 90^\circ + 1\angle\theta + 1\angle 0^\circ + 1\angle 90^\circ + \theta\right|^2$$

$$= \frac{A^2K}{8}\left|\begin{array}{l}\cos 90^\circ + j\sin 90^\circ + \cos\theta + j\sin\theta + \cos 0^\circ \\ + j\sin 0^\circ + \cos(90^\circ + \theta) + j\sin(90^\circ + \theta)\end{array}\right|^2$$

$$= \frac{A^2K}{8}\left|(1 + \cos\theta - \sin\theta) + j(1 + \cos\theta + \sin\theta)\right|^2$$

$$= \frac{A^2K}{8}\left[\begin{array}{l}1 + 2\cos\theta - 2\sin\theta - 2\sin\theta\cos\theta + \sin^2\theta + \cos^2\theta \\ + 1 + 2\cos\theta + 2\sin\theta + 2\sin\theta\cos\theta + \sin^2\theta + \cos^2\theta\end{array}\right]$$

$$= \frac{A^2K}{8}(4 + 4\cos\theta)$$

$$= \frac{A^2K}{2}(1 + \cos\theta) \qquad \ldots\ldots (D.3)$$

From (D.1), (D.2) and (D.3)

$$V_1 - V_3 = \frac{A^2K}{2}\left[(1 + \sin\theta) - (1 - \sin\theta)\right]$$

$$= KA^2\sin\theta \qquad \ldots\ldots (D.4)$$

$$2V_2 - (V_1 + V_3) = \frac{A^2K}{2}\left[2(1 + \cos\theta) - (1 + \sin\theta + 1 - \sin\theta)\right]$$

$$= KA^2 \cos\theta \qquad \ldots\ldots (D.5)$$

Mathematically θ can be determined from

$$\theta = \tan^{-1}\left[\frac{V_1 - V_3}{2V_2 - (V_1 + V_3)}\right] \qquad \ldots\ldots (D.6)$$

and

$$A^2 = \frac{1}{K}\left[(V_1 - V_3)^2 + (2V_2 - V_1 - V_3)^2\right]^{\frac{1}{2}} \qquad \ldots\ldots (D.7)$$

The factor 2 that appears on the left of equation (D.5) may be realised by a video amplifier with gain 2. Alternatively the circuit shown in fig D.2 can be used.

Consider, as before, a signal incident at the point marked RF in in fig D.2, and described by $A\cos(2\pi ft + 0°)$ or $A\ \underline{/0°}$. The circuit for the points marked (a) to (m) is identical to that of fig D.1, so that the signals listed above still apply, and V_2 is still as given in equation (D.3).

$$\text{Signal at (n)} : \frac{A}{4}\underline{/90°} + \frac{A}{4}\underline{/\theta}$$

$$\text{at (p)} : \frac{A}{4}\underline{/0°} + \frac{A}{4}\underline{/90° + \theta}$$

Detection yields the signals

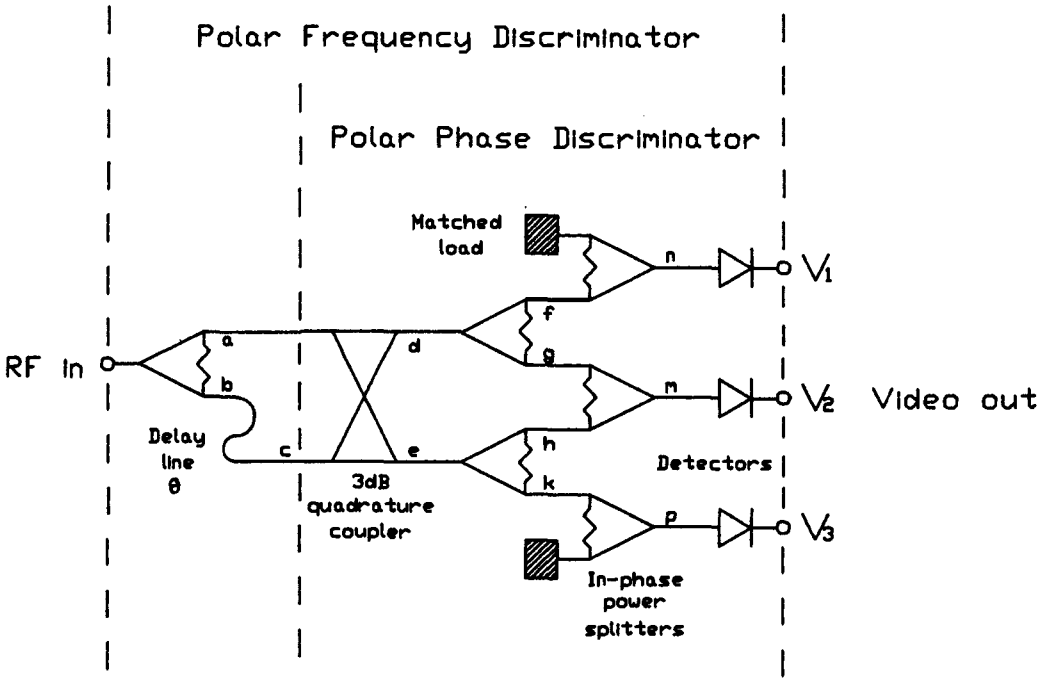

Fig D.2 : **Alternative single QC frequency discriminator**

$$V_1 = 2K \left| \frac{A}{4} \angle 90° + \frac{A}{4} \angle \theta \right|^2$$

$$= \frac{A^2K}{4} (1 + \sin\theta) \qquad \ldots\ldots \text{(D.8)}$$

$$V_3 = 2K \left| \frac{A}{4} \angle 0° + \frac{A}{4} \angle 90° + \theta \right|^2$$

$$= \frac{A^2K}{4} (1 - \sin\theta) \qquad \ldots\ldots \text{(D.9)}$$

from (D.3),(D.8) and (D.9)

$$V_1 - V_3 = \frac{A^2K}{2} \sin\theta \qquad \ldots\ldots \text{(D.10)}$$

$$V_2 - (V_1 + V_3) = \frac{A^2 K}{2} \cos\theta \qquad \ldots\ldots \text{(D.11)}$$

$$\theta = \tan^{-1}\left[\frac{(V_1 - V_3)}{V_2 - (V_1 + V_3)}\right] \qquad \ldots\ldots \text{(D.12)}$$

$$A^2 = \frac{2}{K}\left[(V_1 - V_3)^2 + (V_2 - V_1 - V_3)^2\right] \qquad \ldots\ldots \text{(D.13)}$$

The factor ½ that appears on the right hand side of equations (D.10) and (D.11) indicates that the circuit of fig D.2 has more RF loss than that of fig D.1.

PROPERTY	TEST METHOD, CONDITION		UNITS[1]	DIRECTION	TYPICAL VALUE[2]	
Dielectric constant, ε_r	ASTM D1531	1 MHz	—	Z	2.20	
	ASTM D3380	10 GHz	—	Z	2.20 ± .02 spec.	
Dissipation factor, tan δ	ASTM D1531	1 MHz	—	Z	.0004	
	ASTM D3380	10 GHz	—	Z	.0009	
Volume resistivity	ASTM D257	C96/23/95	M ohm cm	Z	2×10^7	
Surface resistivity	ASTM D257	C96/23/95	M ohm	X,Y	3×10^8	
					Test at 23°C	Test at 100°C
Tensile modulus	ASTM D638	A	MPa (kpsi)	X	1070 (156)	450 (65)
				Y	860 (125)	380 (55)
ultimate stress			MPa (kpsi)	X	29 (4.2)	20 (2.9)
				Y	27 (3.9)	18 (2.6)
ultimate strain			%	X	6.0	7.2
				Y	4.9	5.8
Compressive modulus	ASTM D695	A	MPa (kpsi)	X	710 (103)	500 (73)
				Y	710 (103)	500 (75)
				Z	940 (136)	670 (97)
ultimate stress			MPa (kpsi)	X	27 (3.9)	22 (3.2)
				Y	28 (4.0)	21 (3.1)
				Z	52 (7.5)	43 (6.3)
ultimate strain			%	X	8.5	8.4
				Y	7.7	7.8
				Z	12.5	17.6
Deformation under load	ASTM D621				Test at 150°C	
		24 hr/14MPa(2 kpsi)	%	Z	1.0	
Water absorption	ASTM D570	D 24/23				
		Thickness = 0.8mm(.031 in)	Mg (%)		0.9 (.02)	
		Thickness = 1.6mm(.062 in.)	Mg (%)		1.3 (.015)	
Specific gravity	ASTM D792		—		2.2	
Heat distortion temperature	ASTM D648	1.82MPa(264 psi)	°C(°F)	X,Y	>260 (>500)	
Specific heat	Calculated		J/g/K(BTU/lb/°F)		0.96 (.23)	
Thermal conductivity	Rogers TR2721		W/m/K(BTU in/ft²/hr/°F)	Z	0.26 (1.8)	
Thermal expansion	ASTM D3386		mm/m	→	X	Y	Z
	(10 K/min.)	−100°C			−6.1	−8.7	−18.7
		15			−0.9	−1.8	− 6.9
(Values given are total change from a base temperature of 35°C)		25			−0.5	−0.9	− 4.5
		75			1.1	1.5	8.7
		150			2.3	3.2	28.3
		250			3.8	5.5	69.5

[1] SI units given first with other frequently used units in parentheses.

[2] From internal TR's 1430, 2224, 2854. Tests were at 23°C unless otherwise noted.

RT/duroid® microwave laminate is a registered trademark of Rogers Corporation.

Revised 3/81
Supersedes 1/78

APPENDIX F

BASIC PROGRAM FOR CALCULATING WIDTHS OF OFFSET STRIP CONDUCTORS

Howe[22] presents formulae developed by Rosenzweig in a manner best suited to the analysis of strip transmission lines. The formulae allow calculation of the characteristic impedance of a strip line offset from mid-way between the two ground planes as shown in fig F.1. These formulae are presented here in a manner better suited to the design of a line of given characteristic impedance, ie. calculation of line width w.

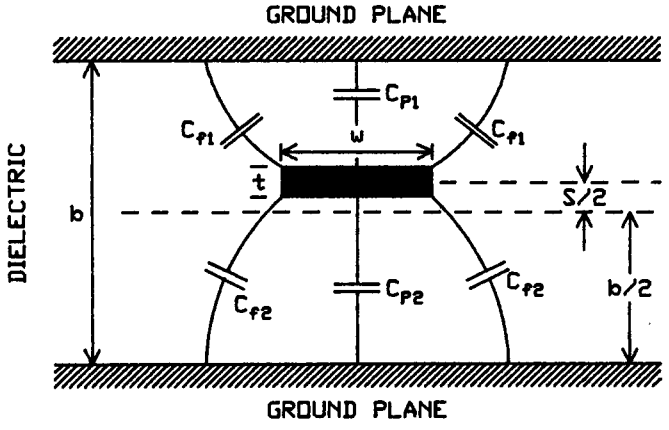

Fig F.1 : Stripline with offset centre conductor

The parameters used in the formulae are shown in fig F.1. 's' is actually the thickness of the centre layer of dielectric in a three layer structure. b, t, s and relative dielectric constant ε_r are defined by the available materials so that w is the only unknown quantity. Other symbols used are:

n = free space impedance = 376.7 ohms
C = static capacitance per unit length between conductors
ε = permittivity of dielectric
ε_r = relative dielectric constant
ε_o = permittivity of free space

Recall that

$$\varepsilon = \varepsilon_r \varepsilon_o \qquad \ldots\ldots \text{(F.1)}$$

then

$$\frac{C_{f_1}}{\varepsilon} = \frac{1}{\pi}\left[2A_1 \ell n(A_1 + 1) - (A_1 - 1)\ell n(A_1^2 - 1)\right] \qquad \ldots\ldots \text{(F.2)}$$

where

$$A_1 = \frac{1}{1 - t/(b-s)} \qquad \ldots\ldots \text{(F.3)}$$

Similarly

$$\frac{C_{f_2}}{\varepsilon} = \frac{1}{\pi}\left[2A_2 \ell n(A_2 + 1) - (A_2 - 1)\ell n(A_2^2 - 1)\right] \qquad \ldots\ldots \text{(F.4)}$$

where

$$A_2 = \frac{1}{1 - t/(b+s)} \qquad \ldots\ldots \text{(F.5)}$$

Now $$\frac{C_{p_1}}{\varepsilon} = K_1 w \qquad \ldots\ldots \text{(F.6)}$$

where $$K_1 = 2/(b-s-t) \qquad \ldots\ldots \text{(F.7)}$$

and $$\frac{C_{p_2}}{\varepsilon} = K_2 w \qquad \ldots\ldots \text{(F.8)}$$

where $$K_2 = 2/(b+s-t) \qquad \ldots\ldots \text{(F.9)}$$

then $$\left(\frac{C}{\varepsilon}\right)_{\text{total}} = (K_1 + K_2)w + 2\frac{C_{f_1}}{\varepsilon} + 2\frac{C_{f_2}}{\varepsilon} \qquad \ldots\ldots \text{(F.10)}$$

But $$\left(\frac{C}{\varepsilon}\right)_{\text{total}} = \frac{n}{\sqrt{\varepsilon_r}\, z_o} \qquad \ldots\ldots \text{(F.11)}$$

Hence

$$w = \frac{\dfrac{n}{\sqrt{\varepsilon_r}\, Z_o} - 2\left[\dfrac{C_{f_1}}{\varepsilon} + \dfrac{C_{f_2}}{\varepsilon}\right]}{(K_1 + K_2)} \qquad \ldots\ldots \text{(F.12)}$$

These approximate formulae give good results provided the following condition holds

$$\frac{w}{b-t} \geq 0.35 \qquad \ldots\ldots \text{(F.13)}$$

The following BASIC program has been written for an IBM PC micro-computer to implement this design routine.

```
100 REM ************************************************
110 REM *                                              *
120 REM *              STRIPLINE DESIGN PROGRAM        *
130 REM *                                              *
140 REM *    Method developed by Rosenzweig and given in *
150 REM *    "Stripline Design" by H.Howe, pp 37-39.   *
160 REM *                                              *
170 REM ************************************************
180 REM
190 REM
200 REM       PROMPT FOR REQUIRED DATA
210 REM
220 PRINT "INPUT GROUND PLANE SPACING (mm)"
230 INPUT B
240 PRINT "INPUT CENTRE LAYER THICKNESS (mm)"
250 INPUT S
260 PRINT "INPUT COPPER THICKNESS (mm)"
270 INPUT T
280 PRINT "INPUT RELATIVE DIELECTRIC CONSTANT"
290 INPUT ER
300 PRINT "INPUT CHARACTERISTIC IMPEDANCE"
310 INPUT ZO
320 REM
330 REM       CALCULATE TOTAL FRINGE CAPACITANCE
340 REM
350 PI=3.1415927#
360 A1=1/(1-T/(B-S))
370 CF1=(2*A1*LOG(A1+1)-(A1-1)*LOG(A1^2-1))/PI
380 A2=1/(1-T/(B+S))
390 CF2=(2*A2*LOG(A2+1)-(A2-1)*LOG(A2^2-1))/PI
400 CF=2*CF1+2*CF2
410 REM
420 REM       CALCULATE CP COEFFICIENTS OF W
430 REM
440 CP1CO=2/(B-S-T)
450 CP2CO=2/(B+S-T)
460 CPCO=CP1CO+CP2CO
470 REM
480 REM       CALCULATE LINE WIDTH W
490 REM
500 G=376.7/(ZO*SQR(ER))
510 W=(G-CF)/CPCO
520 REM
530 REM       CHECK CONDITION
540 REM
550 C=W/(B-T)
560 IF C<.35 GOTO 590
570 PRINT "CALCULATED LINE WIDTH = ";W;" mm"
580 GOTO 600
590 PRINT "CONDITION NOT MET, RESULT NOT RELIABLE"
600 PRINT
610 PRINT "ANOTHER IMPEDANCE ? (Y/N)"
620 INPUT A$
630 IF A$="Y" GOTO 300
640 END
```

APPENDIX G

BASIC PROGRAM FOR CALCULATING WIDTHS OF DIRECTLY OVERLAID COUPLED STRIPLINES

Cohn[31] has analysed the case of two coupled strip conductors laid directly above one another, and suspended in a dielectric between two ground planes as shown in fig G.1. Note that the strips are displaced an equal distance from mid-way between the ground planes so that the structure is symmetrical.

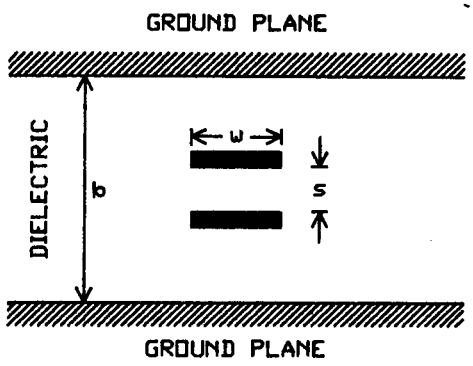

Fig G.1 : Directly overlaid coupled strip lines

In his design procedure Cohn intended that the substrate relative dielectric constant ε_r and ground plane spacing b be determined by the materials in use, and that the strip widths w and separation s be calculated for a given value of characteristic impedance Z_o, and coupling factor described by the even and odd mode impedances Z_{oe} and Z_{oo}.

In practice when soft boards are used, the separation of the conducting strips is determined by the manufacturers' standard substrate thicknesses. Thus dimension s is also specified by the available materials. For a given coupling factor, Z_o cannot now be specified as well but must be calculated along with width w.

Cohn gives a fairly precise method and a simpler more approximate method, plus conditions which must be met for the calculated results to be reliable. For tight coupling the conditions of the more approximate method are rarely met. The more precise method is presented here in a form which allows Z_o and w to be calculated.

Factors b, s and ε_r are specified by the materials in use. The coupling factor required must be specified in terms of the normalised even mode impedance Z_{oen}. The normalised odd mode impedance is then given by

$$Z_{oon} = 1/Z_{oen}, \quad Z_{oen} > Z_{oon} \qquad \ldots\ldots \text{(G.1)}$$

The actual even and odd mode impedances Z_{oe} and Z_{oo} are then given by

$$\begin{aligned} Z_{oe} &= Z_o \, Z_{oen} \\ Z_{oo} &= Z_o \, Z_{oon} \end{aligned} \qquad \ldots\ldots \text{(G.2)}$$

Cohn gives

$$Z_{oe} = \frac{188.3}{\sqrt{\varepsilon_r}} \frac{K(k')}{K(k)} \qquad \ldots\ldots \text{(G.3)}$$

$$Z_{oo} = \frac{296.1}{\sqrt{\varepsilon_r} \frac{b}{s} \tanh^{-1} k} \qquad \ldots\ldots \text{(G.4)}$$

where k = a parameter

$k' = \sqrt{1 - k^2}$

K(k) and K(k') are complete elliptic integrals of the first kind

Setting $$A_1 = \frac{188.3}{\sqrt{\varepsilon_r} \, Z_{oen}} \qquad \ldots\ldots \text{(G.5)}$$

and $$A_2 = \frac{296.1s}{\sqrt{\varepsilon_r}.b.Z_{oon}} \qquad \ldots\ldots \text{(G.6)}$$

and making use of (G.2) we get

$$Z_o = A_1 \frac{K(k')}{K(k)} \qquad \ldots\ldots \text{(G.7)}$$

$$Z_o = A_2/\tanh^{-1}k \qquad \ldots\ldots \text{(G.8)}$$

Equating (G.8) and (G.7) we get

$$\tanh^{-1}k \ \frac{K(k')}{K(k)} - \frac{A_2}{A_1} = 0 \qquad \ldots\ldots \text{(G.9)}$$

Which must be solved for k.

Gupta et al[30] give approximate formulae for K(k')/K(k), reportedly accurate to 8ppm

$$\frac{K(k')}{K(k)} = \begin{cases} \frac{1}{\pi} \ell n\left(2 \frac{1+\sqrt{k'}}{1-\sqrt{k'}}\right) & , 0 \leq k \leq 0.7 \\ \left[\frac{1}{\pi} \ell n\left(2 \frac{1+\sqrt{k}}{1-\sqrt{k}}\right)\right]^{-1} & , 0.7 < k < 1 \end{cases} \qquad \ldots\ldots \text{(G.10)}$$

Making use of (G.10) and

$$\tanh^{-1}(k) = \tfrac{1}{2} \ell n \left[\frac{1+k}{1-k}\right] \quad , -1 < k < 1 \qquad \ldots\ldots \text{(G.11)}$$

equation (G.9) can be solved by trial and error or by a root finding method such as that described below.

Solving (G.9) by the mid-point method we write

$$G(k) = \tanh^{-1}k. \ \frac{K(k')}{K(k)} - \frac{A_2}{A_1} \qquad \ldots\ldots \text{(G.12)}$$

We then choose an interval such that G(k) has different signs at the interval limits. This ensures that a root lies within the interval. The sign of G(k) at the mid-point of the interval is then checked and the previous limiting point with the same sign of G(k) is set equal to this mid-point, so halving the interval size and ensuring a root falls in the new interval. The interval is continuously halved in size until it is as small as some specified allowable value. The limit giving the lowest absolute value of G(k) is then taken to be the root.

Once k has been determined Z_o can be calculated from (G.7) or (G.8), and w can be obtained from

$$w = \frac{2b}{\pi}\left[\tanh^{-1}B_1 - \frac{s}{b}\tanh^{-1}\frac{B_1}{k}\right] \qquad \ldots\ldots \text{(G.13)}$$

where

$$B_1 = \sqrt{\frac{kb/s - 1}{b/ks - 1}} \qquad \ldots\ldots \text{(G.14)}$$

The method gives good results providing the following condition is met

$$\frac{w}{s} > 0.35 \qquad \ldots\ldots \text{(G.15)}$$

Generally w>s so this condition is usually met.

The following BASIC program has been written for an IBM PC micro-computer to implement the above procedure.

```
1000 REM ************************************************************
1010 REM *                                                          *
1020 REM *         DIRECTLY OVERLAID COUPLED STRIPLINES             *
1030 REM *                                                          *
1040 REM *   Cohn's method, IRE T-MTT, vol 8, no.6, Nov 1960        *
1050 REM *   pp 633-637.   Complete elliptic integrals from         *
1060 REM *   approximations presented by Gupta et. al.  in          *
1070 REM *   "Computer Aided Design of Microwave Circuits",         *
1080 REM *   Artech House, Inc., 1981, p 57.                        *
1090 REM *                                                          *
1100 REM ************************************************************
1110 REM
1120 REM
1130 REM       DEFINE FUNCTIONS
1140 REM
1150 REM   INVERSE HYPERBOLIC TANGENT
1160 DEF FNATANH(X)=LOG((1+X)/(1-X))/2
1170 REM
1180 REM   K' FUNCTION
1190 DEF FNKP(K)=SQR(1-K^2)
1200 REM
1210 REM   COMPLETE ELLIPTIC INTEGRALS OF FIRST KIND
1220 REM
1230 REM   0<K<=0.7
1240 DEF FNKK07(K)=LOG(2*(1+SQR(FNKP(K)))/(1-SQR(FNKP(K))))/PI
1250 REM
1260 REM   0.7<K<1
1270 DEF FNKK71(K)=PI/LOG(2*(1+SQR(K))/(1-SQR(K)))
1280 REM
1290 REM   ROOT EQUATIONS
1300 REM
1310 REM   0<K<=0.7
1320 DEF FNR1(K,X)=FNATANH(K)*FNKK07(K)-X
1330 REM
1340 REM   0.7<K<1
1350 DEF FNR2(K,X)=FNATANH(K)*FNKK71(K)-X
1360 REM
1370 REM   ROUND TO 5th DECIMAL PLACE
1380 REM
1390 DEF FNRN5(X)=ABS(X*10^5)/10^5
1400 REM
1410 REM
1420 REM       PROMPT FOR REQUIRED DATA
1430 REM
1440 PRINT "INPUT GROUND PLANE SPACING (mm)"
1450 INPUT B
1460 PRINT "INPUT CENTRE LAYER THICKNESS (mm)"
1470 INPUT S
1480 PRINT "INPUT RELATIVE DIELECTRIC CONSTANT"
1490 INPUT ER
1500 PRINT "INPUT NORMALISED EVEN MODE IMPEDANCE Zoen"
1510 INPUT ZOEN
```

```
1520 REM
1530 REM       CALCULATE ROOT EQUATION CONSTANT
1540 REM
1550 PI=3.1415927#
1560 A1=188.3/(SQR(ER)*ZOEN)
1570 ZOON=1/ZOEN
1580 A2=296.1*S/(SQR(ER)*B*ZOON)
1590 A3=A2/A1
1600 REM
1610 REM       CALCULATE K BY FINDING ROOT
1620 REM
1630 REM
1640 REM       CHECK RANGE OF K BY LOOKING FOR CHANGE OF SIGN
1650 REM
1660 KL=.00001
1670 GL=FNR1(KL,A3)
1680 IF SGN(GL)=0 THEN ROOT=KL: GOTO 2130        ' ROOT FOUND
1690 KR=.7
1700 GR=FNR1(KR,A3)
1710 IF SGN(GR)=0 THEN ROOT=KR: GOTO 2130        ' ROOT FOUND
1720 IF SGN(GL)=SGN(GR) GOTO 1860                ' TRY OTHER RANGE
1730 REM
1740 REM       ROOT IS IN RANGE 0<K<=0.7
1750 REM
1760 IF (KR-KL)<=.00002 GOTO 1840                ' CLOSE ENOUGH
1770 KMID=FNRN5((KL+KR)/2)
1780 GMID=FNR1(KMID,A3)
1790 IF SGN(GMID)=0 THEN ROOT=KMID: GOTO 2130    ' ROOT FOUND
1800 IF SGN(GMID)=SGN(GL) THEN KL=KMID: GL=GMID: GOTO 1760
1810 IF SGN(GMID)=SGN(GR) THEN KR=KMID: GR=GMID: GOTO 1760
1820 ROOT=KMID
1830 GOTO 2130                                   ' ROOT FOUND
1840 IF ABS(GL)<ABS(GR) THEN ROOT=KL ELSE ROOT=KR
1850 GOTO 2130                                   ' ROOT FOUND
1860 KL=.70001
1870 GL=FNR2(KL,A3)
1880 IF SGN(GL)=0 THEN ROOT=KL: GOTO 2130        ' ROOT FOUND
1890 KR=.99999
1900 GR=FNR2(KR,A3)
1910 IF SGN(GR)=0 THEN ROOT=KR: GOTO 2130        ' ROOT FOUND
1920 IF SGN(GL)<>SGN(GR) GOTO 2010
1930 REM
1940 REM       NO SOLUTION CAN BE FOUND
1950 REM
1960 PRINT "NO ROOT TO EQUATION CAN BE FOUND"
1970 GOTO 2220
```

```
1980 REM
1990 REM       ROOT IS IN RANGE 0.7<K<1
2000 REM
2010 IF (KR-KL)<=.00002 GOTO 2090                    ' CLOSE ENOUGH
2020 KMID=FNRN5((KL+KR)/2)
2030 GMID=FNR2(KMID,A3)
2040 IF SGN(GMID)=0 THEN ROOT=KMID: GOTO 2130    ' ROOT FOUND
2050 IF SGN(GMID)=SGN(GL) THEN KL=KMID: GL=GMID: GOTO 2010
2060 IF SGN(GMID)=SGN(GR) THEN KR=KMID: GR=GMID: GOTO 2010
2070 ROOT=KMID
2080 GOTO 2130                                       ' ROOT FOUND
2090 IF ABS(GL)<ABS(GR) THEN ROOT=KL ELSE ROOT=KR
2100 REM
2110 REM       ROOT HAS BEEN FOUND - CALCULATE W
2120 REM
2130 K=ROOT
2140 B1=SQR((K*B/S-1)/(B/K/S-1))
2150 B2=B1/K
2160 W=2*B/PI*(FNATANH(B1)-S/B*FNATANH(B2))
2170 Z0=A2/FNATANH(K)
2180 PRINT
2190 PRINT "CALCULATED LINE WIDTH = ";W;" mm"
2200 PRINT
2210 PRINT "CALCULATED CHARACTERISTIC IMPEDANCE = ";Z0;" ohms"
2220 PRINT
2230 PRINT "ANOTHER Zoen ? (Y/N)"
2240 INPUT A$
2250 IF A$="Y" GOTO 1500
2260 END
```

APPENDIX H

BASIC PROGRAM FOR CALCULATING WIDTHS AND OVERLAPS OF OFFSET PARALLEL COUPLED STRIP TRANSMISSION LINES

Shelton[33] has analysed the case of overlaid coupled lines placed not directly above one another but offset. In tight coupling cases the lines overlap each other while in loosely coupled cases the lines are separated by a gap w_c as shown in fig H.1. The introduction of the offset dimension w_c allows b, s and dielectric constant ε_r to be specified by the materials, and both coupling factor and characteristic impedance to be independently chosen. The lines are always equal in width and distance from mid-way between the ground planes to maintain symmetry.

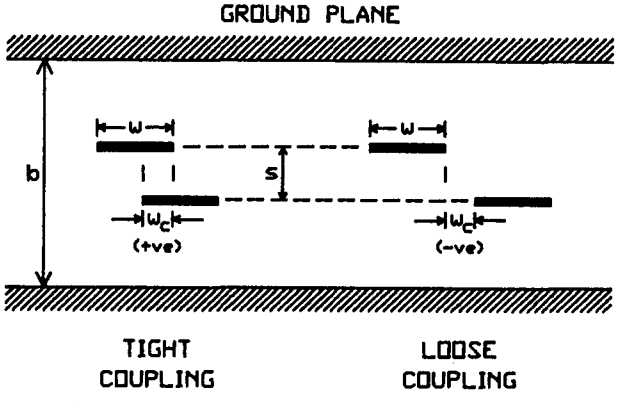

Fig H.1 : Offset parallel coupled strip transmission lines

Shelton recognised that his method was best implemented on a computer and presented his equations accordingly, thus they are not repeated here. The following BASIC program implements Shelton's method. It is an adaptation of a program provided by NIAST[32] and is suited to an IBM PC micro-computer.

The program prompts for wanted data. Coupling is specified in decibels. Shelton's equations are subject to certain conditions to ensure their accuracy. If a particular set of parameters suits neither the loose nor tightly coupled case the program reports this.

```
1000 REM ************************************************************
1010 REM *                                                          *
1020 REM *                OFFSET COUPLED STRIP LINES                *
1030 REM *   Program to implement Shelton's design method for       *
1040 REM *   offset parallel coupled strip transmission lines.      *
1050 REM *   IEEE T-MTT, vol MTT-14, no.1, Jan. 1966, pp 7-15.      *
1060 REM *                                                          *
1070 REM ************************************************************
1080 REM
1090 REM
1100 REM      PREPARE DISPLAY AND PROMPT FOR DATA
1110 REM
1120 PI=3.141593
1130 CLS
1140 LOCATE 2,25
1150 PRINT " STRIPLINE OVERLAY COUPLERS "
1160 LOCATE 3,25
1170 PRINT "----------------------------"
1180 LOCATE 5,1
1190 PRINT "        GROUND PLANE SPACING B (mm)   ";
1200 INPUT R8
1210 LOCATE 7,1
1220 PRINT "             STRIP THICKNESS S (mm)   ";
1230 INPUT R9
1240 LOCATE 9,1
1250 PRINT "    RELATIVE DIELECTRIC CONSTANT E   ";
1260 INPUT S0
1270 LOCATE 11,1
1280 PRINT "CHARACTERISTIC IMPEDANCE Z0 (ohms)   ";
1290 INPUT R5
1300 R9=R9/R8
1310 REM
1320 LOCATE 16,3
1330 PRINT "
1340 LOCATE 16,3
1350 PRINT "ENTER COUPLING COEFFICIENT (dB)   ";
1360 INPUT S2
1370 REM
1380 REM       TRY TIGHT COUPLING CASE
1390 REM
1400 S3=10^(-S2/20)
1410 S1=((1+S3)/(1-S3))^.5
1420 C5=((S0^.5)*R5*LOG(4))/(60*PI*PI)
1430 IF (1-S1*S1*R9)/S1<C5 THEN 2060
1440 S3=EXP(60*(PI^2)*(1-(R9*(S1^2)))/(R5*S1*(S0^.5)))
1450 S4=(S3-2+((S3^2)-(4*S3))^.5)/2
1460 S5=((((1+R9)*(S4-1)/2)^2+4*R9*S4)^.5/2)+((S4-1)*(1+R9)/4)
1470 S6=R9*S4/S5
1480 S7=(LOG((S5*S6)/((R9+S5)*(1+S5)*(S6-R9)*(1-S6))))/(PI*R9)
1490 S7=S7-((2*(LOG(R9)))/(PI*(1-R9)))
1500 S8=120*PI*S1/(R5*(S0^.5))
1510 S9=R9*(1-R9)*(S8-S7)/2
1520 T0=(1-R9)*(LOG(((1+S5)*(S6-R9))/((R9+S5)*(1-S6))))/(2*PI)
1530 T0=T0+((1+R9)*(LOG(S5/S6)))/(2*PI)
1540 T1=S9-T0
1550 IF S9/(1-R9)<=.35 THEN 1760              ' TRY LOOSE COUPLING CASE
1560 IF T1/R9<=.7 THEN 1760                   ' TRY LOOSE COUPLING CASE
```

```
1570 REM
1580 REM       COUPLING IS TIGHT
1590 REM
1600 LOCATE 18,10
1610 PRINT "                                                                    "
1620 LOCATE 18,10
1630 PRINT "COUPLING COEFFICIENT C=";S2;" dB    TIGHT                          "
1640 LOCATE 20,30
1650 PRINT "                                                    "
1660 LOCATE 20,30
1670 PRINT " W=";R8*S9;" mm"
1680 LOCATE 22,30
1690 PRINT "                                                    "
1700 LOCATE 22,30
1710 PRINT "WC=";T1*R8;" mm"
1720 GOTO 1310
1730 REM
1740 REM       TRY LOOSE COUPLING CASE
1750 REM
1760 T2=(120*PI*(S1^2-1))/(S1*R5*(S0^.5))
1770 T3=1/(EXP(PI*T2/2)-1)
1780 T4=(((R9-T3)/(R9+1))^2+T3)^.5-(R9-T3)/(R9+1)
1790 T5=T3/T4
1800 T6=(1/(1+R9)*(LOG((1+T4)/(T4*(1-T5))))-(LOG(T5))/(1-R9))*(2/PI)
1810 T7=-(2/PI)*(LOG((1-R9)/2)/(1+R9)+LOG((1+R9)/2)/(1-R9))
1820 T8=(R9*LOG(T5/T4)+(1-R9)*LOG((1-T5)/(1+T4)))/PI
1830 T9=(1-R9^2)*(S8-T6-T7)/4
1840 U0=T9-T8
1850 IF T9/(1-R9)<=.35 THEN 2060                ' NEITHER CASE FITS
1860 IF 2*U0/(1+R9)<=.85 THEN 2060              ' NEITHER CASE FITS
1870 REM
1880 REM       LOOSE CASE FITS
1890 REM
1900 LOCATE 18,10
1910 PRINT "
1920 LOCATE 18,10
1930 PRINT "COUPLING COEFFICIENT C=";S2;" dB    LOOSE
1940 LOCATE 20,30
1950 PRINT "                                        "
1960 LOCATE 20,30
1970 PRINT " W=";R8*T9;" mm"
1980 LOCATE 22,30
1990 PRINT "                                        "
2000 LOCATE 22,30
2010 PRINT "WC=";T8*R8;" mm"
2020 GOTO 1310
2030 REM
2040 REM       NEITHER CASE FITS
2050 REM
2060 LOCATE 18,10
2070 PRINT "
2080 LOCATE 18,10
2090 PRINT "COUPLING COEFFICIENT C=";S2;" dB    NEITHER
2100 LOCATE 20,20
2110 PRINT "                                                    "
2120 LOCATE 22,20
2130 PRINT "                                                    "
2140 GOTO 1310
2150 END
```

APPENDIX I

BASIC PROGRAM FOR CALCULATING WIDTHS OF MICROSTRIP TRANSMISSION LINES

The method used is that presented by Gupta et al[30] and derived from the work of Wheeler and Schneider. Negligible copper conductor thickness t is assumed and errors are said to be less than two per cent for

$$\frac{t}{h} \leq 0.005 \qquad \ldots\ldots \text{(I.1)}$$

where h is the thickness of the dielectric.

The program prompts for required data and copper strip widths for given characteristic impedances are calculated, as are effective dielectric constants ε_{re}. This allows wavelengths λ to be calculated according to:

$$\lambda = \frac{c}{f\sqrt{\varepsilon_{re}}} \qquad \ldots\ldots \text{(I.2)}$$

where c is the velocity of light in free space and f is the signal frequency.

```
100 REM ************************************************************
110 REM *                                                          *
120 REM *                MICROSTRIP DESIGN PROGRAM                 *
130 REM *                                                          *
140 REM *   Microstrip design for negligible copper thick-         *
150 REM *   ness.  Adapted from methods of Wheeler and             *
160 REM *   Schneider by Gupta et. al. in " Computer Aided         *
170 REM *   Design of Microwave Circuits ",  Artech House,         *
180 REM *   1981, pp 61-62.                                        *
190 REM *                                                          *
200 REM ************************************************************
210 REM
220 REM
230 REM       PROMPT FOR REQUIRED DATA
240 REM
250 PRINT "INPUT DIELECTRIC THICKNESS (mm)"
260 INPUT H
270 PRINT "INPUT RELATIVE DIELECTRIC CONSTANT"
280 INPUT E
290 PRINT "INPUT CHARACTERISTIC IMPEDANCE"
300 INPUT Z
310 REM
320 REM       CHECK RANGE BY CALCULATING A
330 REM
340 PI=3.1415927#
350 A=Z/60*((E+1)/2)^.5+(E-1)/(E+1)*(.23+.11/E)
360 IF A>1.52 THEN 460
370 REM
380 REM       USE EQUATION FOR A<=1.52
390 REM
400 B=60*PI^2/Z/SQR(E)
410 W=2*H/PI*(B-1-LOG(2*B-1)+(E-1)/2/E*(LOG(B-1)+.39-.61/E))
420 GOTO 500
430 REM
440 REM       USE EQUATION FOR A>1.52
450 REM
460 W=H*8*EXP(A)/(EXP(2*A)-2)
470 REM
480 REM       CALCULATE EFFECTIVE DIELECTRIC CONSTANT
490 REM
500 ERE=(E+1)/2+(E-1)/2/SQR(1+10*H/W)
510 REM
520 REM       DISPLAY RESULTS
530 REM
540 PRINT
550 PRINT "CALCULATED LINE WIDTH = ";W;" mm"
560 PRINT
570 PRINT "EFFECTIVE DIELECTRIC CONSTANT = ";ERE
580 PRINT
590 PRINT
600 PRINT "ANOTHER IMPEDANCE ? (Y/N)"
610 INPUT A$
620 PRINT
630 IF A$="Y" GOTO 290
640 END
```

APPENDIX J

FORTRAN PROGRAM FOR CASCADING n-PORT NETWORKS DESCRIBED BY S-PARAMETERS

The following program was written in ASCII FORTRAN for UCT's main frame computer. The program cascades two n-port (n even) networks A and B as shown in fig 6.5. The maximum value of n allowed is 10 but this can easily be increased. The method used is that described in section 6.2.

The first input data required is n, the number of ports. The S-parameters of network A are then required in complex (x,y) form. The order in which they must be entered is S_{11}, S_{12} ... S_{1n}, S_{21}, S_{22}, ... S_{nn}. The S-parameters of matrix B are required next and must be entered in the same form and order.

The program calculates the S-parameters of the overall cascaded network and prints them out in the same order that they are read in.

```
C     ********************************************************************
C     *                                                                  *
C     *                S-PARAMETER CASCADE PROGRAM                       *
C     *                                                                  *
C     *   Program for cascading two n-port (n even) networks             *
C     *   A and B described by their s-parameters.                       *
C     *                                                                  *
C     ********************************************************************
C
C
C     DEFINE COMPLEX ARRAYS
C
      COMPLEX A(10,10),B(10,10),C(10,10),D(15,15),E(15,15)
C
C     DISPLAY HEADINGS AND INPUT NUMBER OF PORTS N
C     N MUST BE EVEN, POSITIVE AND LESS THAN 11
C
      CALL PRTHED
      READ *,N
      PRINT *,' NUMBER OF PORTS = ',N
      PRINT *,' '
C
C     READ IN MATRICES A AND B
C
      CALL REED(A,N)
      CALL PRT(A,N)
      CALL REED(B,N)
      CALL PRT(B,N)
C
C     CASCADE THE NETWORKS
C
      CALL SETC(A,B,C,N)
      CALL SETD(A,B,C,D,N)
      CALL SETA(D,E,A,N)
C
C     PRINT OUT RESULT MATRIX
C
      PRINT *,' '
      PRINT *,' RESULT MATRIX'
      PRINT *,' '
      CALL PRT(A,N)
      END
C
C
C     SUBROUTINE FOR PRINTING HEADINGS
C
      SUBROUTINE PRTHED
C
      PRINT *,' '
      PRINT *,' '
      PRINT *,' N-PORT S-PARAMETER CASCADE PROGRAM'
      PRINT *,' '
      PRINT *,' '
      PRINT *,'      INPUT PORTS ARE PORTS 1 TO N/2'
      PRINT *,' '
      PRINT *,'     OUTPUT PORTS ARE PORTS N/2+1 TO N'
      PRINT *,' '
      PRINT *,' '
C
      RETURN
      END
```

```
C
C
C     SUBROUTINE TO READ IN AN N BY N MATRIX
C
      SUBROUTINE REED(A,N)
      COMPLEX A(10,10)
C
      DO 100 I=1,N
         DO 100 J=1,N
            READ *,A(I,J)
100   CONTINUE
C
      RETURN
      END
C
C
C     SUBROUTINE TO PRINT AN N BY N MATRIX
C
      SUBROUTINE PRT(A,N)
      COMPLEX A(10,10)
C
      PRINT *,' '
      PRINT *,' '
      PRINT *,' MATRIX ORDER = ',N
      PRINT *,' '
C
      DO 100 J=1,N
         DO 100 K=1,N
            PRINT *,J,K,A(J,K)
100   CONTINUE
      PRINT *,' '
C
      RETURN
      END
C
C
C     SUBROUTINE TO SET UP MATRIX C
C
      SUBROUTINE SETC(A,B,C,N)
      COMPLEX A(10,10),B(10,10),C(10,10)
C
      DO 100 I=1,N
         DO 100 J=1,N
C
            C(I,J)=(0.0,0.0)
            DO 200 K=1,N/2
               C(I,J)=C(I,J)+B(I,K)*A(K+N/2,J)
200         CONTINUE
C
100   CONTINUE
C
      RETURN
      END
```

```
C
C
C      SUBROUTINE TO SET UP MATRIX D
C
       SUBROUTINE SETD( A, B, C, D, N)
       COMPLEX  A( 10, 10) , B( 10, 10) , C( 10, 10) , D( 15, 15)
C
       DO 100  I=1, N/2
          DO 100  J=1, N/2
C
              D( I, J) =C( I, J+N/2)
              IF ( I. EQ. J)  D( I, J) =D( I, J) -( 1. 0, 0. 0)
              D( I+N/2, J) =A( I, J+N/2)
              D( I+N, J) =C( I+N/2, J+N/2)
              D( I, J+N/2) =C( I, J)
              D( I+N/2, J+N/2) =A( I, J)
              D( I+N, J+N/2) =C( I+N/2, J)
              D( I, J+N) =B( I, J+N/2)
              D( I+N/2, J+N) =( 0. 0, 0. 0)
              D( I+N, J+N) =B( I+N/2, J+N/2)
C
100    CONTINUE
C
       RETURN
       END
C
C
C      SUBROUTINE TO GAUSS REDUCE MATRIX D AND
C      STORE RESULT BACK IN MATRIX A
C
       SUBROUTINE SETA( D, E, A, N)
       COMPLEX  D( 15, 15) , E( 15, 15) , A( 10, 10)
C
       DO 100  NN=N+N/2, N+1, -1
          CALL SETE( D, E, NN, N)
          CALL RESETD( D, E, NN)
100    CONTINUE
C
       DO 200  I=1, N
          DO 200  J=1, N
             A( I, J) =D( I, J)
200    CONTINUE
C
       RETURN
       END
```

```
C
C
C      SUBROUTINE TO SET UP MATRIX E
C
       SUBROUTINE SETE( D, E, NN, N)
       COMPLEX D( 15, 15), E( 15, 15), TEMP
C
C      LOCATE LARGEST ELEMENT
C
       TEMP2=0.0
       DO 100 I=1, NN-N
          IF (TEMP.LT.CABS( D( I, 1))) THEN
             TEMP2=CABS( D( I, 1))
             II=I
          END IF
100    CONTINUE
C
C      SWOP TOP ROW WITH ROW WITH LARGEST 1st ELEMENT
C
       DO 200 I=1, NN
          TEMP=D( 1, I)
          D( 1, I)=D( II, I)
          D( II, I)=TEMP
200    CONTINUE
C
C      GAUSS REDUCE TO REMOVE TOP ROW
C
       DO 300 I=1, NN-1
          DO 300 J=1, NN-1
             E( I, J)=D( I+1, J+1)-D( I+1, 1)*D( 1, J+1)/D( 1, 1)
300    CONTINUE
C
       RETURN
       END
C
C
C      SUBROUTINE TO RESET MATRIX D
C
       SUBROUTINE RESETD( D, E, NN)
       COMPLEX D( 15, 15), E( 15, 15)
C
       DO 100 I=1, NN-1
          DO 100 J=1, NN-1
             D( I, J)=E( I, J)
100    CONTINUE
C
       RETURN
       END
```

APPENDIX K

BASIC ERROR CALCULATION PROGRAM

The following BASIC program reads S-parameter files created by TOUCHSTONE to compute peak and RMS errors of the various frequency discriminators. Data for the BASIC program should be entered into a dummy S-parameter file called 'DAATA.S2P' through TOUCHSTONE. Fig K.1 shows a sample data file. The standard frequency discriminator is type 0 and types 1 and 2 refer to the simpler single QC FD and the larger single QC FD respectively.

```
          0              4             315            2              6
!      TYPE         CENTRE        DELAY        F-LOWER        F-UPPER
!    (0,1,2)      FREQUENCY    (Degrees)       (GHz)          (GHz)
!                   (GHz)
```

Fig K.1 : **Sample dummy data file DAATA.S2P**

For the standard version, S-parameters should be stored in two three port files named 'STD-FD-1.S3P' and 'STD-FD-2.S3P'. S-parameters for the other two types should be stored in a single four port file named 'MY-FD.S4P'. The disk with these files should be in disk drive A and the TOUCHSTONE program disk should be in drive B, which is usual when using TOUCHSTONE/RF.

The best way to use this program in conjunction with TOUCHSTONE is to use a batch run. Fig K.2 shows the runstream of a suggested batch run started from 'switch-on' or a re-set. 'KEYBUK' merely informs the computer that a UK style key-board is in use, and 'GETCLOCK' retrieves time and calendar information from the real-time clock. The disk should of course be a 'system' disk and the KEYBUK and GETCLOCK programs should be resident on it. 'ERR-CAL' is the name of the BASIC file in which the program is stored. To allow the batch run to be started automatically the runstream should be stored in file 'AUTOEXEC.BAT'.

```
KEYBUK
GETCLOCK
: LOOP
B:
TOUCHSTN
A:
BASICA ERR-CAL
GOTO LOOP
```

Fig K.2 : Batch runstream

The results printed by the program go directly to a printer and are very easy to follow. 'Uncorrected data' refers to errors calculated directly from the S-parameter files with no attempt to improve performance by using linear regression. 'Corrected data' refers to the errors calculated after linear regression is performed on the uncorrected data, to find the best straight line through the data by the least-squares method. For the standard discriminator (type 0) the corrected data is applicable, whereas the uncorrected data should be used for FD types 1 and 2. All errors are printed out in degrees.

Let x be the frequency data and y be the uncorrected error data. Then linear regression to provide corrected data $\hat{y}$ is performed directly by the following set of equations if n is the total number of data :

$$\bar{x} = \frac{\sum^{n} x}{n} \qquad \text{..... (K.1)}$$

$$\bar{y} = \frac{\sum^{n} y}{n} \qquad \text{..... (K.2)}$$

$$b = \frac{\sum^{n} (x - \bar{x})(y - \bar{y})}{\sum^{n} (x - \bar{x})^2} \qquad \text{..... (K.3)}$$

$$c = \bar{y} - b\bar{x} \qquad \text{..... (K.4)}$$

$$\hat{y} = bx + c \qquad \text{..... (K.5)}$$

The program also finds the maximum error in the frequency range specified in DAATA.S2P, and the RMS error according to :

$$\text{RMS error} = \frac{\sum^{n}(y^2)^{\frac{1}{2}}}{n} \qquad \text{..... (K.6)}$$

Note that the linear regression is also performed only over the specified frequency band so that n is the number of frequencies for which S-parameters have been calculated within this band. The S-parameter files may have data outside this band (eg. data over a 1 to 7 GHz band may be calculated whereas the bandwidth of interest is 2 to 6 GHz) to show how the errors worsen.

```
1000 REM ************************************************************
1010 REM *                                                          *
1020 REM *                   FD ERROR CALCULATION PROGRAM           *
1030 REM *                                                          *
1040 REM *    Program reads s-parameter files describing different  *
1050 REM *    frequency discriminators and generated by TOUCHSTONE  *
1060 REM *    to calculate peak and RMS phase errors.               *
1070 REM *                                                          *
1080 REM ************************************************************
1090 REM
1100 REM
1110 REM        READ IN FD TYPE, CENTRE FREQUENCY, DELAY LINE
1120 REM        LENGTH AND UPPER AND LOWER FREQUENCY LIMITS
1130 REM
1140 DIM A(101,4)
1150 PI=3.141592654#
1160 OPEN "A:DAATA.S2P" FOR INPUT AS #1
1170 INPUT #1,DIS,F0,D0,FL,FU
1180 CLOSE #1
1190 REM
1200 REM        READ IN DATA FOP STANDARD FD (TYPE 0)
1210 REM
1220 IF DIS<>0 THEN 1380
1230 OPEN "A:STD-FD-1.S3P" FOR INPUT AS #1
1240 OPEN "A:STD-FD-2.S3P" FOR INPUT AS #2
1250 I=0
1260 IF EOF(1) THEN 1520
1270     I=I+1
1280     INPUT #1,F,A1,B1,C1,D1,E1,F1
1290     INPUT #1,A1,B1,C1,D1,E1,F1
1300     INPUT #1,B1,C1,D1,E1,F1,G1
1310     INPUT #2,FF,A2,B2,C2,D2,E2,F2
1320     INPUT #2,A2,B2,C2,D2,E2,F2
1330     INPUT #2,B2,C2,D2,E2,F2,G2
1340     A(I,1)=F
1350     A(I,2)=180/PI*ATN((A1^2-B1^2)/(A2^2-B2^2))
1360 GOTO 1260
1370 REM
1380 REM        READ IN DATA FOR SINGLE QC FD'S (TYPES 1 & 2)
1390 REM
1400 OPEN "A:MY-FD.S4P" FOR INPUT AS #1
1410 I=0
1420 IF EOF(1) THEN 1520
1430     I=I+1
1440     INPUT #1,F,A1,B1,C1,D1,E1,F1,G1,H1
1450     INPUT #1,B1,C1,D1,E1,F1,G1,H1,I1
1460     INPUT #1,C1,D1,E1,F1,G1,H1,I1,J1
1470     INPUT #1,D1,E1,F1,G1,H1,I1,J1,K1
1480     A(I,1)=F
1490     A(I,2)=180/PI*ATN((B1^2-D1^2)/((3-DIS)*C1^2-B1^2-D1^2))
1500 GOTO 1420
```

```
1510 REM
1520 REM       MAKE INITIAL ERROR CALCULATIONS
1530 REM
1540 N=I
1550 FOR I=1 TO N
1560    A(I,3)=A(I,2)+DO^A(I,1)/FO
1570    WHILE A(I,3)>90
1580       A(I,3)=A(I,3)-180
1590    WEND
1600 NEXT I
1610 REM
1620 REM       PERFORM LINEAR REGRESSION
1630 REM
1640 FOR I=1 TO N
1650    IF A(I,1)=FL THEN LET NL=I
1660    IF A(I,1)=FU THEN LET NU=I
1670 NEXT I
1680 X=0: Y=0
1690 FOR I=NL TO NU
1700    X=X+A(I,1)
1710    Y=Y+A(I,3)
1720 NEXT I
1730 XBAR=X/(NU-NL+1)
1740 YBAR=Y/(NU-NL+1)
1750 B=0: C=0
1760 FOR I=NL TO NU
1770    B=B+(A(I,1)-XBAR)*(A(I,3)-YBAR)
1780    C=C+(A(I,1)-XBAR)^2
1790 NEXT I
1800 M=B/C
1810 C=YBAR-M*XBAR
1820 FOR I=1 TO N
1830    A(I,4)=A(I,3)-M*A(I,1)-C
1840 NEXT I
1850 REM
1860 REM       FIND MAXIMUM AND CALCULATE RMS ERRORS
1870 REM
1880 E1MAX=0: E2MAX=0
1890 E1TOT=0: E2TOT=0
1900 FOR I=NL TO NU
1910    IF ABS(A(I,3))>E1MAX THEN LET E1MAX=ABS(A(I,3))
1920    IF ABS(A(I,4))>E2MAX THEN LET E2MAX=ABS(A(I,4))
1930    E1TOT=E1TOT+ABS(A(I,3))
1940    E2TOT=E2TOT+ABS(A(I,4))
1950 NEXT I
1960 E1RMS=E1TOT/(NU-NL+1)
1970 E2RMS=E2TOT/(NU-NL+1)
```

```
1980 REM
1990 REM       PRINT OUT DATA
2000 REM
2010 PGLEN=50
2020 LPRINT :LPRINT "     DISCRIMINATOR TYPE = ";DIS
2030 LPRINT :LPRINT "       CENTRE FREQUENCY = ";F0;" GHz"
2040 LPRINT :LPRINT "           DELAY LENGTH = ";D0;" Degrees"
2050 LPRINT :LPRINT " LOWER FREQUENCY LIMIT = ";FL;" GHz"
2060 LPRINT :LPRINT " UPPER FREQUENCY LIMIT = ";FU;" GHz"
2070 LPRINT :LPRINT
2080 LPRINT "    UNCORRECTED CASE"
2090 LPRINT "   ------------------"
2100 LPRINT :LPRINT "    PEAK ERROR = ";E1MAX;" Degrees"
2110 LPRINT :LPRINT "     RMS ERROR = ";E1RMS;" Degrees"
2120 LPRINT :LPRINT
2130 LPRINT "      CORRECTED CASE"
2140 LPRINT "     ----------------"
2150 LPRINT :LPRINT "    PEAK ERROR = ";E2MAX;" Degrees"
2160 LPRINT :LPRINT "     RMS ERROR = ";E2RMS;" Degrees"
2170 LPRINT CHR$(12)
2180 LPRINT
2190 LPRINT "    FREQUENCY    UNCORRECTED    CORRECTED"
2200 LPRINT "      (GHz)          ERROR          ERROR"
2210 LPRINT " ---------------------------------------"
2220 LPRINT
2230 LCNT=5
2240 FOR I=1 TO N
2250    LPRINT "      ";
2260    LPRINT USING "##.#";A(I,1);
2270    LPRINT "         ";
2280    LPRINT USING "###.###";A(I,3);
2290    LPRINT "        ";
2300    LPRINT USING "###.###";A(I,4)
2310    LCNT=LCNT+1
2320    IF LCNT=50 THEN LPRINT CHR$(12):LPRINT :LCNT=1
2330 NEXT I
2340 LPRINT CHR$(12)
2350 CLOSE
2360 SYSTEM
2370 END
```

APPENDIX L

PUBLICATION

The following brief article was published in the 7th November 1985 edition of ELECTRONICS LETTERS.

NOVEL POLAR FREQUENCY DISCRIMINATOR

Indexing term: Signal processing

An alternative form of polar frequency discriminator is described. It reduces the complexity of previous circuits and makes microstrip integration much simpler by eliminating the need to cross over transmission lines. As a result phase errors are significantly reduced.

Polar frequency discriminators (PFDs) form the basis of instantaneous frequency measuring receivers (IFMRs) and have been extensively covered in the literature.[1-4] Fig. 1 shows a common PFD configuration. In essence it consists of a polar phase discriminator (PPD) which measures the phase delay in a transmission line, the phase being linearly dependent on frequency.

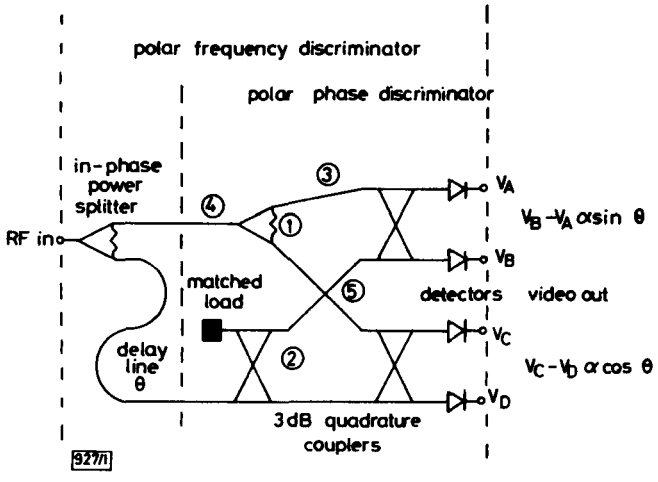

Fig. 1 *Usual PFD circuit*

The major problem with the PFD is the crossover required at point (5) in Fig. 1. Air bridges work well in monolithic circuits and at low frequencies in microstrip[4] but are structurally weak. Cascaded quadrature couplers have been considered[4] but they unnecessarily increase the circuit complexity. The usual solution is to integrate the PPD separately and attach the delay line externally.[3,4] Alternatively the detector video outputs may be taken from the interior of the board via coaxial cables.

The lack of symmetry between the in-phase power splitter and quadrature coupler labelled (1) and (2) also gives rise to phase errors. One solution is to use a hybrid coupler in place of (1) and to add a 90° phase shifter at (3). Sometimes a phase shift network is added at (4) to compensate for the difference in the physical length of components (1) and (2), and the slight nonlinearities in phase against frequency between input and output ports of quadrature couplers. All these refinements increase the complexity of the PPD. It is also worth noting that in the authors' experience in-phase power splitters exhibit more nearly ideal behaviour over wide bandwidths than quadrature couplers.

Figs. 2 and 3 show alternative layouts which this letter serves to introduce. That shown in Fig. 2 is the simpler configuration. Note that no crossover at all is required, so the PFD is easily integrated in its entirety. Since only one quadrature coupler is required the circuit is less sensitive to 3 dB coupling and 90° phase deviations which occur within these components in wideband applications. Only three detectors are required, which reduces cost and errors that arise if detectors do not track each other exactly. The disadvantages are the slightly more complex video processing and the additional power loss, 3 dB in the case of the layout shown in Fig. 3. Since PFDs are usually fed by limiting amplifiers the additional loss can be tolerated. It is common practice anyway to place resistive matching networks before the detectors.[3,4]

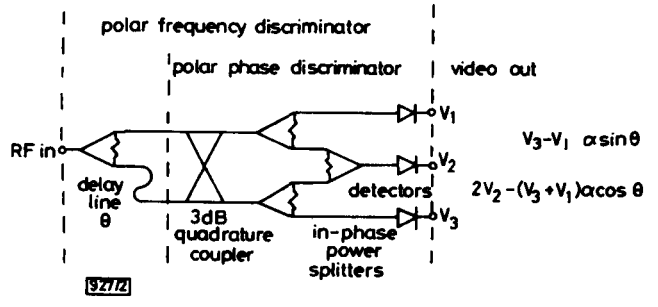

Fig. 2 *Simpler PFD configuration*

Referring to Fig. 2 the video processing required is given by

$$\sin\theta \propto V_3 - V_1$$

$$\cos\theta \propto 2V_2 - (V_3 + V_1)$$

The factor 2 which occurs in the second equation is required if the voltage split factor of the power splitters is $(\sqrt{2})^{-1}$. In fact, if the voltage split is a, V_2 needs to be multiplied by a factor a^{-2}. This is achieved with a video amplifier with a voltage gain of a^{-2}. This multiplicative factor can be avoided by using the configuration shown in Fig. 3. Slightly greater RF complexity is then required. Whether this leads to a better or worse error performance depends on the input match of the two added power combiners. Once the various components have been developed computer analysis should be used to determine which circuit gives better results, but in most cases the simpler version performs as well or better.

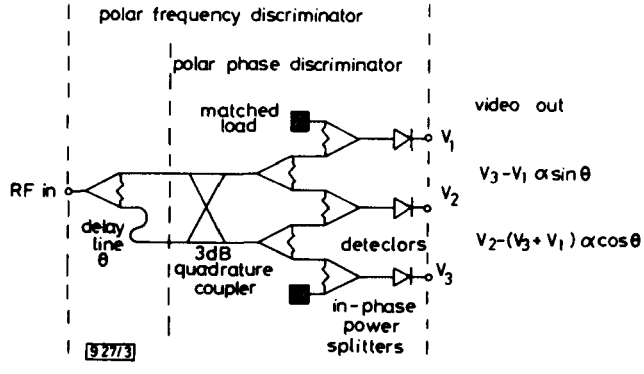

Fig. 3 *Slightly more complex PFD*

Fig. 4 shows photographs of 2–6 GHz stripline prototypes of these two circuits manufactured on RT Duroid 5880 (ξ_r = 2·2). The size of these circuits can be greatly reduced by using RT Duroid 6010 (ξ_r = 10) or alumina, and by working in microstrip. The available materials made construction of the three-section 3 dB overlay couplers with a characteristic impedance of 50 Ω much easier than single-section couplers, but the minimal improvement in theoretical performance would not otherwise have justified their use. Based on *s*-parameter measurements the 2–6 GHz PFD on the left in Fig. 4 exhibited a peak error of 3·3° and an RMS error of 1·5°, while the other had a peak error of 6° and an RMS error of 1·4°.

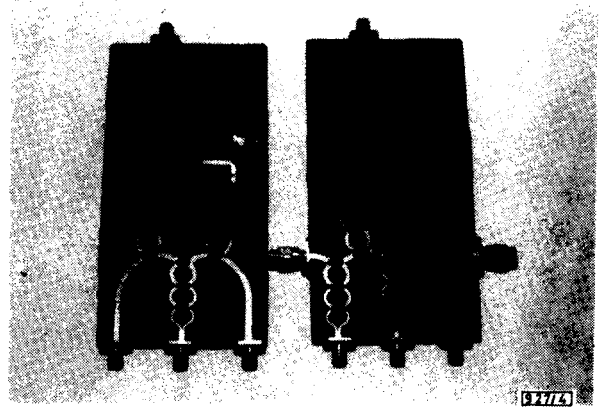

Fig. 4 *Prototype 2–6 GHz PFDs*

Reprinted from ELECTRONICS LETTERS 7th November 1985 Vol. 21 No. 23 pp. 1108-1109

REFERENCES

1 HOFMANN, C.B., BARON, A.R.: 'Wideband ESM receiving systems, Part I', Microwave Journal, Sept 1980, pp 24-34.

2. HOFMANN, C.B., BARON, A.R.: 'Wideband ESM receiving systems, Part II', Microwave Journal, Feb 1981, pp 57-61.

3. MARGOSIAN, J.: 'EW and the instantaneous frequency measurement receiver (IFMR):', Conf. proc., Military Electronics Defence Expo, Wiesbaden, Germany, 7-9 Oct 1980, pp 179-196.

4. EAST, P.W.: 'Design techniques and performance of digital IFM', IEE Proc. F, Commun., Radar & Signal Process., 1982, Vol 129, pp 154-163.

5. RHODES, J.D.: 'A review of radar warning receivers', European Microwaves Conference, Paris, August 1985, pp 3-12.

6. SKOLNIK, M.I.: 'Introduction to Radar Systems', 2nd ed., McGraw-Hill International Book Company, 1980.

7. DROGIN, E.M.: 'Frequency encoding essential for overlapping pulses', MSN, July 1979, pp 50-63.

8. COLLINS, J. H., GRANT, P.M.: 'A review of current and future components for electronic warfare receivers', IEEE Transactions on Microwave Theory and Techniques, Vol MTT-29, No 5, May 1981, pp 395-403.

9. RAPPOLT, F., STONE, N.: 'Receivers for signal acquisition', Conf. proc., Military Electronics Defence Expo, 1976, pp 403-420.

10. SULLIVAN, W.B.: 'Ultra-wideband IFM receiver fulfills design requirements', MSN & CT, April 1985, pp 105-107.

11. TSUI, J., SHAW, R., CISAR, J., RATCLIFF, T.: 'Instantaneous simultaneous signal detecting', Microwave Journal, 1982, pp 118-122.

12. HAMILTON, R.J., OSBRINK, N.K.: 'EW applications of new dual-gate GaAs FETs', Defence Electronics, Sept 1979, pp 101-107.

13. GODDARD, N.E.: 'Instantaneous frequency-measuring receivers', IEEE Trans on Microwave Theory & Techniques, Vol. MTT-20, April 1972, pp 292-293.

14. HEATON, D.: 'The system engineer's primer on IFM receivers', Microwave Journal, Feb 1980, pp 71-85.

15. KONIG, C.: 'ELINT design melds classic methods', Microwaves & RF, Sept 1984, pp 150-151, 155, 225.

16. RACHMAN, D.M., DOWNING, B.J.: 'A novel polar frequency discriminator', Electronics Letters, Vol 21, No 23, 7th November 1985, pp 1108-1109.

17. MYERS, G.A., CUMMING, R.C.: 'Theoretical response of a polar-display instantaneous-frequency meter', IEEE Transactions on Instrumentation and Measurement, Vol IM-20, No 1, Feb 1971, pp 38-48.

18. YOUNG, L: 'The analytical equivalence of TEM-mode directional couplers and transmission-line stepped-impedance filters', Proceedings of the IEE, Vol 110, No 2, Feb 1963, pp 275-281.

19. ALLEN, D.E., LARSON, I.D., CONTY, E.: 'Surface accoustic wave components for frequency sorting receivers', IEEE Ultrasonics Syumposium, 1979, pp 555-557.

20. CHUA, L.W., GIBSON, P.J.: 'MIC frequency discriminators for K-Ka band IFM receivers', Proceedings of the Military Microwaves Conference, London, England, 20-22 Oct 1982, pp 262-266.

21. CHELLI, R., GASPERINI, S., QUAGLIA, A.: 'MIC polar discriminators and multifunction modules in EW systems', Proceedings of the Military Microwave Conference, London, England, 20-22 Oct, 1982, pp 256-261.

22. HOWE, H.: 'Instantaneous Frequency Monitors', Stripline Circuit Construction, pp 266-267.

23. SCHIFFMAN, B.M.: 'A new class of broad-band microwave 90-degree phase shifters', IRE Transactions on Microwave Theory & Techniques, Vol 6, No 2, April 1958, pp 232-237.

24. Narda Microwave Corp.: 'Polar frequency discriminators', Microwave Journal, Sept 1974, p 36.

25. GROSSBACH, R.: 'Degradation of polar-discriminator performance by non-ideal components', Microwave Journal, Dec 1974, pp 53-68.

26. DUHAMEL, R.H., ARMSTRONG, M.E.: 'The tapered-line magic-T', 'Parallel Coupled Lines and Directional Couplers', edited L. Young, Artech House, Inc. 1972, pp 207-233.

27. REHNMARK, S.: 'Wide-band balanced line microwave hybrids', IEEE Transactions on Microwave Theory & Techniques, Vol MTT-25, No 10, Oct 1977, pp 825-830.

28. MISHRA, S.R., WADHWA, R.P.: 'Development of an X-band waveguide frequency discriminator', IEEE Transactions on Microwave Theory & Techniques, Vol MTT-18, Sept 1970, pp 660-661.

29. NIGRIN, J., MANSOUR, N.A., VOSS, W.A.G.: 'Single hybrid tee frequency discriminator', IEEE Transactions on Microwave Theory & Techniques, Vol MTT-23, Sept 1975, pp 776-778.

30. GUPTA, K.C., GARG, R., CHADHA, R.: 'Computer Aided Design of Microwave Circuits', Artech House, Inc., 1981.

31. COHN, S.B.: 'Characteristic impedance of broadside-coupled strip transmission lines', IRE Transactions on Microwave Theory & Techniques, Vol MTT-8, No 6, Nov 1960, pp 633-637.

32. NIAST-CSIR: 'Program for calculating Shelton's equations', Private communication.

33. SHELTON, J.P.: 'Impedances of offset parallel-coupled strip transmission lines', IEEE Transactions on Microwave Theory & Techniques, Vol MTT-14, No 1, Jan 1966, pp 7-15.

34. COHN, S.B.: 'A class of broadband three-port TEM-mode hybrids', IEEE Translations on Microwave Theory & Techniques, Vol MTT-16, No 2, Feb 1968, pp 110-116.

35. LANGE, J.: 'Interdigitated stripline quadrature hybrid', IEEE Transactions on Microwave Theory and Techniques, Vol. MTT-17, Dec 1969, pp 1150-1151.

36. DOWNING, B.J.: 'Lange Coupler', Private communication.

37. GARCIA, J.A.: 'A wide-band quadrature hybrid coupler', IEEE Transactions on Microwave Theory and Techniques, Vol MTT-19, July 1971, pp 660-661.

38. SCHIEK, B.: 'Hybrid branchline couplers - a useful new class of directional couplers', IEEE Transactions on Microwave Theory and Techniques, Vol MTT-22, No 10, Oct 1974, pp 864-869.

39. CRISTAL, G.E., YOUNG, L.: 'Theory and tables of optimum symmetrical TEM-mode coupled-transmission-line directional couplers', IEEE Transactions on Microwave Theory and Techniques, Vol MTT-13, Sept 1965, pp 544-558.

40. KAMMLER, D.W.: 'The design of discrete N-section and continuously tapered symmetrical microwave TEM directional couplers', IEEE Transactions on Microwave Theory and Techniques, Vol MTT-17, No 8, Aug 1969, pp 577-590.

41. TRESSELT, C.P.: 'Design and computed theoretical performance of three classes of equal-ripple non-uniform line couplers', IEEE Transactions on Microwave Theory and Techniques, Vol MTT-17, No 4, April 1969, pp 218-230.

42. HO, C.Y., MOSER, L.: 'Symmetrical coupler reduces phase error', Microwaves, Vol 20, April 1981, pp 82-84.

43. HARROD, J.E.: 'The analysis of non-ideal stripline directional couplers', MSc dissertation, University of Stellenbosch, 1976.

44. MATTHEI, G., YOUNG, L., JONES, E.M.T.: 'Microwave Filters, Impedance-Matching Networks, and Coupling Structures', Artech House, 1980.

45. SHURMER, H.V.: 'Microwave Semi-conductor Devices', Pitman Publishing, 1971.

46. Alpha Microwave Semiconductors, 'Schottky barrier diodes for mixers and detectors', Alpha Industries, Inc.

47. BLACHMAN, N.M.: 'The effect of noise upon polar-display instantaneous frequency measurement', IEEE Transactions on Instrumentation and Measurement, Vol IM-25, No 3, Sept 1976, pp 214-221.